



MONASH University

***Measurement of Atmospheric Volatile Organic Compounds
with Proton Transfer Reaction- Mass Spectrometry***

Erin Dunne

BSc Hons.

A thesis submitted for the degree of Doctor of Philosophy at
Monash University in 2015
Faculty of Science, School of Chemistry

Copyright notice

© The author (2015). Except as provided in the Copyright Act 1968, this thesis may not be reproduced in any form without the written permission of the author.

I certify that I have made all reasonable efforts to secure copyright permissions for third-party content included in this thesis and have not knowingly added copyright content to my work without the owner's permission.

Abstract

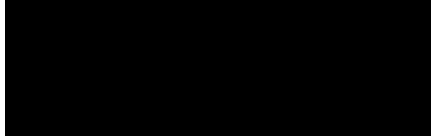
The instrument employed in this study was a PTR-MS with switchable reagent ion capability (SRI-MS), which enables the use of O_2^+ and NO^+ as reagent ions in addition to H_3O^+ . The application of SRI-MS to measurements of inorganic and organic compounds in the atmosphere is still in its infancy and studies such as those reported here are critical to determine what, if any, additional information can be acquired through the use of reagent ions other than H_3O^+ .

The laboratory studies described in this thesis represent one of the most extensive characterizations of the performance of SRI-MS instruments for the identification and quantification of volatile organic compounds (VOCs) to date. This was followed by one of the first real-world comparisons of the measurement of VOCs using O_2^+ , NO^+ and H_3O^+ reagent ions in SRI-MS and this work represents a significant contribution to the available information on the application of SRI-MS to atmospheric observations of VOCs. In addition, two novel applications of SRI-MS were developed: A study of acetonitrile showed that in some cases corrections may be made for the coincidence of several VOC signals at the same mass/charge ratio, and an improved analyte signal obtained. Finally some promising results concerning the measurement of total non-methane organic carbon with SRI-MS were presented.

Declaration

This thesis contains no material which has been accepted for the award of any other degree or diploma at any university or equivalent institution and that, to the best of my knowledge and belief, this thesis contains no material previously published or written by another person, except where due reference is made in the text of the thesis.

Signature:

A solid black rectangular box used to redact the signature.

Erin Dunne

Date: 21/12/2015

Thesis including published works declaration

I hereby declare that this thesis contains no material which has been accepted for the award of any other degree or diploma at any university or equivalent institution and that, to the best of my knowledge and belief, this thesis contains no material previously published or written by another person, except where due reference is made in the text of the thesis.

This thesis includes one original paper published in a peer-reviewed journal. The core theme of the thesis is the identification and quantification of atmospheric volatile organic compounds using Proton Transfer Reaction – Mass Spectrometry. The ideas, development and writing up of all the papers in the thesis were the principal responsibility of myself, the candidate, working within the School of Chemistry under the supervision of Dr Ian Galbally (CSIRO Marine and Atmospheric Research) and Assoc. Prof. Antonio Patti (School of Chemistry, Faculty of Science)

The inclusion of co-authors reflects the fact that the work came from active collaboration between researchers and acknowledges input into team-based research.

In the case of *Chapter 5* my contribution to the work involved the following:

Thesis Chapter	Publication Title	Status	Nature and % of student contribution	Co-author name(s) Nature and % of Co-author's contribution*	Co-author(s), Monash student
5	<i>Interference in the measurement of acetonitrile at m/z 42 in polluted urban air by PTR-MS – A study using switchable reagent ion PTR-MS</i>	<i>published</i>	<i>70%. Concept and collecting data and writing first draft</i>	<i>1) Ian Galbally 25% input into concept and manuscript 2) Sarah Lawson 5% input into measurements 3) Antonio Patti 5% input into manuscript</i>	<i>No No No</i>

I have not renumbered sections of submitted or published papers in order to generate a consistent presentation within the thesis.

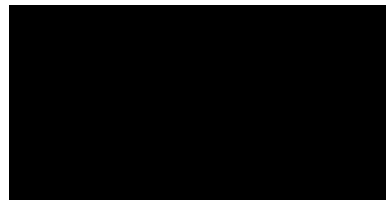
Student signature:



Date: 21/12/2015

The undersigned hereby certify that the above declaration correctly reflects the nature and extent of the student's and co-authors' contributions to this work. In instances where I am not the responsible author I have consulted with the responsible author to agree on the respective contributions of the authors.

Main Supervisor signature:



Date: 21/12/2015

Acknowledgements

I have been fortunate to work with many wonderful people over the course of my thesis. First and foremost, I thank my supervisor at CSIRO, Ian Galbally for the enormous amount of time, effort and enthusiasm he has invested in supporting me through this long journey. Ian, I deeply appreciate the opportunities you have provided for me, your guidance and perseverance through challenging times, and your patience and friendship throughout.

I would like say a special thanks to thank Sarah Lawson for her help in tackling the ‘The Beast’, and the humour, patience and friendship she has offered me over my PhD journey.

Thanks also to Tony Patti, my Monash supervisor for his support and constant encouragement to find the finish line.

To the rest of the CSIRO team who have helped and supported me along the way- Min Cheng, Paul Selleck, Suzie Molloy, Jamie Harnwell, Jason Ward, Jennifer Powell, Melita Keywood, and the late Simon Bentley- thank you all sincerely. In particular, I would like to gratefully acknowledge the work of Paul Selleck, Min Cheng, and Jason Ward, from CSIRO and Branka Miljevic from QUT for the supporting measurements they have provided for this thesis.

Finally, thanks to my family- especially my three beautiful sons Gabe, Reuben and Jude, and my partner Lachlan – for their love and support without which, none of this would have been possible.

This work was supported by CSIRO Marine and Atmospheric Research and a Monash University Faculty of Science Scholarship.

Contents

Copyright notice	iv
Abstract	v
General Declaration.....	vi
Acknowledgements	vii
Thesis Overview	1
Original hypothesis.....	1
Thesis Structure and Approach	1
Part A: PTR-MS Theory and Laboratory Studies.....	6
Chapter 1. The Principles and Components of PTR-MS	8
1.1 Introduction	8
1.2 Chemical Ionization Mass Spectrometry.....	10
1.3 Chemical Ionization in PTR-MS	12
1.3.1 Thermochemistry of Proton Transfer Reactions.....	13
1.3.2 Proton Transfer Reaction Kinetics	15
1.3.2.1 Proton transfer reaction kinetics for non-polar reactants.....	15
1.3.2.2 Proton transfer reaction kinetics for polar reactants	16
1.3.2.3 Proton transfer reaction kinetics at supra-thermal conditions	17
1.4 Reaction processes occurring in PTR-MS.....	19
1.4.1 Proton transfer from H_3O^+	19
1.4.2 Association Reactions	21
1.4.3 Reactions with hydrated hydronium ions	22
1.4.4 Thermoneutral Reactions.....	23
1.4.5 Reactions of O_2^+ and NO^+ reagent ions in PTR-MS.....	24
1.4.6 Summary of Reaction Processes in PTR-MS	27
1.5 PTR-MS Instrumentation	30
1.5.1 The Hollow Cathode Ion Source	31
1.5.2 Switchable Reagent Ion Mass Spectrometry (SRI-MS)	36
1.5.3 The PTR-MS Drift Tube	38
1.5.4 The PTR-MS Ion Detection System.....	43
1.5.5 The Quadrupole Mass Spectrometer	43
1.5.6 Secondary Electron Multiplier	44
1.5.7 Digitising the signal.....	46
1.5.8 Mass Dependent Transmission.....	47
1.6 PTR-MS Quantification.....	49

1.7. Empirical Calibration	53
1.8 Summary	54
Chapter 2. PTR-MS Spectra of some simple oxygenated VOCs	56
2.1 Introduction.....	56
2.2 Methods.....	58
2.2.1 Preparation of gas standards	58
2.2.2 PTRMS instrument set-up	59
2.3 Results & Discussion	60
2.3.1 Aldehydes and ketones	63
2.3.2 Alcohols	70
2.3.3 Carboxylic acids.....	77
2.3.4 Esters	81
2.3.5 Multifunctional VOCs.....	84
2.4 Discussion	92
Chapter 3. Switchable reagent ion mass spectrometry (SRI-MS): measurements of certified gas standards of a range of VOCs.	96
3.1 Introduction.....	96
3.2 Interpretation of the SRI-MS spectra of mixtures	98
3.2.1 Rules for the interpretation of the mass spectra.....	99
3.2.2 Supplementary Information.....	101
3.3 Methodology	106
3.4. SRI-MS measurements of certified gas standards with H_3O^+	115
3.5 SRI-MS measurements of certified gas standards with O_2^+	131
3.6 SRI-MS measurements of certified gas standards with NO^+	146
3.7 SRI-MS Sensitivity.....	158
3.7 Conclusions	162
Part B: Measurements of VOCs in urban air with SRI-MS	166

Chapter 4. An exploratory study of the use of switchable reagent ion mass spectrometry (SRI-MS) for the measurement of VOCs in urban air..... 168

4.1 Introduction	168
4.2 Methodology	170
4.2.1 Study location.....	170
4.2.2 SRI-MS measurement set-up.....	170
4.3 SRI-MS calibrations	173
4.4 Selection and identification of key m/z.....	175
4.5 Supporting Measurements	178
4.6 Considerations for quantitative inter-comparisons.....	180
4.7 SRI-MS measurements of selected VOCs in urban air with H_3O^+	183
4.7.1 H_3O^+ SRI-MS m/z 93: Toluene	184
4.7.2 H_3O^+ SRI-MS m/z 107: C_8 Aromatics.....	186
4.7.3 H_3O^+ SRI-MS m/z 121: C_9 aromatics.....	187
4.7.4 H_3O^+ SRI-MS m/z 69: Isoprene	188
4.7.5 H_3O^+ SRI-MS m/z 81 & 137: Monoterpenes	190
4.7.6 H_3O^+ SRI-MS m/z 31: Formaldehyde	192
4.7.7 H_3O^+ SRI-MS m/z 45: Acetaldehyde	194
4.7.8 H_3O^+ SRI-MS m/z 59: Acetone & Propanal.....	197
4.7.9 H_3O^+ SRI-MS m/z 71: Methacrolein & Methyl Vinyl Ketone.....	198
4.7.10 H_3O^+ SRI-MS m/z 73: Methyl Ethyl Ketone, Methyl Glyoxal & Butanal.....	201
4.7.11 Summary of the comparison of measurements of VOCs in urban air with H_3O^+ SRI-MS, AT-VOC and DNPH techniques	202
4.8 SRI-MS measurements of VOCs in urban air with O_2^+	205
4.8.1 O_2^+ SRI-MS m/z 92: Toluene	207
4.8.2 O_2^+ SRI-MS m/z 106: C_8 Aromatic compounds.....	208
4.8.3 O_2^+ SRI-MS m/z 120: C_9 Aromatic compounds.....	209
4.8.4 O_2^+ SRI-MS m/z 67: Isoprene	210
4.8.5 O_2^+ SRI-MS m/z 93: Monoterpenes	211
4.8.6 Summary of the comparison of measurements of VOCs in urban air with O_2^+ and H_3O^+ SRI-MS	212
4.9 SRI-MS measurements of VOCs in urban air with NO^+	215
4.9.1 NO^+ SRI-MS m/z 92: Toluene	216
4.9.2 NO^+ SRI-MS m/z 106: C_8 Aromatics	217
4.9.3 NO^+ SRI-MS m/z 68: Isoprene.....	218

4.9.4 Summary of the comparison of measurements of VOCs in urban air with NO ⁺ and H ₃ O ⁺ SRI-MS	220
4.10 Conclusions	221
Chapter 5. Interference in the PTR-MS measurement of acetonitrile at m/z 42 in polluted urban air – A study using switchable reagent ion PTR-MS.....	224
Chapter 6. Measurement of total non-methane organic carbon (TNMOC) in urban air using O₂⁺ SRI-MS	233
6.1 Introduction	233
Definitions of total non-methane organic carbon.....	235
6.2 Methodology	237
6.2.1 Speciated VOC measurements	237
6.2.2 SRI-MS set-up	238
6.3 O ₂ ⁺ SRI-MS Sensitivity	239
6.4 Quantification of total non-methane organic carbon [TNMOC] from the O ₂ ⁺ SRI-MS signal	242
6.6 Tests against certified gas standards.....	244
6.7 TNMOC measurements in urban air	250
6.8 Correlations of TNMOC with other atmospheric constituents.....	253
6.9 Conclusions	257
Chapter 7. Thesis Conclusions	259
8. Bibliography	263

Thesis Overview

This thesis will be presented as a combination of five traditional thesis chapters and one published paper. Journal formatting has been maintained for the published paper. The thesis concludes with a general discussion followed by a complete bibliography

Original hypothesis

The overall research hypothesis for this thesis was:

PTR-MS can be used to accurately identify and quantify VOCs in the atmosphere.

This hypothesis was examined in two parts:

- What information can be reliably determined about VOC identification from PTR-MS?
- What compounds can the PTR-MS unequivocally quantify in measurements of the atmosphere?

Subsequent to the commencement of this work, switchable reagent ion PTR-MS (SRI-MS) became available and the thesis was extended to include SRI-MS in addressing the questions above.

Thesis Structure and Approach

The body of this thesis is presented in two parts: Part A concerns PTR-MS theory and laboratory studies; and Part B concerns the application of PTR-MS in measurements of VOCs in ambient air.

Part A – Chapter 1, provides a review of the principles of PTR-MS and it's application to measurements of VOCs in the atmosphere. Chapters 2 and 3, describe a series of PTR-MS laboratory studies of pure gaseous VOC standards. The Objectives of Part A were to:

- understand the processes occurring in the PTR-MS;
- evaluate the capability of a proton-transfer reaction mass spectrometer to identify volatile organic compounds in the atmosphere

- characterize the sensitivity of the PTR-MS in multiple reagent ion modes (H_3O^+ , NO^+ , and O_2^+) in terms of ion-molecule collision theory and our understanding of the mass dependent transmission of ions through a quadrupole mass spectrometer.

Chapter 1- The principles and components of PTR-MS

At the commencement of this thesis project in 2007 a comprehensive review of the principles underlying PTR-MS, its structure and its application to measurements of VOCs in the atmosphere was undertaken. This review is presented in Chapter 1, with only minor modifications to include information on switchable reagent ion PTR-MS. Since the original review was undertaken, a number of other reviews of the principles and applications of proton transfer mass spectrometry have been published. de Gouw and Warneke (2007) described the basic instrumentation, measurement principles and application of PTRMS to the measurements of VOCs in the atmosphere. Blake, Ellis and Monks (2009) reviewed the development, principles and application of PTR-MS to environmental, food and medical science. The most comprehensive description of the principles and application of PTR-MS was produced more recently in a dedicated book by Ellis and Mayhew (2014).

Thus, while the review provided in Chapter 1 would not be included if the thesis project was commenced today, it is included here to provide a comprehensive background to the experimental work completed for this thesis.

Chapter 2- Studies of PTR-MS spectra of some simple, oxygenated VOCs

While the PTR-MS was operating with H_3O^+ as the primary reagent ion, the mass spectra of 27 simple VOCs relevant to atmospheric chemistry were measured across a range of PTR-MS operating conditions. The reaction processes occurring in the PTR-MS that result in the observed mass spectra of each compound were identified and compared with theoretical expectations. These mass spectra provide essential reference information for the interpretation of PTR-MS spectra of atmospheric VOCs and to optimize the operating conditions for the measurement of species of interest.

Chapter 3- Switchable reagent ion mass spectrometry (SRI-MS): measurements of certified gas standards of a range of VOCs.

A set of simple rules were developed for the interpretation of the SRI-MS mass spectra of VOC mixtures of known composition. These rules were applied to a series of measurements of certified gas standard mixtures containing in total 73 VOCs, analysed while the SRI-MS was switched sequentially through H_3O^+ , O_2^+ and NO^+ reagent ion modes. The systematized

approach to identify compounds in SRI-MS mass spectra of VOCs was used to determine which compounds the SRI-MS can detect in each reagent ion mode, and of these, which compounds can be detected without interference in the mass spectra of VOC mixtures.

Finally, this chapter presents a characterization of the sensitivity of the SRI-MS in each reagent ion mode (H_3O^+ , NO^+ , and O_2^+). The difference in the empirically derived instrument sensitivities between each reagent ion mode is described in terms of ion-molecule collision theory and our understanding of the mass dependent transmission of ions through a quadrupole mass spectrometer.

Part B- Chapters 4 – 6 present the results of a series of measurements of urban air with SRI-MS. The objective of Part B was to evaluate what information can be reliably determined about the identity of VOCs in an urban atmosphere and which compounds could be accurately quantified.

Chapter 4 - An exploratory study of the use of switchable reagent ion mass spectrometry (SRI-MS) for the measurement of VOCs in urban air

Results of the mass spectral studies undertaken as part of the laboratory work carried out under this thesis along with many published studies indicate that some VOCs can be measured by PTR-MS without significant interference. However the best validation of VOC measurements by PTR-MS are obtained by comparing measurement results with those from independent standard analytical techniques.

An exploratory study of the use of NO^+ , O_2^+ in addition to H_3O^+ reagent ions was undertaken in a series of PTR-MS measurements of VOCs in urban air in Sydney 2011. The sensitivity of the PTR-MS was empirically determined from a series of calibration measurements in each reagent ion mode.

The PTR-MS was operated alongside two other well established VOC measurement techniques using integrated samples of VOCs on adsorbent tubes analysed by GC-FID-MS and carbonyls sampled on DNPH cartridges analysed by HPLC. The SRI-MS observations were compared with the concentrations measured by the two established analytical techniques for a number of atmospherically important VOCs. Specific qualifications for the analysis of each compound are presented.

Chapter 5 - Interference in the measurement of acetonitrile at m/z 42 in polluted urban air – A study using switchable reagent ion PTR-MS

The interpretation of the PTR-MS mass spectra of ambient air is also complicated by the presence of isotopes, and side reactions occurring within the PTR-MS with reagent ions other than H_3O^+ . A detailed investigation of the potential for mass interference in the detection of a species of interest (acetonitrile) due to the presence of isotopologues and the presence of product ions from reactions with impurity reagent ions was performed. A methodology to quantify mass interference was developed and applied to a set of ambient data and is presented as a published case study- Dunne et al. (2012), “Interference in the measurement of acetonitrile at m/z 42 in polluted urban air – A study using switchable reagent ion PTR-MS” *Int. J. Mass Spectrom.*, 319-320, p 40 - 47.

Chapter 6- Measurements of total non-methane organic carbon (TNMOC) in urban air using O_2^+ SRI-MS

While a multitude of speciated VOC measurement systems exist, few techniques to measure total non-methane organic carbon (TNMOC) at concentrations typical in ambient air with high time resolutions have been developed. Measurements of total organic carbon and speciated VOCs using present techniques confirm that a significant fraction of TNMOC in the atmosphere remains unidentified with conventional VOC measurement techniques. (Chung et al. 2003, Goldstein & Galbally 2007, Heald et al. 2008).

Chapter 6 outlines the development of a methodology for quantifying (TNMOC) from the O_2^+ SRI-MS signal and the application of this technique to measurements of urban air undertaken in Sydney, 2011. The results are compared with the sum of the speciated VOCs measured using standard measurement techniques. The characteristics of TNMOC concentrations in urban air, and their relationship to NO_x , and organic aerosol were investigated.

The thesis concludes with a general discussion (Chapter 7) of the research presented and its practical and theoretical significance.

Part A: PTR-MS Theory and Laboratory Studies

Chapter 1. The Principles and Components of PTR-MS

1.1 Introduction

Volatile organic compounds (VOCs) are minor components of atmospheric composition, and have key roles in the chemistry of the atmosphere, processes affecting climate, and processes affecting the health of humans and other life forms on earth. These organic compounds exist in the atmosphere at concentrations that range from parts per billion (10^{-9} mole/mole) to parts per trillion (10^{-12} mole/mole). VOCs belong to different classes of organic compounds including aliphatic hydrocarbons, aromatics, oxygenated VOCs, organo-nitrogen compounds, organ-sulphur compounds, halocarbons and multifunctional compounds. VOCs are emitted into the atmosphere from both biogenic and anthropogenic sources (Seinfeld & Pandis 2006). In the atmosphere, these compounds undergo numerous chemical processes resulting in transformation to a range of oxidised organic products (Atkinson & Arey 2003). It has been estimated that 10^4 - 10^5 different organic species have been identified in the atmosphere and that this range may represent only a fraction of the organic species actually present (Goldstein & Galbally 2007)

The Proton Transfer Reaction-Mass Spectrometer (PTR-MS) is a chemical analysis instrument for analyzing gases for compounds that have a proton affinity greater than water. These compounds are mainly volatile organic compounds. The first commercial proton transfer reaction mass spectrometer (PTR-MS) was described in 1995 (Hansel et al. 1995) followed by a more thorough description in Lindinger et al (1998).

A number of reviews of the principles and applications of proton transfer mass spectrometry have been written since the beginning of this thesis project in 2007. de Gouw and Warneke (2007) described the basic instrumentation, measurement principles and application of PTRMS to the measurements of VOCs in the atmosphere. Blake, Ellis and Monks (2009) reviewed the development, principles and application of PTR-MS to environmental, food and medical science. The most comprehensive description of the principles and application of PTR-MS was produced more recently in a dedicated book by Ellis and Mayhew (2014).

The following description of the development, instrumentation and measurement principles of PTR-MS was completed in 2010 and there is significant cross over with these

other PTR-MS reviews. The work is included here as it was conducted as part of the development of the thesis.

All mass spectrometers operate on the same principle, that is: to ionize chemical compounds to generate charged molecules or molecule fragments and measure them according to their mass-to-charge ratio. A simple model of a mass spectrometer consists of 7 components (Dass 2006):

- An inlet system that transfers the sample from atmospheric pressure to the low pressure of the ion source without interference to the sample's integrity.
- An ion source that transforms gaseous compounds into ions;
- A mass analyzer that sorts ions according to their mass to charge ratio by passing them through an electromagnetic field;
- A detector that measures and amplifies the ion current for each mass-to-charge value and converts it into a mass spectrum.
- A data system to record, process and store the mass spectral data;
- An electronics system to control the operation of the above components.

Proton transfer mass spectrometers belong to a class of mass spectrometers known as chemical ionization mass spectrometers that utilize ion-molecule reactions to ionize the sample rather than conventional ionization such as electron impact (Harrison 1992). The ion source in a PTR-MS consists of 2 parts: a source of primary reagent ions that take part in the chemical ionization reactions, and a drift tube reactor in which the chemical ionization of neutral reactants takes place under controlled conditions.

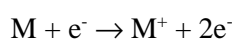
Of prime interest is the drift tube reaction section of the PTR-MS which incorporates chemical ionization first described by Munson and Field (1966) with the flow-drift tube techniques originally invented by Ferguson and colleagues at the National Oceanic and Atmospheric Administration (NOAA) in the 1970s (McFarland et al. 1973). Within the PTR-MS drift tube, compounds with a proton affinity greater than that of water (691 kJ mol^{-1}) undergo proton transfer reactions with protonated water molecules, H_3O^+ , and are thus chemically ionized. The natural components of air (e.g. N_2 , CO_2 , O_2 , Ar) have proton affinities much less than that of water and are invisible to the PTRMS. Conversely a large number of volatile organic compounds have proton affinities high enough to undergo highly efficient proton transfer reactions with protonated water molecules. The well-defined conditions in the reaction chamber permit calculation of the analyte gas concentration without

the need for internal standards or calibration. That is, the constant drift field and pressure define the reaction time, and the proton transfer reaction rates are constant and known. The PTR-MS instrument is sensitive (sub ppbv), and capable of measuring in real time, labile compounds that might not survive the pre-treatment required in other analytical methods.

Firstly, in this chapter we will discuss chemical ionization reactions and aspects of their thermochemistry and reaction kinetics relevant to PTR-MS. Secondly, this chapter will describe the structure and function of the three key components of the PTR-MS: the hollow cathode ion source, the flow-drift tube and the mass spectrometer; as well as the important chemical and physical processes that occur within each. Understanding these processes provides the basis for utilizing PTR-MS for the quantitative and qualitative analysis of volatile organic compounds in gas mixtures, as outlined in the final sections of this chapter.

1.2 Chemical Ionization Mass Spectrometry

Conventional mass spectrometry systems utilize electron impact ionization, a simple, well-characterized technique that can be applied to all volatile compounds that produces high ion currents for sensitive detection, and highly reproducible results. Given its widespread use, a large database of electron impact mass spectra exists to assist in interpretation of EI-MS data (Silverstein et al. 2005). In electron impact ionization, a beam of energized electrons emitted from a hot filament remove an electron from a neutral molecule resulting in a positive ion:



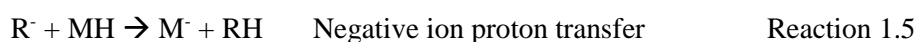
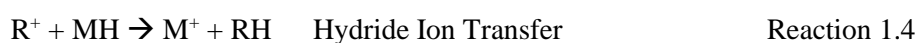
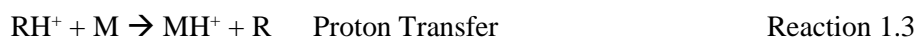
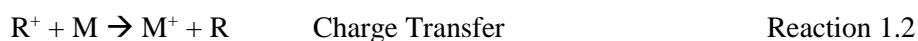
Reaction 1.1

Typical electron energies of 70eV are utilized in electron impact mass spectrometry, of which approximately 15eV, but as much as 30eV, is transferred during the ionization process (Silverstein et al 2005). Typical chemical bond energy is around 3eV and ionization potentials of organic molecules are 8 – 12 eV, therefore the transferred energy in electron impact ionization is sufficient to cause excitation and extensive fragmentation and rearrangement of organic molecules.

Ionization resulting predominantly in the formation of the molecular ion is ideal for molecular mass determination, structure elucidation and identification and quantification of compounds (Harrison 1992). The high energies associated with electron impact ionization regularly result in fragmentation and/or rearrangement followed by fragmentation to produce

an array of fragment ions making identification of the parent molecule more complex. Electron impact is not a selective ionization technique and inorganic constituents in air: nitrogen, oxygen and carbon dioxide, overwhelm the mass spectrum at the low mass range. Due to fragmentation of target molecules and interference by other molecules, the mass spectra of gas mixtures such as atmospheric samples are complex.

Chemical ionization, first described by Munson and Field (1966) and thoroughly reviewed by Harrison (1992), is a ‘soft’ ionization process which utilizes gas-phase ion-molecule reactions to ionize an unknown material in the gas phase. A positive or negative reagent ion, R^+ / R^- is produced from a reagent gas in a conventional ion source such as an electron impact, glow discharge, or ionizing radiation source. The reagent ion (R) undergoes gas-phase ion molecule reactions under controlled conditions with an analyte molecule (M), resulting in a positive or negative stable product ion and a neutral product.



There is a large array of organic and inorganic reagent ions available so the chemical ionization mass spectrometry system can be selected to suit the application.

The aim of chemical ionization is to produce abundant product ions characteristic of the parent molecule/s by choosing the most suitable reagent ion. As these ion/molecule reactions occur at low relative kinetic energy there is usually not enough energy available to cause significant fragmentation of the product ions making it simpler to identify the parent molecules (Munson & Field 1966).

To be utilized for measurements of analyte gas density, chemical ionization must occur under well-defined conditions. As will be shown in Section 1.6, when reaction conditions are known, ion signals detected by the mass spectrometer can be related to the density of reactant and reagent ions in the reaction vessel. In a drift tube, chemical ionization conditions are defined by the pressure and the electric field, which in turn determine the reaction time, reaction frequency and the kinetic energy between the reactants.

In the early 1990s Lindinger and coworkers at the University of Innsbruck, investigated the use of an ion molecule mass spectrometer for trace gas analysis using charge transfer from Xe^+ and Kr^+ to ionize a range of organic and inorganic species (Lindinger et al. 1993). The apparatus included an ion storage section in which ions created in a conventional electron impact source were injected and trapped in a multipole electric field that acted as the reactor. The gas mixture to be analysed was introduced to the reactor where it was chemically ionized and detected by a downstream mass spectrometer. Using this technique the authors were able to quantify a range of inorganic compounds in car exhaust gas. However, charge transfer from Xe^+ and Kr^+ to hydrocarbons resulted in extensive fragmentation, making quantification difficult.

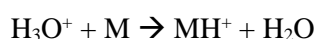
This study identified hydronium ions (H_3O^+) as potentially an ideal primary reagent ion for the analysis of gas mixtures containing a wide variety of hydrocarbons at very low concentrations, as proton transfer from H_3O^+ only occasionally causes extensive product ion fragmentation and reaction efficiency is high, thus generating strong ion signals. Furthermore, the natural components of air (N_2 , O_2 , etc) have proton affinities lower than that of water and most non-alkane VOCs have PA higher than that of water making H_3O^+ an ideal reagent gas for trace VOC detection in air.

The viability of proton transfer reactions involving H_3O^+ was further demonstrated by the University of Innsbruck group, using an Selected ion flow drift tube (SIFDT) (Lagg et al. 1994) in which methanol, ethanol and acetone from human breath samples were ionized resulting in a single product ion for each trace component with detection limits as low as 0.1 ppb.

The remainder of this chapter will deal with the chemical ionization reaction processes occurring in the PTR-MS drift tube, the kinetic and thermodynamic factors of interest, and the quantification of product ions

1.3 Chemical Ionization in PTR-MS

Ideally in the PTR-MS, hydronium ions (H_3O^+) will undergo fast proton transfer reactions resulting in a positive, stable product ion, MH^+ and a neutral water molecule.



Reaction 1.6

In order for M to be ionized, Reaction 1.6 must be thermodynamically favourable. To achieve the high product ion signals required for sensitive trace gas detection Reaction 1.6 must also occur with high reaction efficiency. Furthermore, in order to produce abundant product ions characteristic of the parent molecule/s, fragmentation of the product ion must be minimized. The extent of fragmentation of the product ion, MH^+ , depends on its internal energy, which in part is dependent on the energy transferred from the reagent ion to the neutral in the proton transfer reaction.

1.3.1 Thermochemistry of Proton Transfer Reactions

Reaction 1.6 is thermodynamically favourable if the Gibbs free energy change (ΔG) is negative. The thermodynamic factors of interest in proton transfer reactions are the proton affinity (PA) and the gas phase basicity (GB). Proton affinity is related to enthalpy, H , and gas phase basicity is related to Gibbs free energy. These thermodynamic properties are brought together in the Gibbs free energy equation:

$$\Delta G = \Delta H - T\Delta S \quad \text{Equation 1.1}$$

The proton affinity (PA) of a molecule M, in the gas phase is defined as the standard enthalpy (ΔH°) of the hypothetical de-protonation reaction, r :



(standard conditions ($^\circ$), $T = 298.15 \text{ }^\circ\text{K}$, $P = 1 \text{ bar}$)

Proton affinity is usually expressed in units of kilocalories per mole (kcal mol^{-1}) but can also be expressed in kilojoules per mole (kJ mol^{-1}) or electron volts (eV) where ($1 \text{ kcal mol}^{-1} = 4.184 \text{ kJ mol}^{-1} = 0.434 \text{ eV}$). The proton affinity of water is $165 \text{ kcal mol}^{-1}$. Proton affinities of organic species are in the range of $\sim 50 - 250 \text{ kcal/mol}$. Proton affinities for many organic compounds are available at the National Institute of Standards and Technology, NIST, chemistry webbook (<http://webbook.nist.gov/chemistry>).

The gas phase basicity of a gaseous species is the standard Gibbs free energy of the de-protonation reaction (Reaction 1.7):

$$GB(M) = \Delta G_r^\circ \quad \text{Equation 1.2}$$

The gas phase basicity of a species can be related to its proton affinity via a derivation of the Gibbs free energy equation:

$$GB(M) = PA(M) - T\Delta S_r^\circ \quad \text{Equation 1.3}$$

Where T is the temperature and ΔS_r° is the standard entropy change for the reaction, *r*. Proton transfer is a simple process, and the entropy change between the reactants and products is small therefore $GB(M) \approx PA(M)$. Thus, it is reasonable to use PAs as a substitute for GBs when assessing whether Reaction 1.6 will occur spontaneously.

For Reaction 1.6, the standard enthalpy of the reaction is:

$$\Delta H_r^\circ = -PA(M) + PA(R) \quad \text{Equation 1.4}$$

and the standard Gibbs free energy of reaction is:

$$\Delta G_r^\circ = -GB(M) + GB(R). \quad \text{Equation 1.5}$$

Proton transfer is exothermic, when $\Delta H_r^\circ < 0$, that is if $PA(R) < PA(M)$. Proton transfer is exoergic when $\Delta G_r^\circ < 0$, that is if $GB(R) < GB(M)$.

Proton transfer from H_3O^+ is an ideal reagent ion for organic trace gas analysis for two reasons. Firstly the natural components of air (N_2 , O_2 , etc) have proton affinities lower than that of water and most non-alkane VOCs have PA higher than that of water making H_3O^+ a selective VOC ionizing reagent.

Secondly the stability of the product ion, MH^+ , depends on its internal energy, which depends on the exothermicity of the proton transfer reaction. The exothermicity of the proton transfer reaction is given by the proton affinity (PA) of R minus the PA of M and the energy transferred in proton transfer reactions is often small enough ($< 100 \text{ kcal mol}^{-1}$) to avoid extensive fragmentation.

1.3.2 Proton Transfer Reaction Kinetics

Highly efficient reaction systems are required to gain the high ion signals required for sensitive trace gas detection. The reaction efficiency (RE) and enthalpy of the proton transfer reactions are positively related, and high RE (RE ~ 1) is observed for exothermic proton transfer reactions ($\Delta H^\circ \leq -20 \text{ kJ mol}^{-1}$) (Bouchoux et al. 1996) and a reaction occurs on nearly every collision between the reagent ion and the neutral.

SIFT-MS and Flowing afterglow studies have shown that not only are exothermic proton transfer processes almost always fast ($10^{-9} \text{ cm}^3 \text{ s}^{-1}$) but that the experimentally determined reaction rate coefficients agree well (~15%) with theoretical rate coefficients based on barrier-less collision and capture processes (Lindinger et al. 1998). Given, the agreement between experimentally and theoretically derived reaction rates the absence of an experimentally determined reaction rate is not an impediment to quantifying concentrations as theoretical values with similar error limits can be determined.

Several theoretical approaches to determining the rate of ion-molecule reactions have been proposed and are described briefly below.

1.3.2.1 Proton transfer reaction kinetics for non-polar reactants

The Langevin (Giousmouis-Stevenson) theory shows reasonable agreement with the experimental reaction rate coefficients for efficient ion-molecule reactions involving non-polar neutral molecules (Langevin 1905, Giousmouis & Stevenson 1958). This Langevin model describes the long-range interaction between a point charge (in this case H_3O^+) and a polarizable molecule (R). The Langevin theory determines the reaction rate coefficient as follows:

$$k_L = \sqrt{\frac{\pi \alpha e^2}{\mu \epsilon_0}} \quad (\text{Units: m}^3\text{s}^{-1}) \quad \text{Equation 1.6}$$

where, k_L is the Langevin reaction rate coefficient, α is the polarizability of the neutral, μ is the reduced mass of the colliding partners, e is the fundamental unit charge, and ϵ_0 is the permittivity of free space.

1.3.2.2 Proton transfer reaction kinetics for polar reactants

The Langevin (Giousmouis-Stevenson) underestimates the collision rate for polar compounds due to the greater attraction of ion-dipole forces. For an ion-molecule interaction a ‘locked dipole’ model assumes the dipole moment to be fixed in the most energetically favourable orientation in relation to the reagent ion resulting in an overestimation of the reaction rate, as less favourable orientations are neglected. Su and Bowers (Su & Bowers 1973a, Su & Bowers 1973b, Su & Bowers 1973c) developed Average-Dipole-Orientation (ADO) theory which incorporates a locking parameter, C, that is a measure of the average orientation of the neutral’s dipole moment. When C=1 a locked dipole model is in effect.

$$k_{ADO} = \sqrt{\frac{\pi\alpha e^2}{\mu\epsilon_0} + \frac{C\mu_D e}{\epsilon_0}} \sqrt{\frac{1}{2\pi\mu kT}} \quad \text{Equation 1.7}$$

where, μ_D is the dipole moment of the neutral. C is a function of the ratio $\mu_D/\alpha^{1/2}$. ADO underestimates the reaction rate as it neglects the dipole moment of the reagent ion and is considered an outdated approach.

Su and Chesnavich (1982) performed model trajectory simulations and parameterization of the results:

$$k_{cap}(T) = k_L \times K_{cap}(T)$$

$$K_{cap} = \begin{cases} \frac{(x + 0.5090)^2}{10.526} + 0.9754 & x \geq 2 \\ 0.4767x + 0.6200 & 2 \leq x \leq 3 \\ 0.5781x + 0.3165 & 3 \leq x \leq 35 \\ 0.6201x - 1.153 & 35 \leq x \leq 60 \\ 0.6347x - 2.029 & 60 \leq x \end{cases} \quad \text{Equation 1.8}$$

K_{cap} is a dipole locking effect parameter and is a function of μ_D and α . x is the inverse square root of the reduced temperature, $x = T_r^{-1/2}$. Parameterized Capture Rate theory shows very good agreement with experimentally determined reaction rate coefficients for efficient ion-polar molecule reactions.

Experimental values of the polarizability and the dipole moment are not available for all neutrals however Zhao and Zhang (2004) calculated these for 78 hydrocarbons and found

good agreement between experimental values and theory. The reaction rate coefficients for polar molecules determined by the Su and Chesnavich model underestimate the reaction rate at supra-thermal conditions whereas the Langevin rate coefficients for non-polar molecules are independent of temperature.

1.3.2.3 Proton transfer reaction kinetics at supra-thermal conditions

A large amount of the kinetic theory underlying our understanding of proton transfer reactions was generated in flow tube instruments that operate at thermal energies (room temperature). The drift tube of a PTR-MS is a supra-thermal system as ions are transported through the drift tube by an electric field, E ($V\ cm^{-1}$). The effective ion temperature can be determined from (McFarland et al. 1973):

$$T_{eff} = T + \frac{m_b v_d^2}{3k_B} \quad \text{Equation 1.9}$$

where, T is the drift tube temperature, m_b is the mass of the buffer gas (for PTR-MS the weighted mass of O_2 and N_2), and v_d is the ion drift velocity and k_B is the Boltzmann constant. At typical operating conditions ($E/N > 100\text{Td}$) in PTR-MS, effective ion temperatures are in excess of 1000°K . The uncertainty associated with the use of thermal reaction rate constants for PTR-MS data analysis significantly contributes to the overall uncertainty in quantification of concentrations. The calculation of concentrations from PTR-MS raw signals is discussed in Section 1.6.

To determine the energy dependence of reaction rate constants they are often described as a function of the mean relative kinetic energy between the reactants, KE_{CM} , and can be calculated by a modified version of the Wannier equation for KE_{ion} (McFarland et al 1973):

$$KE_{CM} = \frac{M}{m+M} \left(KE_{ion} - \frac{3}{2} k_B T \right) + \frac{3}{2} k_B T$$

$$KE_{ion} = \frac{3}{2} k_B T + \frac{m v_d^2}{2} + \frac{M_{ion} v_d^2}{2} \quad \text{Equation 1.10}$$

Where M is the mass of the neutral reactant, m is the mass of the ion and T is the drift tube temperature. Typically ion molecule reactions in PTR-MS occur at KE_{CM} values of 0.15 – 0.30. Increasing KE_{CM} leads to a decrease in proton transfer reaction rate, and increases the fragmentation of the product ions. Figure 1.1 from Lagg et al. (1994) illustrates the reaction

rate coefficient (Figure 1.1 (top)) and the product branching ratio (Figure 1.1(bottom)) of the reaction between H_3O^+ and acetone as a function of KE_{CM} , discussed below.

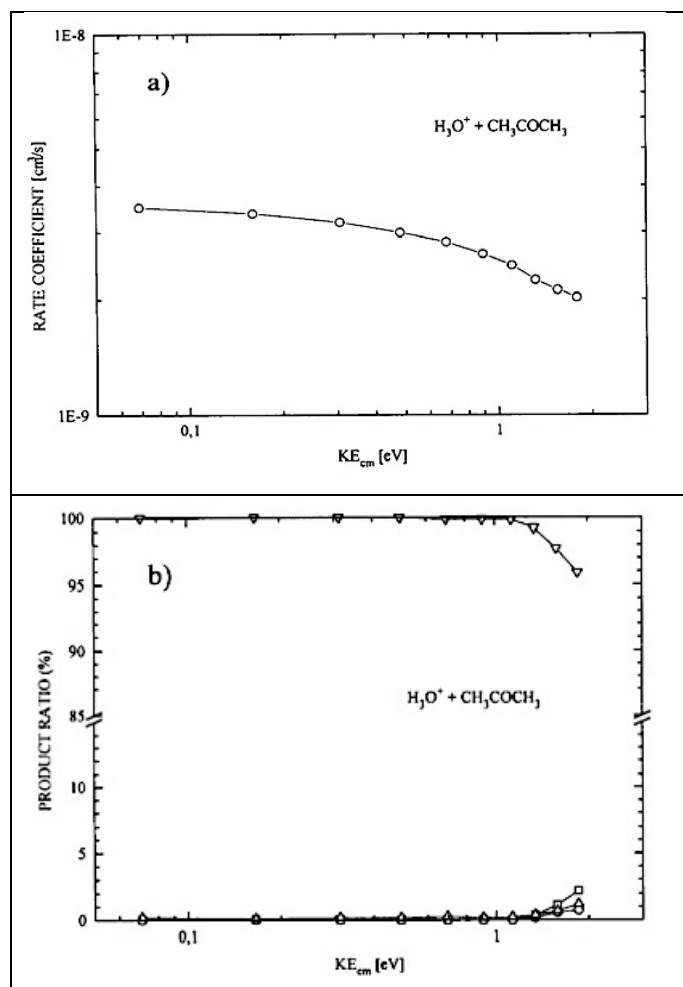


Figure 1.1: (top) Reaction rate coefficient versus mean centre of mass kinetic energy (KE_{CM}) for reaction between H_3O^+ and acetone. (Bottom) Product ion branching ratio (%) versus KE_{CM} for reactions between H_3O^+ and acetone. (Open circles) mass 41, (open squares) mass 31, (triangle) mass 43, (upside down triangle) mass 59. (Source: Lagg et al. (1994)).

1.4 Reaction processes occurring in PTR-MS

Proton transfer reactions are the primary chemical ionization reaction process occurring in PTR-MS, however, in practice there are several reaction processes occurring within the PTR-MS whose product ions can contribute to the observed mass spectra. These reaction processes include:

- dissociative and non-dissociative proton transfer from H_3O^+
- reactions with reagent ion water clusters ($\text{H}_3\text{O}^+ \cdot \text{H}_2\text{O}_n$) and
- reactions with other reagent ions (O_2^+ , NO^+) present as impurities in the reagent ion matrix.

1.4.1 Proton transfer from H_3O^+

As we have discussed, in PTR-MS H_3O^+ reagent ions undergo proton transfer reactions with the constituents in the sample gas that have a higher PA than the $\text{PA}(\text{H}_2\text{O})$ yielding a protonated molecular ion with m/z equal to the molecular mass plus one due to proton addition:



Proton transfer can be non-dissociative (as above) or dissociative:



In dissociative proton transfer the internal energy of the protonated molecular ion approaches the limits of dissociation denoted as $(\text{MH}^+)^*$. Dissociation occurs resulting in a fragment ion F^+ and a neutral fragment N.

The extent of fragmentation of the product ion, MH^+ , depends on its internal energy, which in part depends on the exothermicity of the proton transfer reaction. The exothermicity of the proton transfer reaction is given by the proton affinity (PA) of R minus the PA of M. If the energy transferred is sufficient uni-molecular dissociation occurs.

There is an electric field applied across the drift tube reactor that accelerates the ions to a higher kinetic energy (KE_{CM}) and ion-molecule collision energies are ~ 20 eV. Upon

collisions with other molecules, some of the kinetic energy is converted to internal energy and if sufficient, can result in dissociation of the product ion. Figure 1.1 (bottom panel) shows the product ion branching ratios from the reaction of H_3O^+ with acetone as a function of KE_{CM} . Consequently, increasing the voltage of the drift field will increase the frequency and extent of collision induced dissociation of MH^+ ions. The presence of fragment ions complicates the PTR-MS spectra, and PTR-MS instruments are typically operated at $E/N < 140 \text{ Td}$ (see sect 1.5.3.2) in order to minimize product ion fragmentation.

Generally, in the fragmentation of protonated parent ions in the PTR-MS it is expected that the even electron rule applies, wherein fragmentation of even-electron MH^+ usually involves elimination of an even electron neutral to form an even electron fragment ion (Harrison 1992). Also if the molecule contains functional group Y, the initial fragmentation often involves the loss of stable molecule HY from MH^+ . Following Field's rule, the tendency of the functional group Y to be eliminated as HY is inversely related to the proton affinity of HY, that is the higher the proton affinity the lower the tendency to be eliminated (Harrison 1992).

In the original papers describing PTR-MS it was assumed the energy deposited in the product ion upon proton transfer would not be sufficient to cause extensive fragmentation for many organic compounds (Hansel et al. 1995, Lindinger et al. 1998). Consequently, in measurements of the atmosphere the PTR-MS spectra were expected to be simple and predominantly comprised of protonated parent ions at m/z equivalent to their molecular weight plus one due to proton addition. In practice, fragmentation is commonly observed in PTR-MS studies. Table 1.1 provides a summary of the major reaction pathways of H_3O^+ with several organic compound classes observed in PTR-MS studies.

A more detailed description of fragmentation in PTR-MS will be presented in Chapters 2 and 3 of this thesis alongside a series of laboratory studies of PTR-MS spectra of a range of organic compound groups.

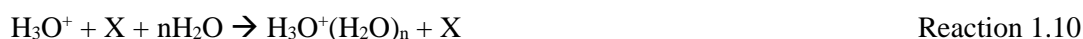
Table 1.1: A summary of the major proton transfer reaction pathways observed in PTR-MS studies of several organic compound classes.

	H₃O⁺ Reaction pathway	Refs
Alcohols	Alcohols > C ₂ undergo both dissociative and non-dissociative proton transfer. Fragmentation occurs via H ₂ O elimination	[1], [2], [3]
Carboxylic Acids	Proton transfer to carboxylic acids largely non-dissociative, with minor fragmentation via H ₂ O elimination	[1], [2],[3]
Aldehydes	Proton transfer to aldehydes largely non-dissociative, with minor fragmentation via H ₂ O elimination for aldehydes > C ₃	[1], [2],[3]
Ketones	Proton transfer to ketones almost exclusively non-dissociative	[1], [2],[3]
Alkanes	Proton transfer to alkanes < C ₅ endothermic. > C ₅ proton transfer reactions are slow with some minor fragmentation	[1], [2]
Alkenes	Proton transfer to alkenes C ₂ – C ₄ largely non dissociative, > C ₅ minor fragmentation.	[1], [2]
Monoterpenes	Monoterpenes undergo both dissociative and non-dissociative proton transfer.	[4]
Aromatics	Proton transfer to aromatics almost exclusively non-dissociative	[1], [3]

References: [1] Warneke et al. (2003), [2] Buhr et al. (2002), [3] Lindinger et al. (1998), [4] Tani et al. (Tani et al. 2003).

1.4.2 Association Reactions

In addition to proton transfer reactions, association reactions can occur between reagent ions (H₃O⁺) or analyte ions (M) and water molecules:



The presence of these hydrated products can potentially complicate the mass spectra. The major advantage of a drift tube reactor is the applied electric field, which suppresses formation of these hydrates.

The density of hydrated ions is also dependent upon and the water vapour content of the sampled air. Even in dry air, approximately 5% of the water vapour flow to the ion source reaches the drift tube resulting in the formation of water clusters (Warneke et al. 2001) . Over the course of a measurement, the ratio of H_3O^+ to $\text{H}_3\text{O}^+\cdot\text{H}_2\text{O}_n$ is not constant at a given set of operating conditions due to changes in the ion source intensity and variation in water vapour content of the sampled air.

The presence of hydrated hydronium ions can complicate the PTR-MS spectra as they may or may not undergo reactions with analyte molecules in the drift tube and the frequency of some reactions may vary as the proportion of H_3O^+ to $\text{H}_3\text{O}^+\cdot\text{H}_2\text{O}$ reagent ions present in the drift tube changes.

1.4.3 Reactions with hydrated hydronium ions

The hydrated reagent ions, $\text{H}_3\text{O}^+(\text{H}_2\text{O})_n$ can undergo direct proton transfer and ligand switching reactions with analyte molecules. In the case of the monohydrate ($n = 1$), direct proton transfer is exothermic and highly efficient if the proton affinity of the analyte molecule, $\text{PA}(\text{A})$, is $> \text{PA}(\text{H}_2\text{O}\cdot\text{H}_2\text{O}) = 194.6\text{kcal mol}^{-1}$ (813.4 kJ mol^{-1}) .



The weakly bound $\text{H}_2\text{O}(\text{H}_2\text{O})$ cluster is dissociated in exothermic reactions.

Ligand switching reactions occur when a hydrated reagent ion reacts with a neutral analyte, M:

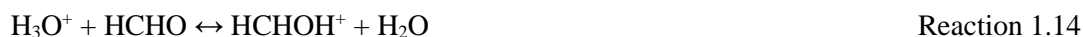


For some compounds, such as benzene, and toluene reaction with hydrated hydronium ions is not energetically favourable due to their low proton affinities and the PTR-MS sensitivity to these compounds is lower when a significant fraction of the H_3O^+ reagent ions in the drift tube are present as hydrated clusters (Warneke et al. 2001). Consequently, in measurements of the atmosphere the PTR-MS sensitivity to these compounds will be dependent on the ambient water vapour concentrations and may change with humidity over the course of a measurement.

The fraction of $\text{H}_3\text{O}^+(\text{H}_2\text{O})_n$ versus H_3O^+ reagent ions in the drift tube can also affect the product ion distributions of some compounds. For example, the PA of limonene is $\sim 209 \text{ kcal mol}^{-1}$, which is higher than the PA of H_2O by 44 kcal mol^{-1} and the energy transferred in reactions with H_3O^+ reagent ions is sufficient to cause dissociation of the protonated parent ion (Tani et al. 2004). Conversely, proton transfer from $\text{H}_3\text{O}^+(\text{H}_2\text{O})$ is only exothermic by $\sim 15 \text{ kcal mol}^{-1}$. In PTR-MS, when the fraction of $\text{H}_3\text{O}^+(\text{H}_2\text{O})$ in the reagent ion matrix was high, limonene was observed to undergo less fragmentation (Tani et al. 2004). Consequently, in measurements of the atmosphere, the PTR-MS sensitivity to a particular compound at a given product ion mass (m/z), may be dependent on the ambient water vapour concentrations and change over the course of a measurement.

1.4.4 Thermoneutral Reactions

If only a small difference exists between the proton affinity (PA) of H_2O and the PA of the analyte M, the protonated analyte (MH^+) may undergo a back reaction with the abundant water molecules in the drift tube. An important case of this is formaldehyde:



$\Delta H = \text{PA}(\text{H}_2\text{O}) - \text{PA}(\text{HCHO}) = 166.5 \text{ kcal mol}^{-1} - 171.6 \text{ kcal mol}^{-1} = -5.2 \text{ kcal mol}^{-1}$
(Hansel et al 1997).

Hansel et al (1997) demonstrated the energy dependence of the rates forward and back reactions of formaldehyde with H_3O^+ (Figure 1.2). At KE_{cm} values typical of PTR-MS ($> 0.20 \text{ eV}$) the rate of the endothermic back reaction increases considerably and the rate of the forward reaction decreases slightly. In measurements of ambient air the concentration of water molecules in the drift tube is considerably higher than the concentration of formaldehyde molecules and loss via back reaction is significant (Karl et al. 2003, Steinbacher et al. 2004, Inomata et al. 2008).

Consequently, the PTR-MS sensitivity to formaldehyde needs to be empirically calibrated and this calibration must be done over the range of ambient water vapour concentrations occurring over the measurement period.

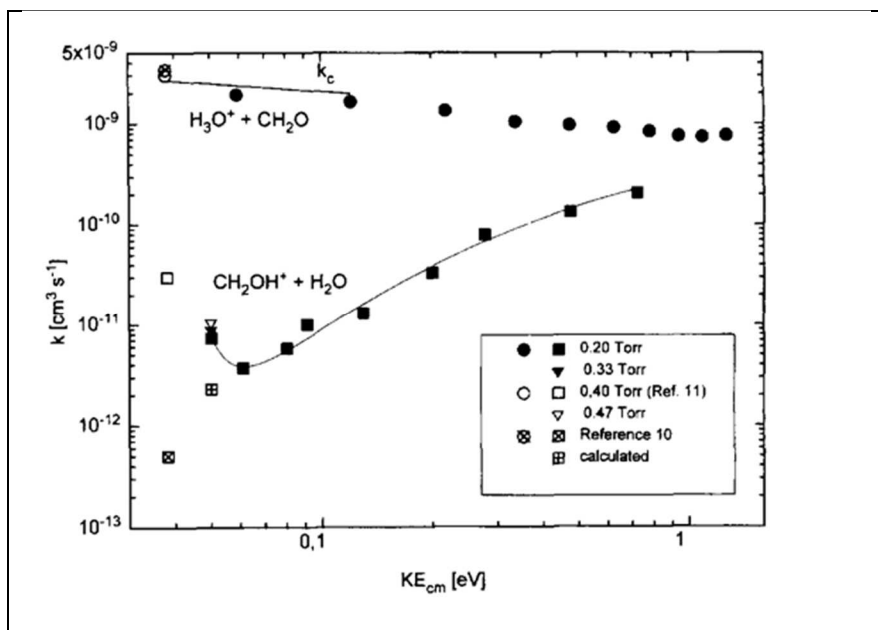


Figure 1.2: Energy dependence of the forward (circles) and back (squares) reactions of formaldehyde with H_3O^+ . Source: Hansel et al (1997).

1.4.5 Reactions of O_2^+ and NO^+ reagent ions in PTR-MS

The majority of PTRMS instruments are operated with H_3O^+ as the only primary chemical ionization reagent ion. The use of reagent ions other than H_3O^+ was proposed in the early development of PTR-MS (Lindinger et al. 1998) to enable the detection of some species that do not react with H_3O^+ or to differentiate isobaric compounds on the basis of differences in their ionization reactions or fragmentation products. The development and application of multiple reagent ion analysis in PTR-MS has only occurred more recently (Wyche et al. 2005, Blake et al. 2006, Norman et al. 2007, Inomata & Tanimoto 2008). These studies have demonstrated the production of a range of alternative reagent ions including O_2^+ , NO^+ , NH_4^+ and protonated VOC reagent ions (VOCH^+) with little to no modification of the PTR-MS instrument.

The instrument employed for the experimental work for this thesis was a commercially built PTR-MS (Ionicon Analytik GmbH, Innsbruck, Austria) modified with the addition of a switchable reagent ion source system to enable the use of NO^+ and O_2^+ reagent ions in addition to H_3O^+ . In these systems chemical ionization is not confined to proton transfer reactions. Thus, for the purposes of this thesis these instruments are referred to as switchable reagent ion mass spectrometers (SRI-MS).

In PTR-MS operating with H_3O^+ as the primary reagent ion, the ion source is tuned to produce reagent ions with a purity of > 95 % but there are always some O_2^+ and NO^+ reagent ions present in the reagent ion matrix as a result of air back-streaming into the ion source. These trace reagent ions also undergo chemical ionization reactions and the products of these reactions can complicate the PTR-MS mass spectra.

Regardless of whether they are being employed as alternative primary reagent ions or are present as impurities in the H_3O^+ reagent ion matrix, the reaction processes of O_2^+ and NO^+ with neutrals in the analyte gas are the same.

Oxygen cations will undergo efficient charge transfer reactions with all species that have a lower first ionization energy (IE) than O_2 (12.07eV) (Smith & Spanel 1996, Blake et al. 2006):



The IE of O_2 is higher than nearly all organic compounds (Lias 2015). The IE of most VOCs is in the range of 8 – 11 eV, and there is a significant amount of excess energy deposited in the product ion upon charge transfer from O_2^+ , which may result in dissociation of the excited nascent molecular ion to fragment ions (F^+). The strongest single bonds in organic molecules have strengths of about 4 eV ($1 \text{ eV} \approx 23 \text{ kcal mol}^{-1} \approx 96 \text{ kJ mol}^{-1}$) (McMurry 1992), and charge transfer from O_2^+ to VOCs frequently results in more extensive product ion fragmentation than that observed in proton transfer from H_3O^+ (Blake et al. 2006, Jordan et al. 2009).

In addition to dissociative and non-dissociative charge transfer, (Cappellin et al. 2014) recently reported an additional O_2^+ reaction pathway via oxygen insertion, in measurements of the PTR-Time of Flight mass spectra of ethene:



NO^+ can undergo charge transfer reactions with compounds with an $\text{IE} < \text{IE}(\text{NO})$, (9.26eV) (Smith & Spanel 1996, Blake et al. 2006). Due to its low ionization energy, NO^+ undergoes charge transfer with a limited number of VOCs, specifically the aromatics, alkenes $> \text{C}_4$, isoprene and monoterpenes. NO^+ will not undergo charge transfer reactions with most alkanes, ethene, propene, and oxygenated VOCs $< \text{C}_6$ due to their higher proton affinities.

The reaction chemistry of NO^+ and VOCs is not limited to charge transfer processes. If the heat of formation of the products is lower than the heat of formation of the reactants, NO^+ may undergo hydride ion transfer reactions.



NO^+ can also undergo hydroxide ion ($-\text{OH}$) transfer reactions yielding $(\text{M-OH})^+$ product ions, and alkoxide ion ($-\text{OR}$) transfer yielding $(\text{M-OR})^+$ ions. The NO^+ mass spectra will be discussed for each calibration gas in turn below.

NO^+ can also undergo association reactions with some compounds. The molecular product ion is detected as the molecular mass plus 30 due to NO^+ addition.



This process is similar to the hydration reactions observed in the H_3O^+ reagent ion regime. That being the case, it is expected that association reactions with NO^+ would be suppressed by the high collision energies resulting from the applied voltage electric field in the PTR-MS drift tube.

The reactions of NO^+ with VOCs usually proceeds via only one of these reaction processes resulting in only one or two product ions, but for some compounds two reaction processes can occur simultaneously (Blake et al 2006).

The reactions of O_2^+ and NO^+ in an SRI-MS with over 70 VOCs in certified gas standard mixtures is described in Chapter 3 of this thesis. Chapter 5 of this thesis describes a detailed investigation of the potential for mass interference in the detection of a species of interest (acetonitrile) due to the presence of product ions from reactions with the impurity reagent ions (O_2^+ , NO^+).

1.4.6 Summary of Reaction Processes in PTR-MS

As discussed in the preceding sections, in addition to proton transfer from H_3O^+ resulting in the formation of a single protonated parent ion for each compound present, there are multiple reaction processes that may be occurring within the PTR-MS, the products of which can complicate the interpretation of PTR-MS mass spectra. These include product ion fragmentation, association reactions, and reactions with trace reagent ions present as impurities in the reagent ion matrix. Furthermore, compounds may produce signals at several mass to charge (m/z) values due to the presence of naturally occurring isotopes in the compounds e.g. ^{13}C , ^{18}O , ^{15}N , etc.

In PTR-MS only the nominal mass of the product ions is determined and isobaric species cannot be distinguished. The mass (m) of product ions is expressed as a mass to charge (z) ratio (m/z) however the PTR-MS only generates singly charge product ions so $m/z = m$.

The aim of this discussion is to define the number of possible reaction pathways that could contribute to a given m/z in PTR-MS mass spectra. The reaction pathways and product ions that contribute to the signal at $m/z = x$ and the molecular weight (MW) of the analyte molecule (M) in relation to the m/z of the product ion are listed in Table 1.2.

Table 1.2: The number of reaction pathways and product ions that could contribute to the signal at $m/z = x$ and the molecular weight (MW) of the analyte molecule (M) in relation to the m/z of the product ion

	Reaction	Reaction pathway that yields $m/z = x$ from M.
1	$\text{H}_3\text{O}^+ + \text{M} \rightarrow \text{MH}^+ + \text{H}_2\text{O}$	Direct proton transfer where M has $\text{MW} = x - 1$.
2	$\text{H}_3\text{O}^+ + \text{M} \rightarrow \text{FH}^+ + \text{N} + \text{H}_2\text{O}$	Dissociative proton transfer where F has $\text{MW} = x - 1$, and M has $\text{MW} = \text{MW}(\text{F}) + \text{MW}(\text{N})$.
3	$\text{H}_3\text{O}^+ + \text{M}_i \rightarrow \text{M}_i\text{H}^+ + \text{H}_2\text{O}$	Direct proton transfer where M has $\text{MW} = x - 2$ and one carbon in M_i is a ^{13}C isotope <u>or</u> M has $\text{MW} = x - 3$ and one oxygen in M_i is ^{18}O .
4	$\text{H}_3\text{O}^+ + \text{M}_i \rightarrow \text{F}_i\text{H}^+ + \text{N} + \text{H}_2\text{O}$	Dissociative proton transfer where F_i has $\text{MW} = x - 2$ and one carbon in F_i is a ^{13}C isotope <u>or</u> F has $\text{MW} = x - 3$ and one oxygen in F_i is ^{18}O . M_i has $\text{MW} = \text{MW}(\text{F}_i) + \text{MW}(\text{N})$.
5	$\text{MH}^+ + \text{H}_2\text{O} \rightarrow \text{H}_3\text{O}^+ + \text{M}$	Reverse proton transfer reaction where H_3O^+ ions at m/z 19 are reproduced, and M is not detected.
7	$\text{H}_3\text{O}^+\bullet\text{H}_2\text{O} + \text{M} \rightarrow \text{MH}^+ + 2\text{H}_2\text{O}$	Direct proton transfer where M has $\text{MW} = x - 1$.
8	$\text{H}_3\text{O}^+\bullet\text{H}_2\text{O} + \text{M}_i \rightarrow \text{M}_i\text{H}^+ + 2\text{H}_2\text{O}$	Direct proton transfer where M has $\text{MW} = x - 2$ and one carbon in M_i is a ^{13}C isotope <u>or</u> M has $\text{MW} = x - 3$ and one oxygen in M_i is ^{18}O . M_i has $\text{MW} = \text{MW}(\text{F}_i) + \text{MW}(\text{N})$.
9	$\text{H}_3\text{O}^+\bullet\text{H}_2\text{O} + \text{M} \rightarrow \text{PH}^+\bullet\text{H}_2\text{O} + \text{H}_2\text{O}$	Non-dissociative ligand switching where M has $\text{MW} = x - 19$.
10	$\text{H}_3\text{O}^+\bullet\text{H}_2\text{O} + \text{A}_i \rightarrow \text{P}_i\text{H}^+\bullet\text{H}_2\text{O} + \text{H}_2\text{O}$	Non-dissociative ligand switching where M has $\text{MW} = x - 20$ and one carbon in M_i is a ^{13}C isotope <u>or</u> M has $\text{MW} = x - 3$ and one oxygen in M_i is ^{18}O .
11	$\text{H}_3\text{O}^+\bullet\text{H}_2\text{O} + \text{M} \rightarrow \text{MH}^+ + 2\text{H}_2\text{O}$	Dissociative ligand switching where M has $\text{MW} = x - 1$.
12	$\text{H}_3\text{O}^+\bullet\text{H}_2\text{O} + \text{M}_i \rightarrow \text{M}_i\text{H}^+ + 2\text{H}_2\text{O}$	Dissociative ligand switching where M has $\text{MW} = x - 2$ and one carbon in M_i is a ^{13}C isotope <u>or</u> M has $\text{MW} = x - 3$ and one oxygen in M_i is ^{18}O .

Table 1.2 (cont.)

	Reaction	Reaction pathway that yields $m/z = x$ from M.
13	$O_2^+ + M \rightarrow M^+ + O_2$	Charge transfer where M has MW = x.
14	$O_2^+ + M \rightarrow F^+ + N + O_2$	Dissociative charge transfer where F has MW = x and M has MW = MW(F) + MW(N).
15	$O_2^+ + M_i \rightarrow P_i^+ + O_2$	Charge transfer where M has MW = x - 1 and one carbon in M_i is a ^{13}C isotope <u>or</u> M has MW = x - 2 and one oxygen in M_i is ^{18}O .
17	$NO^+ + M \rightarrow M^+ + NO$	Charge transfer where M has MW = x.
18	$NO^+ + M \rightarrow F^+ + N + NO$	Dissociative charge transfer where F has MW = x and M has MW = MW(F) + MW(N).
19	$NO^+ + M_i \rightarrow P_i^+ + NO$	Charge transfer where M has MW = x - 1 and one carbon in M_i is a ^{13}C isotope <u>or</u> M has MW = x - 2 and one oxygen in M_i is ^{18}O .
20	$NO^+ + M_i \rightarrow F_i^+ + N + NO$	Dissociative charge transfer where F has MW = x - 1 and one carbon in F_i is a ^{13}C isotope <u>or</u> F has MW = x - 2 and one oxygen in F_i is ^{18}O . M_i has MW = MW(F_i) + MW(N).
21	$NO^+ + MH \rightarrow M^+ + NOH$	Hydride ion transfer where M has MW = x , and MW(MH) = x + 1.
22	$NO^+ + M_iH \rightarrow M_i^+ + NOH$	Hydride ion transfer where M has MW = x - 1, and MW(M_iH) = x + 1.
23	$NO^+ + M + N_2 \rightarrow (NO \bullet M^+)^+ + N_2$ $\rightarrow (NO)M^+ + N_2$	Association reactions where M has MW = x - 30.
24	$NO^+ + M_i + N_2 \rightarrow (NO \bullet M_i^+)^+ + N_2$ $\rightarrow (NO)M_i^+ + N_2$	Association reactions where M has MW = x - 31 and one carbon in M_i is a ^{13}C isotope <u>or</u> M has MW = x - 32 and one oxygen in M_i is ^{18}O .

In summary, 24 possible reaction pathways were identified that can occur in PTR-MS. Therefore, in the identification of a signal from PTR-MS, one must consider the contributions to a particular m/z ratio from:

- Product ions with molecular mass plus one due to proton addition.
- Product ions from fragmentation of molecular ions following proton transfer.
- Isotopologue product ions whose ion signals occur at the molecular mass plus one due to naturally occurring ^{13}C isotopes, the molecular mass plus two due to naturally occurring ^{18}O isotopes, etc.
- Product ions from reactions with O_2^+ , NO^+ and $\text{H}_3\text{O}^+(\text{H}_2\text{O})$.

Thus, while the PTR-MS spectra of VOCs are relatively simple in comparison to their respective electron impact mass spectra, their interpretation can still be potentially complex, as a result of the multiple reaction processes that may be occurring within the instrument.

In practice, the number and frequency of different reaction types occurring in the PTR-MS will be limited by:

1. the composition of the reagent ion matrix
2. the composition of the sample air matrix
3. the reaction rate of the individual reactions
4. the reaction conditions in the drift tube (pressure, electric field and temperature).

Factors 1, 3 and 4 above are in part controlled by the reaction conditions in the ion source and drift tube of the PTR-MS. In the proceeding sections the three key components of the PTR-MS: ions source, drift tube, ion detection system, and their operation will be described.

1.5 PTR-MS Instrumentation

Structurally a PTR-MS can be described as a stainless steel tube, composed of three regions, that terminates at the ion detection system (Figure 1.3). The sections of the tube in the order encountered by the ions are a hollow cathode ion source ($\sim 45 \text{ mm} \times \text{i.d. } 12 \text{ mm}$) (HC in Figure 1.3), a short source drift region ($\sim 12 \text{ mm} \times \text{i.d. } 12 \text{ mm}$) (IC1 in Figure 1.3), and a drift-tube reaction section (length $\sim 9.3 \text{ cm}$) from which ions exit to the quadrupole mass spectrometer. The drift tube operates with an electric field of $\sim 400 - 600 \text{ V}$ and pressure of \sim

2 mbar. The tube terminates with a lens system that focuses the ions into the detector, a quadrupole mass spectrometer.

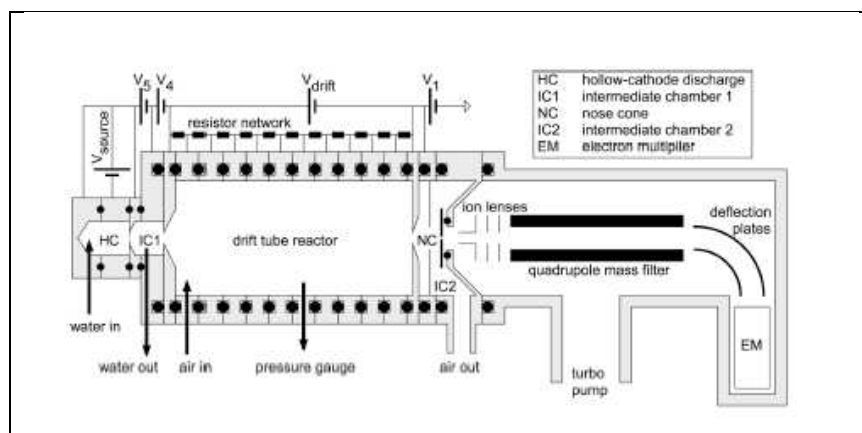


Figure 1.3: A schematic diagram of a PTR-MS. Note the hollow cathode ion source (HC), the source drift region (IC1), and the electrodes V_4 and V_5 . Source: de Gouw and Warneke (2007).

The function of these three key components is as follows. The hollow cathode ion source provides a pure concentrated source of protonated water molecules, (H_3O^+). The flow-drift tube is a reactor vessel in which protonated water molecules and neutral analytes mix and undergo proton transfer chemical ionization reactions under well-defined conditions. The quadrupole mass spectrometer measures a mass-to-charge ratio signal for both the reagent ions and the product ions of the chemical ionization reactions.

1.5.1 The Hollow Cathode Ion Source

Physical principles

The physical principles of conduction of electricity through gases are discussed in detail in Bleaney and Bleaney (1965) of which the following is a summary. An ideal gas contains no charged particles and can therefore not carry a current however in reality this is never the case. External actions (cosmic rays or UV light) release electrons ensuring there are always a few ions present. The density of ions at low electric fields is determined by the equilibrium between formation by external action and recombination within the gas. As the voltage is increased the ion velocity increases and the density of ions is reduced, as ions are increasingly lost at the electrodes. No ions are lost by recombination and the current becomes independent of the voltage and is solely determined by the formation of ions by external action. This regime is known as the voltage limited regime.

At atmospheric pressure both positive and negative ions in a gas have similar mobilities however, as the pressure is lowered the mobility of negative ions increases much more rapidly than that for positive ions. This is due to the fact that most of the negative ions at low pressure are electrons which have a negligible diameter relative to a charged molecule, therefore their mean free path (i.e. distance traveled between collisions) significantly increases with decreasing pressure.

As the pressure decreases (and the density decreases) the mean free path increases and there is more distance for the electron to gain energy from the applied electric field between collisions. The quantity of energy gained is determined by the applied electric field E and the mean free path, which is itself proportional to the pressure p , therefore the energy of the electrons is a function of E/p . Electrons with sufficient energy can undergo inelastic collisions resulting in the transfer of most of their energy to the colliding molecule resulting in excitation or ionization of the molecule. The mean free path of the larger positive ions increases less rapidly than that of electrons due to their larger cross sections.

Excitation occurs when an electron with sufficient energy collides with the molecule in its ground energy state and transfers some of its kinetic energy to the molecule raising it to an excited state. Generally the excited molecule rapidly decays and emits the excess energy as light. When the energy of the electrons is sufficient the molecule is raised to a sufficiently excited state such that an electron is completely removed leaving the molecule as a positively charged ion. The energy required to do this is known as the 'ionization energy' or 'ionization potential' of the molecule. Therefore if the electric field applied to a gas is high enough, ions are created in collisions between charged particles and neutral molecules and the density of ions in the gas is dramatically increased and is no longer limited by formation via external action. This process of ionization through electron impact increases the number of charged ions/electrons and when the value of E/p is large enough for it to occur the current of the gas is greatly increased. This regime is known as the current limited regime.

Hollow cathode discharges

The principles described above have been applied in the development of ion sources for mass spectrometry. Hollow cathode discharges belong to a group known as glow discharges and consist of a cell with an anode and a cathode filled with gas at low pressure (Mavrodineanu 1984). By applying a potential difference between the two electrodes the gas can be broken down into positive and negative ions and electrons. These positive ions are

accelerated and bombard the cathode wall emitting secondary electrons. The electrons arrive in the negative glow of the plasma and take part in excitation and ionization collisions with the source gas. The release of light energy in excitation collisions gives the plasma its characteristic glow, and the ionization collisions are the primary source of new ions in the body of gas.

Throughout the 1970s Lindinger and co-workers at the University of Innsbruck investigated the characteristics of steady-state, low pressure gas discharges in cylindrical hollow cathodes for the determination of ion-molecule reaction rate constants. Elementary processes (i.e. ion-molecule reactions) between ions and neutrals within the negative glow of a cylindrical hollow cathode proved to be intensive sources of secondary and tertiary ions including hydronium ions (H_3O^+) (Märk et al. 1972, Howorka et al. 1973, Lindinger 1973, Howorka et al. 1974). Thus, following initial electron impact ionization, as described in the preceding section, secondary ionization via ion-molecule reactions produces secondary and tertiary ions.

The plasma (as shown in Fig.1.4) in the hollow cathode exists as a glowing cylinder close to anode potential, along the axis of the cylindrical cathode known as the negative glow (Howorka et al. 1973). The plasma is produced by the highly energetic electrons emitted when positively charged ions collide with the cathode wall. The dark space between the negative glow and the cathode wall is the cathode fall region, referred to as KFR in Figure 1.4; an area with a potential drop of a few hundred electronvolts in which these electrons become highly energetic as they are accelerated back to the negative glow region (Howorka et al. 1974). Electrons typically gain several hundred electron volts of kinetic energy traversing the cathode fall region, which enables them to make several ionizing collisions within the negative glow region (Hansel et al. 1995).

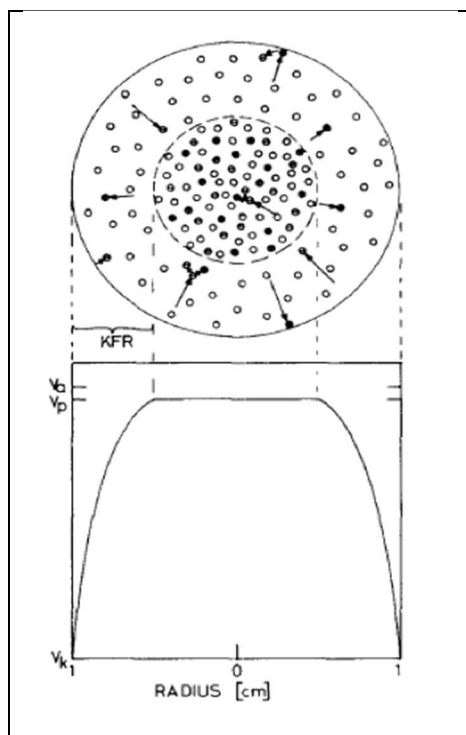


Figure 1.4: (top) Section through the plasma of a cylindrical hollow cathode illustrating the high density of the axial negative glow regions and the acceleration of electrons in the cathode fall region (KFR); (bottom) potential distribution. V_a anode potential; V_p negative glow potential; V_k cathode potential; Source: Howorka et al (1974).

In the PTR-MS a hollow cathode discharge is used to produce hydronium reagent ions (H_3O^+). In the hollow cathode these fast electrons collide with water vapour molecules to form the primary ions H_2O^+ , O^+ , H^+ , H_2^+ and OH^+ by electron impact (Hansel et al. 1995). These primary ions undergo ion-molecule reactions in the negative glow region to form secondary ion species (See Table 1.3). A high-density plasma of $10^{10} - 10^{11}$ molecules cm^{-3} (Hansel et al. 1995) is formed in axial region of negative glow due to the lower relative mobility of the heavy ions compared to the electrons. The plasma is self sustaining as some positive ions diffuse from the negative glow through the cathode fall and collide with the cathode wall producing further highly energised electrons (Howorka et al. 1974).

The source gas for the PTR-MS hollow cathode is a pure water vapour flow of around 6 - 8 STP $\text{cm}^{-3} \text{ min}^{-1}$ (Lindinger et al. 1998). Anode plates at either end of the cathode cylinder contain the negative glow. One anode plate has a small centrally located hole with a diameter of 1mm, through which the ions from the axis of the plasma are carried in the stream of water vapour via pumping action into a source drift region.

H_3O^+ is an ideal reagent ion as all potential primary ions generated in the hollow cathode discharge such as O^+ , H^+ , H_2^+ , OH^+ and H_2O^+ undergo fast reactions with water molecules to form H_3O^+ as detailed in Table 1.3 below. In the current PTR-MS system most of the ions emerging from the hollow cathode source are in the form of H_3O^+ with a small fraction of primary ions. Between the ion source and the drift tube there is a short source drift region in which the emerging hydronium ions become collisionally equilibrated and the primary ions undergo further reaction with water and form hydronium ions (Hansel et al. 1995).

Table 1.3: Reactions and reaction rates of primary ions generated from water vapour in the hollow cathode ion source.

Reactions of primary ions	Reaction rate constants k ($\text{cm}^3 \text{s}^{-1}$)
$\text{O}^+ + \text{H}_2\text{O} \rightarrow \text{H}_2\text{O}^+ + \text{O}$	2.6×10^{-9}
$\text{H}^+ + \text{H}_2\text{O} \rightarrow \text{H}_2\text{O}^+ + \text{H}$	8.2×10^{-9}
$\text{H}_2^+ + \text{H}_2\text{O} \rightarrow \text{H}_3\text{O}^+ + \text{H}$	3.4×10^{-9}
$\text{H}_2^+ + \text{H}_2\text{O} \rightarrow \text{H}_2\text{O}^+ + \text{H}_2$	3.7×10^{-9}
$\text{OH}^+ + \text{H}_2\text{O} \rightarrow \text{H}_3\text{O}^+ + \text{O}$	1.3×10^{-9}
$\text{OH}^+ + \text{H}_2\text{O} \rightarrow \text{H}_2\text{O}^+ + \text{OH}$	1.8×10^{-9}
$\text{H}_2\text{O}^+ + \text{H}_2\text{O} \rightarrow \text{H}_3\text{O}^+ + \text{OH}$	1.8×10^{-9}

Most of the neutral water vapour in the source drift region is pumped away via an outlet to a turbo molecular pump resulting in an ion source pressure of 2.5 - 3.5 mbar. Approximately 5% ($0.3 - 0.4 \text{ STP cm}^3 \text{ min}^{-1}$) of neutral water vapour from the ion source reaches the drift tube (Warneke et al. 2001).

From the source drift region, reagent ions are focused via an aperture in the centre of a venturi inlet located at the tube axis. Venturi inlets are designed to minimise back streaming of reactant gas into the source drift region (Dupeyrat et al. 1982) which would deplete the source gas and generate impurity ions such as O_2^+ and NO^+ which result from direct electron impact or from ionization by H_2O^+ . A voltage applied to the venturi inlet plate operates as an electrostatic lens to inject hydronium ions into the drift tube.

The ion source is tuned to produce reagent H_3O^+ ions with a purity of > 95 % but there are always some O_2^+ , NO^+ and other ions present in the reagent ion matrix as a result of air back-streaming into the ion source. As discussed in section 1.4.5, these impurity reagent ions can also undergo reactions with VOCs in the drift tube and their presence can complicate the mass spectra. The instrument manufacturer (Ionicon Analytik GmbH) suggests that < 2 % of O_2^+ and NO^+ impurities is optimal.

The performance of the ion source in terms of reagent ion signal intensity and purity, can be optimised by adjusting the voltages of the two elements (labelled as V_4 and V_5 in Figure 1.3) in the source drift region; adjusting the water vapour flow to the ion source; and adjusting a proportional valve that is located in a line between the ion source and the vacuum pump attached to the drift tube. Lower voltages increase the residence time of the primary ions in the source and source drift region allowing more collisions leading to the production of H_3O^+ ions. Closing the proportional valve also increases the residence time of ions in the source. Increasing the water vapour flow to the ion source increases the number of collisions between the primary ions and water molecules leading to production of H_3O^+ . The output of the source is also dependent on variables such as the water vapour flow, the humidity of the sample air and the cleanliness of the source.

Selected ion flow tube mass spectrometers (SIFT-MS) (Smith and Spanel (1996) employ an electron impact source combined with a quadrupole mass analyzer to pre-select reagent ions prior to injecting them into the reaction region. A major advantage of PTR-MS over SIFT-MS is the hollow cathode ion source produces the high intensity of hydronium ions ($10^6 - 10^7$ counts per second) required for sensitive trace gas detection (sub ppb) without the need for quadrupole pre-selection of reagent ions. A number of other alternative ion sources have been developed for use in PTR-MS instruments, and have been reviewed by Blake et al (2009) and Ellis and Mayhew (2014) and will not be discussed further here.

1.5.2 Switchable Reagent Ion Mass Spectrometry (SRI-MS)

As discussed in Section 1.4.5, the majority of PTRMS instruments are operated with H_3O^+ as the only primary chemical ionization reagent ion. Jordan et al (2009) reported the development of the first commercially available PTR-MS instrument with switchable reagent ion capability (SRI-MS) in which different reagent ion source gases and ion source tuning are used to selectively produce O_2^+ , NO^+ in addition to H_3O^+ in the hollow cathode ion source. In this modified PTR-MS system the source gas is switched from water vapour to UHP O_2 to produce the O_2^+ reagent ions via the pathways listed in Table 1.4. The source gas for the NO^+ reagent can be either air that has passed through an appropriate charcoal filter to remove VOCs, or a mixture of UHP N_2 and O_2 . NO^+ ions are produced via the reaction pathways listed in Table 1.4.

Table 1.4: Reaction pathways occurring in the hollow cathode ion source of the SRI-MS in the production of O_2^+ reagent ions and NO^+ reagent ions.

O_2^+ reagent ion production	
$e^- + O_2 \rightarrow O_2^+ + 2e^-$	
$e^- + O_2 \rightarrow O^+ + O + 2e^-$	
$O^+ + O_2 \rightarrow O_2^+ + O$	
NO^+ reagent ion production	
$e^- + O_2 \rightarrow O_2^+ + O + 2e^-$	$e^- + N_2 \rightarrow N_2^+ + 2e^-$
$e^- + O_2 \rightarrow O^+ + O + 2e^-$	$e^- + N_2 \rightarrow N^+ + N + 2e^-$
$O^+ + N_2 \rightarrow NO^+ + N$	
$N^+ + O_2 \rightarrow NO^+ + O$	

High intensity (10^9 cps) and high purity (> 95%) reagent ion signals are achieved for both O_2^+ and NO^+ reagent ions in the modified system (Jordan et al 2009). When the source gas is O_2 , the ion source can be operated at high voltages with the proportional valve open as only short residence times are required to produce the O_2^+ reagent ions. Conversely, the mechanism to produce NO^+ is more complex and requires longer residence times of ions in the source and source drift region. This is achieved by applying lower voltages and closing the proportional valve.

The usefulness of multiple reagent ions has been extensively studied with a technique similar to SRI-MS, selected ion flow tube mass spectrometry (SIFT-MS), since its inception in the mid-nineties. The reference spectra of hundreds of VOCs have since been determined for these instruments (Smith & Španěl 2005).

In comparison, the study of the performance and application of SRI-MS is still in its infancy. Much of the work to date has focused on the use of alternative reagent ions for the differentiation of isobaric compounds (Lindinger et al. 1998, Wyche et al. 2005, Blake et al. 2008, Inomata & Tanimoto 2008, Knighton et al. 2009, Karl et al. 2012, Lanza et al. 2013, Karl et al. 2014). Other studies have investigated the use of alternative reagent ions in order to detect compounds that do not react with H_3O^+ including the detection of ammonia with O_2^+ (Norman et al. 2007), the detection of alkanes with NO^+ (Inomata et al. 2013), and the use of Kr^+ and Xe^+ reagent ions for the detection of compounds other than VOCs including (CH_4 , CO , CO_2 , N_2O , NO_2 , SO_2) (Sulzer et al. 2012).

It is likely the problems inherent in interpreting PTR-MS mass spectra, using H_3O^+ , will also occur for the mass spectra determined using alternative reagent ions. Further work is required to determine the potential application of multiple reagent ion analysis with SRI-MS, and what, if any, additional information can be acquired through the use of reagent ions other than H_3O^+ in measurements of the atmosphere.

An extensive laboratory characterization of an SRI-MS instrument is provided in Chapter 3 of this thesis followed in Chapter 4, by an exploratory study of the application of SRI-MS to measurements of VOCs in an urban atmosphere.

1.5.3 The PTR-MS Drift Tube

The function of the drift tube in PTR-MS is as a reaction region in which compounds of interest are chemically ionized via ion-molecule reactions under well-defined conditions for mass spectrometric analysis. In drift tubes, the pressure and the electric field determine the reaction time, reaction frequency and the kinetic energy between the reactants (Shamlouei & Tabrizchi 2008). This is necessary for the application of chemical ionization to atmospheric concentration measurements as the ion signals detected by the quadrupole mass spectrometer can be related to the density of reactant and reagent ions in the drift tube. The following is an outline of the development of drift tube instruments.

1.5.3.1 Development of the PTR-MS drift tube

The precursor to the drift tube was the flowing afterglow technique conceived by E.E. Ferguson, F.C Fehensfeld and A.L. Schmeltekopf (Fehensfeld et al. 1966, Goldan et al. 1966), at the Environmental Science Services Administration (ESSA) Aeronomy Laboratory (now NOAA), for atmospheric ion chemistry studies at thermal energies for a wide variety of ion and neutral reactants.

The flowing afterglow system was further developed in the NOAA lab by incorporating a drift tube (McFarland et al. 1973). In a drift tube the ions can be accelerated from thermal energy to several electron volts ion kinetic energy by an applied electric field thus allowing measurement of the energy dependence of ion molecule reactions over an energy range not covered by flowing afterglow or ion-neutral beam techniques. Early flow tubes such as the flowing afterglow and flow-drift tube utilized immersed ion sources that suffered from a lack

of versatility in the ions that could be produced, and the presence of other unwanted reactive species, which lead to a complex ion-neutral matrix.

The selected ion flow tube (SIFT) apparatus was developed in the mid 1970s to overcome some of the limitations of immersed ion source flow tubes (Adams & Smith 1976). This technique employs a quadrupole mass spectrometer as a mass filter to select a single ion species (typically He^+ , N^+ , Ar^+) from the ion source and then injects it into a flowing neutral gas thus the ion source is separated from the flow tube. These ions then react with reactant gases added downstream.

In 1979 Lindinger et al. (1979) reported on the use of a flow-drift tube with a separated hollow cathode ion source for the measurement of the rate coefficients of reactions of He^+ with N_2 , CH_4 and O_2 within a drift tube (Lindinger et al. 1979). This pure source of reagent ions removed the requirement for a mass filter between the ion source and the reaction tube, and very closely resembles modern PTR-MS systems.

Up to this point, flow reactor techniques had been used to study gas-phase ion chemistry, in particular the reaction rate coefficients of ion-molecule reactions. The reaction rate coefficients were determined by introducing a flow of reactant gas into a flow/drift tube filled with chemical ionization reagent ions and measuring the ion signal with and without the addition of reactant gas, using the following equation (Lindinger et al. 1998):

$$k = \frac{F_{\text{He}}}{F_{\text{R}}} \frac{k_{\text{B}} T}{P} \frac{v_d}{L} \ln \left(\frac{i(A^+)_0}{i(A^+)_R} \right)$$

Equation 1.11

where, k is the reaction rate coefficient, F_{He} and F_{R} are the flow rates of the buffer gas (He) and reactant gas, R, respectively. k_{B} is the Boltzmann constant, T is the temperature and P is the buffer gas pressure. V_d is the ion velocity and L is the length of the reaction vessel. $i(A^+)_0$ and $i(A^+)_R$ are the primary ion signals for the reagent ion measured with and without the reactant gas respectively.

The potential of flow/drift tube systems as analytical instruments became increasingly apparent. In the early 1990s a selected ion flow drift tube apparatus was used to investigate the use of drift tubes as a method for trace gas analysis (Lagg et al. 1994) closely followed by the simultaneous development of two commercially available instruments for trace gas detection: the Selected Ion Flow Mass Tube Spectrometer (SIFT-MS) technique developed by

Smith and Spanel (1996) from the University of Keele, and the Proton Transfer Reaction Mass Spectrometer (PTR-MS) (Ionicon Analytik GmbH) by Lindinger and colleagues from the University of Innsbruck (Hansel et al. 1995, Lindinger et al. 1998). In this new application the previous technique for measuring rate coefficients was reversed and the known rate coefficients were used with the observed count rates to determine trace gas density.

There are several important differences between these two techniques. Firstly, PTR-MS employs a hollow cathode ion source from which reagent ions are directly injected in to the reactor, without the need for a mass filter to pre-select reagent ions. SIFT-MS employs a microwave discharge ion source with a quadrupole mass filter to preselect reagent ions prior to injection into the reactor (Smith & Spanel 1996).

Secondly, in PTR-MS chemical ionization reactions occur under the influence of the applied a high electric field of the drift tube reactor. In SIFT-MS, chemical ionization reactions occur at thermal energies and ions are transported along the reaction vessel in the buffer gas flow. Lastly, in PTR-MS the sample air itself acts as the buffer gas and the analyte molecules are not diluted in helium, as occurs in SIFT-MS, resulting in higher product ion currents and thus higher sensitivity in PTR-MS (Lindinger et al. 1998).

Thus, by employing chemical ionization via proton transfer from H_3O^+ , and the interfacing of a hollow cathode ion source with a drift tube in a mass spectrometer, PTR-MS has emerged as a potentially powerful tool specifically designed for the measurement of mixtures of organic compounds in the gas phase with conceivable applications in atmospheric, medical and food science.

1.5.3.2 PTR-MS Drift Tube Operating Parameters

Structurally the PTR-MS drift tube is a tube ~ 9.5cm long with an inner diameter of 5 cm composed of a series of electrically isolated stainless steel rings across which a voltage of 400 - 600V can be applied (Figure 1.3). Reactant gas is continuously pumped through the drift tube at a pressure of ~ 2 mbar and at a rate of ~ 15 – 25 mL min⁻¹. Reagent hydronium ions enter the drift tube from the ion source via a Venturi inlet in which there is a small hole on the downstream side of the ion source through which reactant gas is drawn into the drift tube. The swarm of reagent ions and reactant neutrals undergo multiple reactive and non-reactive collisions whilst traversing the drift tube.

The specific physical and chemical processes that occur in the drift tube are dependent on the operating parameters of voltage, pressure and temperature. Here we describe the variables used to specify conditions in the drift tube.

The drift velocity, v_d , that ions will move through a buffer gas, under the action of an electric field is determined by the ratio E/N :

$$v_d = \mu \times E \quad \text{Equation 1.12}$$

$$\mu_0 = \frac{p}{p_0} \times \frac{T_0}{T} \times \mu = \frac{N}{N_0} \times \mu \quad \text{Equation 1.13}$$

where μ is the ion mobility usually expressed as μ_0 , the reduced ion mobility for which a value of $2.8 \text{ cm}^2 \text{ V}^{-1} \text{ s}^{-1}$ is typically used (Dotan et al 1976, Viehland and Mason, 1995). E is the electric field strength (V cm^{-1}) and N (molecules cm^{-3}) is the buffer gas density and is presented in units of Townsend ($1 \text{ Townsend} = 1 \text{ Td} = 10^{17} \text{ V cm}^{-2}$):

$$E = V \text{ cm}^{-1} = V_{\text{Drift}}/L(\text{cm}) \quad \text{Equation 1.14}$$

where V_{Drift} is the applied drift tube voltage and L , is the drift tube length; N is determined from the ideal gas equation using the pressure in the drift tube (P_{drift}), temperature in the drift tube (T_{drift}), Avogadro's number (N_A) and the gas constant (R):

$$N(\text{molecules cm}^{-3}) = \frac{N_A T_0 P_{\text{drift}}}{RT_{\text{drift}}} \quad \text{Equation 1.15}$$

In Equation 1.12 μ is the ion mobility, generally reported as the reduced mobility μ_0 , for which a value of $2.8 \text{ cm}^2 \text{ V}^{-1} \text{ s}^{-1}$ is usually used (Dotan et al 1976, Viehland and Mason, 1995); p and p_0 are the drift tube pressure and standard pressure respectively. T and T_0 are the drift tube temperature and standard temperature respectively and N and N_0 are the number gas density and the number gas density at standard pressure and temperature respectively.

The ion drift velocity and the length of the drift tube (L) determine the reaction time, Δt :

$$\Delta t = \frac{L}{\mu_0 N_0} (E/N)^{-1} \quad \text{Equation 1.16}$$

In Section 1.3.2, it was demonstrated that reaction rates based on ion-molecule collision theory have a negative temperature dependency (Equations 1.7 – 1.8). At typical operating conditions ($E/N > 100 \text{ Td}$) effective ion temperatures are in excess of 1000°K and increasing E/N will result in a decrease in the ion-molecule reaction rates in the drift tube. Therefore, both reaction time and reaction rate are a function of E/N and the instrument response (product ion signal intensity) to a given compound will decrease with increasing E/N .

An investigation of the PTR-MS sensitivity to a series of prepared VOC standards as a function of E/N will be presented in Chapter 2 of this thesis.

As described in section 1.4.1, the electric field applied across the drift tube reactor accelerates the ions to a high kinetic energies (KE_{CM}) and ion-molecule collision energies are $\sim 20 \text{ eV}$. Upon collisions with other molecules, some of the kinetic energy is converted to internal energy and if sufficient, can result in dissociation of the product ion.

This has the advantage that the formation of reagent and product ion clusters ($\text{H}_3\text{O}^+(\text{H}_2\text{O})_n$ and $\text{MH}^+(\text{H}_2\text{O})_n$) is suppressed as they rapidly dissociate at E/N Values $> 100 \text{ Td}$. As can be seen in Figure 1.5, H_3O^+ detected at m/z 19 dominates the primary reagent ion signal in the normal PTR-MS operating range of E/N 110-130 Td, with some contribution from the monohydrate (m/z 37) and only minor contributions from the dihydrates (m/z 55).

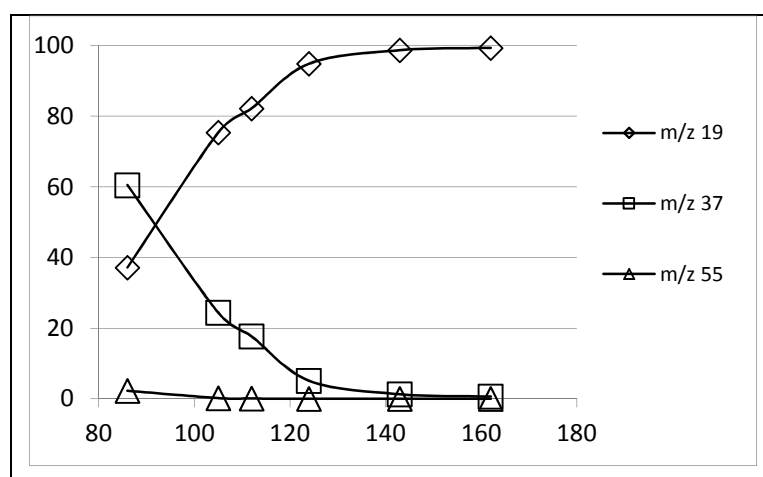


Figure 1.5 The relative abundance (%) of the H_3O^+ primary reagent ions detected at m/z 19, and the reagent ion clusters: $\text{H}_3\text{O}^+(\text{H}_2\text{O})$ (m/z 37) and $\text{H}_3\text{O}^+(\text{H}_2\text{O})_2$ (m/z 55) as a function of E/N (This study).

Warneke et al (2001) observed that the density of cluster ions in the drift tube is greater than that determined by the detection system due to collisional dissociation in the small chamber between the drift tube and the quadrupole (IC2 in Figure 1.3). These authors

measured ion mobilities in the drift tube across a range of E/N and found an individual ion in the drift tube will undergo numerous hydration and subsequent dissociation reactions with neutral water molecules so the ion's measured mobility is a weighted average of the mobilities of the different cluster ions. The weights are determined from the respective densities of H_3O^+ and $\text{H}_3\text{O}^+(\text{H}_2\text{O})_n$ ions.

As well as suppressing the formation of cluster ions, the additional collision energy imparted by the electric field in the drift tube in PTR-MS can enhance the degree of fragmentation of product ions. Ionization resulting predominantly in the formation of the molecular ion is ideal for molecular mass determination, structure elucidation and identification and quantification of compounds (Harrison 1992) and the operating conditions in the drift tube must be optimized to limit fragmentation of species of interest.

The key to identifying and quantifying VOCs in PTR-MS spectra is understanding the chemistry and fragmentation in the drift tube. An investigation of the PTR-MS spectra of a series of prepared VOC standards as a function of E/N will be presented in Chapter 2 of this thesis.

1.5.4 The PTR-MS Ion Detection System

Once they have traversed the drift tube, the sample air and ions enter the second intermediate chamber by a small orifice where most of the air is pumped away. A fraction of the ions are extracted through the nose cone into the ion detection system.

The ion detection system in a standard PTR-MS consists of a quadrupole mass spectrometer that separates the ions according to their mass/charge ratio (m/z) and a secondary electron multiplier (SEM) operated in count mode that detects the number of impinging ions at each m/z channel.

1.5.5 The Quadrupole Mass Spectrometer

The performance of quadrupole mass analyzers was thoroughly reviewed by Dawson (Dawson 1986) and need only be briefly described here. A quadrupole mass filter consists of four parallel rods which act as electrodes (See Figure 1.6). A voltage consisting of a dc component and an rf component is applied between adjacent rods, via electrical connections between opposite pairs of rods. One electrode pair has a positive dc potential with an rf

potential while the other pair have a negative dc potential and an rf potential. Oscillating the electric fields across the electrodes cause the ions to oscillate in x and y directions along the z axis (Figure 1.6). For a given set of *dc* and *rf* operating conditions only ions in a narrow band of *m/z* values will have stable ion trajectories and be transmitted to the detector. The width of the stable region determines the resolution of the mass spectrometer. By varying the *rf* and *dc* operating conditions the quadrupole mass filter can selectively transmit ions of desired *m/z* to the detector for counting.

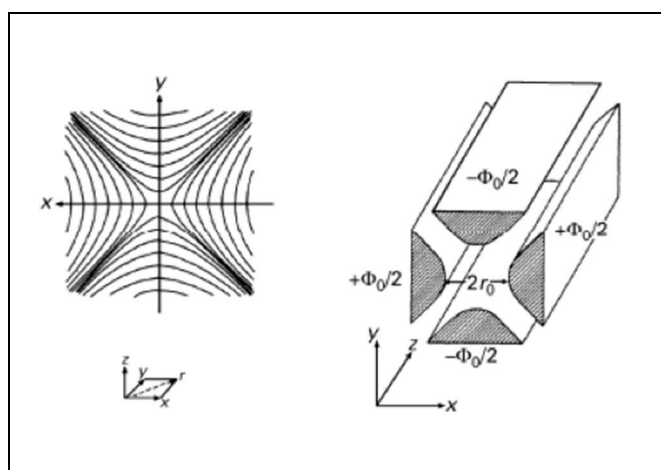


Figure 1.6: Cross section of the quadrupole mass filter indicating x, y and z axis. Source Dawson et al (1986).

The mass range (*m/z*) detectable by PTR-MS is roughly 1 - 500 amu however ions with *m/z* > 250 amu are not routinely measured. The resolution of the quadrupole mass filter is 1 amu. This low resolution is a significant limitation on the analysis of complex gas matrices as ions of the same nominal molecular mass cannot be distinguished from one another.

PTR-MS must be considered as a low selectivity tool for high time resolution measurements not a method for providing detailed speciated VOC measurements. Unequivocal VOC identification requires higher resolution mass spectrometers such as the recently developed PTR- time-of-flight mass spectrometers (Jordan et al. 2009), or co-located techniques with lower time resolutions that are capable of better speciation such as gas chromatography.

1.5.6 Secondary Electron Multiplier

Proton Transfer Reaction – (Quadrupole) Mass Spectrometers utilize commercially available Secondary Electron Multipliers (SEMs) in pulse counting mode to detect the count rate of ions exiting the quadrupole.

An SEM type commonly used in PTR-MS applications (Manufactured by Mascom GmbH) consists of a series of Cu-Be coated dynodes mounted sequentially on ceramic rods insulated from each other by ceramic spacers. A high voltage is applied to the dynode series in order that a single charged particle impinging on the first dynode triggers a cascade of electrons from the first and subsequent dynodes. The end result is a gain of $10^4 - 10^6$ charged particles impinging on the collector of the SEM as a countable electrical pulse per single charged particle impinging on the first dynode of the SEM.

Ideally there is a linear relationship between the ion current applied to the SEM and its output count rate. However, in addition to the design characteristics of different SEM types the factors that affect the count rate response of an SEM include the velocity and angle of incidence of ion impact on the first dynode; the release of electrons at each dynode; the acceleration of electrons between dynodes and the surface charge effects of the final dynode and collector (Richter et al. 2001). As the SEM ages, the gain achieved is reduced and a higher voltage is required to maintain yield and a linear SEM response.

The linear relationship between input ion current and output count rate has a y-intercept determined from the dark noise counts, that is, the output count rate registered by the counting electronics when there are no incident ions. In PTR-MS the count rate at mass 25 is used for this purpose as no known compounds are detected at this mass channel. Increasing SEM voltage increases dark noise counts (Fig. 1.7).

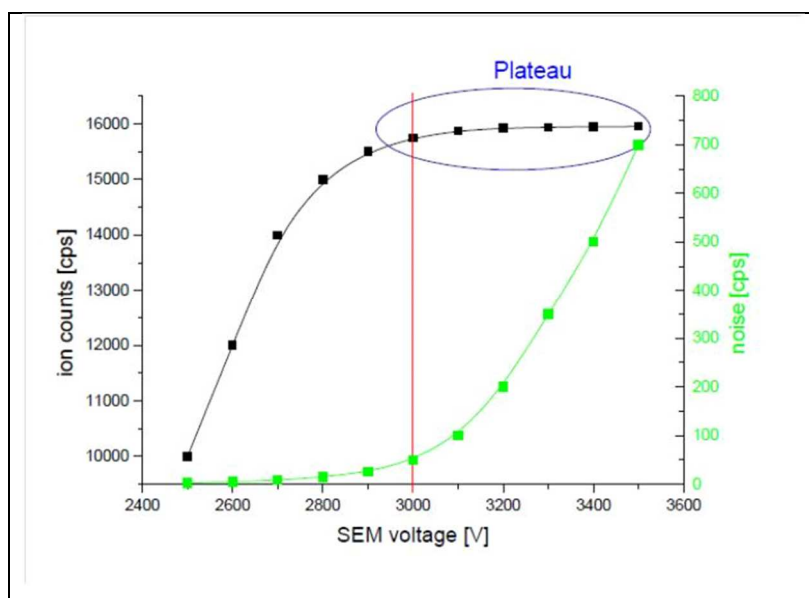


Figure 1.7: SEM voltage versus ion counts (left hand-y axis) and dark noise counts (right hand y-axis). Source: HS-PTR-MS Manual, Ionicon Analytik .

Figure 1.7. illustrates the ideal SEM voltage range to maintain high SEM sensitivity (gain) and linearity. The yield of an SEM is close to unity (measured count rate/true count rate) when the applied voltage is set to a value where the output counts are close to the plateau and the noise level is still low. This setting also maximizes the lifespan of the SEM.

The lifetime of the SEM is reduced by a high applied voltages and high ion currents impinging on the first dynode. Direct measurement of ion signals greater than 10^5 cps significantly shorten the lifetime of the SEM and the period that the SEM remains optimized. The intense ion signals of the primary H_3O^+ reagent ions overwhelm the ion detection system and shorten the lifetime of the SEM. In order to avoid this, the ion isotopes of the primary and impurity reagent ions are often measured rather than the primary ion signal: $\text{H}_3^{18}\text{O}^+$ detected at m/z 21 is multiplied by 500 to approximate the H_3O^+ signal at m/z 19; the ion isotopes of impurity reagent ions were measured rather than the primary ion signal: $\text{H}_3^{18}\text{O}^+(\text{H}_2\text{O})$ or $\text{H}_3\text{O}^+(\text{H}_2^{18}\text{O})$ is detected at m/z 39 was multiplied by 250 to approximate the $\text{H}_3\text{O}^+(\text{H}_2\text{O})$ signal; and, $^{18}\text{O}^{16}\text{O}^+$, detected at m/z 34 is multiplied by 250 to approximate the $^{16}\text{O}_2^+$ signal at m/z 32.

1.5.7 Digitising the signal

For an input pulse (ion or photon) the SEM produces a brief output peak in current, or voltage if a small resistance is placed in line. This peak is recorded as a single pulse by a pulse counter. It is important to understand over what range this process is linear i.e., one ion impact on the first dynode results in one pulse counted. In understanding this transformation, 4 factors need to be considered:

- the peak width (time)
- the peak height,
- the detection threshold of the pulse counter (how high a peak needs to be to be counted)
- the resolution time (dead time) of the counting system.

Pulse counting electronics require a non-zero dead time to handle a single pulse, and cannot in the meantime process another pulse (a coincident count). The dead time affects the counting of events from a random process as two events which occur in a time interval shorter than the dead time are considered as a single pulse and the measured count rate is lower than the true count rate.

If the counting system records N counts in time T (secs), and each recorded count is followed by a dead time of interval τ (secs), the true rate of ion counts, R (counts per second, cps) is given by (Lucke 1976):

$$R = N / (T - N\tau) \quad \text{Equation 1.17}$$

The ion signals routinely measured with PTR-MS range from very high (10^5 cps) down to a few cps. At high count rates the occurrence and undercounting of coincident counts occurring due to dead time results in non-linearity in the SEM response i.e the true count rate versus the measured count rate. For this and other reasons, the reagent ions are measured through their less abundant isotopes, thereby at lower count rates.

1.5.8 Mass Dependent Transmission

Ions of different m/z are not transmitted from the drift tube through the ion detection system with equal efficiency. This mass discrimination has three components that relate to the extraction of ions from the drift tube, the transmission of ions through the quadrupole and the deflection efficiency of the lenses of the SEM.

The extraction efficiency of ions from the drift tube into the quadrupole is m/z dependent as lighter ions are preferentially lost due to their greater tendency to scatter in the drift tube than heavier ions (Steinbacher et al. 2004).

Transmission of ions through the quadrupole itself is m/z dependent as heavier ions spend more time in the fringing fields thus reducing their transmission efficiency. Fringing field refers to the region at the edge of the stable ion path where the applied voltage is slightly less than that required for a stable path (Dawson 1975, Dawson 1976, Dawson 1986).

The SEM is attached perpendicular to the ion source-drift tube-quadrupole combination to prevent photons and fast neutral particles from triggering a pulse on the detector. An electrostatic field is used to transmit the ions through this perpendicular configuration from the quadrupole to the SEM. The deflection efficiency of this electrostatic field is also mass dependent (Steinbacher et al. 2004).

Given this, a mass discrimination factor must be determined for the PTR-MS in order to calculate concentrations from raw counts. This is commonly referred to as a transmission factor however it also includes the mass dependent extraction and deflection of ions.

Several authors have described methods to determine the mass discrimination of the PTR-MS (Ammann et al. 2004, Steinbacher et al. 2004). Steinbacher et al (2004) reported large differences between the experimentally determined transmission curve provided by the instrument manufacturer and their own experimentally derived mass discrimination curve, highlighting the need for recurring measurements of mass discrimination.

The relative transmission of an ion (MH^+) with a protonated mass x , can be determined by sampling a pure, non-fragmenting compound at high enough concentrations that the H_3O^+ reagent ion (m/z 19 amu) signal decreases by $\sim 10\%$. This is essentially continuous ion titration where the decline in the reagent ion signal at m/z 19 is assumed to be exclusively due to the formation of MH^+ and the ratio of the of the product ion (I_x) increase to the reagent ion (I_{19}) decrease differs from unity due to mass discrimination. By definition, if I_{19} and I_x are the signal intensities (cps) of the two masses ($m/z = x$ and $m/z = 19$) the transmission of mass x , M_x , is (Steinbacher et al. 2004):

$$T_{rel}(M_x) = \frac{-\Delta I_x}{\Delta I_{19}} \quad \text{Equation 1.18}$$

Note that $T_{rel}(M_x)$ is the transmission of the ion at $m/z = x$ relative to that of the H_3O^+ ion at m/z 19.

If this process is repeated for several non-fragmenting compounds across the working mass range an overall mass discrimination curve can be determined.

Figure 1.8 below shows the relative transmissions measured for a series of 9 compounds: methanol (m/z 33), acetonitrile (m/z 42), acetaldehyde (m/z 45), acetone (m/z 59), methyl ethyl ketone (m/z 73), benzene (m/z 79), toluene (m/z 93), m-xylene (m/z 107) and 1,3,5-trimethyl benzene. The transmission of each compound was normalized to the highest value, in this case acetone at m/z 59. The mass discrimination of the PTR-MS quadrupole to lighter ions ($< m/z$ 59) and heavier ions ($> m/z$ 59) such is evident.

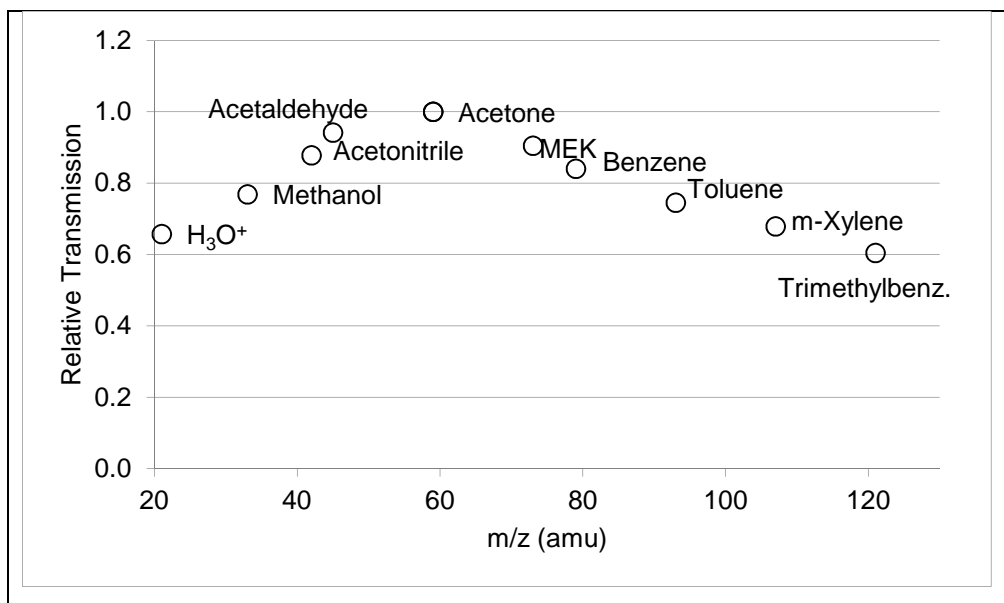


Figure 1.8: Relative transmissions measured using a series of pure liquid standards of methanol (m/z 33), acetonitrile (m/z 42), acetaldehyde (m/z 45), methyl ethyl ketone (m/z 73), toluene (m/z 93), m -xylene (m/z 107) and 1,3,5-trimethyl benzene. Values were normalized to the highest value (acetone).

1.6 PTR-MS Quantification

The well-defined conditions in the drift tube permit calculation of the analyte gas concentration from the raw ion signals, without the need for internal standards or calibration. The constant drift field and pressure define the reaction time and the proton transfer reaction rates are constant and known. The procedure for determining the volume mixing ratio of an analyte gas from the PTR-MS ion signals is described below.

For the proton transfer reaction:



The reaction proceeds with a reaction rate k , in units of $\text{cm}^3 \text{s}^{-1}$, determined via (Lindinger et al. 1979):

$$\frac{d[H_3O^+]}{dt} = -k[H_3O^+][A] \quad \text{Equation 1.19}$$

where the ratio $d[H_3O^+]/dt$ is the change in H_3O^+ density over time (t) due to proton transfer reactions with A, present at concentration $[A]$.

if $[A] \gg [H_3O^+] \gg [AH^+]$, and the density of H_3O^+ does not change significantly following the addition of A, the density of AH^+ can be determined (Hansel et al. 1995, Lindinger et al. 1998):

$$[AH^+] = [H_3O^+]_{t=0} (1 - e^{-k[A]\Delta t}) \approx [H_3O^+]_{t=0} [A] k \Delta t \quad \text{Equation 1.20}$$

As discussed, the ion drift velocity and the length of the drift tube determine the reaction time, Δt (de Gouw & Warneke 2007):

$$\Delta t = \frac{L}{\mu_0 N_0} (E/N)^{-1} \quad \text{Equation 1.21}$$

where μ_0 is the reduced ion mobility ($2.8 \text{ cm}^2 \text{ V}^{-1} \text{ s}^{-1}$) (Dotan et al 1976, Viehland and Mason, 1995); N_0 is the number gas density at standard temperature and pressure. E is the drift tube voltage in V cm^{-1} and N is the number gas density in the drift tube (molecules cm^{-3}).

If k and Δt are known, the absolute concentration of trace gas A can be determined from:

$$[A] = \frac{[AH^+]}{[H_3O^+]_{t=0}} \frac{1}{k \Delta t} \quad \text{Equation 1.22}$$

The PTR-MS data output is an ion signal in counts per second for each m/z in the chosen m/z range. The ratio of the ion signals $I(AH^+)$ and $I(H_3O^+)$ is linearly proportional to the concentration of AH^+ and H_3O^+ ions in the drift tube (de Gouw et al. 2003).

$$\frac{[AH^+]}{[H_3O^+]} = \frac{I(AH^+)}{I(H_3O^+)} = [A] k \Delta t \quad \text{Equation 1.23}$$

If k and Δt are known, and the measured ion signals are proportional to the ion concentration then the absolute concentration of trace gas A can be determined from the raw signals:

$$[A] = \frac{I(AH^+)}{I(H_3O^+)} \frac{1}{k \Delta t} \quad \text{Equation 1.24}$$

Due to the variability in H_3O^+ reagent ion count rates over time, it is common to express the product ion signals relative to 10^6 counts per second of H_3O^+ , referred to as normalized counts per second (ncps):

$$I(\text{AH}^+)(\text{ncps}) = \frac{I(\text{AH}^+)\text{cps}}{I(\text{H}_3\text{O}^+)\text{cps}/10^6} \quad \text{Equation 1.25}$$

As discussed in section 1.5.8, the transmission of ions through the ion detection system is mass dependent and a mass discrimination factor (T) must be experimentally determined for the reagent and product ions and incorporated into Equation 1.25:

$$[\text{A}] = \frac{I(\text{AH}^+)}{I(\text{H}_3\text{O}^+)} \times \frac{T(\text{AH}^+)}{T(\text{H}_3\text{O}^+)} \times \frac{1}{k\Delta t} \quad \text{Equation 1.26}$$

Equation 1.26 determines the number gas density (molecules cm^3) of [A] in the drift tube. However, the factor of interest is the concentration of the analyte [A] in the sample prior to entering the instrument. Rather than expressing the concentration of A, as a density, in measurements of the atmosphere volume mixing ratio is typically used.

In theory, the VMR of the analyte will be the same inside and outside of the instrument. In practice ~5% of the water vapour flow from the ion source enters the drift tube (Warneke et al. 2001). Thus for a typical water vapour flow of 6 - 8 STP $\text{cm}^3 \text{min}^{-1}$, 0.3 – 0.4 STP $\text{cm}^3 \text{min}^{-1}$ water vapour is added to the reactant gas flow of 15 – 20 STP $\text{cm}^3 \text{min}^{-1}$. The contribution of the water vapour flow is small, $\leq 3\%$, and can therefore be neglected in the following calculation of volume mixing ratio.

The VMR is expressed in units of parts per million by volume (ppmv), parts per billion (ppbv) or parts per trillion (pptv). To calculate [A] as a VMR, the number density of molecules in the drift tube (N) in molecules cm^{-3} is incorporated into equation 1.26.

For example, to calculate the VMR of [A] in ppbv:

$$[\text{A}] = \frac{I(\text{AH}^+)}{I(\text{H}_3\text{O}^+)} \times \frac{T(\text{AH}^+)}{T(\text{H}_3\text{O}^+)} \times \frac{1}{k\Delta t} \times \frac{10^9}{N} \quad \text{Equation 1.27}$$

As described in section 1.5.3 (Equation 1.15) the number gas density of molecules in the drift tube, N, is determined from the ideal gas equation using the pressure in the drift tube

(mbar) (P_{drift}), temperature ($^{\circ}\text{K}$) in the drift tube (T_{drift}), Avogadro's number and the gas constant.

From Equation 1.27 we can characterize the sensitivity (S) of the PTR-MS to analyte A as the signal of AH^+ ions at a VMR of 1 ppbv expressed as normalized counts per second per ppbv (ncps ppbv^{-1}):

$$S(A)(\text{ncps ppbv}^{-1}) = \frac{T(\text{AH}^+)}{T(\text{H}_3\text{O}^+)} \times \frac{1}{k\Delta t} \times \frac{10^9}{N} \quad \text{Equation 1.28}$$

Combining Equations 1.21 and 1.28 gives:

$$S(A)(\text{ncps ppbv}^{-1}) = 10^{-3} \frac{T(\text{AH}^+)}{T(\text{H}_3\text{O}^+)} \times \frac{kL}{\mu_0 N_0} \times \frac{N^2}{E} \quad \text{Equation 1.29}$$

Calculated sensitivities have been observed to differ from measured sensitivities by a factor of 2 (Warneke et al. 2003) as a result of uncertainties associated with calculated or thermally derived reaction rate coefficients with uncertainties of up to 50% and the ratio $T_{\text{AH}^+}/T_{\text{H}_3\text{O}^+}$ with an associated uncertainty up to 25% (Steinbacher et al 2004). Figure 1.7 presents calibrated versus calculated sensitivities for a number of different volatile organic compounds reported by Warneke et al (2003).

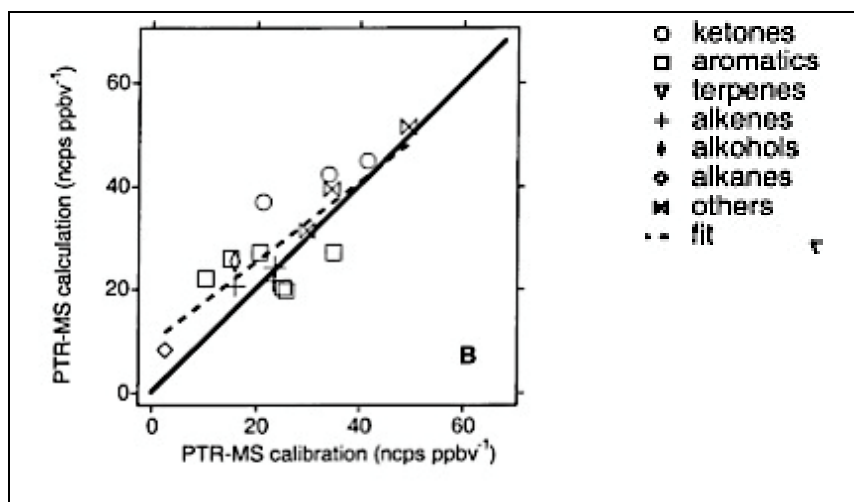


Figure 1.7: Calibrated versus calculated sensitivity for a number of different volatile organic compounds. Source: Warneke et al (2003).

It was shown in Equation 1.21 that reaction time, Δt , is dependent upon the drift tube operating parameters of voltage and pressure. Consequently the sensitivity of the PTR-MS to a given analyte will be dependent on the operating conditions in the drift tube as well as the reaction rate (k), and the mass dependent transmission factor (T). In Chapter 2 of this thesis,

the expected response of the PTR-MS to a series of compounds, based on equation 1.28, is compared to the observed response.

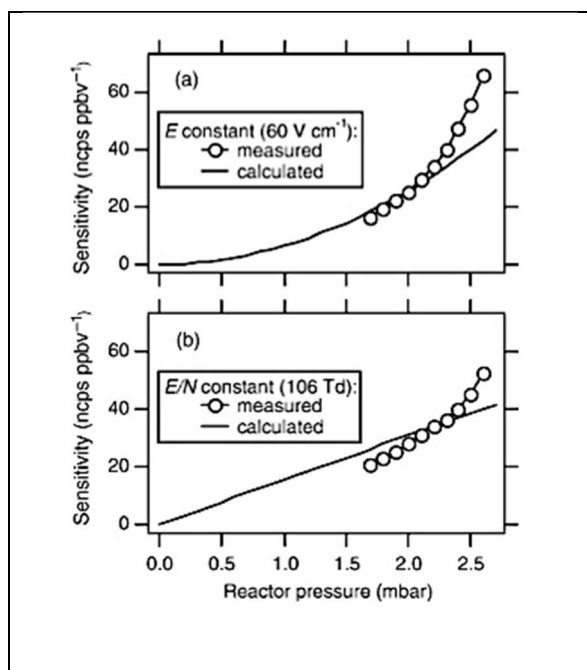


Figure 1.8: Measured (open circles) and calculated sensitivity of PTR-MS to acetonitrile as a function of pressure at (a) a constant voltage and (b) at a constant E/N . Source: (de Gouw et al. 2003).

Figure 1.8 illustrates the effect of drift tube parameters electric field and pressure on the instrument's sensitivity as it was measured, and as it is calculated according to equation 1.28. The sensitivity is dependent on the pressure squared as both the reaction time and frequency are linearly dependent on pressure. At a constant E/N , sensitivity is linearly dependent on pressure, as only the reaction frequency is varied Figure 1.8.

1.7. Empirical Calibration

Given the uncertainty associated with calculating the concentration from theoretical principles it is preferable to determine the sensitivity of a PTR-MS empirically by calibration using certified gas standards to determine the sensitivity in ncps/ppbv for all compounds of interest.

$$S = \frac{I(AH^+)_{norm}}{VMR}$$

Equation 1.30

$I(\text{AH}^+)_{\text{norm}}$ is the ion signal of the product ion normalized to a H_3O^+ signal of 10^6 cps and a volume mixing ratio (VMR) of 1 ppbv. Warneke et al (2003) compared the sensitivity determined from direct calibration with those calculated from theoretical principles and found reasonable agreement for most compounds, however some significant variations support direct calibration for improved accuracy (Figure 1.7). This is especially the case for compounds that undergo thermoneutral proton transfer reactions such as formaldehyde as the theoretical approach does not account for the reverse reaction outlined in section 1.4.4.

In practice, it is not feasible to calibrate for all compounds potentially measured by the PTR-MS and the theoretically derived sensitivities can be used in lieu of measured sensitivities. The determination of empirically derived, mass dependent sensitivity curves is described in Chapter 3 of this thesis, which allow the user to determine the sensitivity of the instrument at each m/z without the need for calculation via equation 1.29 or explicit calibration for each compound.

1.8 Summary

This chapter provides a systematic account of the principles and components of PTR-MS including switchable reagent ion PTR-MS (SRI-MS). Two important questions are highlighted in this examination of PTR-MS:

- *What information can be reliably determined about VOC identification from PTR-MS?*
- *What compounds can the PTR-MS unequivocally quantify in measurements of the atmosphere without interference?*

The key to identifying and quantifying VOCs in PTR-MS spectra is understanding the chemistry and fragmentation in the drift tube. This can be done by use of the use of:

- studies of VOCs standards
- manipulation of drift tube conditions
- use of different reagent ions
- comparison of atmospheric measurements by PTR-MS with other measurement techniques.

Answers to these two key questions are explored by the methods outlined above in the proceeding chapters of this thesis.

Chapter 2. PTR-MS spectra of some simple oxygenated VOCs

2.1 Introduction

The formation of ozone and secondary organic aerosol (SOA) in the troposphere results from the reactive chemistry of volatile organic compounds. In the atmosphere, these compounds undergo numerous chemical processes resulting in transformation to a range of oxidised organic products (Atkinson and Arey, 2003). The ability to measure oxygenated VOCs in the atmosphere is a major advantage of PTR-MS as the number and concentration of OVOCs present in the atmosphere has, until recently, been poorly understood. It is expected that individually OVOCs are present in small quantities but their combined contribution represents a significant fraction of total VOCs in the atmosphere (Goldstein & Galbally 2007). Therefore accurate and robust methods for measuring OVOCs in the atmosphere are critical to improve our understanding of the reactive organic carbon budget and the formation of ozone and SOA.

Proton transfer reaction mass spectrometry is a highly sensitive (sub ppb) chemical ionization mass spectrometry technique capable of quantifying VOCs, including many oxygenated VOCs, at high time resolutions (< 1 min) (Lindinger et al 1998). The major limitation of measurements of VOCs in the atmosphere by PTR-MS is that product ions of the same molecular weight cannot be distinguished. In measurements of the atmosphere, the PTR-MS is potentially responding to a large number of VOCs simultaneously, and the challenge is to determine what the PTR-MS is responding to when it gives a spectrum of counts at a range of m/z values during PTR-MS analysis of atmospheric VOCs.

Theory predicts the excess energy deposited in the product ions upon proton transfer from H_3O^+ is not sufficient to result in extensive product ion dissociation. Consequently, the H_3O^+ SRI-MS spectra of VOCs is expected to be simple and predominantly comprised of protonated parent ions detected at m/z equivalent to their molecular weight (MW) plus one due to proton addition.

In practice, there are numerous reaction processes occurring in the drift tube of the PTR-MS including:

- Simple proton transfer yielding product ions with molecular mass plus one due to proton addition:



- Dissociative proton transfer yielding product ions from fragmentation of molecular ions following proton transfer:



- Reactions with $H_3O^+(H_2O)$;



The chemical ionization conditions in a PTR-MS drift tube are controlled by the applied drift voltage and pressure described by the variable E/N , where E is the applied voltage ($V\text{ cm}^{-1}$) and N is the number gas density in the drift tube (molecules cm^{-3}). E/N is expressed in units of Townsend ($1\text{ Td} = 10^{-17}\text{ V cm}^2$). At high values of E/N , the additional collision energy imparted by the electric field in the drift tube in PTR-MS can enhance the degree of fragmentation, and suppress the formation of cluster ions $(H_3O^+(H_2O)_n)$ and $MH^+(H_2O)_n$. Consequently, the product ions and their respective branching ratios from reactions occurring in the PTR-MS are dependent on E/N .

Development of a comprehensive mass spectral database, determined for a range of drift tube operating conditions, is a key step in enabling accurate measurements of VOCs with PTR-MS. A study of the mass spectra patterns of prepared gaseous standards of 25 individual VOCs relevant to atmospheric chemistry was undertaken for this study. The compound classes studied included carboxylic acids, esters, alcohols, aldehydes and ketones. Additionally, four multifunctional compounds were investigated including hydroxyacetone, glyoxal and methyl glyoxal, and glycolic acid.

The density of MH^+ and FH^+ product ions in the drift tube is given by:

$$[AH^+] = [H_3O^+]_{t=0}(1 - e^{-k[A]\Delta t}) \approx [H_3O^+]_{t=0}[A]k\Delta t \quad \text{Equation 2.1}$$

Where, $[H_3O^+]$ is the number density of reagent ions in the drift tube, k is the reaction rate and Δt is the reaction time. The time it takes for an ion to traverse the drift tube, given by:

$$t = L \left(\mu_0 N_0 \frac{E}{N} \right)^{-1} \quad \text{Equation 2.2}$$

As discussed in Chapter 1, Sections 1.3 and 1.6, both the reaction rate k and Δt vary with E/N. Using theoretically derived reaction rates for each setting of E/N, it is possible to calculate the sensitivity of the PTR-MS to a given compound. In the present study observed changes in PTR-MS response with changes to E/N for each compound are compared with calculated values based on theoretically derived reaction rates and reaction times for each E/N setting.

The aim of this study was to identify the product ions in the mass spectra of some simple ($C_1 - C_6$) oxygenated VOCs (OVOCs) and 4 multifunctional OVOCs and to investigate the effect of different operating conditions on the PTR-MS sensitivity to each compound.

2.2 Methods

2.2.1 Preparation of gas standards

Pure gaseous standards were prepared for each compound by filling a 10 L tedlar bag with zero (VOC free) air. Zero air was generated by diverting ambient air through a zero furnace (350°C) with a Platinum wool catalyst that destroyed VOCs in the air. Then approximately 1 μ L per litre of bag volume of pure liquid standard was added to the bag using a clean glass syringe. The liquid standards used in this study had stated purities of 98 – 99% purity and were obtained from Sigma Aldrich (Milwaukee USA). It is important to state that while the concentration of the compound in the standards prepared in this way were fixed for each experiment, the absolute concentration of the compound was unknown.

The combined background of the instrument plus the tedlar bag was determined from measurements of an additional bag containing only zero air. All ion signals from the measurements of prepared gaseous standards referred to in this study are background corrected.

2.2.2 PTRMS instrument set-up

The instrument employed in this work is a commercially built PTR-MS, a more detailed description of which is contained in Chapter 1. And only the details of the PTR-MS operation relevant to this study will be described below.

Before starting these experiments the hollow cathode ion source was detuned by adjusting the ion source voltages in order to reduce the H_3O^+ ion signal to ~ 1 million counts per second to prevent saturation of the SEM.

The inlet of the PTR-MS was set to sample the standards at a flow 100 mL min^{-1} . The drift tube and inlet were maintained at a constant temperature of 60°C for all experiments. The mass spectra of each compound was determined over a range of drift tube settings with E/N of 86 – 170 Td, by adjusting the applied drift tube voltage between 450 V - 600 V and the drift tube pressure between 2.1 – 2.3 mbar (Table 2.1).

Table 2.1: The PTR-MS drift tube operating voltages and pressures for each E/N setting employed in this study.

	E/N (Td)					
	90	110	130	140	150	170
Drift Tube Pressure (mbar)	2.1	2.1	2.1	2.1	2.1	2.0
Drift Tube Voltage (V)	380	475	540	580	620	700

The PTR-MS quadrupole continuously scanned 181 masses between 21 and 200 amu. The dwell time for a single mass measurement was 1 second, generating a full mass scan approximately every 3 minutes. To preserve the lifetime of the SEM, the ion isotopes of the reagent ion were measured rather than the primary ion signal: $\text{H}_3^{18}\text{O}^+$ detected at m/z 21 was multiplied by 500 to approximate the H_3O^+ signal at m/z 19.

The product ion signals were normalized to 10^6 cps of H_3O^+ ions and is expressed as normalized counts per second (ncps).

The observed reagent and product ion signals are dependent on the concentration of ionized VOCs and H_3O^+ ions in the drift tube and the mass discrimination factor, T. Ions of different m/z are not transmitted from the drift tube through the ion detection system with equal efficiency. Given this, a mass discrimination factor was determined for the PTR-MS using the procedure described in Chapter 1 in order to calculate actual product ion signals from raw counts. The product ion signals reported in this Chapter are transmission corrected normalized counts per second.

2.3 Results & Discussion

The product ions and branching ratios observed in the PTR-MS spectra of a series of oxygenated VOCs as a function of E/N are presented in Tables 2.2 – 2.5. The PTR-MS spectra of the multifunctional compounds are for several reasons, complex and their PTR-MS spectra are discussed separately in section 2.3.5.

In addition to the product ion distributions as a function of E/N for each compound, the present study also investigated the PTR-MS sensitivity to each compound as a function of E/N. While the absolute concentration of the analyte compound in the prepared gaseous standards was unknown, a fixed input concentration was supplied to the PTR-MS throughout the measurement of each compound. For each setting of E/N the total ion signal (TIS) of a compound was calculated from the sum of the transmission corrected ion signals of the product ion peaks observed in the mass spectra. This represents the total ion signal for a fixed input concentration of analyte gas.

Table 2.2 presents calculated reaction rates for E/N of 110 Td and 170 Td PTR-MS for a selection of the compounds employed in this study that were determined from the values reported by Cappellin et al. (2012). When E/N is changed from 110 Td to 170 Td the reaction rates for all compounds decline by ~ 10 - 15%. In addition, when E/N was changed from 110 Td to 170 Td the reaction time decreased by 36% from (127 μs to 106 μs). Therefore, due to changes in the reaction rate and reaction time, the PTR-MS sensitivity to a given compound will decrease with increasing E/N.

Table 2.2: The calculated change in PTR-MS sensitivity (ΔS_{calc}) to the VOCs employed in this study expected when E/N is changed from 110 Td to 170 Td. ΔS_{calc} was calculated from theoretically derived reaction rates (k_{calc}) based on the values reported by Cappellin et al (2012); and the change in the observed total ion signal this study (ΔTIS %) when E/N was changed from 110 Td to 170 Td. Values for acetone were also included for comparison.

E/N (Td)	110 k_{calc} ($10^{-9} \text{ cm}^3 \text{ s}^{-1}$)	170 k_{calc} ($10^{-9} \text{ cm}^3 \text{ s}^{-1}$)	ΔS_{calc} %	ΔTIS %
Formaldehyde	2.79	2.52	- 42%	- 75%
Acetaldehyde	3.19	2.87	- 41%	- 57%
Acetone	3.38	3.02	- 42%	- 60%
MEK	3.34	2.89	- 44%	- 88%
MIBK	-	-	-	- 72%
Methanol	2.26	1.98	- 43%	- 33%
Ethanol	2.23	1.87	- 45%	- 93%
1-Propanol	2.17	1.88	- 44%	- 64%
2-Propanol	2.29	1.95	- 45%	- 67%
1-Butanol	2.22	1.99	- 42%	- 89%
2-Butanol	2.45	2.03	- 43%	- 71%
2-Methyl-2-Propanol				- 87%
Formic Acid	2.03	1.72	- 45%	- 85%
Acetic Acid	2.29	1.92	- 46%	- 72%
Propionic Acid	-	-	-	- 68%
Methyl Formate	2.44	2.06	- 45%	- 81%
Ethyl Formate	-	-	-	- 84%
Propyl Formate	-	-	-	- 66%
Butyl Formate	-	-	-	- 86%
Methyl Acetate	4.40	3.94	- 46%	- 78%
Ethyl Acetate	2.46	2.06	- 42%	- 71%
Hydroxyacetone	-	-	-	- 96%

The PTR-MS sensitivity at 110 Td and 170 Td was calculated for a selection the compounds employed in this study via:

$$S_{calc}(ncps\ ppbv^{-1}) = \frac{kL}{\mu_0 N_0} \frac{N^2}{E} \quad \text{Equation 2.3}$$

Where, L is the length of the drift tube, μ_0 is the reduced ion mobility ($2.8\text{ cm}^2\text{ V}^{-1}\text{ s}^{-1}$) and N_0 is the number density of air at standard pressure.

Where, L is the length of the drift tube, μ_0 is the reduced ion mobility ($2.8\text{ cm}^2\text{ V}^{-1}\text{ s}^{-1}$) and N_0 is the number density of air at standard pressure. S_{calc} was determined for each value of E/N employed in this study, $S_{calc}(E/N = X)$. The change in the calculated sensitivities (ΔS_{calc}) when E/N was increased from 110 Td was calculated via:

$$\Delta S_{calc} = 1 - (S_{calc}(E/N = X) / (S_{calc}(E/N = 110))) \quad \text{Equation 2.4}$$

The calculated change in PTR-MS sensitivity (ΔS_{calc}) to the VOCs employed in this study expected when E/N was changed from 110 Td to 170 Td are presented in Table 2.1 as a percentage ($\Delta S_{calc}\%$). When E/N was changed from 110 to 170 Td the calculated changes in sensitivity were similar (41 - 46%) for all of the compounds employed in this study.

In this study, the PTR-MS response to a given compound was described by the total ion signal (TIS) observed for that compound. TIS is the sum of the transmission corrected ion signals at each m/z scanned, in normalized counts per second. The concentration of the compound in the prepared standards were fixed for each experiment, however the absolute concentration of the compound was unknown. Thus, in this study TIS represents the PTR-MS response to a fixed concentration of analyte and any changes in TIS with E/N are due to a change in reaction conditions.

Given the similarity in ΔS_{calc} when E/N was changed from 110 Td to 170 Td for each compound listed in Table 2.2, one would expect the changes in the observed PTR-MS total ion signal, for fixed input concentrations of each compound would also be similar. The change in the observed total ion signal in this study (ΔTIS) when E/N was increased from 110 Td was calculated via:

$$\Delta\text{TIS} = 1 - (\text{TIS}(E/N = X) / \text{TIS}(E/N = 110)) \quad \text{Equation 2.5}$$

The observed change in TIS for each of the VOCs employed in this study when E/N was changed from 110 Td to 170 Td are presented in Table 2.1 as a percentage (Δ TIS %). When E/N was changed from 110 to 170 Td the observed changes in TIS for the compounds employed in this study ranged from 33 – 96%.

The product ion distributions and PTR-MS sensitivity as a function of E/N are discussed in turn for each compound below.

2.3.1 Aldehydes and ketones

The PTR-MS spectra of five C₁ – C₆ carbonyl compounds were determined in this study. The product ions and branching ratios (as a percentage of the total ion signal (%TIS)) from reactions of H₃O⁺ with the aldehydes and ketones employed in this study are listed in Table 2.2.

Formaldehyde (CH₂O): Across the range of E/N settings, the protonated parent ion was the dominant ion observed in the PTR-MS spectra of formaldehyde in this study. In addition to the protonated parent ion at m/z 31, there were 8 other peaks observed in the PTR-MS spectra of the formaldehyde standard employed in this study. In solution, formaldehyde readily forms diols and oligomers (Utterback et al. 1984) and the peaks at m/z 49, 51, 77, 88, and 95 were attributed to the presence of these formaldehyde derivatives in the prepared formaldehyde standard. Product ions that correspond with protonated methanol (m/z 33) and protonated acetaldehyde (m/z 45) were also observed in the mass spectra of the formaldehyde standard, and these peaks were likely due to impurities present in the formaldehyde standard or fragment ions of the formaldehyde derivatives.

When we subtract the ion signals attributed to the products of the formaldehyde derivatives, the protonated formaldehyde ion abundance is 92 - 99 % across all E/N with a trace peak at m/z 29 (Table 2.3). These results were consistent with previously reported mass spectra from the reactions of H₃O⁺ with formaldehyde (Hansel et al. 1997, Spanel et al. 1997, Inomata et al. 2008).

The proton affinity of formaldehyde is only slightly greater than the proton affinity of water and back reaction occurs. The reaction rates of the forward reaction is several orders of magnitude higher than the reverse reaction, however the concentration of water molecules in the PTR-MS drift tube is considerably higher than the concentration of formaldehyde and loss via back reaction is significant (Hansel et al. 1997, Inomata et al. 2008). Consequently, the

PTR-MS sensitivity to formaldehyde is low and the response is humidity dependent. Furthermore, the rate of the back reaction has a significant positive energy dependence and the rate of the forward reaction has a slight negative energy dependence (Hansel et al. 1997). Consequently, the PTR-MS sensitivity to formaldehyde has been observed to decrease with increasing E/N (Wisthaler et al. 2006, Inomata et al. 2008, Wisthaler et al. 2008).

In the present study, for a fixed input concentration of formaldehyde the total ion signal (TIS) decreased by 75% when E/N was changed from 110 Td to 170 Td (Table 2.3, Fig. 2.1). This was much greater than the expected decline of 42% based on calculated sensitivities at E/N of 110 and 170 Td, and also greater than the 57% decline in TIS observed for acetaldehyde over the same E/N range.

The decrease in sensitivity occurs due to back reaction of formaldehyde with H_2O to reproduce H_3O^+ . At high E/N (> 130 Td) the back reaction was a significant loss term. Consequently, the decline in PTR-MS response to formaldehyde with increasing E/N was due to a combination of an increase in loss via the back reaction and a coincident decrease in both the rate of the forward reaction and the reaction time.

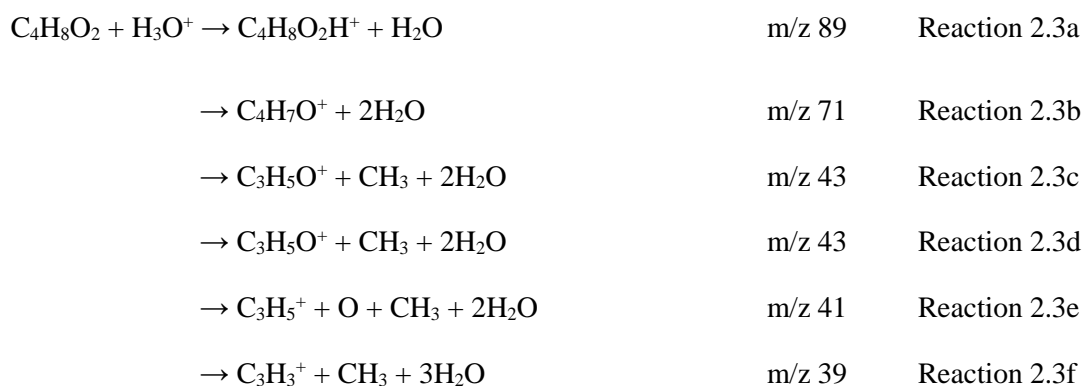
Table 2.3: The aldehydes and ketones employed in this study, their formula, molecular weight (MW) and proton affinity (PA), and their product ions and branching ratios from the PTR-MS mass spectra determined across a range of E/N.

Compound	MW	PA (kJ mol ⁻¹)	Product ion formula	m/z	PTR-MS E/N (Td)					
					90	110	130	140	150	170
					Product ion branching ratios (%)					
Formaldehyde CH ₂ O	30	712.9	HCO ⁺	29	<1	<1	<1	2	<1	<1
			CH ₂ OH ⁺	31	99	96	97	92	95	98
Acetaldehyde C ₂ H ₄ O	44	768.5	C ₃ H ₃ ⁺	39		<1	<1	1	3	8
			C ₂ HO ⁺ /C ₃ H ₅ ⁺	41		<1	2	3	3	3
			C ₂ H ₃ O ⁺	43		4	4	3	3	3
			C ₂ H ₅ O ⁺	45		86	88	88	87	82
			¹³ CCH ₅ O ⁺	46		1	1	1	1	1
			C ₂ H ₅ O ⁺ •H ₂ O	63		1	>1	>1	>1	>1
			C ₃ H ₃ O ₂ ⁺ /C ₄ H ₇ O ⁺	71		7	4	3	2	2
			C ₄ H ₉ O ₂ ⁺ / (C ₂ H ₄ O) ₂ H ⁺	89		1	<1	<1	<1	<1
Acetone C ₃ H ₆ O	58	812	C ₃ H ₇ O ⁺	59		98	98	98	97	96
			¹³ CC ₃ H ₇ O ⁺	60		2	2	2	2	2
Methyl ethyl ketone C ₄ H ₈ O	72	827.3	C ₂ H ₅ O ⁺	45		<1	<1	<1	<1	3
			C ₄ H ₅ ⁺	53		<1	<1	<1	<1	1
			C ₄ H ₇ ⁺ /C ₃ H ₃ O ⁺	55		<1	<1	3	5	8
			C ₄ H ₉ O ⁺	73		97	96	93	88	75
			¹³ CC ₃ H ₉ O ⁺	74		2	2	3	3	3
Methyl isobutyl ketone C ₆ H ₁₂ O	100	>PA(H ₂ O)	C ₃ H ₃ ⁺	39		<1	<1	3	8	19
			C ₃ H ₅ ⁺	41		<1	3	7	8	6
			C ₂ H ₃ O ⁺ / C ₃ H ₇ ⁺	43		<1	<1	1	1	2
			C ₂ H ₅ O ⁺	45		<1	5	8	10	12
			C ₄ H ₇ ⁺	55		<1	3	5	5	3
			C ₄ H ₉ ⁺ /C ₃ H ₅ O ⁺	57		5	26	25	22	13
			C ₃ H ₆ O ⁺	58		<1	2	2	2	1
			C ₃ H ₇ O ⁺	59		<1	7	12	19	26
			C ₅ H ₇ O ⁺	83		<1	2	2	2	1
			C ₆ H ₁₃ O ⁺	101		87	48	28	17	9
			¹³ CC ₅ H ₁₃ O ⁺	102		3	2	1	<1	<1

Acetaldehyde: The PA of acetaldehyde is > PA (H₂O) and the protonated parent ion (m/z 45) was the dominant product ion observed across the E/N range studied (110 -170 Td) (Table 2.3). The additional product ion signal at m/z 63 was attributed to either the acetaldehyde monohydrate or the acetaldehyde gem diol.

The product ion signals observed at m/z 43, 41, and 39 may be formed via fragmentation of acetaldehyde. With the exception of H₂ elimination from protonated acetaldehyde to form C₂H₃O⁺ (m/z 43), it is difficult to determine a logical reaction mechanism to explain the product ion signals at m/z 39 (C₃H₃⁺) and 41 (C₃H₅⁺/ C₂HO⁺).

Alternatively, the product ion signal at m/z 89 observed in the acetaldehyde mass spectra was likely due to the presence of the acetaldehyde dimer (C₄H₈O₂H⁺) that formed in the standard solution and may undergo protonation and subsequent fragmentation in the PTR-MS via:



The presence of the acetaldehyde dimer was a by-product of the acetaldehyde standard preparation process. Blake et al (2006) also observed product ion signals at m/z 39, 41, and 43, in addition to m/z 45 in the mass spectra of an acetaldehyde standard also prepared from an evaporated standard solution. The absence of product ion signals at m/z 89 and 71 in that study was likely due to the high E/N settings employed (E/N = 165 Td).

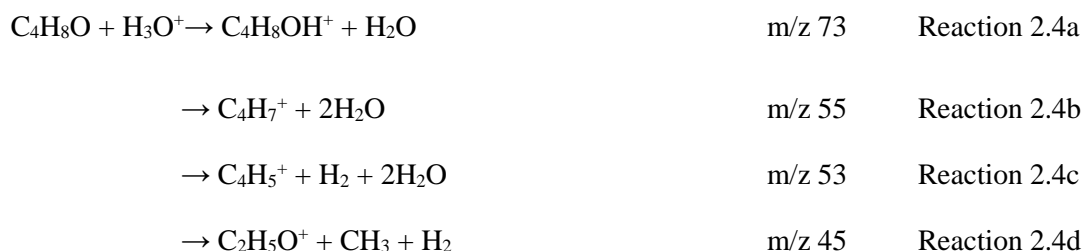
The total ion signal of acetaldehyde declined by 57% when E/N was changed from 110 to 170 Td, which was close to the value of ΔS_{calc} of 41% (Table 2.2).

In the atmosphere, acetaldehyde is likely to be present largely in its monomer form and it was concluded that in measurements of the atmosphere with PTR-MS the product ion signal of acetaldehyde would largely occur at m/z 45 across a range of E/N settings.

Acetone: The PTR-MS mass spectra of acetone observed in this study was very simple and was consistent with previous PTR-MS studies (Warneke et al. 2003, Blake et al. 2006). The protonated parent ion and its ^{13}C isotopologue accounted for > 98% of the total ion signal (Table 2.3). The PTR-MS sensitivity to acetone did not decline significantly as E/N was increased from 110 to 170 Td (Table 2.1, Fig. 2.1). We concluded that in measurements of the atmosphere with PTR-MS acetone would be sensitively detected at m/z 59 across a range of PTR-MS operating conditions.

Methyl ethyl ketone (MEK): The PTR-MS spectra of methyl ethyl ketone was dominated by the protonated parent ion detected at m/z 73 across the range of E/N settings studied (110 – 170 Td) (Table 2.3).

In addition to the protonated parent ion, four fragment ions were observed at m/z 55, 53, and 45 that were presumably formed via:



The protonated parent ion was the only product observed in a SIFT-MS studies the reactions of H_3O^+ with MEK (Spanel et al. 1997). The PA of MEK is only 136 kJ mol^{-1} higher than the PA(H_2O), and the energy available upon protonation is not sufficient to rupture bonds in these molecules. The fragmentation of these compounds occurs in the PTR-MS but not in the SIFT-MS due to the higher collision energies in the PTR-MS drift tube.

In this study, for a fixed input concentration of MEK the total ion signal (TIS) decreased 88% when E/N was changed from 110 Td to 170 Td (Table 2.1 and Figure 2.1). This is much greater than the 46% decline observed for acetone. This suggests there was an additional process occurring that affected the PTR-MS sensitivity to MEK.

The PA of MEK is \gg PA(H_2O) and it is unlikely significant loss via back reaction with H_2O is responsible for the apparent loss in sensitivity with E/N. It is possible that at higher E/N MEK undergoes fragmentation to an ion that was not measured such as CH_y^+ ions where $y = 1 - 5$ whose m/z would be less than m/z 17 and were not included in the mass range

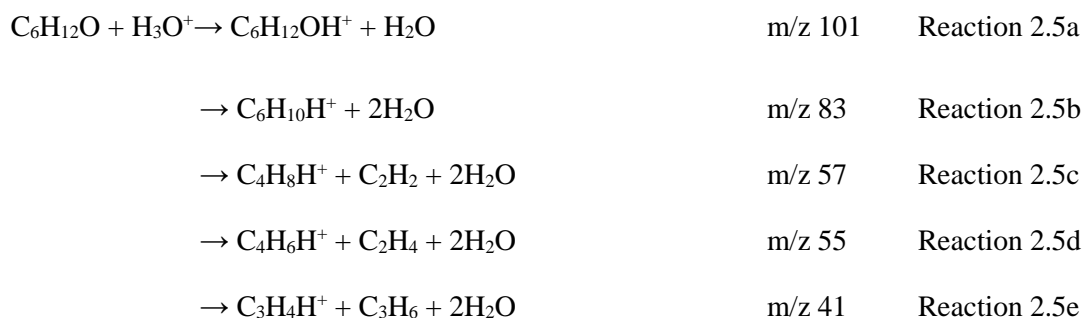
scanned (21 – 200 amu). The other possibility is fragmentation to H_3O^+ (m/z 19) the ion signal of which would be obscured by the PTR-MS H_3O^+ reagent ion signals and is therefore unmeasurable.

The results observed in the present study are contrary to those reported by Cappellin et al. (2012) who compared the known concentration of MEK in a certified gas standard ($[\text{MEK}]_{\text{std}}$) versus the theoretically predicted concentration of MEK. The theoretically predicted concentration of MEK was calculated from the reagent and product ion signals observed in the PTR-time of Flight (ToF) spectra of the MEK standard and the calculated reaction rate coefficients ($[\text{MEK}]_{\text{calc}}$). The ratio of $[\text{MEK}]_{\text{std}}/[\text{MEK}]_{\text{calc}}$ was $1 \pm 10\%$ at E/N of 120 and 150 Td and at relative humidity of 0, 50 and 100%. These results suggest the change in PTR-ToF sensitivity to MEK with E/N can be fully explained by the change in reaction rate and reaction time and no additional processes were occurring that affected the PTR-ToF sensitivity to MEK. The reasons behind the discrepancy between the study by Cappellin et al (2012) and the present study are unclear.

Overall, in measurements of the atmosphere with PTR-MS, MEK can be detected at m/z 73 however the PTR-MS sensitivity to MEK considerably declined at $E/N > 110$ Td.

Methyl isobutyl ketone (MIBK): The PA of MIBK is unknown, however the presence of the protonated molecular ion in the mass spectra of MIBK reported here indicates the $\text{PA}(\text{MIBK}) > \text{PA}(\text{H}_2\text{O})$. No known mass spectra for MIBK exist for PTR-MS or SIFT-MS. The abundance of protonated MIBK declined from 87 % of the TIS at E/N 110 Td to only 48% of TIS at E/N 130 Td due to extensive fragmentation.

In addition to the protonated parent ion, there were eight other significant peaks in the PTR-MS spectra of methyl isobutyl ketone formed via two competing fragmentation processes (Table 2.3). Firstly, elimination of H_2O and subsequent breakdown of the carbon skeleton:





Secondly, MIBK may fragment via elimination of a hydrocarbon fragment to yield an oxygenated product ion:

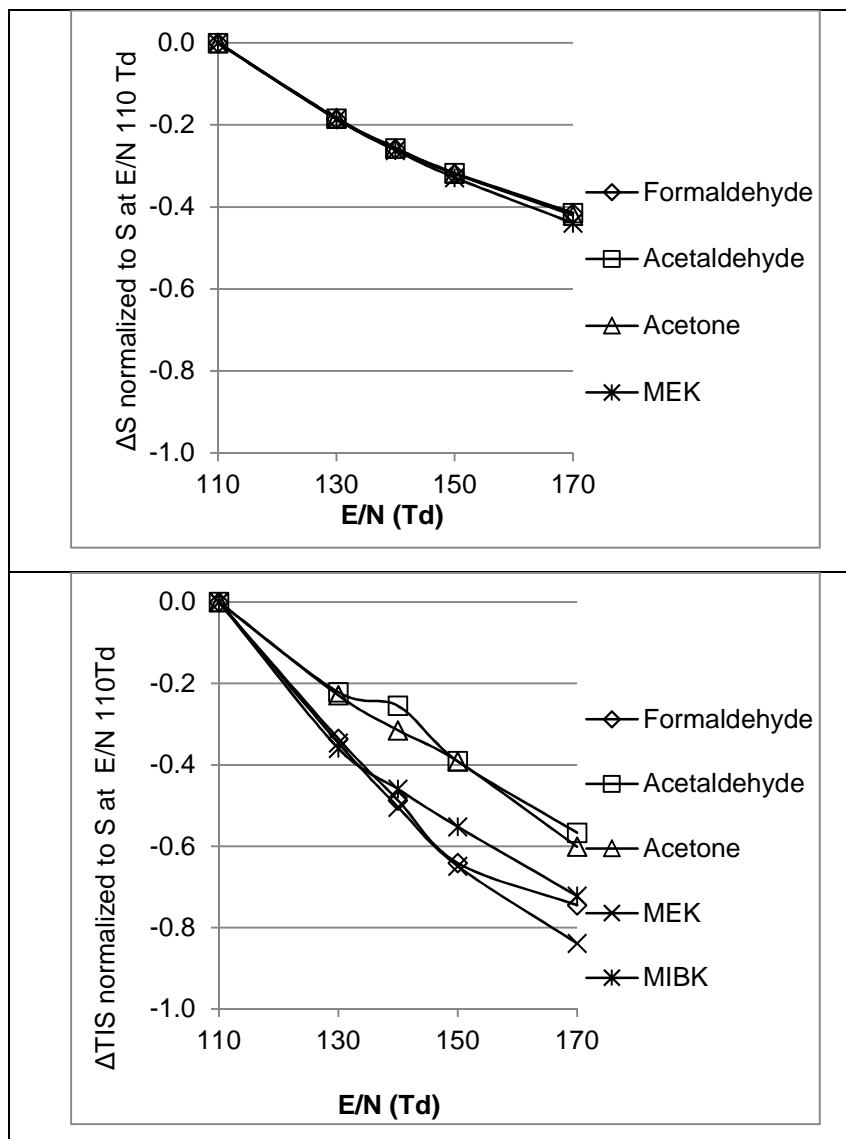


Figure 2.1: (Top panel) The change in calculated PTR-MS sensitivity (ΔS) to carbonyl based on theoretically derived reaction rates, when E/N is changed from 110Td to 170Td. Note: reaction rates for MIBK were not available. (Bottom panel) The change in observed total ion signal (ΔTIS) for fixed input concentrations of carbonyl compounds when E/N is changed from 110Td to 170Td.

In measurements of the atmosphere with PTR-MS, MIBK can be sensitively detected at its protonated parent ion mass (m/z 101) when operating at low E/N values, however, at E/N > 130 Td protonated MIBK undergoes extensive fragmentation and the sensitivity to MIBK at m/z 101 significantly declines.

In summary, acetaldehyde and acetone can be sensitively detected at their respective protonated parent ion signals across a range of E/N settings. Conversely, formaldehyde, MEK and MIBK showed an increasing tendency to fragment with increasing E/N. At E/N of 110 Td and higher, the PTR-MS sensitivity to formaldehyde and MEK, was significantly reduced due to significant loss via back reaction to H_3O^+ in the case of formaldehyde, and possible fragmentation to unmeasured product ions in the case of MEK.

2.3.2 Alcohols

The PTR-MS spectra of seven $C_1 - C_4$ alcohols were determined in this study. The product ions and branching ratios (as a percentage of the total ion signal (%TIS)) from reactions of H_3O^+ with the alcohols employed in this study are listed in Table 2.4.

Methanol: The PTR-MS mass spectra of methanol observed in this study was very simple and was consistent with previous PTR-MS studies (Buhr et al. 2002, Warneke et al. 2003). The protonated parent ion accounted for > 95% of the total ion signal across all E/N settings (Table 2.4). The PTR-MS sensitivity to methanol did not significantly decline with E/N (Table 2.2) and it was concluded that in measurements of the atmosphere methanol will be sensitively detected at m/z 33 across a range of PTR-MS operating conditions.

Ethanol: Across the range of E/N settings employed in this study (95 – 170 Td), the protonated ethanol ion, detected at m/z 47, was the dominant ion observed in the PTR-MS spectra of ethanol (Figure 2.2, Table 2.4). In addition to the protonated parent ion signal, four other important product ion channels were observed in the ethanol mass spectra corresponding to:

$\text{C}_2\text{H}_5\text{OH} + \text{H}_3\text{O}^+ \rightarrow \text{C}_2\text{H}_5\text{OHH}^+ + \text{H}_2\text{O}$	m/z 47	Reaction 2.6a
$\rightarrow \text{C}_2\text{H}_5\text{O}^+ + \text{H}_2 + \text{H}_2\text{O}$	m/z 45	Reaction 2.6b
$\rightarrow \text{CH}_2\text{OH}^+ + \text{CH}_4 + \text{H}_2\text{O}$	m/z 31	Reaction 2.6c
$\rightarrow \text{C}_2\text{H}_5^+ + 2\text{H}_2\text{O}$	m/z 29	Reaction 2.6d
$\rightarrow \text{C}_2\text{H}_5\text{OHH}^+ + \text{H}_2\text{O}$	m/z 65	Reaction 2.6e

The product ions observed in the PTR-MS spectra of ethanol in this study resemble those reported by other authors (Buhr et al. 2002, Warneke et al. 2003, Blake et al. 2006, Inomata & Tanimoto 2009, Brown et al. 2010) with the exception of the ion signal at m/z 45 (Reaction 2.6b) which was only observed in two other studies (Buhr et al. 2002, Brown et al. 2010).

The $\text{C}_2\text{H}_5\text{O}^+$ product ion detected at m/z 45 is the dominant product ion in charge transfer reactions of O_2^+ with ethanol (Blake et al. 2006) and it is possible this is a product of reaction with O_2^+ reagent ions present as impurities in the reagent ion matrix.

In this study, the total ion signal for a fixed input concentration of ethanol decreased from 2.0×10^5 cps at 110 Td to 1.4×10^4 cps at 170 Td, a decrease of 93% (Table 2.2 and Figure 2.1). In comparison, when E/N was changed from 110 to 170 Td, the total ion signal of methanol declined by only 33% despite the expected decline based on theoretically derived reaction rates and reaction times being almost equivalent (Figure 2.3). Thus, it appears there is an additional mechanism affecting the PTR-MS sensitivity to ethanol.

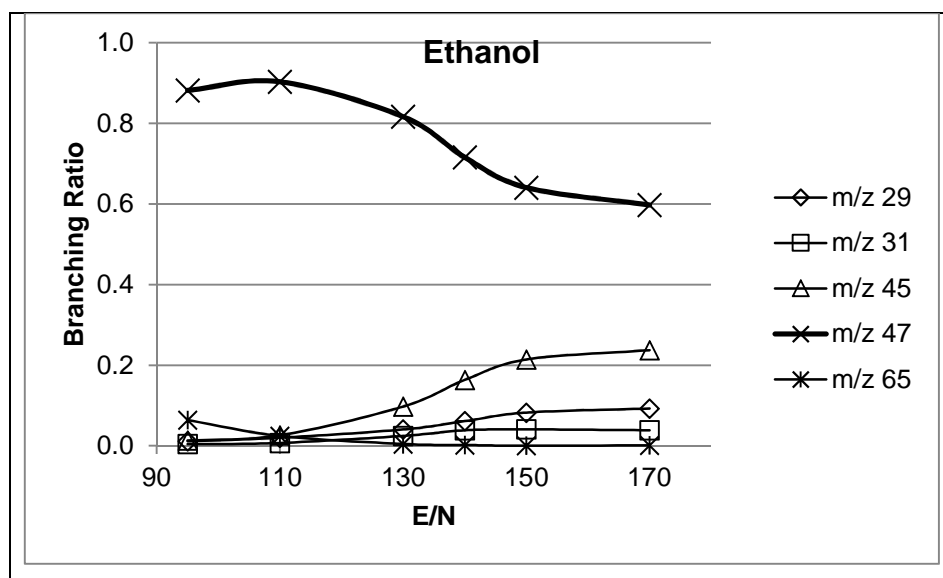


Figure 2.2: The major product ions and their branching ratios for the reaction of H_3O^+ with ethanol at 6 values of E/N .

Warneke et al. (2003), observed that the measured PTR-MS sensitivity to ethanol was ~ 12% of the calculated sensitivity based on ion –molecule collision theory. These authors proposed that the loss in sensitivity to ethanol was due to fragmentation to an unmeasurable ion, perhaps m/z 19 or 37. In PTR-MS, fragment ions that occur at m/z 19 and 37 would be obscured by the PTR-MS reagent ion signals of H_3O^+ and $\text{H}_3\text{O}^+(\text{H}_2\text{O})$ and are therefore unmeasurable.

Another early clue to this potential reaction pathway was provided by Kok et al. (2003) who reported a product ion at m/z 19 in the mass spectrum of proton transfer from CH_4^+ to ethanol. Subsequently, in a PTR-MS study with deuterium labelled ethanol, Inomata and Tanimoto (2009) confirmed the reproduction of H_3O^+ with H-atoms on both the 1st and 2nd carbon of the ethanol molecule:



In the study by Inomata and colleagues (2009), at low E/N (108Td), the branching ratio of H_3O^+ formation (Reaction 2.6f) was almost equivalent to the branching ratio of the protonated parent ion production (Reaction 2.6a), H_3O^+ reproduction was the dominant product ion channel at E/N 119 – 162. Thus, reproduction of H_3O^+ largely explains the loss in sensitivity with increasing E/N in PTR-MS studies of ethanol.

Table 2.4 The alcohols employed in this study, their formula, molecular weight (MW) and proton affinity (PA), and their product ions and branching ratios from the PTR-MS mass spectra determined across a range of E/N.

Compound	MW	PA (kJ mol ⁻¹)	Product ion formula	m/z	PTR-MS E/N (Td)					
					95	110	130	140	150	170
					Product ion branching ratios (%)					
Methanol CH ₄ O	32	754.3	CH ₃ O ⁺	31	<1	<1	<1	<1	<1	1
			CH ₅ O ⁺	33	95	98	98	97	97	
			CH ₅ O ⁺ •H ₂ O	51	2	<1	<1	<1	<1	
Ethanol C ₂ H ₆ O	46	776.4	C ₂ H ₂ ⁺	26	<1	<1	<1	<1	<1	1
			C ₂ H ₃ ⁺	27	<1	<1	<1	<1	<1	1
			C ₂ H ₅ ⁺	29	1	2	4	6	8	9
			CH ₂ O ⁺	31	<1	1	2	4	4	4
			C ₂ H ₅ O ⁺	45	1	3	10	16	21	24
			C ₂ H ₇ O ⁺	47	88	90	82	72	64	60
			¹³ CCH ₇ O ⁺	48	1	2	2	1	1	1
			C ₂ H ₇ O ⁺ •H ₂ O	65	6	2	<1	<1	<1	<1
				E/N						
				90	110	130	140	150	170	
1-Propanol C ₃ H ₈ O	60	786.5	C ₃ H ₃ ⁺	39	<1	<1	8	23	40	61
			¹³ CC ₂ H ₃ ⁺	40	<1	<1	<1	<1	1	2
			C ₃ H ₅ ⁺	41	<1	11	41	41	34	20
			¹³ CC ₂ H ₅ ⁺	42	<1	<1	1	1	1	<1
			C ₃ H ₇ ⁺	43	83	81	44	29	20	13
			¹³ CCH ₅ O ⁺	44	3	3	2	1	<1	<1
			C ₃ H ₇ O ⁺	59	1	2	2	1	<1	<1
			C ₃ H ₉ O ⁺	61	9	1	<1	<1	<1	<1
C ₃ H ₉ O ⁺ •H ₂ O	79	3	<1	<1	<1	<1	<1			
2- Propanol C ₃ H ₈ O	60	793	C ₃ H ₃ ⁺	39	<1	<1	4	16	33	57
			¹³ CC ₂ H ₃ ⁺	40	<1	<1	<1	<1	<1	1
			C ₃ H ₅ ⁺	41	<1	6	36	43	36	21
			¹³ CC ₂ H ₅ ⁺	42	<1	<1	<1	1	1	<1
			C ₃ H ₇ ⁺	43	<1	88	52	32	22	14
			¹³ CCH ₅ O ⁺	44	<1	1	1	<1	<1	<1
			C ₂ H ₅ O ⁺	45	<1	1	2	2	2	2
			C ₃ H ₇ O ⁺	59	<1	1	1	1	1	1
C ₃ H ₉ O ⁺	61	<1	<1	<1	<1	<1	<1			

Table 2.4 (cont.)

Compound	MW	PA (kJ mol ⁻¹)	Product ion formula	PTR-MS E/N (Td)						
				m/z	95	110	130	140	150	170
				Product ion branching ratios (%)						
1-butanol C ₄ H ₁₀ O	74	789	HCO ⁺ / C ₂ H ₅ ⁺	29	<1	<1	<1	<1	1	2
			C ₃ H ₃ ⁺	39	<1	1	7	19	44	
			¹³ CC ₂ H ₃ ⁺	40	<1	<1	<1	<1	1	
			C ₃ H ₅ ⁺	41	1	8	17	21	18	
			C ₄ H ₈ ⁺	56	1	1	1	<1	<1	
			C ₄ H ₉ ⁺	57	94	84	70	53	31	
			¹³ CC ₃ H ₉ ⁺	58	3	3	2	2	1	
			C ₄ H ₁₁ O ⁺	75	<1	<1	<1	<1	<1	
2-butanol C ₄ H ₁₀ O	74	815	HCO ⁺ / C ₂ H ₅ ⁺	29	<1	<1	<1	<1	1	2
			C ₃ H ₃ ⁺	39	<1	<1	2	10	22	42
			¹³ CC ₂ H ₃ ⁺	40	<1	<1	<1	<1	<1	1
			C ₃ H ₅ ⁺	41	<1	2	11	17	19	15
			C ₄ H ₉ ⁺	57	89	90	78	63	49	32
			¹³ CC ₃ H ₉ ⁺	58	5	5	4	3	2	1
			C ₄ H ₉ O ⁺	73	1	1	2	2	2	1
			C ₄ H ₁₁ O ⁺	75	3	<1	<1	<1	<1	<1
2-methyl-2-propanol C ₄ H ₁₀ O	74	802.6	HCO ⁺ / C ₂ H ₅ ⁺	29	<1	<1	<1	<1	<1	2
			C ₃ H ₃ ⁺	39	<1	<1	5	16	37	
			C ₃ H ₅ ⁺	41	<1	5	12	16	14	
			C ₄ H ₉ ⁺	57	96	90	77	60	39	
			¹³ CC ₃ H ₉ ⁺	58	2	3	2	2	2	
			C ₃ H ₇ O ⁺	59	2	3	4	5	7	

1-and 2- Propanol: The protonated parent ion was a minor product ion in the PTR-MS spectra of the C₃ alcohols in this study (Table 2.4). In SIFT-MS studies, at thermal energies, H₂O elimination was the dominant process in reactions of H₃O⁺ with C₃ alcohols with a small (< 20%) contribution from non-dissociative proton transfer (Spanel & Smith 1997). These results suggest the reaction pathways for the formation of both the MH⁺ and (M-H₂O)⁺ ions are exothermic and occur at thermal energies upon protonation for C₃ alcohols. Due to the additional collision energies in the PTR-MS, proton transfer to C₃ alcohols is almost completely dissociative (Buhr et al. 2002, Brown et al. 2010).

The dominant reaction channel in the PTR-MS spectra of C₃ alcohols was H₂O elimination:



with subsequent H-elimination yielding:



The mass spectra of 1- and 2- propanol reported here closely resemble those reported in other PTR-MS studies (Buhr et al. 2002, Brown et al. 2010).

As we will see in this study, and has been reported in other PTR-MS studies of multiple compound classes, (Warneke et al. 2003, Blake et al. 2006) product ions at m/z 43 occur for a large number of VOCs. Consequently, in PTR-MS measurements of complex mixtures of VOCs, specific measurements of C₃ alcohols at m/z 43 would not be possible due to contributions from multiple compounds at m/z 43.

Furthermore, as was the case for ethanol, Inomata et al. (2010) observed that measured PTR-MS sensitivity to 2-propanol was ~ 75% of the calculated sensitivity based on ion – molecule collision theory, and further deuterium labelling studies showed the reproduction of H₃O⁺ also occurred for 2-propanol (Inomata & Tanimoto 2010). In the present study, the total ion signal (TIS) for a fixed input concentration of propanol decreased by ~ 65% (Table 2.2 and Figure 2.3) indicating the reproduction of H₃O⁺ was a less important pathway for propanol than it was in the mass spectra ethanol in this study.

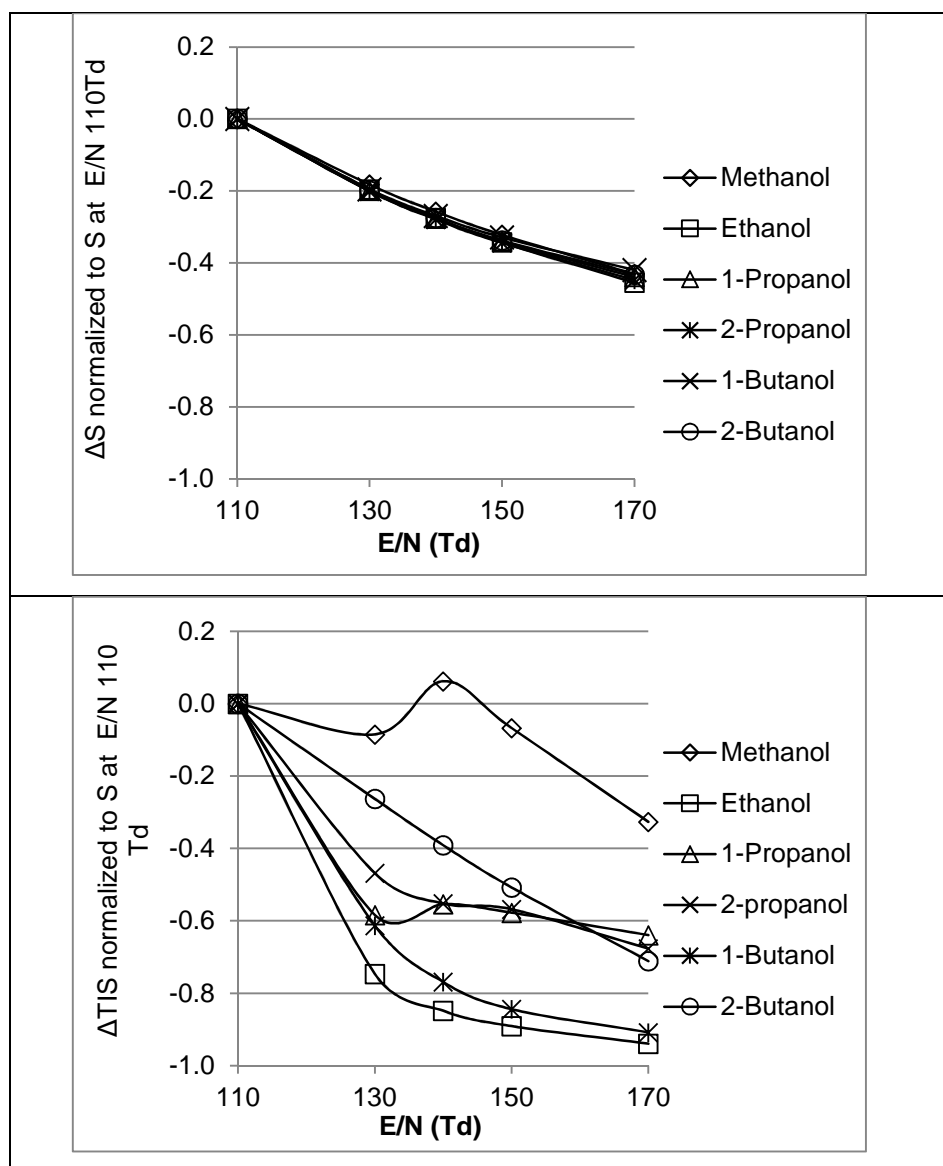


Figure 2.3: (Top panel) The change in calculated PTR-MS sensitivity (ΔS) to alcohols based on theoretically derived reaction rates, when E/N is changed from 110 Td to 170 Td. (Bottom panel) The change in observed total ion signal (ΔTIS) for a fixed input concentration of alcohols when E/N is changed from 110 Td to 170 Td.

C₄ alcohols: Consistent with previous studies, H₂O elimination was also the dominant reaction pathway for the C₄ alcohols yielding a significant peak at m/z 57 and subsequent minor peaks at m/z 41 and 39 at higher E/N settings (Buhr et al. 2002, Brown et al. 2010). Product ions at m/z 57 also occur for a large number of VOCs (Warneke et al. 2003, Blake et al. 2006) and in PTR-MS measurements of complex VOC mixtures, specific measurements of C₄ alcohols at m/z 57 would not be possible due to contributions from multiple compounds at m/z 57.

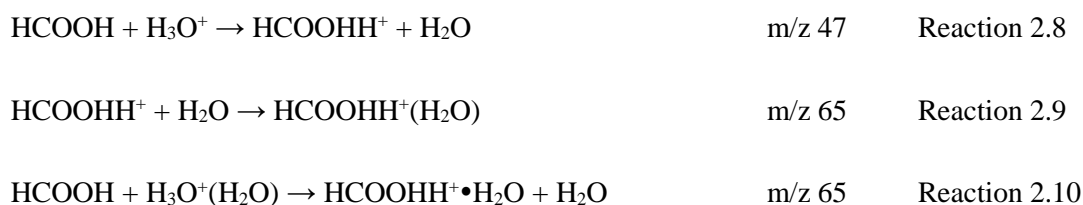
The total observed ion signal for a fixed input concentration of 1-butanol decreased by 89% when E/N was changed from 110 Td to 170 Td (Table 2.2 and Figure 2.3) suggesting the reproduction of H_3O^+ could be an important reaction pathway for 1-butanol. In comparison, the total observed ion signal of tertiary butyl alcohol and 2-butanol declined by ~ 70% (Table 2.2).

In summary, methanol can be sensitively detected at its protonated parent ion signal across a range of E/N settings. The $\text{C}_2 - \text{C}_4$ alcohols employed in this study showed an increasing tendency to fragment with both increasing carbon chain length and increasing E/N. At E/N of 110 Td and higher, the PTR-MS sensitivity to $\text{C}_2 - \text{C}_4$ alcohols, in particular ethanol and 1-butanol, was significantly reduced due to fragmentation to unmeasurable H_3O^+ product ions.

2.3.3 Carboxylic acids

The PTR-MS spectra of formic-, acetic- and propionic acids were determined in this study across a range of E/N settings. The product ions and branching ratios (as a percentage of the total ion signal (%TIS)) from reactions of H_3O^+ with the alcohols employed in this study are listed in Table 2.5.

Formic Acid: Across the range of E/N settings employed in this study, the protonated parent ion was the dominant ion observed in the PTR-MS spectra of formic acid. In addition to the protonated parent ion signal (Reaction 2.8), the monohydrate product ion was observed in high abundance at E/N = 90 Td in the PTR-MS spectra of formic acid. The monohydrate ion is formed by association reactions (Reaction 2.9) and/or ligand switching reactions (Reaction 2.10):



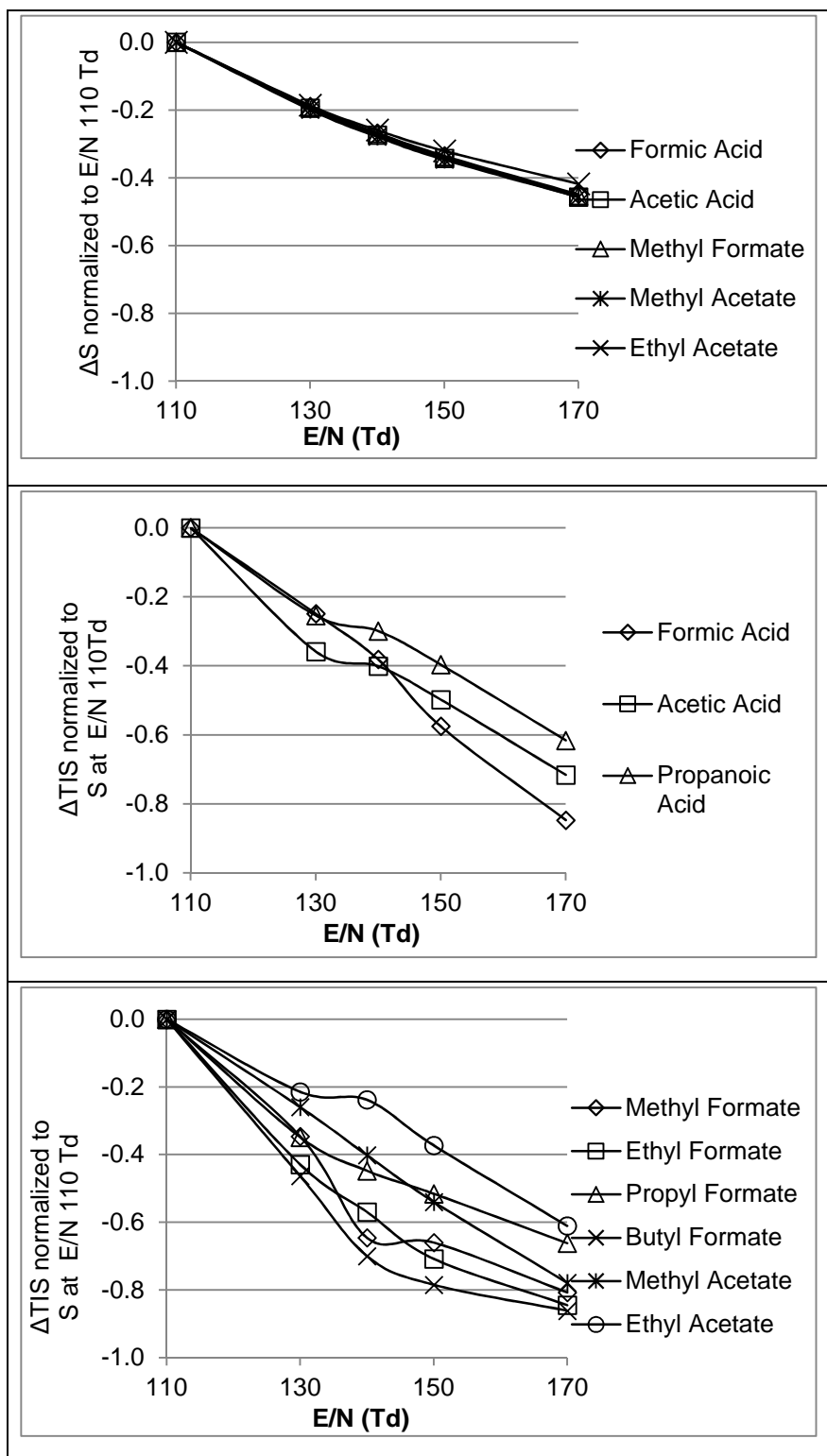


Figure 2.4: (Top panel) The change in calculated PTR-MS sensitivity (ΔS) to carboxylic acids and esters based on theoretically derived reaction rates, when E/N is changed from 110 Td to 170 Td. (Middle and Bottom panels) The change in observed total ion signal (ΔTIS) for a fixed input concentration of carboxylic acids and esters when E/N is changed from 110 Td to 170 Td.

In this study, the total ion signal for a fixed input concentration of formic acid decreased by 85% when E/N was changed from 110 Td to 170 Td which is more than the ~ 60 - 70% decline observed for acetic and propionic acid (Table 2.2 and Figure 2.4). Again, the loss in sensitivity to formic acid is presumably due to reproduction of H_3O^+ at m/z 19, which is obscured by the PTR-MS reagent ion signals of H_3O^+ and therefore unmeasurable.

The carbonyl oxygen has a higher proton affinity than the hydroxyl group oxygen, however both protonation sites are close together and protonation at both sites could occur. Protonation at the hydroxyl oxygen and subsequent fragmentation may be responsible for the formation of H_3O^+ product ions, as was observed for ethanol in the previous section.

In a detailed study of the PTR-MS response to formic and acetic acid, Baasandorj et al (2014), proposed that at high E/N, protonated formic acid undergoes high energy collisions with water molecules to form H_3O^+ :



In the same study, the PTR-MS sensitivity to formic acid showed negative humidity dependence at high E/N, which supports the theory that reproduction of H_3O^+ occurred via this mechanism.

In a selected ion flow drift tube (SIFDT) mass spectrometer, protonated formic acid ions were observed to dissociate upon collisions with He buffer gas, to form HCO^+ and H_3O^+ detected at m/z 29 and 19 respectively (Glosik et al. 1993). In the present study, no significant peak at m/z 29 was observed in the PTR-MS spectra of formic acid.

Overall, in measurements of the atmosphere with PTR-MS, formic acid will be detected at m/z 47, however at high values of E/N the PTR-MS sensitivity to formic acid will be poor.

Acetic Acid: Across the range of E/N settings employed in this study, the protonated parent ion was the dominant ion observed in the PTR-MS spectra of acetic acid. In addition to the protonated parent ion signal (Reaction 2.7a) H_2O elimination yielded a product ion signal at m/z 43.



At E/N = 90 Td, trace ion signals (< 3%) of hydration reaction products were also observed in the PTR-MS spectra of acetic acid (Table 2.5).

In PTR-MS measurements across a range of E/N values Haase et al. (2012) reported a 37% decline in the observed sensitivity to acetic acid from 23 ncps ppbv⁻¹ at E/N 95 Td to 8.5 ncps ppbv⁻¹ at E/N of 132 Td, which is almost identical to the 39% decline in TIS observed across the same E/N range in the present study (Figure 2.4).

In summary, in measurements of the atmosphere with PTR-MS, acetic acid will be detected at m/z 61, with good sensitivity across a range of E/N values.

Propionic Acid: The major products of the reactions of H₃O⁺ with propionic acid were the protonated parent ion detected at m/z 75 and the product of H₂O elimination (m/z 57) (Table 2.5). This was consistent with the PTR-MS spectra (E/N 148 Td) of propionic acid reported by von Hartungen (2004).

In the present study, both the signal at m/z 75 and 57 declined with E/N, but contrary to expectations the fraction of the TIS detected as the protonated parent ion at m/z 75 increased with E/N and the fraction of the TIS detected as the fragment ion signal at m/z 57 decreased with increasing E/N. The reason for this unusual behaviour is uncertain.

Table 2.5: The carboxylic acids employed in this study, their formula, molecular weight (MW) and proton affinity (PA), and their product ions and branching ratios from the PTR-MS mass spectra determined across a range of E/N

Compound	MW	PA (kJ mol ⁻¹)	Product ion formula	m/z	PTR-MS E/N (Td)					
					90	110	130	140	150	170
					Product ion branching ratios (%)					
Formic Acid CH ₂ O ₂	46	742	CH ₃ O ₂ ⁺	47	69	95	98	99	99	98
			¹³ CH ₃ O ₂ ⁺	48	<1	<1	1	1	1	1
			CH ₃ O ₂ ⁺ •H ₂ O	65	30	4	1	0	0	0
Acetic acid C ₂ H ₄ O ₂	60	783.7	C ₂ H ₃ O ⁺	43	6	12	17	21	26	40
			C ₂ H ₅ O ₂ ⁺	61	89	86	81	77	72	57
			¹³ CCH ₅ O ₂ ⁺	62	1	1	1	1	1	1
			C ₂ H ₅ O ₂ ⁺ •H ₂ O	79	3	<1	<1	<1	<1	<1
Propionic acid C ₃ H ₆ O ₂	74	797.2	C ₂ H ₅ ⁺ /HCO ⁺	29	<1	<1	<1	1	2	2
			C ₃ H ₅ O ⁺	57	19	16	8	5	5	5
			C ₃ H ₇ O ₂ ⁺	75	73	78	86	88	89	87
			¹³ CC ₂ H ₇ O ₂ ⁺	76	3	3	3	3	3	3
			C ₃ H ₇ O ₂ ⁺ •H ₂ O	93	2	<1	<1	<1	<1	<1

In summary, acetic and propionic acid can be sensitively detected at their respective protonated parent ions across a range of E/N settings. While formic acid was also predominantly detected as the protonated parent ion, the PTR-MS sensitivity to formic acid was significantly reduced at high E/N due to fragmentation to unmeasurable H₃O⁺ product ions.

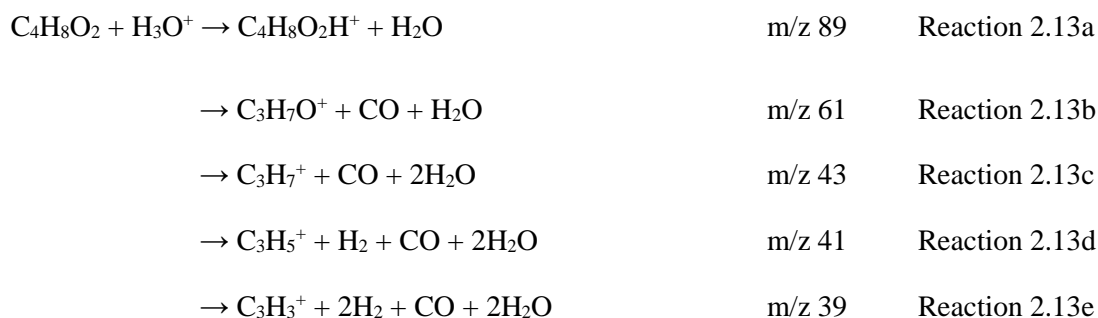
2.3.4 Esters

The PTR-MS spectra of six acetate and formate esters were determined in this study across a range of E/N settings. The product ions and branching ratios (as a percentage of the total ion signal (%TIS)) from reactions of H₃O⁺ with the esters employed in this study are listed in Table 2.6.

C₂ – C₅ Formate esters : The protonated parent ion detected at m/z 61 was the dominant ion in the mass spectra of methyl formate across all E/N settings, however at E/N > 150 Td fragmentation to protonated methanol and a neutral CO was also a significant reaction pathway (Table 2.6).

The protonated product ion at m/z 75 was abundant at low E/N in the mass spectra of ethyl formate, however CO elimination resulting in a protonated ethanol fragment ion at m/z 47 was the dominant product ion in the PTR-MS spectra of ethyl formate across all settings of E/N.

The reactions of H₃O⁺ with propyl and butyl formate were more complex, with CO elimination resulting in the formation of the corresponding protonated alcohols, followed by H₂O elimination from the alcohol and subsequent breakdown of the hydrocarbon chain. For instance, the reactions of propyl formate proceed via:

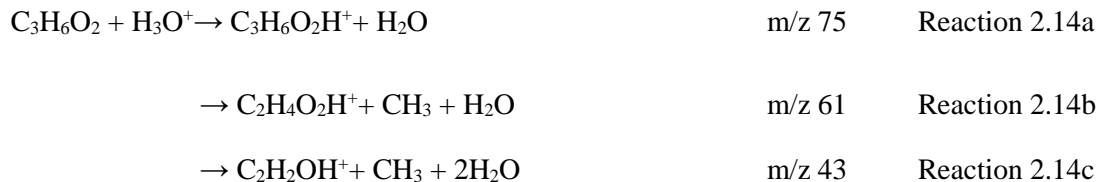


As we saw in the section 2.3.2, propanol rapidly dissociates to form a product ion at m/z 43, which explains the absence of a significant peak at m/z 61 in the spectra of propyl formate

The product ions and branching ratios of reactions of H_3O^+ with methyl-, ethyl- and butyl formate measured by PTR-MS in this study closely resembled those reported in other studies with PTR-MS (Aprea et al. 2007) and SIFT-MS instruments (Spanel & Smith 1998).

When E/N was changed from 110 Td to 170 Td the total ion signals for fixed concentrations of methyl formate, ethyl formate or butyl formate decreased by 81% - 86 % (Table 2.2 and Figure 2.4), suggesting high energy collisions with water molecules in the PTR-MS resulted in reproduction of H_3O^+ ions from both of these compounds. In comparison, the total ion signal of propyl formate decreased by 66% across the same E/N range.

C₃ – C₄Acetate esters: The protonated parent ion detected at m/z 75 was the dominant ion in the mass spectra of methyl acetate across all E/N settings. As E/N increased from 90 to 170 Td the fragment ion peak at m/z 43 increased in intensity. These $C_2H_3O^+$ fragment ions were presumably formed via:



As we saw in section 2.3.2, propanol (m/z 61) dissociates to form a product ion at m/z 43, which explains the small (~ 0.03 %) peak at m/z 61 in the spectra of methyl acetate.

The protonated parent ion was a minor product in the mass spectra of ethyl acetate, with the dominant peaks observed at m/z 61 and 43, which are fragment ions formed via a similar reaction mechanism to that described above for methyl acetate.

The products of reactions of H_3O^+ with methyl- and ethyl acetate observed in this study were similar those reported in previous PTR-MS studies of esters (Buhr et al. 2002, Aprea et al. 2007). In contrast, in SIFT-MS studies at thermal energies, only the protonated parent ion was observed in the mass spectra of methyl- and ethyl- acetate (Spanel & Smith 1998).

When E/N was changed from 110 Td to 170 Td the total ion signals for fixed concentrations of methyl acetate, ethyl acetate decreased by 78 % and 71 % respectively

(Table 2.1 and Figure 2.4) suggesting reproduction of H_3O^+ ions from high energy collisions with water molecules may not be as significant as for the corresponding formate esters.

Table 2.6: The organic ester compounds employed in this study, their formula, molecular weight (MW) and proton affinity (PA), enthalpy of reaction with H_3O^+ (ΔH_p°) and their product ions and branching ratios from the PTR-MS mass spectra determined across a range of E/N.

Compound	MW	PA (kJ mol ⁻¹)	Product ion formula	m/z	PTR-MS E/N (Td)				
					110	130	140	150	170
			Product ion branching ratios (%)						
Methyl formate C ₂ H ₄ O ₂	60	782.5 (-91.5)	CH ₅ O ⁺	33	2	7	16	30	47
			C ₂ H ₅ O ₂ ⁺	61	96	91	82	68	50
			¹³ CCH ₅ O ₂ ⁺	62	1	1	1	1	<1
Ethyl formate C ₃ H ₆ O ₂	74	799.4 (-108.4)	C ₂ H ₇ O ⁺	47	53	83	89	91	89
			C ₂ H ₇ O ⁺ •H ₂ O	65	3	<1	<1	<1	<1
			C ₃ H ₇ O ₂ ⁺	75	42	14	9	7	8
Propyl formate C ₄ H ₈ O ₂	88	804.9 (-113.9)	C ₃ H ₃ ⁺	39	<1	3	13	31	56
			¹³ CC ₂ H ₃ ⁺	40	<1	<1	<1	<1	1
			C ₃ H ₅ ⁺	41	5	33	42	36	22
			¹³ CC ₂ H ₅ ⁺	42	<1	1	2	1	1
			C ₂ H ₃ O ⁺ /C ₃ H ₇ ⁺	43	80	51	32	21	13
			¹³ CCH ₃ O ⁺	44	1	1	<1	<1	<1
			C ₂ H ₇ O ⁺	47	7	9	9	8	6
			C ₄ H ₉ O ₂ ⁺	89	5	2	<1	<1	<1
Butyl formate C ₅ H ₁₀ O ₂	102	806 (115)	HCO ⁺ / C ₂ H ₅ ⁺	29	<1	<1	<1	1	2
			C ₃ H ₃ ⁺	39	<1	1	6	19	44
			¹³ CC ₂ H ₃ ⁺	40	<1	<1	<1	<1	1
			C ₃ H ₅ ⁺	41	<1	8	16	20	17
			CH ₅ O ⁺	47	<1	<1	<1	1	<1
			C ₄ H ₉ ⁺ /C ₃ H ₅ O ⁺	57	95	87	72	54	31
			¹³ CC ₃ H ₉ ⁺ / ¹³ CC ₂ H ₅ O ⁺	58	2	2	2	2	1
			C ₅ H ₁₁ O ₂ ⁺	103	<1	<1	<1	<1	<1
Methyl acetate C ₃ H ₆ O ₂	74	821.6 (130.6)	C ₂ H ₃ O ⁺	43	2	7	16	26	46
			¹³ CCH ₅ O ⁺	44	<1	<1	<1	<1	1
			C ₃ H ₇ O ₂ ⁺	75	94	90	80	69	49
			¹³ CC ₂ H ₇ O ₂ ⁺	76	3	3	3	2	2
Ethyl acetate C ₄ H ₈ O ₂	88	835.7 (144.7)	C ₂ H ₅ O ⁺ / C ₃ H ₇ ⁺	43	7	13	16	22	36
			C ₂ H ₅ O ₂ ⁺	61	49	75	77	73	60
			¹³ CCH ₅ O ₂ ⁺	62	<1	1	1	1	1
			C ₄ H ₉ O ₂ ⁺	89	41	9	5	3	2
			¹³ CC ₃ H ₉ O ₂ ⁺	90	1	<1	<1	<1	<1

In summary, the major product ions of esters employed in this study (m/z 43, 47, 57, 61, 75) overlap with the product ions of $\text{C}_2 - \text{C}_4$ alcohols and carboxylic acids which would complicate their unique their measurement in the atmosphere by PTR-MS

2.3.5 Multifunctional VOCs

The PTR-MS spectra of four compounds with multiple functional groups were examined: glyoxal, methyl glyoxal, glycolic acid and hydroxyacetone. These compounds are common secondary oxidation products of isoprene, terpenes and aromatics and are important intermediates in the formation of secondary organic aerosol. These highly oxygenated VOCs are often poorly detected by widely used techniques such as gas chromatography, and their measurement in the atmosphere is a major potential advantage of PTR-MS.

Hydroxyacetone (*1-hydroxy-2-propanone*): The proton affinity of hydroxyacetone is unknown. In this study, the dominant ion signal in the PTR-MS mass spectra of hydroxyacetone was detected at m/z 75 which corresponds to the protonated hydroxyacetone ion, and one can assume the $PA(\text{hydroxyacetone}) > PA(\text{H}_2\text{O})$.

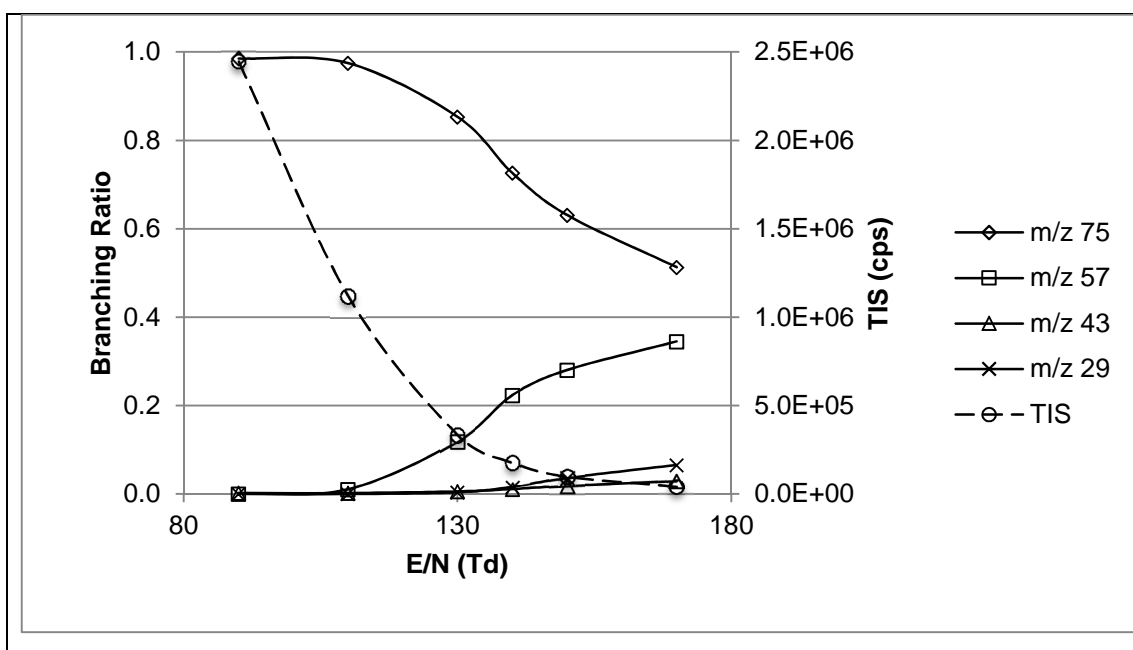
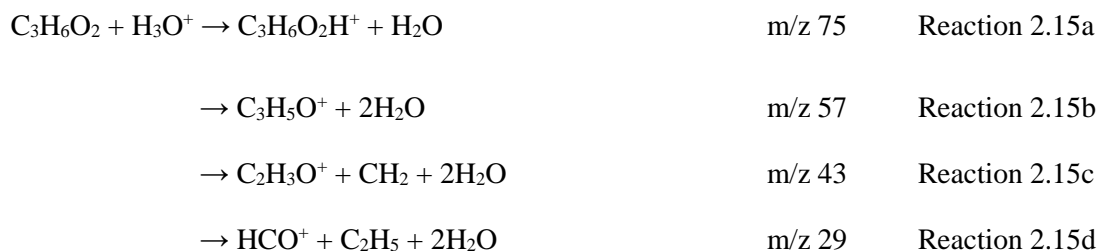


Figure 2.5: The major product ions of hydroxyacetone and their respective branching ratios at each setting of E/N employed in this study. Also included is the total ion signal (TIS) at each E/N .

In addition to the protonated parent ion, there were three fragment ions observed in the PTR-MS spectra of hydroxyacetone at m/z 57, 43 and 29 (Figure 2.5). The product ion at m/z 57 is presumably $\text{C}_3\text{H}_5\text{O}^+$ formed via H_2O elimination with subsequent breakdown of the carbon chain at higher values of E/N resulting in formation of $\text{C}_2\text{H}_3\text{O}^+$ (m/z 43) and HCO^+ (m/z 29):



The product ion branching ratios reported here are in agreement with those reported by Karl et al. (2007) who observed 80% of the hydroxyacetone signal as the protonated parent ion (m/z 75) at E/N 120 Td.

When E/N was changed from 110 Td to 170 Td the total ion signal for a fixed input concentration of hydroxyacetone decreased by ~ 96% (Figure 2.5). In comparison, when E/N was changed from 110 to 170 Td, the total ion signal of the related compounds 1-propanol and acetone declined by 64 % and 60% respectively. At high values of E/N it is possible hydroxyacetone fragments to an unmeasurable ion such as H_3O^+ as has been described for several other compounds containing either hydroxyl or carbonyl groups in this study such as MEK, and ethanol.

In summary, in measurements of the atmosphere with PTR-MS, the ion signal at m/z 75 may contain contributions from hydroxyacetone. At E/N of 110 Td and higher, the PTR-MS sensitivity to hydroxyacetone was significantly reduced due to fragmentation to unmeasurable H_3O^+ product ions.

Glyoxal: In the present study, 4 significant peaks were detected in the PTR-MS spectra of glyoxal (CHOCHO) at m/z 95, 88, 47 and 45 (Figure 2.6). Notably a signal at m/z 59 corresponding with protonated glyoxal was not observed.

Several of the peaks observed in the mass spectra of the glyoxal standard had m/z > m/z 59 and may therefore be products of hydration reactions with glyoxal or products of impurities in the standard. Glyoxal is extremely water soluble and undergoes hydration and oligomerization processes in the presence of water (Loeffler et al. 2006). In this study, ions signals that corresponded with known products of glyoxal oligomers were detected at m/z 95, 88, 61 (Liggio et al. 2005). This suggests that a significant fraction of the glyoxal was present in its oligomeric form in the prepared gas standard employed in this study.

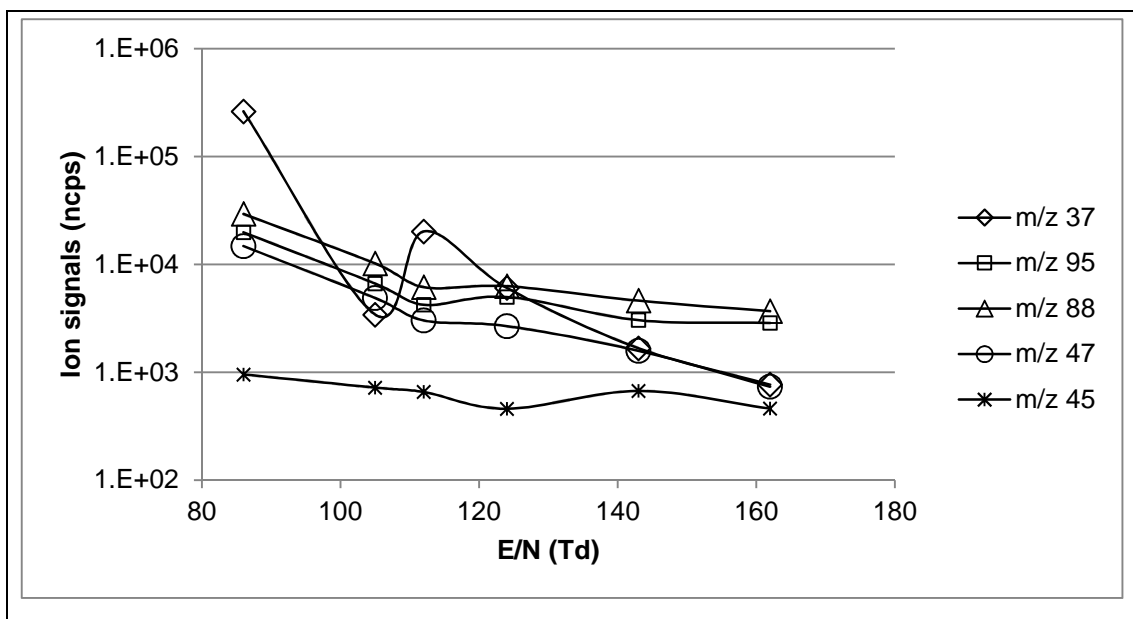


Figure 2.6: The ion signals of the major product ions of observed in measurements of the prepared glyoxal standard at each setting of E/N employed in this study.

Due to the presence of these derivative compounds, the products of reactions of H_3O^+ with glyoxal could not be distinguished from the products of the glyoxal derivatives or possible impurities and accurate branching ratios for glyoxal could not be determined and only the product ion signals are reported in Figure 2.6.

It is reasonable to assume that a fraction of the glyoxal present would have partitioned to the monomer form and the following discussion will focus on the possible reasons the protonated glyoxal parent ion was not observed in the PTR-MS spectra in this study.

The absence of a protonated glyoxal parent ion in this study may be due to one or a combination of factors, including:

- $\text{PA}(\text{Glyoxal}) < \text{PA}(\text{H}_2\text{O})$ and proton transfer did not occur
- $\text{PA}(\text{Glyoxal}) \approx \text{PA}(\text{H}_2\text{O})$ and in humid conditions loss via back reaction is significant
- $\text{PA}(\text{Glyoxal}) \gg \text{PA}(\text{H}_2\text{O})$ and proton transfer is completely dissociative.

A computational study determined the PA of glyoxal to be $673.7 \text{ kJ mol}^{-1}$, which is slightly lower than the $\text{PA}(\text{H}_2\text{O})$ of 691 kJ mol^{-1} . This is unsurprising given the structure of glyoxal is very similar to that of formaldehyde, which as discussed, has proton affinity $\approx \text{PA}(\text{H}_2\text{O})$. As in the case of formaldehyde, the reaction rates of the forward reaction may be

higher than the reverse reaction however, the concentration of water molecules in the PTR-MS drift tube is considerably higher than the concentration of glyoxal and loss via back reaction would be significant.

In a SIFT-MS study of the reactions of H_3O^+ with *cis*- and *trans*- glyoxal isomers, a protonated parent ion signal was observed at m/z 59 (Michel et al. 2005). In SIFT-MS, the reactions occur in helium buffer gas and the concentration of water molecules is significantly lower than in PTR-MS, thus limiting the H_2O available for the back reaction. In the SIFT-MS study, when water was added to the carrier gas, the signal of protonated glyoxal decreased significantly (Michel et al. 2005) without a coincident increase in the signal of the hydrates of glyoxal suggesting loss via back reaction with H_2O was occurring.

Two separate peaks at m/z 59 were observed with a higher mass resolution PTR-time of flight mass spectrometer (PTR-ToF) exposed to a mixture containing acetone (m/z 59.050) and glyoxal (m/z 59.013) (Graus et al. 2010). The dilution gas used in the prepared mixture of acetone + glyoxal in the study by Graus et al. (2010) was not specified, however if H_2O -free gas was used (e.g. nitrogen, zero-grade air) loss via the back reaction would not have been significant, providing a plausible explanation for the presence of a protonated glyoxal peak in the PTR-ToF spectra in that study.

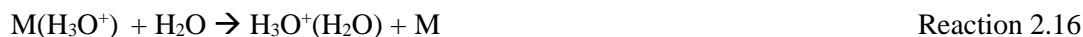
In the present study, the glyoxal standard was diluted with zero (VOC free) air which was generated by diverting ambient air through a zero furnace (350°C) with a Platinum wool catalyst that destroyed VOCs in the air. This zero air had the same mole fractions of H_2O as the ambient air. Consistent with this study, Thalman et al (2015) also reported no response to glyoxal in their PTR-ToF instrument when challenged with up to 30 ppbv of a prepared glyoxal standard. These experiments were conducted in a chamber, at typical ambient relative humidity. Thus, in both studies, sufficient water was present for the back reaction to occur, and protonated glyoxal was not detected.

A third possible explanation for the absence of protonated glyoxal in the PTR-MS spectra in this study may be that glyoxal undergoes complete dissociation upon proton transfer from H_3O^+ . Given we have established that the PA of glyoxal is likely to be close to that of water, the energy transferred in proton transfer from H_3O^+ to glyoxal is unlikely to be sufficient to cause complete dissociation. Furthermore, the charged parent ion is observed in the much higher energy electron impact mass spectra of glyoxal, which adds weight to the argument that complete dissociation of glyoxal does not occur in PTR-MS (Stein 2005).

Given that proton transfer from H_3O^+ to glyoxal appears to be endothermic it is unlikely there is sufficient energy transferred in the proton transfer reaction to cause dissociation and it is likely the product ions signals at m/z 45 and 47, observed in the mass spectra of the glyoxal standard in this study, are products from the glyoxal derivatives and/ or impurities in prepared standard.

Another peculiarity of the PTR-MS spectra of glyoxal observed in this study was the behaviour of the m/z 37 ion signal with increasing E/N (Figure 2.2). Typically in PTR-MS measurements, as E/N is increased, the abundance of hydrated hydronium ions ($\text{H}_3\text{O}^+\cdot\text{H}_2\text{O}$) detected at m/z 37, declines. In the present study, for a fixed glyoxal concentration, the m/z 37 ion signal increased at E/N 112 and 124 and then resumed its decline from E/N 143.

In the SIFT-MS study by Michel et al (2005), when the water content of the carrier gas was kept constant and the concentration of glyoxal supplied to the SIFT-MS instrument was increased the signal at m/z 37 also increased. These authors proposed rapid ligand switching reactions of glyoxal with $\text{H}_3\text{O}^+\cdot\text{H}_2\text{O}$ were responsible for these phenomena:



Clearly, the reactions of H_3O^+ with glyoxal in the presence of water are complex and not fully resolved. However, it can be concluded from this and previous studies, that in PTR-MS measurements of the atmosphere at typical ambient humidity, the signal at m/z 59 will not contain substantial contributions from protonated glyoxal.

Methyl glyoxal: The proton affinity of methyl glyoxal is also unknown. In this study, an ion signal at m/z 73 was detected in the PTR-MS spectra of methyl glyoxal which can be attributed to protonated methyl glyoxal, and one can assume the $\text{PA}(\text{methyl glyoxal}) > \text{PA}(\text{H}_2\text{O})$.

In addition to protonated methyl glyoxal at m/z 73, five other significant peaks were observed in the methyl glyoxal mass spectra at m/z 33, 43, 45, 61, and 75, with minor signals (1 - 5 %) observed at another 10 m/z (m/z 31, 51, 57, 59, 79, 87, 88, 89, 91, 131). Like glyoxal, methyl glyoxal is extremely water soluble and undergoes hydration and oligomerization processes in the presence of water to form diols and tetrols (Axson et al. 2009). These methyl glyoxal derivatives would have been present in the liquid methyl glyoxal solution (~ 40 % in H_2O) and in the prepared gaseous standard.

Given, there were potentially multiple compounds present in the prepared methyl glyoxal standard used in this study the products of the reactions of H_3O^+ with methyl glyoxal could not be distinguished from those of other compounds present and the PTR-MS spectra of pure methyl glyoxal could not be determined. As such only the ion signals of the m/z observed in the mass spectra of methyl glyoxal are shown in Figure 2.7.

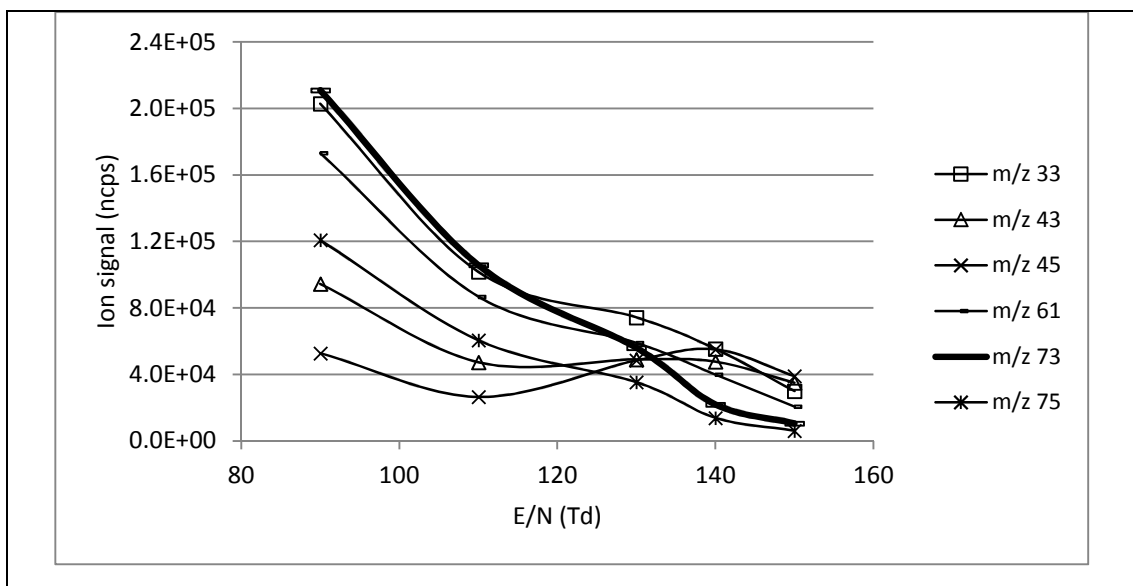


Figure 2.7: The signals of the major product ions of observed in measurements of the prepared methyl glyoxal standard at each setting of E/N employed in this study.

The measurement of methyl glyoxal at m/z 73 was also demonstrated in a chamber study, in which the PTR-ToF signal at m/z 73 (0 – 2000 ppbv) was in close agreement ($\pm 10\%$) with two established methyl glyoxal measurement techniques: fourier transform infra-red spectrometry (FTIR) and light- emitting diode cavity-enhanced differential optical absorption spectrometry (CE-DOAS) (Thalman et al. 2015).

For a fixed concentration of methyl glyoxal, the ion signal at m/z 73 declined 95% when E/N was changed from 90 Td to 150 Td. Presumably some of this decline could be attributed to fragmentation to lower molecular weight ions, for example those detected at m/z 45 and 43.

In summary, in measurements of the atmosphere with PTR-MS, the signal at m/z 73 may contain contributions from protonated methyl glyoxal. The PTR-MS sensitivity to methyl glyoxal at m/z 73 considerably declines at $E/N > 110$ Td due to fragmentation, the products of which could not be determined in this study.

Glycolic acid (*hydroxy-acetic acid*): The proton affinity of glycolic acid is unknown, however the protonated parent ion signal of glycolic acid at m/z 77 was detected in the PTR-MS spectra in this study indicating the PA(Glycolic Acid) > PA (H₂O).

In addition to the protonated parent ion, there were six other significant product ions observed in the PTR-MS spectra of glycolic acid at m/z 29, 31, 33, 45, 47, and 95. Trace ion signals (1 - 2%) were also detected at m/z 46, 49, 61, 73, 78, 89, 91, and 108.

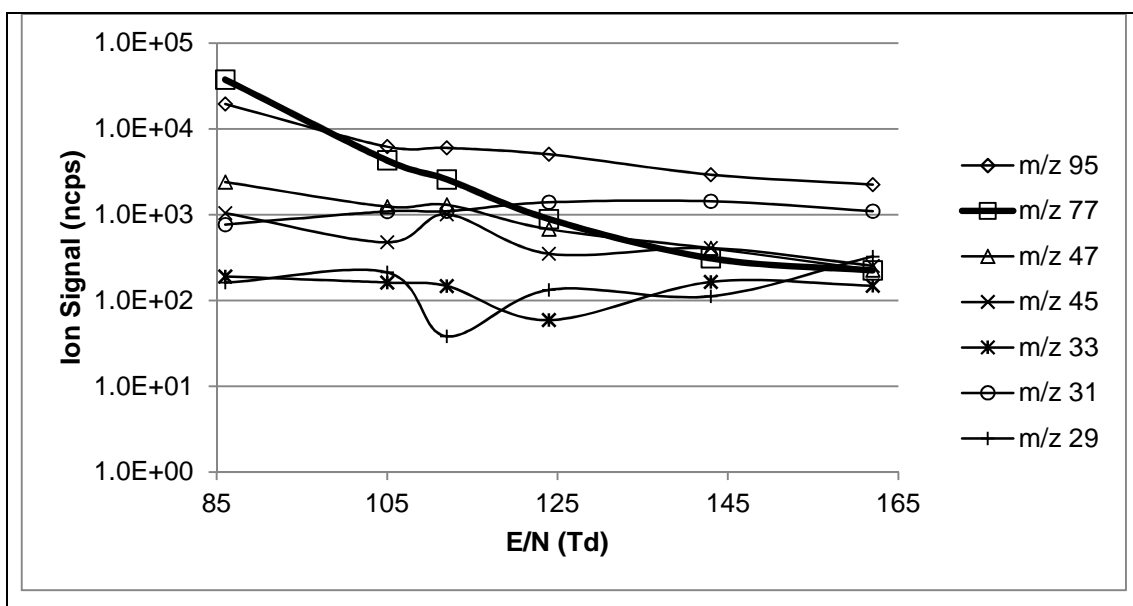


Figure 2.8 The major product ions of observed in measurements of the prepared glycolic acid standard and their respective branching ratios at each setting of E/N employed in this study.

Like glyoxal and methyl glyoxal, glycolic acid is extremely water-soluble and in the presence of H₂O it may undergo transformation to a tetrol, which could yield a protonated parent ion at m/z 95:

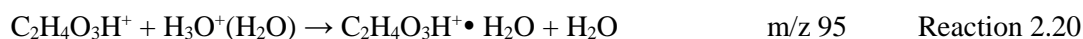


The product ion at m/z 95 could also be the product of association reactions between protonated glycolic acid and H₂O or ligand switching reactions of protonated glycolic acid with H₃O⁺(H₂O).

Association reaction:



Ligand switching reaction:



Given, there were potentially multiple compounds present in the prepared glycolic acid standard used in this study the product ions and branching ratios from the reactions of H₃O⁺ with glycolic acid could not be distinguished from those of other compounds present and accurate branching ratios of glycolic acid could not be determined and only the product ion signals are reported in Figure 2.8.

The product ion signals observed at 29, 31, 33, 45 and 47 might be the result of fragmentation processes in multiple compounds. The fragmentation products of glycolic acid observed in this study closely resembled those obtained from electron impact mass spectra (Stein 2005) and ion trap mass spectra (Baker & Gabryelski 2007) of glycolic acid.

Proposed fragmentation pathways from reactions of H₃O⁺ with glycolic acid are as follows:



and /or



While the product ions and branching ratios of glycolic acid could not be defined in this study due to the likely presence of impurities in the prepared standard, we can conclude that in measurements of the atmosphere with PTR-MS, the ion signal at m/z 77 may contain contributions from protonated glycolic acid. At $E/N > 110$ Td the sensitivity of the PTR-MS to glycolic acid significantly declines.

In summary, the PTR-MS spectra of glyoxal, methyl glyoxal and glycolic acid could not be determined in this study due to the presence of higher molecular weight derivatives of these compounds in the prepared standards. Nevertheless, several important factors relating to the detection of these species can be determined. Firstly, at typical ambient humidities the PTR-MS is insensitive to glyoxal due to its low PA. Methyl glyoxal and glycolic acid can be detected at their respective protonated parent ion signals.

2.4 Discussion

In this study a PTR-MS was challenged with 25 oxygenated VOCs from a range of compound classes. All but one of these 25 compounds was detectable with PTR-MS including three important multifunctional VOCs (hydroxyacetone, methyl glyoxal and glycolic acid). Thus, PTR-MS appears to be a powerful tool for the detection of oxygenated VOCs, whose presence in the atmosphere has, until recently, been poorly understood.

The major limitation of measurements of VOCs in the atmosphere by PTR-MS is that product ions of the same molecular weight cannot be distinguished. In theory the excess energy deposited in the product ions upon proton transfer from H_3O^+ is considered to be insufficient to result in extensive product ion dissociation. Consequently, the H_3O^+ SRI-MS spectra of the 25 VOCs employed in this study was expected to be simple and predominantly comprised of protonated parent ions detected at m/z equivalent to their molecular weight (MW) plus one.

In practice, the protonated parent ion was rarely the only product ion observed in the PTR-MS spectra of the VOCs employed in this study. Even at E/N of 110 Td there were only two compounds that produced a single product ion (acetone, MEK). Instead, there were multiple reaction processes observed to occur in the drift tube of the PTR-MS including:

- Simple proton transfer yielding product ions with molecular mass plus one due to proton addition;
- Dissociative proton transfer yielding product ions from fragmentation of molecular ions following proton transfer;
- Reactions with $\text{H}_3\text{O}^+(\text{H}_2\text{O})$ reagent ions
- Back reactions with H_2O

In measurements of the atmosphere, the PTR-MS employed in this study is typically operated at E/N of 130 Td to minimise the formation of hydrated product ions ($\text{MH}^+\cdot\text{H}_2\text{O}$). Of the 24 VOCs studied here, there were eight compounds whose protonated parent ion signal was $\geq 90\%$ of their total ion signal at E/N 130 Td, they were formaldehyde (m/z 31), acetaldehyde (m/z 45), acetone (m/z 59), MEK (m/z 73), methanol (m/z 33), formic acid (m/z 47), methyl formate (m/z 61), methyl acetate (m/z 75).

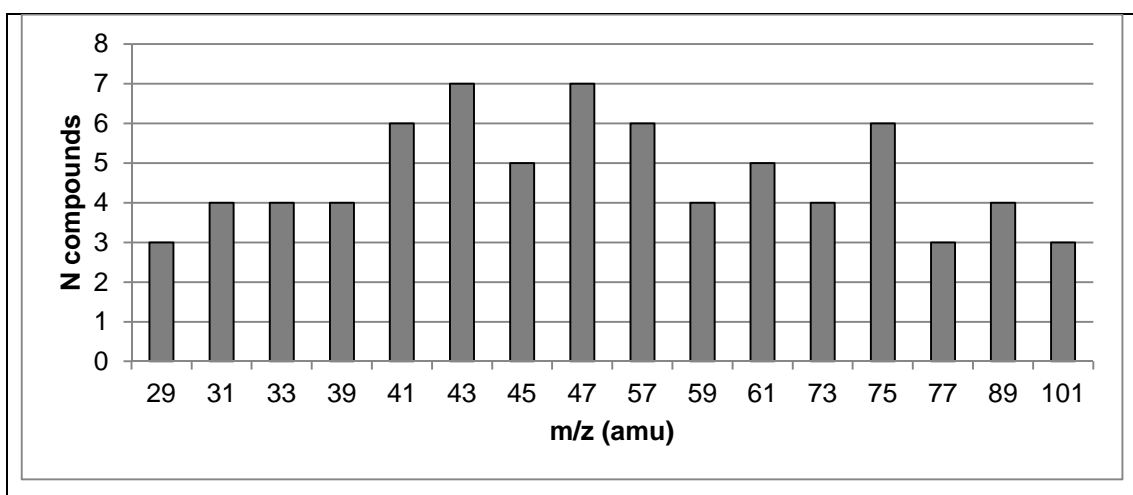


Figure 2.9: Frequency distribution of the number of compounds detected (> 5% TIS) at each m/z.

Figure 2.9 shows a frequency distribution of the number of compounds detected (> 5% TIS) at each m/z. All eight of the compounds listed above had protonated parent ion signals that overlapped product ions of other compounds measured in this study. Thus, in a

hypothetical mixture containing all 25 VOCs, it would not be possible to uniquely measure these 8 compounds at their protonated m/z without interference from other compounds present.

It has been estimated that $> 10^4$ VOC species have been detected in the atmosphere, and this may represent only a fraction of the species actually present (Goldstein & Galbally 2007). Given the complexity of atmospheric VOC composition, in measurements of the atmosphere, PTR-MS must be considered as a low selectivity method. PTR-MS is a tool for high time resolution measurements not a tool for providing detailed speciated VOC measurements. Unequivocal VOC identification requires higher resolution mass spectrometers such as the recently developed PTR- time-of-flight mass spectrometers (Jordan et al. 2009), or co-located techniques with lower time resolutions that are capable of better speciation such as gas chromatography.

The PTR-MS spectra of VOCs employed in this study were determined across a range of operating conditions (E/N). For several compounds the PTR-MS response significantly declined at $E/N > 110$ Td. Previous studies have shown that formaldehyde, ethanol, 2-propanol, and formic acid reaction processes that result in the reproduction of H_3O^+ ions (Hansel et al. 1997, Inomata et al. 2008, Inomata & Tanimoto 2009, Inomata & Tanimoto 2010, Baasandorj et al. 2015). H_3O^+ product ions occur at m/z 19 and are obscured by the PTR-MS reagent ion signals resulting in the apparent low PTR-MS sensitivity to these compounds.

In this study, most compounds showed a decline in TIS of 33 – 75% when E/N was changed from 110 Td to 170 Td, there were several species whose TIS decreased $> 85\%$, including formaldehyde, ethanol, and formic acid. Previous studies have shown the decline in apparent PTR-MS sensitivity to these compounds is due to loss via back reaction in the case of formaldehyde (Hansel et al. 1997, Inomata et al. 2008) and collision induced dissociation resulting in the reproduction of H_3O^+ , in the case of ethanol and formic acid (Inomata & Tanimoto 2009, Baasandorj et al. 2015).

Glyoxal was not detected by PTR-MS in this study and this was attributed to complete loss via back reaction. There were several other species whose TIS declined 80 – 96% when E/N was changed from 110 Td to 170 Td, including MEK, 1-butanol, methyl formate, ethyl formate and hydroxyacetone. These compounds have not been previously reported to undergo reaction processes resulting in reproduction of H_3O^+ or other unmeasured product ions. Thus,

it appears the reproduction of H_3O^+ or other unmeasured ions from protonated VOCs in the PTR-MS may be more widespread than previously reported. These results suggest lower E/N conditions should be employed in PTR-MS measurements of the atmosphere to maximise sensitivity to oxygenated VOCs.

Overall, sensitivity and selectivity are critical factors in the application of PTR-MS to measurements of VOCs in the atmosphere. Simple studies such as those described here provide important information to optimize PTR-MS operation for the sensitive detection of VOCs and are valuable references for interpretation of PTR-MS spectra of the atmosphere.

Chapter 3. Switchable reagent ion - mass spectrometry (SRI-MS): Measurements of certified gas standards containing a range of VOCs.

3.1 Introduction

PTR-MS is a highly sensitive (sub ppb) chemical ionization mass spectrometry technique capable of quantifying VOCs, including many oxygenated VOCs, at high time resolutions (<1 min). The major limitation of measurements of VOCs in complex air matrices by PTR-MS is that product ions of the same nominal molecular weight cannot be distinguished. In the measurement of complex mixtures of VOCs by PTR-MS, the presence of isobaric parent ions, fragment and cluster ions often result in overlapping product ion signals, complicating the interpretation of the mass spectra.

The number of VOCs potentially present in the atmosphere is in excess of 10^4 (Goldstein & Galbally 2007), a significant number of which will produce a response in PTR-MS. Consequently, the interpretation of PTR-MS spectra of the atmosphere is complex and studies of the atmosphere generally only identify and quantitatively measure a limited number of compounds, including isoprene, aromatics and simple oxygenated compounds (e.g. formaldehyde, methanol, acetaldehyde, acetone) that have been shown to be detectable without significant interference (de Gouw et al. 2003, Warneke et al. 2003).

Alternative instrumental systems have been developed to overcome this limitation, notably, the use of high-resolution time-of-flight mass spectrometers (PTR-ToF) (Jordan et al. 2009) that can differentiate between isobaric product ions but not isomers. A second approach is to exploit the use of alternative reagent ions to differentiate compounds on the basis of differences in their ionization reactions or fragmentation products.

The use of multiple reagent ions has been extensively studied with selected ion flow tube mass spectrometry (SIFT-MS) since its inception in the mid-nineties. The reference spectra of hundreds of VOCs have since been determined for these instruments (Smith & Španěl 2005) which has enabled its use in food science, medical and environmental applications (Smith & Španěl 2011).

Despite the fact that the use of reagent ions other than H_3O^+ was proposed in the early development of PTR-MS (Lindinger et al. 1998) the development and application of this technique has only occurred more recently (Wyche et al. 2005, Blake et al. 2006, Norman et al. 2007, Inomata & Tanimoto 2008). These studies have demonstrated the production of a range of reagent ions (H_3O^+ , NO^+ and O_2^+ , NH_4^+ and protonated VOC reagent ions (VOCH^+)) with little to no modification of the PTR-MS instrument. Jordan et al (2009) reported the development of the first commercially available PTR-MS instrument with switchable reagent ion capability (SRI-MS) in which different reagent ion source gases and ion source tuning are used to selectively produce O_2^+ , NO^+ or H_3O^+ in the hollow cathode ion source.

Much of the work to date has focused on the use of alternative reagent ions for the differentiation of isobaric compounds (Lindinger et al. 1998, Wyche et al. 2005, Blake et al. 2008, Inomata & Tanimoto 2008, Knighton et al. 2009, Karl et al. 2012, Lanza et al. 2013, Karl et al. 2014). Other studies have investigated the use of alternative reagent ions in order to detect compounds that do not react with H_3O^+ including the detection of ammonia with O_2^+ (Norman et al. 2007), the detection of alkanes with NO^+ (Inomata et al. 2013), and the use of Kr^+ and Xe^+ reagent ions for the detection of compounds other than VOCs including (CH_4 , CO , CO_2 , N_2O , NO_2 , SO_2) (Sulzer et al. 2012).

It is likely the problems inherent in interpreting PTR-MS mass spectra, using H_3O^+ , will also occur for the mass spectra determined using alternative reagent ions. Further work is required to determine the potential application of multiple reagent ion analysis with SRI-MS, and what, if any, additional information can be acquired through the use of reagent ions other than H_3O^+ in measurements of the atmosphere.

As a start towards this, the performance of the SRI-MS in each reagent ion mode (H_3O^+ , O_2^+ , NO^+) was characterized, via a series of measurements of five of certified gas standards containing in total, 73 atmospherically relevant VOCs, from a range of compound classes including multiple alkanes, alkenes, aromatic hydrocarbons, aldehydes, ketones, chlorobenzenes and terpenoids, as well as acetylene, methanol, acetonitrile, ethyl acetate, and dimethyl sulphide.

A set of rules were developed for the interpretation of the SRI-MS spectra of these complex standard mixtures to determine, which compounds can be detected by the SRI-MS in each reagent ion mode, and of these, which compounds could be detected without significant mass overlap in the SRI-MS spectra of gas mixtures of known composition.

Finally, this chapter presents a characterization of the sensitivity of the SRI-MS in each reagent ion mode (H_3O^+ , NO^+ , and O_2^+). The difference in the empirically derived instrument sensitivities between each reagent ion mode is described in terms of ion-molecule collision theory and our understanding of the mass dependent transmission of ions through a quadrupole mass spectrometer.

3.2 Interpretation of the SRI-MS spectra of mixtures

In the mass spectra of a mixture, the optimum situation is one in which the spectra contain characteristic peaks unique to each of the components present in the sample mixture. In practice, overlapping contributions from two or more components, to peaks in the mass spectra frequently occurs and the interpretation of the mass spectra is complex.

Electron impact mass spectrometry is a well-established technique and methods for the interpretation of EIMS spectra of mixtures of organic compounds are well known. Put simply, the interpretation of the EIMS spectra of organic compound mixtures has been performed by comparing the mass spectra with a series of reference spectra for the individual compounds present. When a component in the mixture is correctly identified, its reference spectrum is subtracted from the spectra of the mixture and the process is then repeated for the residual mass spectra.

The PTR-MS spectra of numerous individual VOCs have been studied using PTR-MS and SIFT-MS systems. However, unlike EIMS, the SRI-MS and SIFT-MS techniques do not generate mass spectra that are highly reproducible between instruments. As a result, the current body of chemical ionization mass spectral data is useful for identifying probable product ions in SRI-MS mass spectra, but the ion abundances cannot be employed to perform “spectrum stripping” as described above for EIMS analyses.

Another major difference with EIMS is that electron impact ionization is capable of ionizing all organic compounds and thus all organic compounds present will be detected in an array of product ion peaks in the mass spectra. In SRI-MS and SIFT-MS, the reaction between the compound and the reagent ion must be thermochemically favourable for ionization reactions to occur. Therefore, dependent upon their thermochemical properties, some compounds will be ionized and mass analyzed by the mass spectrometer, and some compounds will pass through the instrument undetected.

3.2.1 Rules for the interpretation of the mass spectra

Here, a set of logical rules was developed for the interpretation of the SRI-MS spectra of mixtures of known composition. These rules were used to determine, which compounds can be detected by the SRI-MS in each reagent ion mode, and of these, which compounds could be detected without significant mass overlap.

For the following analysis $m/z = x$ refers to a known product ion signal of compound M, that was present in a hypothetical mixture containing multiple components. The rules applied to the mass spectral interpretation are summarized in Figure 3.1 and the underlying logic of each rule is discussed in turn below:

Rule 1: *Chemical ionization reactions between M and R^+ are thermochemically favourable.*

The thermochemistry of the ionization reactions between the analyte and the reagent ions is fundamental to whether or not the SRI-MS is able to detect the analyte. Exothermic chemical ionization reactions are highly efficient (Bouchoux et al 1996), that is a reaction occurs on nearly every collision. In SRI-MS, highly efficient reaction systems are required to gain the high intensity ion signals required for sensitive trace gas detection. If the reaction between a reagent ion and a neutral is not energetically favourable, the product ion signals will either be below the limit of detection; or, trace ion signals will result and the compound will be detected with poor sensitivity.

Thus, if Rule 1 is satisfied we can say that compound M is probably detected by the SRI-MS (and one can proceed to Rule 2). If Rule 1 is not satisfied, refer directly to Rule 5.

Rule 2: *A significant peak at m/z x, a known product ion of M, must be observed in the mass spectra*

If inspection of an independent reference mass spectra of compound M reveals a product ion signal at m/z x, one can say, a known product ion of M occurs at m/z x. If a peak at m/z x was then also observed in the mass spectra of the analyte mixture containing M, it is possible that compound M contributed to the observed peak at m/z x. For the purposes of this study a significant peak was defined as a peak whose intensity was $>0.3\%$ of the total ion signal summed across all m/z .

If Rule 2 is not satisfied, we can say that compound M was not detected at m/z x.

If Rules 1 and 2 are satisfied one can say that m/z x , a known product ion signal of compound M , was probably detected by SRI-MS. It must then be verified if the signal at m/z x is exclusively due to the presence of compound M (Rule 3).

Rule 3: *No other compounds were present with known product ions at m/z x .*

Independent reference spectra of all other compounds present in the analyte mixture must be inspected to determine if any of the other compounds present had known product ion signals at m/z x .

Thus if Rules 1, 2 and 3 are satisfied it can be said that compound M was detected by the SRI-MS, and a known reaction product ion signal at m/z x was observed that can only be attributed to compound M , or in other words, compound M was detected without interference. Conversely, if Rules 1 and 2 are satisfied but Rule 3 is not, we can say that compound M was detected at m/z x with interference.

Rule 4: *Compound M probably contributed $\geq 90\%$ of the ion signal at m/z x .*

Rule 4 is used to determine whether the interference in the measurement of compound M at m/z x was likely to be significant or minor. This is based on the branching ratios observed in the independent reference spectra of all compounds that had product ions at that m/z .

For example, in the case of H_3O^+ SRI-MS, 100 % of the toluene product ion signal, and ~3 % of the C_9 aromatic compound fragment ion signal has been reported to occur at m/z 93 (Gueneron et al. 2015). If these compounds were present in equivalent concentrations it is reasonable to assume toluene contributed $>90\%$ to the total ion signal at m/z 93 and the interference due to fragment ions of C_9 aromatic compounds was minor ($< 10\%$).

Rule 5: *A trace peak at m/z x , a known product ion of M , must be observed in the mass spectra.*

As discussed in relation to Rule 1, if the chemical ionization reaction of compound M with the reagent ion is not energetically favourable, reaction may occur with a low reaction efficiency resulting in a trace ion signal at m/z x .

If Rule 1 and 5 are not satisfied we can say that compound M was not detected at m/z x . Conversely, if Rule 1 is false and Rule 5 is true we can say that compound M was possibly detected at m/z x with poor sensitivity.

We then refer to back to Rule 3 - "no other compounds were present with known product ions at m/z x " - to determine if compound M was possibly detected at m/z x with or without interference.

Overall, for a given compound, M, there are four possible outcomes (decisions) from the procedure outlined above:

- Compound M was detected at $m/z = x$ without interference
- Compound M was detected at $m/z = x$ with minor interference from other compounds present that also produce product ions at $m/z = x$.
- Compound M was detected at $m/z = x$ with significant interference from other compounds present that also produce product ions at $m/z = x$.
- Compound M was not detected at $m/z = x$.

3.2.2 Supplementary Information

The application of these rules requires prior knowledge of:

- the composition of the mixture being analysed
- the mass spectra of the mixture
- the thermochemical threshold for efficient reactions between the reagent ion and each of the components in the mixture
- the thermochemical properties of the reagent ion and the components in the mixture
- individual reference spectra of the products of reaction between the reagent ion and each of the components present in the mixture

In the present study, the rules outlined above were applied to the interpretation of the mass spectra of five certified gas standard mixtures. The prior knowledge required for this procedure was obtained from a variety of sources, which are described in turn below

<i>Decision tree for the detection & identification of compound M, at m/z x, in a gas mixture using CIMS with reagent ion R⁺:</i>											
Prior Knowledge required (see also section 4.2.3 of text):								Decision			
The composition of the analyte gas mixture & the mass spectra of the analyte gas mixture											
The thermochemical constraints of the reaction M + R ⁺ and the thermochemical properties of M and R											
		The reference spectra of compound M							Compound M was :		
				The thermochemical properties and reference spectra of all other components in the analyte gas mixture							
Rule 1 Chemical ionization reactions between M and R ⁺ is thermochemically favourable	TRUE	Rule 2 A significant peak at m/z x, a known product ion of M, was observed in the mass spectra	TRUE	Rule 3 No other compounds were present with known product ions at m/z x	TRUE			Detected at m/z x without inteference			
								FALSE	Rule 4 Compound M probably contributed ≥ 90% of the ion signal at m/z x (see text)	TRUE	Probably detected at m/z x with minor interference
										FALSE	Probably detected at m/z x with significant interference
	FALSE	Rule 5 A trace peak at m/z x, a known product ion of M, was observed in the mass spectra	TRUE	Rule 3 No other compounds were present with known product ions at m/z x	TRUE			Detected at m/z x without interference but with poor sensitvity			
								FALSE		Possibly detected at m/z x with interference and poor sensitvity	
										FALSE	

Figure 3.1: A decision tree summarizing the rules for the interpretation of the SRI-MS spectra of mixtures of known composition.

Firstly, the analyte mixtures employed in this study were certified gas standards and as such their composition was known. Secondly, the mass spectra of each certified gas standard was measured by the SRI-MS in each reagent ion mode.

In the present study, there were three reagent ion systems employed (H_3O^+ , O_2^+ , NO^+) and the thermochemical threshold for efficient reactions between the reagent ion and each of the components in the mixture can be defined for each:

- In the case of H_3O^+ , proton transfer is exothermic when the proton affinity of the analyte is $> \text{PA}(\text{H}_2\text{O})$.
- Charge transfer from O_2^+ to the analyte is exoergic when the ionization energy of the analyte is $< \text{IE}(\text{O}_2)$.
- Charge transfer from NO^+ is exoergic when $\text{IE}(\text{Analyte}) < \text{IE}(\text{NO})$.

The relevant gas phase ion energetic data (proton affinity, ionization energy) for the reagent ions (H_3O^+ , O_2^+ , NO^+) and the analytes employed in this study were sourced from the NIST chemistry web book database (Lias 2015). For some compounds the relevant thermochemical values were unknown, in which case the value was estimated to be simply $<$ or $>$ the threshold value, based on those for closely related compounds. The three reagent ion systems are discussed in more detail in sections 4.4 – 4.6.

In this study, the contribution of a compound to a given m/z in the mass spectra of the gas standard mixtures, was determined via consultation of published reference spectra for each compound present. SRI-MS reference spectra for each component in the gas standards were sourced from the previous chapters in this thesis and the available literature. The literature sources of each reference spectra used are listed in Tables 3.1 – 3.3 below.

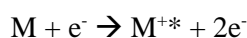
For some compounds, no independent SRI-MS reference spectra were available. In lieu, of SRI-MS reference spectra, the more extensive database of spectra determined in the related SIFT-MS instruments were employed. It is important to note, due to the applied electric field in the drift tube reactor, the ion-molecule collision energies (~ 20 eV) in the SRI-MS are higher than in the flow tube of SIFT-MS instruments. As a result, more extensive product ion fragmentation has been observed in studies using SRI-MS than for SIFT-MS (Blake et al. 2006) and the application of SIFT-MS mass spectral data to predict the products of ion-molecule reactions in the SRI-MS must be treated with caution. For some of the components

studied here, no reference H_3O^+ and NO^+ spectra were available, in which case the product ions and branching ratios of closely related isomers were substituted.

Table 3.1: Sources of reference H_3O^+ spectra for each compound present in the certified gas standards employed in this study.

	Reference	Instrument	Compounds
[1]	This thesis, Chapter 2	SRI-MS	Isoprene Formaldehyde, acetaldehyde Acetone, methyl ethyl ketone Methanol Ethyl acetate Acetonitrile
[2]	Spanel et al. (1997)	SIFT-MS	Acrolein
[3]	Blake et al. (2006)	SRI-MS	Methacrolein
[4]	Maleknia et al. (2007)	PTR-MS	α -pinene, 1,8-cineole
[5]	Gueneron et al. (2015)	PTR-MS	$\text{C}_6 - \text{C}_9$ aromatics
[6]	Jordan et al. (2009)	SRI-MS	Chlorobenzenes
[7]	Warneke et al. (2003)	PTR-MS	C_{10} aromatics Dimethyl sulphide
[8]	Wilson et al. (2003)	SIFT-MS	$\text{C}_2 - \text{C}_4$ alkanes, alkenes, alkynes
[9]	Spanel & Smith (1998b)	SIFT-MS	$\text{C}_4 - \text{C}_9$ alkanes, alkenes
[10]	Erickson et al. (2014)	PTR-MS	$\text{C}_{11} - \text{C}_{12}$ alkanes

In the case of O_2^+ the mass spectra of VOCs generated by O_2^+ SRI-MS often resemble the spectra obtained by electron ionization mass spectrometry (EI-MS) a ‘harder’ ionization process in which electrons accelerated to $\sim 70\text{eV}$ are used to ionize the sample by removing an electron.



Again, due to differences in the ionization energy and processes, using EIMS mass spectra to predict the products of ion-molecule chemistry in the O_2^+ SRI-MS must also be treated with caution. Nevertheless, one can assume the products of charge transfer to a given VOC in SRI-MS will share characteristics with both the lower energy SIFT-MS and higher energy EI-MS mass spectra for the given compound. When applying the rules listed in Figure 3.1 for interpreting the O_2^+ SRI-MS spectra in this study, SIFT-MS or EI-MS reference spectra (Stein 2005) were used in lieu of O_2^+ SRI-MS reference data.

Table 3.2: Sources of reference O_2^+ spectra for each compound present in the certified gas standards employed in this study.

	Reference	Instrument	Compounds
[1]	Spanel et al. (1997)	SIFT-MS	Formaldehyde, Acrolein Methyl ethyl ketone
[2]	Ionicon (2009) unpublished	SRI-MS	Methanol
[3]	Blake et al. (2006)	SRI-MS	Benzene, toluene Acetaldehyde Acetone Ethyl acetate Acetonitrile
[4]	Schoon et al. (2003)	SIFT-MS	α -pinene,
[5]	Spanel & Smith (1998b)	SIFT-MS	$C_4 - C_{12}$ alkanes, $C_4 - C_5$ alkenes Isoprene
[6]	Jordan et al. (2009)	SRI-MS	Chlorobenzenes
[7]	Spanel et al. (1998a)	SIFT-MS	Dimethyl sulphide
[8]	Amelnyck et al. (2005)	SIFT-MS	1,8-cineole
[9]	Cappellin et al. (2014)	SRI-MS	Ethene
[10]	Wilson et al. (2003)	SIFT-MS	Acetylene $C_2 - C_3$ alkanes, $C_3 - C_4$ alkenes
[11]	Diskin et al. (2002)	SIFT-MS	hexene
[12]	Labsyft software suite	SIFT-MS	$C_6 - C_9$ alkanes
[13]	NIST chemistry web book (Stein 2005)	EIMS	$C_6 - C_{12}$ alkanes $C_6 - C_7$ cycloalkanes Styrene, $C_9 - C_{10}$ aromatics

Table 3.3: Sources of reference NO⁺ spectra for each compound present in the certified gas standards employed in this study.

	Reference	Instrument	Compounds
[1]	Spanel et al. (1997)	SIFT-MS	Formaldehyde, acetaldehyde, acrolein methyl ethyl ketone
[2]	Spanel & Smith (1997)	SIFT-MS	Methanol
[3]	Ionicon (2009) unpublished	SRI-MS	Formaldehyde Methanol
[4]	Blake et al. (2006)	SRI-MS	Benzene, toluene Acetaldehyde, methacrolein Acetone Ethyl acetate Acetonitrile
[5]	Michel et al. (2005)	SIFT-MS	Methacrolein
[6]	Spanel & Smith (1998c)	SIFT-MS	Acetonitrile
[7]	Schoon et al. (2003)	SIFT-MS	α -pinene,
[8]	Spanel & Smith (1998b)	SIFT-MS	C ₄ – C ₁₂ alkanes, C ₄ – C ₅ alkenes Isoprene Xylene, trimethylbenzene
[9]	Jordan et al. (2009)	SRI-MS	Chlorobenzenes
[10]	Spanel et al. (1998a)	SIFT-MS	Dimethyl sulphide
[11]	Karl et al. (2012)	SRI-MS	Isoprene
[12]	Amelnyck et al. (2005)	SIFT-MS	1,8-cineole
[13]	Wilson et al. (2003)	SIFT-MS	C ₂ – C ₄ alkanes, C ₂ – C ₄ alkenes
[14]	Inomata et al. (2013)	SRI-MS	C ₃ – C ₄ alkanes

3.3 Methodology

The instrument employed in this work was a commercially built PTR-MS (Ionicon Analytik GmbH, Innsbruck, Austria) modified with the addition of a switchable reagent ion source system to enable the use of NO⁺ and O₂⁺ reagent ions in addition to H₃O⁺. A detailed description of PTR-MS instruments and their application was provided in Chapter 1 of this thesis and in Ellis and Mayhew (2014) and a description of the switchable reagent ion system is provided in Jordan et al (2009).

Briefly, in the hollow cathode ion source, the relevant source gas was ionized by electron impact to produce the desired reagent ions: H₃O⁺, O₂⁺ and NO⁺. The H₃O⁺ reagent ions were

produced from water vapour introduced at a flow of ~ 6 mL/min (STP). The source gas for the O_2^+ reagent ions was UHP O_2 (BOC, Australia) introduced to the ion source at a flow rate of 5 mL/min (STP). The source gas for the NO^+ reagent ions was a combination of UHP O_2 and UHP N_2 (BOC, Australia) introduced to the ion source at flow rates of 5.0 mL min^{-1} (STP) and 3.8 mL min^{-1} (STP), respectively.

The hollow cathode ion source generated high intensity ion signals (10^7 cps) in all three reagent ion modes. The mean ion signals and the relative concentration of trace impurity ions for each reagent ion system are listed in Table 3.4. The ion source was tuned to produce the primary reagent ions with a purity of $>95\%$ but there were always other ions present in trace amounts in the reagent ion matrix as a result of air back-streaming into the ion source and the humidity of the sampled air. The presence of these trace impurity reagent ions complicate the SRI-MS spectra, as they also undergo chemical ionization reactions with VOCs present in the reagent–analyte matrix.

The intense ion signals of the primary reagent ions H_3O^+ , O_2^+ and NO^+ overwhelm the ion detection system and shorten the lifetime of the secondary electron multiplier (SEM). In order to avoid this, the ion isotopes of the reagent ion were measured rather than the primary ion signal: $\text{H}_3^{18}\text{O}^+$ detected at m/z 21 was multiplied by 500 to approximate the H_3O^+ signal at m/z 19; $^{15}\text{NO}^+$, detected at m/z 31, was multiplied by 274 to approximate the NO^+ signal at m/z 30; and, $^{18}\text{O}^{16}\text{O}^+$, detected at m/z 34 was multiplied by 250 to approximate the $^{16}\text{O}_2^+$ signal at m/z 32. Likewise, the ion isotopes of impurity reagent ions were measured rather than the primary ion signal: $\text{H}_3^{18}\text{O}^+(\text{H}_2\text{O})$ or $\text{H}_3\text{O}^+(\text{H}_2^{18}\text{O})$ was detected at m/z 39 was multiplied by 250 to approximate the $\text{H}_3\text{O}^+(\text{H}_2\text{O})$ signal; and $\text{N}^{18}\text{O}_2^+$ detected at m/z 48 was multiplied by 250 to approximate the NO_2^+ signal.

Table 3.4: Primary reagent ion signals and the relative concentration of impurity ions. Also listed are the ionization energies (IE) and proton affinities (PA) of primary and impurity reagent ions.

Primary reagent ion	Mean primary reagent ion signal (cps)	Impurity reagent ions	MW	PA (kJ mol ⁻¹)	IE (eV)	% primary reagent ion signal
H ₃ O ⁺	2.8 ± 0.1 × 10 ⁷	O ₂ ⁺	32	421	12.07	2.9 – 3.5%
		NO ⁺	30	532	9.26	0.4 – 0.6%
		H ₃ O ⁺ (H ₂ O)	37	808	-	1.5 – 6.0%
O ₂ ⁺	4.3 ± 0.1 × 10 ⁷	H ₃ O ⁺	19	691	-	2.2 – 7.0 %
		NO ⁺	30	531	9.26	4.6 – 5.4%
		NO ₂ ⁺	46	591	9.59	0.4 – 0.6%
NO ⁺	5.0 ± 0.2 × 10 ⁷	H ₃ O ⁺	19	691	-	0.2 – 0.3%
		O ₂ ⁺	32	421	12.07	0.6 – 1.1%
		NO ₂ ⁺	46	591	9.59	4.8 – 8.2%

In the present study, the drift tube was operated at 60°C and an applied voltage of 445 V. The pressure in the reactor was 2.16 mbar when sampling in H₃O⁺ mode (E/N 102 Td), 2.26 mbar in NO⁺ mode (E/N 97 Td) and 2.23 mbar in O₂⁺ mode (E/N 99 Td).

The reagent ions and analytes underwent chemical ionization reactions in the drift tube and the resultant product ions were detected downstream by a quadrupole mass spectrometer and secondary electron multiplier. The SRI-MS quadrupole continuously scanned 181 masses between 14 and 200 amu. The dwell time for a single mass measurement was 1 second, generating a full mass scan approximately every 3 minutes.

The PTR-MS operated with the aid of a custom built auxiliary system that regulated the flow of air in the sample inlet and controlled whether the PTR-MS was sampling ambient or zero air or calibration gas. Zero readings were made by diverting the sample air through a zero furnace (350°C) with a platinum wool catalyst that destroyed VOCs in the air before it entered the PTR-MS. Zero measurements were conducted prior to calibration measurements in each reagent ion mode. All ion signals from the calibration gas measurements referred to in this chapter were background corrected.

The stability and purity of the NO⁺ plasma is more sensitive to the operating conditions of the ion source than the H₃O⁺ plasma (Knighton et al. 2009). In the present study, the hollow cathode ion source was operated with a discharge current of 4.8 mA which was optimized for H₃O⁺ production. At the time, it was not possible to automatically change the discharge current on the ion source during measurement. The production of a stable NO⁺ plasma in the

hollow cathode ion source requires a higher discharge current (~ 6 mA). As a result of the sub-optimal NO^+ ion source settings, the instrument background was high and unstable during NO^+ measurement periods.

There are no known compounds that contribute to the signal at m/z 25, and it is commonly regarded as a measure of the background ‘noise’ in the ion signal. This ‘noise’ may result from dark counts, or from light escaping the ion source and travelling into the detection system.

The m/z 25 ion signal exhibited a steady decrease over each NO^+ measurement period. Consequently, the instrument background was lower during the zero measurements than in the preceding ambient measurement period. Consequently, an additional background correction, based on the relative signals of m/z 25 during zero and calibration measurements, was applied to the NO^+ calibration data to account for this. There were also several occasions during measurement in which the NO^+ plasma became unstable and the reagent ion signal “dropped out”. These measurement periods were excluded from the following analysis.

Following this study, further modification of the SRI-MS instrument has allowed the automatic switching of the source current when switching between reagent ion source gases.

Multiple measurements of certified gas standards were performed with the SRI-MS in H_3O^+ , O_2^+ and NO^+ mode. For each measurement a set flow of $10 - 20 \text{ mL min}^{-1}$ of the certified gas standard was diluted in a flow of 1500 mL min^{-1} of ambient air that had been passed through the zero furnace and delivered to the SRI-MS inlet. This zero air had the same mole fractions of H_2O and CO_2 as the ambient air being sampled, neglecting minor contributions from the oxidation of VOCs present.

Table 3.5: The contents of calibration standards 1 – 3 employed in this study

Calibration Gas 1		Calibration Gas 2	
Methanol	CH ₃ OH	Formaldehyde	CH ₂ O
Acetonitrile	CH ₃ CN	Acetone	C ₃ H ₆ O
Acetaldehyde	C ₂ H ₄ O		
Acrolein	C ₃ H ₄ O	Calibration Gas 3	
Acetone	C ₃ H ₆ O	Acetone	C ₃ H ₆ O
Methacrolein	C ₄ H ₆ O	Dimethyl sulphide	C ₂ H ₆ S
Methyl ethyl ketone	C ₄ H ₈ O	Isoprene	C ₅ H ₈
α-pinene	C ₁₀ H ₁₆	Ethyl acetate	C ₄ H ₈ O ₂
Benzene	C ₆ H ₆	1,8-cineole	C ₁₀ H ₁₈ O
Toluene	C ₇ H ₈		
m-xylene	C ₈ H ₁₀		
1,3,5-trimethylbenzene	C ₉ H ₁₂		
Chlorobenzene	C ₆ H ₅ Cl		
1,2-dichlorobenzene	C ₆ H ₄ Cl ₂		
1,2,4-trichlorobenzene	C ₆ H ₃ Cl ₃		

The components, of each gas standard are listed in Tables 3.5 – 3.6. Calibration gas 1 was supplied by AiR Environmental Inc, calibration gases 2-4 were supplied by AirLiquide-Scott Specialty Gases and calibration gas 5 was a PAMS Standard supplied by Spectra gases. Each component was present in the standard at a VMR of ~1 ppmv. The stated accuracy for each component in the standards was $\pm 5\%$.

A series of measurements of gas standards 1- 4 were undertaken as part of a larger field study (Cope et al. 2014). At a later date additional measurements of calibration gases 1 and 5 were performed with the SRI-MS in H₃O⁺ and O₂⁺ reagent ion mode. Calibration gas 5 was not measured using NO⁺ reagent ion mode.

Table 3.6: The hydrocarbon compounds present in calibration gases 4 and 5 employed in this study.

Compound			Cal Gas	Compound			Cal Gas
Acetylene	C ₂ H ₂	5		2,2,4-trimethylpentane	C ₈ H ₁₈	5	
Ethene	C ₂ H ₄	4, 5		2,3,4-trimethylpentane	C ₈ H ₁₈	5	
Ethane	C ₂ H ₆	4, 5		n-heptane	C ₇ H ₁₆	5	
Propene	C ₃ H ₆	4, 5		Methylcyclohexane	C ₇ H ₁₄	5	
Propane	C ₃ H ₈	4, 5		2-methylheptane	C ₈ H ₁₈	5	
1-butene	C ₄ H ₈	5		3-methylheptane	C ₈ H ₁₈	5	
cis-2-butene	C ₄ H ₈	4, 5		n-octane	C ₈ H ₁₈	5	
trans-2-butene	C ₄ H ₈	4		Nonane	C ₉ H ₂₀	5	
Isobutane	C ₄ H ₁₀	5		n-decane	C ₁₀ H ₂₂	5	
n-butane	C ₄ H ₁₀	4, 5		n-undecane	C ₁₁ H ₂₄	5	
Isoprene	C ₅ H ₈	4, 5		n-dodecane	C ₁₂ H ₂₆	5	
1-pentene	C ₅ H ₁₀	5		Benzene	C ₆ H ₆	5	
trans-2-pentene	C ₅ H ₁₀	4, 5		Toluene	C ₇ H ₈	5	
cis-2-pentene	C ₅ H ₁₀	4, 5		Styrene	C ₈ H ₈	5	
Isopentane	C ₅ H ₁₂	4, 5		Ethylbenzene	C ₈ H ₁₀	5	
n-pentane	C ₅ H ₁₂	4, 5		p-xylene	C ₈ H ₁₀	5	
2,2-dimethylbutane	C ₆ H ₁₄	5		m-xylene	C ₈ H ₁₀	5	
2,3-dimethylbutane	C ₆ H ₁₄	5		o-xylene	C ₈ H ₁₀	5	
2-methylpentane	C ₆ H ₁₄	5		Isopropylbenzene	C ₉ H ₁₂	5	
3-methylpentane	C ₆ H ₁₄	5		n-propylbenzene	C ₉ H ₁₂	5	
1-hexene	C ₆ H ₁₂	5		m-ethyltoluene	C ₉ H ₁₂	5	
n-hexane	C ₆ H ₁₄	5		p-ethyltoluene	C ₉ H ₁₂	5	
Methylcyclopentane	C ₆ H ₁₂	5		o-ethyltoluene	C ₉ H ₁₂	5	
2,4-dimethylpentane	C ₇ H ₁₆	5		1,3,5-trimethylbenzene	C ₉ H ₁₂	5	
Cyclohexane	C ₆ H ₁₂	5		1,2,4-trimethylbenzene	C ₉ H ₁₂	5	
2-methylhexane	C ₇ H ₁₆	5		1,2,3-trimethylbenzene	C ₉ H ₁₂	5	
2,3-dimethylpentane	C ₇ H ₁₆	5		m-diethylbenzene	C ₁₀ H ₁₄	5	
3-methylhexane	C ₇ H ₁₆	5		p-diethylbenzene	C ₁₀ H ₁₄	5	

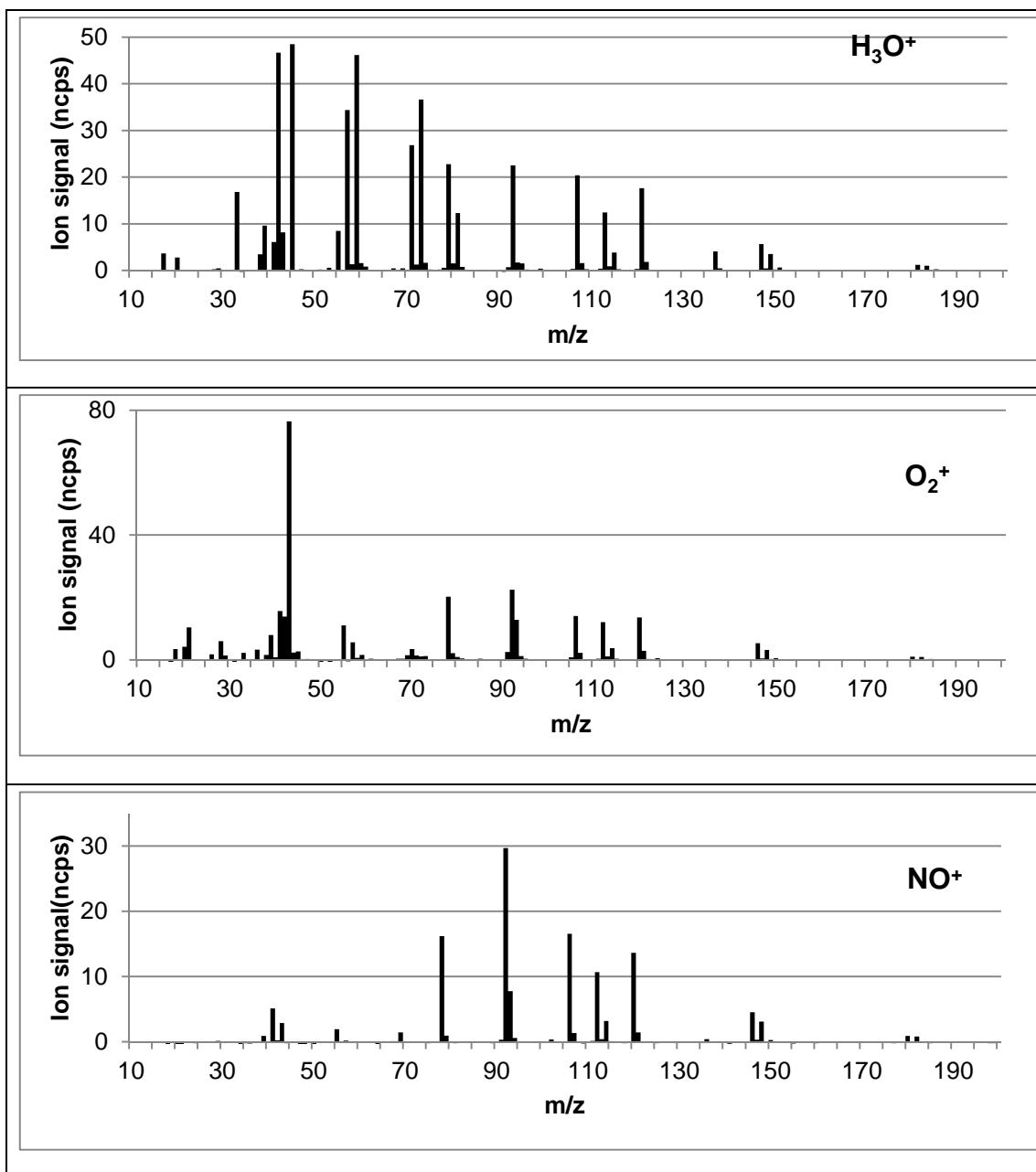


Figure 3.2: Mass spectra, for each reagent ion mode, of calibration gas 1 methanol, acetonitrile, acetaldehyde, acrolein, acetone, methacrolein, methyl ethyl ketone, benzene, toluene, *m*-xylene, 1,3,5-trimethylbenzene, alpha-pinene, chlorobenzene, 1,2-dichlorobenzene, 1,2,4-trichlorobenzene.

Note: in Figures 3.2 – 3.6 H₃O⁺ measurements occurred at E/N 102 Td, O₂⁺ measurements occurred at E/N 99 Td, and NO⁺ measurements occurred at E/N 97 Td.

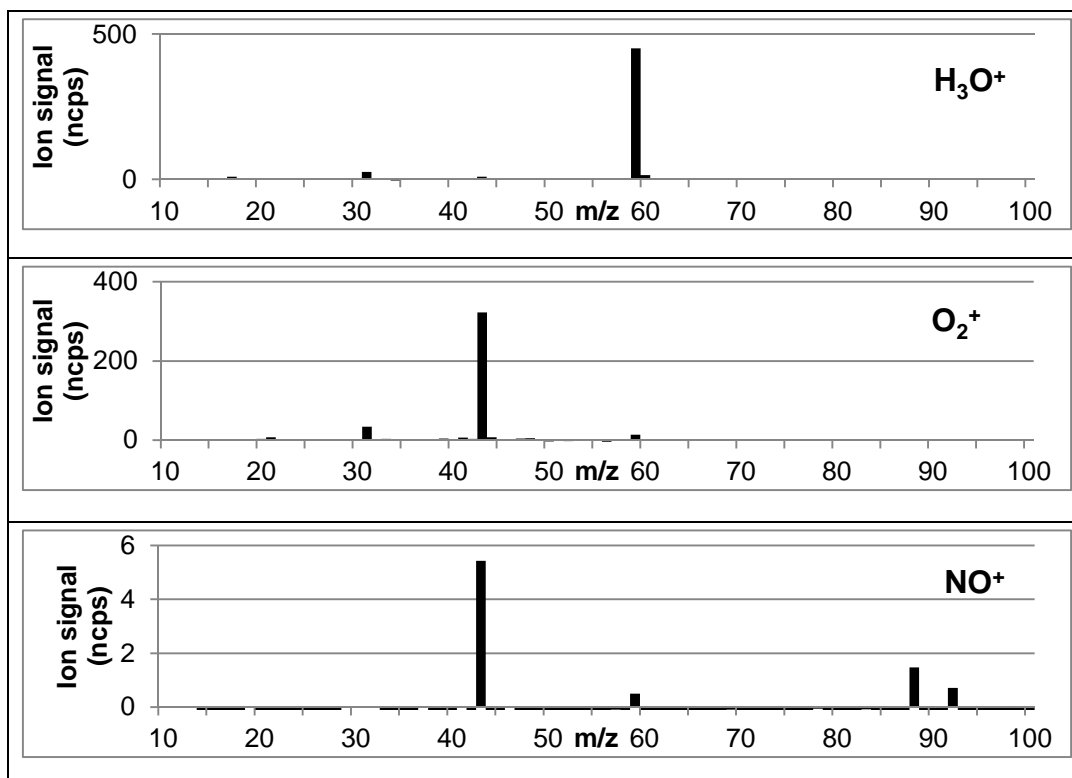


Figure 3.3: Mass spectra, for each reagent ion mode, of calibration gas 2 containing formaldehyde and acetone.

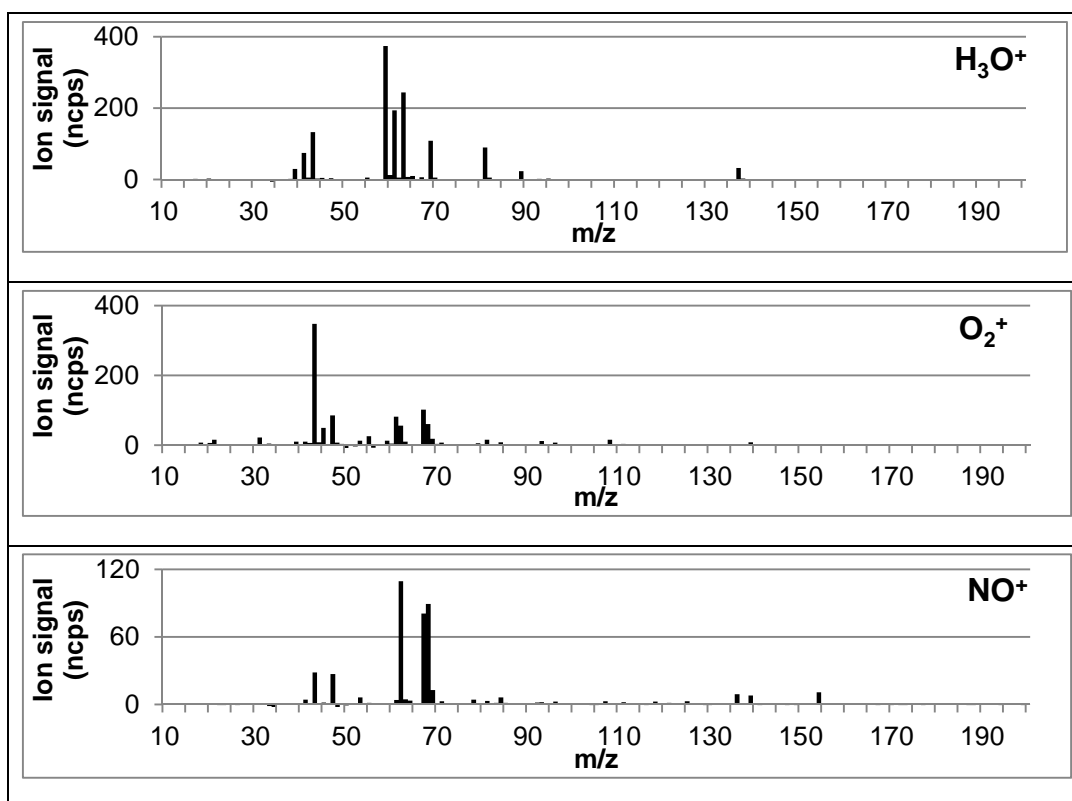


Figure 3.4: Mass spectra, for each reagent ion mode, of calibration gas 3 containing acetone, dimethyl sulphide, isoprene, ethyl acetate, and 1,8-cineole.

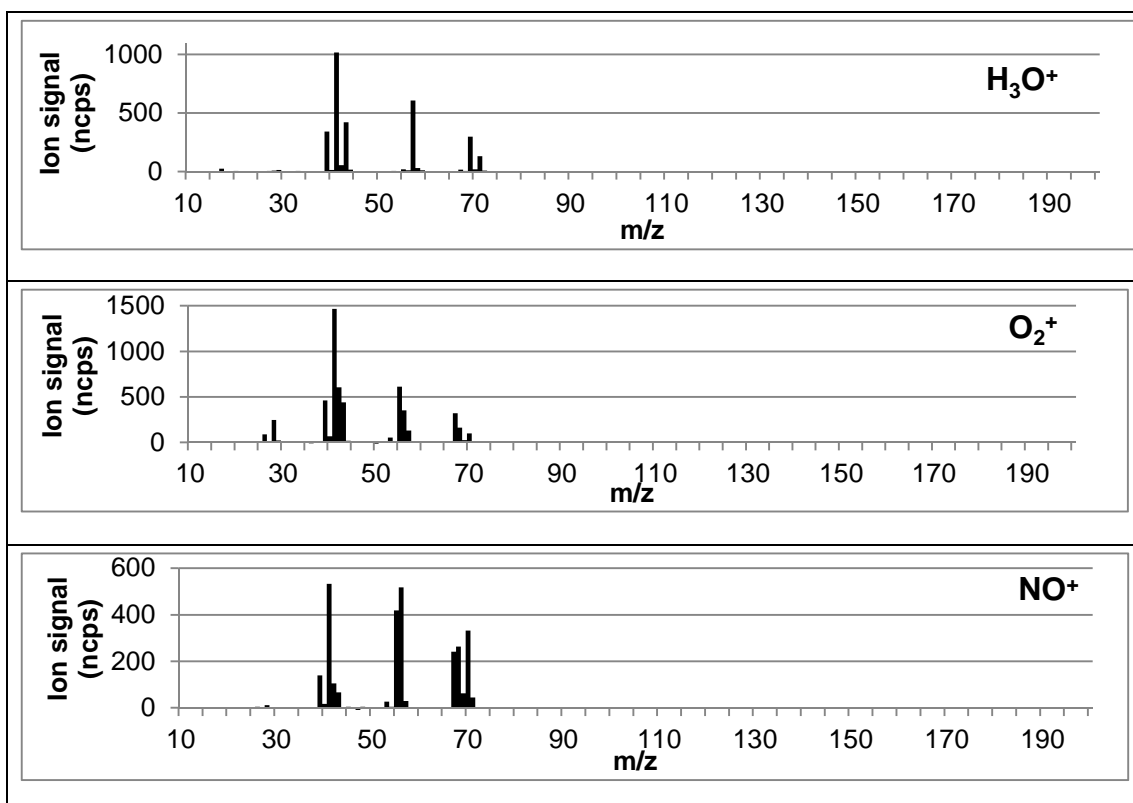


Figure 3.5: Mass spectra, for each reagent ion mode, of calibration gas 4 containing 12 C₂ – C₅ alkanes and alkenes.

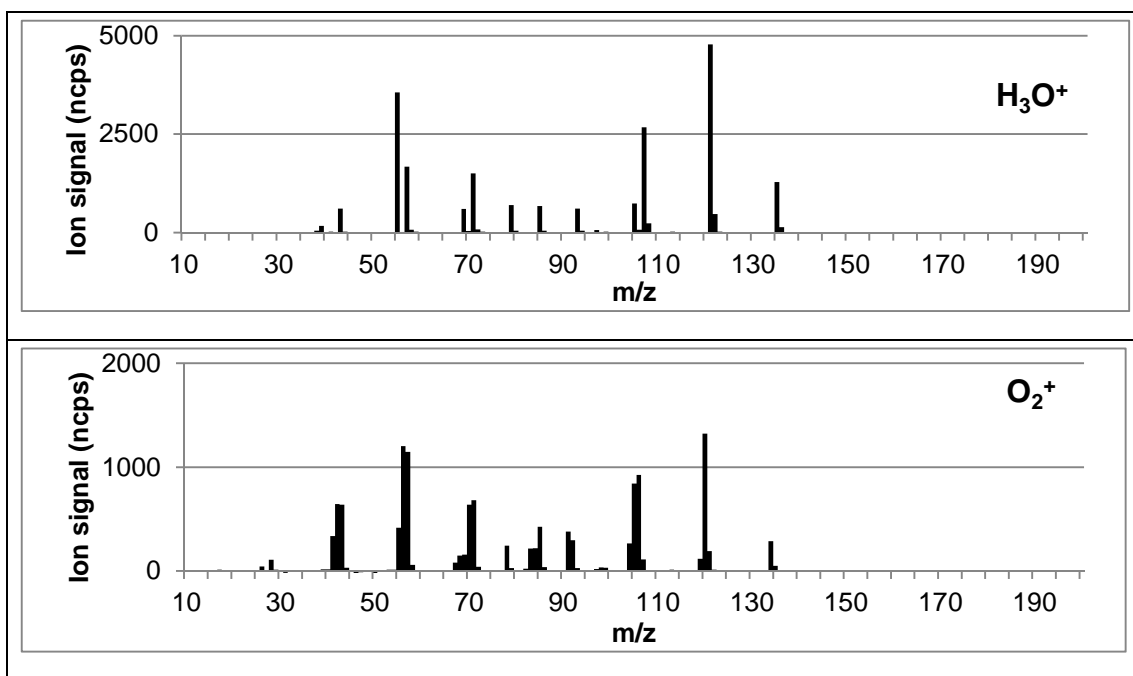


Figure 3.6: Mass spectra, for each reagent ion mode, of a calibration standard containing 55 hydrocarbons including C₂ – C₁₂ alkanes and alkenes, and C₆ – C₁₀ aromatics. This standard was not measured using NO⁺ reagent ion mode.

3.4. SRI-MS measurements of certified gas standards with H_3O^+

The rules for mass spectral interpretation described in section 3.2, were applied to the H_3O^+ SRI-MS spectra of the five calibration gases to determine the compounds that can be detected by the H_3O^+ SRI-MS, and of these, which compounds could be unambiguously identified without significant mass overlap in the H_3O^+ SRI-MS spectra of gas mixtures of known composition.

Rule 1 (Figure 3.1) stated, “Chemical ionization reactions between M and R^+ is thermochemically favourable”. In the case of H_3O^+ SRI-MS, hydronium ions will undergo efficient proton transfer ionization reactions with any compound that has a proton affinity $>$ the $\text{PA}(\text{H}_2\text{O})$. Thus Rule 1 is restated as:

Rule 1: The $\text{PA}(\text{M}) > \text{PA}(\text{H}_2\text{O})$

The PA of a range of VOCs is plotted versus the PA of water in Figure 3.7. Clearly, almost all VOCs are expected to react with H_3O^+ with the notable exception of acetylene, ethene, and alkanes ($< \text{C}_4$).

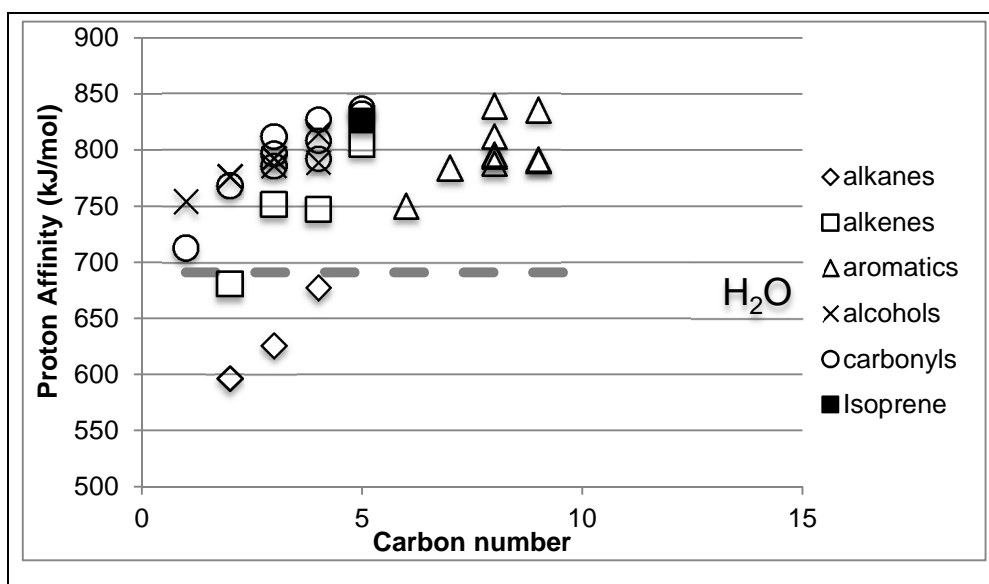


Figure 3.7: The proton affinity (PA) of a range of VOCs in relation to the PA of H_2O . If the $\text{PA}(\text{VOC})$ is $> \text{PA}(\text{H}_2\text{O})$ proton transfer from H_3O^+ reagent ions will occur

The PA of each compound in the gas standards employed in this study are included in Tables 3.7 – 3.12. For some compounds the proton affinity was unknown, in which case the PA was estimated to be simply $<$ or $> \text{PA}(\text{H}_2\text{O})$ based on the proton affinity of closely related

compounds. For example with reference to Figure 3.7 an alkane compound $\leq C_4$ with an unknown PA, can be assumed to have a $PA < PA(H_2O)$. Whereas, for an aromatic compound whose PA is unknown it is reasonable to assume the PA is $> PA(H_2O)$.

Proton transfer is considered a “soft” ionization process. The PA of most VOCs is in the range of 700 - 850 kJ mol⁻¹, and only a small amount of excess energy is deposited in the product ion upon proton transfer from H₃O⁺ which limits dissociation of the excited nascent protonated molecular ion. Consequently, The H₃O⁺ SRI-MS spectra of the VOCs studied were expected to be simple and predominantly comprised of protonated parent ions (MH⁺) detected at m/z equivalent to their molecular weight (MW) plus one. The SRI-MS mass spectra of calibration gases 1- 5 are shown in Figures 3.2 – 3.6.

The number of compounds present in each gas standard analyzed and the number of compounds that were detected by the H₃O⁺ SRI-MS are shown in Table 3.7. The H₃O⁺ SRI-MS detected 50 out of the 73 compounds studied. In order to identify the major reaction processes occurring in H₃O⁺ SRI-MS, the different types of reaction products identified were listed, and the number of compounds that yielded each product ion type was determined. These are also shown in Table 3.7.

From Table 3.7 it is clear that the protonated parent ion was the most frequently detected reaction product across all of the H₃O⁺ mass spectra, with some minor fragmentation products also observed. Calibration gases 1 – 4 contained mostly simple, short chain VOCs (C₁ – C₅) and aromatic compounds. These compounds are not prone to extensive fragmentation, and as a result fewer fragmentation products were identified in the mass spectra of calibration gases 1 - 4. Conversely, a larger number fragment ions were detected in the mass spectra of calibration gas 5, as it contained a significant number of more labile, long chain VOCs ($> C_5$).

Table 3.7: The number and types of reaction products identified in the H_3O^+ SRI-MS spectra of calibration gases 1-5.

	Calibration Gas				
	1	2	3	4	5
Components	OVOCs Aromatics α -pinene acetonitrile	HCHO Acetone	Isoprene DMS Ethyl acetate 1,8-cineole	Isoprene C_2-C_5 alkanes & alkenes	Isoprene C_2-C_{12} alkanes C_2-C_6 alkenes C_6-C_{10} aromatics
VOCs measured	15	2	5	12	55
VOCs detected	15	2 (1)	5	8 (6)	50 (28)
<i>Number of compounds that yielded each product ion type</i>					
MH^+	15	2 (1)	4	7 (6)	27 (25)
$(M-H)^+$	1			2 (1)	9 (3)
$(M-CH)^+$				2	
$(M-CH_3)^+$				2	17 (8)
$(M-C_nH_{2n-1})^+$	2		2	2	15 (12)
$(M-C_nH_{2n+1})^+$					18 (1)
$(M-C_nH_{n-1})^+$					8
$(M-CHO)^+$	1				
$(M-C_nH_{2n+1}O)^+$			2		
$(MH-H_2O)^+$			1		
$MH^+(H_2O)$					1 (0)

Note: The number in brackets represents the number of compounds detected with good sensitivity.

The known product ions for each compound studied and the results of the mass spectral interpretation for each calibration gas mixture are summarized in Tables 3.8- 3.13 and are discussed in turn below.

Calibration Gas 1: The H_3O^+ SRI-MS spectra of calibration gas 1 is shown in Figure 3.2 and the results of the mass spectral interpretation of each component in Calibration gas 1 are listed in Table 3.8. All of the compounds in calibration gas 1 were detected at their respective protonated molecular ion (MH^+) m/z .

Based on their known product ions and proton affinities, fifteen compounds were detected without interference, including: methanol (m/z 33), acetonitrile (m/z 42), acetaldehyde (m/z 45), acrolein (m/z 57), acetone (m/z 59), methacrolein (m/z 71), methyl ethyl ketone (MEK) (m/z 73), α -pinene (m/z 137, 95, 81), benzene (m/z 79), toluene (m/z 93), m -xylene (m/z 107), trimethyl benzene (m/z 121), chlorobenzene (m/z 113), dichlorobenzene (m/z 147),

trichlorobenzene (m/z 181). Combined, these ion signals constituted 89% of the total ion signal (TIS) observed in the mass spectra of calibration gas 1.

The peak at m/z 43 contained contributions from acetaldehyde and methacrolein fragment ions. The sum of these ion signals constituted 1% of the TIS observed in calibration gas 1. Isotopic ion signals contributed an additional 5% of the TIS of calibration gas 1, with the remaining 4% of TIS unidentified

Table 3.8: The outcome of the mass spectral interpretation procedure (Figure 3.1) for the H_3O^+ Spectra of Calibration Gases 1 and 2. The numbered references are listed in Table 3.1.

Compound	PA kJ mol^{-1}	MW	m/z	Product ion	Decision	Ref
Formaldehyde	712.9	30	31	MH^+	Detected without interference but with poor sensitivity	[1]
Methanol	754.3	32	33	MH^+	Detected without interference	[1]
			31 51	$(M-H)^+$	Not detected	
Acetaldehyde	768.5	44	45	MH^+	Detected without interference	[1]
			43	$(M-H)^+$	Probably detected with significant interference	
			63	$MH^+ \cdot H_2O$	Not detected	
Acrolein	797.0	56	57	MH^+	Detected without interference	[2]
Acetone	812.0	58	59	MH^+	Detected without interference	[1]
Methacrolein	808.7	70	71 41	MH^+ $(M-CHO)^+$	Detected without interference	[3]
			43	$(M-C_2H_3)^+$	Probably detected with significant interference	
Methyl ethyl ketone	827.3	72	73	MH^+	Detected without interference	[1]
Acetonitrile	779.2	41	42	MH^+	Detected without interference	[1]
Alpha-pinene	>PA (H_2O)	137	81	$(M-C_4H_7)^+$	Detected without interference	[4]
			95	$(M-C_3H_5)^+$		
			137	MH^+		

Table 3.8(cont)

Compound	PA kJ mol ⁻¹	MW	m/z	Product ion	Decision	Ref
Benzene	750.4	78	79	MH ⁺	Detected without interference	[5]
Toluene		92	93	MH ⁺	Detected without interference	[5]
m-xylene	812.1	106	107	MH ⁺	Detected without interference	[5]
Trimethylbenzene	836.2	120	121	MH ⁺	Detected without interference	[5]
Chlorobenzene	753.1	112	113 115	MH ⁺ ³⁷ Cl MH ⁺	Detected without interference	[6]
Dichlorobenzene	>PA (H ₂ O)	146	147 149	MH ⁺ ³⁷ Cl MH ⁺	Detected without interference	[6]
Trichlorobenzene	>PA (H ₂ O)	180	181 183	MH ⁺ ³⁷ Cl MH ⁺	Detected without interference	[6]

Calibration gas 2: contained formaldehyde and acetone. The H₃O⁺ SRI-MS mass spectra of calibration gas 2 is shown in Figure 3.3 and the results of the mass spectral interpretation of each component are listed in Table 3.8. Consistent with the results for calibration gas 1, acetone was sensitively detected at m/z 59 without interference.

Protonated formaldehyde was detected without interference at m/z 31, however only a small peak was observed in the mass spectra in Figure 3.3. The measurement of formaldehyde by H₃O⁺ SRI-MS is complex as its proton affinity is only slightly greater than the proton affinity of water and loss via back reaction in humid air is non-negligible (Inomata et al. 2008). Consequently, the H₃O⁺ SRI-MS sensitivity to formaldehyde is low and the response is humidity dependent.

The sum of the ion signals at m/z 31 and 59 comprised 91% of the TIS observed in the mass spectra of calibration gas 2 with an additional 5% attributable to the ¹³C and ¹⁸O isotopes of acetone at m/z 60 and 61. The remaining 4% of the TIS was unidentified.

Calibration Gas 3: The H₃O⁺ SRI-MS mass spectra of calibration gas 3 is shown in Figure 3.4 and the results of the mass spectral interpretation of each component are listed in Table 3.9. All of the compounds in calibration gas 3, with the exception of 1,8-cineole, were detected at their respective protonated molecular ion (MH⁺), without interference, including:

acetone (m/z 59), dimethyl sulphide (DMS) (m/z 63), isoprene (m/z 69), and ethyl acetate (m/z 89). 1,8-cineole (MW = 154) was detected without interference at its fragment ion signals at m/z 137 and 81.

Combined the ion signals at these m/z contributed 96% of the TIS observed in the mass spectra of calibration gas 3 with an additional 4% attributed to the ^{13}C and ^{18}O isotopes of these compounds.

Table 3.9: The outcome of the mass spectral interpretation procedure (Figure 3.1) for the H_3O^+ Spectra of Calibration Gas 3. The numbered references are listed in Table 3.1.

Compound	PA kJ mol^{-1}	MW	m/z	Product ion	Decision	Ref
Acetone	812.0	58	59	MH^+	Detected without interference	[1]
Dimethyl sulphide	830.9	62	63	MH^+	Detected without interference	[7]
Isoprene	826.4	68	69 41	MH^+ $(\text{M}-\text{C}_2\text{H}_3)^+$	Detected without interference	[1]
Ethyl Acetate	835.7	88	89 61 43	MH^+ $(\text{M}-\text{C}_2\text{H}_3)^+$ $(\text{M}-\text{C}_2\text{H}_5\text{O})^+$	Detected without interference	[1]
1,8-cineole	>PA (H_2O)	154	137 95 81	$(\text{MH}-\text{H}_2\text{O})^+$ $(\text{M}-\text{C}_3\text{H}_7\text{O})^+$ $(\text{M}-\text{C}_4\text{H}_9\text{O})^+$	Detected without interference	[4]
			155 93	MH^+ $(\text{M}-\text{C}_3\text{H}_9\text{O})^+$	Not detected	

Calibration Gas 4: contained 11 $\text{C}_2 - \text{C}_5$ alkanes and alkenes plus isoprene. The H_3O^+ SRI-MS mass spectra of calibration gas 4 is shown in Figure 3.5. Table 3.10 lists the known product ions for each compound in calibration gas 4 that were / were not detected, as well as whether mass interference occurred for each.

The proton affinities of ethene, and the $\text{C}_2 - \text{C}_6$ alkanes are known or estimated to be $\leq \text{PA}(\text{H}_2\text{O})$ and proton transfer does not occur or occurs at a rate less than 5% of the collisional limit resulting in a poor instrument response to these compounds (Wilson et al., 2003, Arnold et al 1998).

The PA of propene, cis-2-butene, trans-2-butene, isoprene, cis-2-pentene, and trans-2-pentene, are known or expected to be greater than the PA of H₂O and efficient proton transfer was assumed to occur in each case. The H₃O⁺ SRI-MS spectra of cis-2-butene and trans-2-pentene have been previously reported by Guerenon et al (2015) whereas, the mass spectra of trans-2-butene and cis-2-pentene have not been previously reported. For the purposes of this analysis it was assumed the butene isomers behaved similarly and the pentene isomers behaved similarly, and as such the results for the sum of butenes and sum of pentenes are reported here.

Table 3.10: The outcome of the mass spectral interpretation procedure (Figure 3.1) for the H₃O⁺ Spectra of Calibration Gas 4. The numbered references are listed in Table 3.1.

Compound	PA kJ mol ⁻¹	MW	m/z	Product ion	Decision	Ref
Ethene	680.5	28	29	MH ⁺	Detected without interference, but poor sensitivity	[8]
			47	MH ⁺ (H ₂ O)	Not detected	
Ethane	596.3	30	No reaction			[8]
Propene	751.6	42	41 43	(M-H) ⁺ MH ⁺	Probably detected with significant interference	[7]
Propane	625.7	44	No reaction			[8]
Σ cis- & trans-2-butene isomers	747	56	57	MH ⁺	Probably detected with minor interference	[5]
			41 43	(M-CH ₃) ⁺ (M-CH) ⁺	Probably detected with significant interference	
n-butane	<PA (H ₂ O)	58	57	(M-H) ⁺	Possibly detected with significant interference, and poor sensitivity	[8]
			75	MH ⁺ (H ₂ O)	Not detected	
Isoprene	826.4	68	69	MH ⁺	Detected without interference	[1]
			41	(M-C ₂ H ₃) ⁺	Probably detected with significant interference	
Σ cis- & trans-2-pentene isomers	>PA (H ₂ O)	70	71	MH ⁺	Detected without interference	[5]
			41 43	(M-C ₂ H ₅) ⁺ (M-C ₂ H ₃) ⁺	Probably detected with significant interference	
Isopentane	<PA (H ₂ O)	72	No reaction			[9]
n-pentane	<PA (H ₂ O)	72	No reaction			[9]

In the H_3O^+ SRI-MS mass spectra of calibration gas 4 there were two m/z that could be attributed to individual compounds/isomers without interference. They were protonated isoprene (m/z 69), and the sum of the protonated pentenes (m/z 71). The sum of the ion signals at m/z 69 and 71 contributed 18% of the TIS in the mass spectra of calibration gas 4.

The sum of the protonated butenes detected at m/z 57 may have suffered very minor interference from butane $(\text{M}-\text{H})^+$ fragment ions. The signal at m/z 43 was composed of product ion signals from protonated propene, plus pentene fragment ions. The signal at m/z 41 was composed of fragment ions from propene- and butene- isomers, isoprene and pentene isomers. The combined ion signals at m/z 57, 43 and 41 accounted for 71% of the TIS in the mass spectra of calibration gas 4.

4% of TIS was attributed to the presence of ^{13}C isotopologues of the compounds detected and/or the products of reactions with O_2^+ present as an impurity in the reagent ion matrix. 7% of the TIS in the calibration gas 3 mass spectra remained unidentified.

Calibration gas 5: contained 55 hydrocarbons including, acetylene, isoprene, $\text{C}_2 - \text{C}_6$ alkenes, $\text{C}_2 - \text{C}_{12}$ alkanes, $\text{C}_6 - \text{C}_7$ cycloalkanes, and $\text{C}_6 - \text{C}_{10}$ aromatic compounds. The H_3O^+ SRI-MS mass spectra of calibration gas 4 is shown in Figure 3.6. Tables 3.11 - 3.13 lists the known product ions for each compound in calibration gas 5 that were / were not detected, as well as whether mass interference occurred for each.

The $\text{C}_3 - \text{C}_6$ alkenes and, isoprene all have $\text{PA} > \text{PA}(\text{H}_2\text{O})$ and it was concluded that these compounds were well detected in the mass spectra of calibration gas 5. The $\text{C}_3 - \text{C}_6$ alkenes are known to undergo both dissociative and non-dissociative proton transfer with H_3O^+ yielding a protonated molecular ion in addition to a series of $\text{C}_n\text{H}_{2n+1}^+$ ($n \geq 3$) product ions (Diskin et al 2003, Warneke 2003, Gueneron et al 2015) with overlapping m/z .

The results of the mass spectral interpretation of the unsaturated hydrocarbons in Calibration gas 5 are listed in Table 3.11. Based on their known product ions and proton affinities it was concluded acetylene and ethene were not detected in the mass spectra of calibration gas 5. Isoprene was detected at m/z 69 without significant interference; and the known product ions of the $\text{C}_3 - \text{C}_6$ alkenes at m/z 43, 57, 71, 85 were probably detected with significant interference.

Table 3.11: The outcome of the mass spectral interpretation procedure (Figure 3.1) for the alkenes present in the H_3O^+ Spectra of Calibration Gas 5. The numbered references are listed in Table 3.1.

Compound	PA kJ mol ⁻¹	MW	m/z	Product ion	Decision	Ref
Acetylene	641.4	26	45	MH ⁺ (H ₂ O)	Not detected	[8]
Ethene	680.5	28	29 47	MH ⁺ MH ⁺ (H ₂ O)	Not detected	[8]
Propene	751.6	42	43	MH ⁺	Probably detected with significant interference	[7]
			41	(M-H) ⁺	Not detected	
Sum butenes	747	56	57 43	MH ⁺ (M-CH) ⁺	Probably detected with significant interference	[5]
			41	(M-CH ₃) ⁺	Not detected	
Isoprene	826.4	68	69	MH ⁺	Detected without interference	[1]
			41	(M-C ₂ H ₃) ⁺	Not detected	
Sum pentenes	>PA (H ₂ O)	70	71 43	MH ⁺ (M-C ₂ H ₃) ⁺	Probably detected with significant interference	[5]
			41	(M-C ₂ H ₅) ⁺	Not detected	
1-hexene	805.2	84	85	MH ⁺	Probably detected with significant interference	[5]
			57	(M-C ₂ H ₃) ⁺		
			43	(M-C ₃ H ₅) ⁺		
			41	(M-C ₃ H ₇) ⁺	Not detected	

As discussed previously, the proton affinities of C₂ – C₆ alkanes are known or estimated to be \leq PA(H₂O) and proton transfer does not occur or occurs at a rate less than the collisional limit (Wilson et al., 2003, Arnold et al 1998). Quantum mechanical calculations of alkane C-C bond proton affinities have shown that the bonds near the centre of the alkane carbon skeleton have higher proton affinities and for larger alkanes these proton affinities can be $>$ PA(H₂O) (Hunter & East 2002). Previous studies have shown that proton transfer does not occur efficiently for alkanes $<$ C₈ (Arnold et al 1998, Jobson et al 2005, Erickson et al 2014).

The alkanes that do undergo reaction with H₃O⁺ are known to fragment yielding a series of C_nH_{2n+1}⁺ (n \geq 3) product ions (Spanel et al 1998, Jobson et al 2005, Erickson et al 2014, Gueneron et al 2015) with overlapping m/z.

The results of the mass spectral interpretation of the alkanes in Calibration gas 5 are listed in Table 3.12. Based on their proton affinities and the published mass spectral data, we concluded that ethane, propane and pentane were not detected in the mass spectra of

calibration gas 5 and the remaining C₄ and C₆ – C₁₂ alkanes were possibly detected with poor sensitivity.

Both the alkanes and alkenes present in calibration gas 5, that undergo reaction with H₃O⁺, are known to fragment yielding a series of C_nH_{2n+1}⁺ (n ≥ 3) product ions and the precise contribution of alkanes to the mass spectra of calibration gas 5 cannot be determined due to these overlapping ion signals. However, due to their lower protonation efficiencies, we concluded that the alkanes made only minor contributions to the observed ion signals at m/z 41, 43, 57, 71 and 85, and the majority of the observed ion signals at these m/z in the mass spectra of calibration gas 5, were attributed to the alkenes.

Calibration gas 5 contained the cyclic alkanes methylcyclopentane, cyclohexane and methylcyclohexane. The proton affinity of cyclohexane is 686.9 kJ mol⁻¹ which is ≈ PA(H₂O). The PAs of methylcyclopentane and methylcyclohexane are unknown. Gueneron et al., (2015) reported poor PTR-MS sensitivity to cyclopentane, cyclohexane, and methylcyclopentane, due to their proton affinities being ≤ PA(H₂O).

Cycloalkanes are known to undergo both dissociative and non-dissociative proton transfer with H₃O⁺ yielding a protonated molecular ion in addition to a series of C_nH_{2n+1}⁺ (n ≥ 3) product ions at m/z 43, 57, and 85 (Gueneron et al 2015) which overlap with the known product ions of the aliphatic alkanes and alkenes also present in calibration gas 5 and discussed previously.

The results of the mass spectral interpretation of the cycloalkanes in Calibration gas 5 are listed in Table 3.13. Apart from the protonated parent ion of methyl cyclohexane identified at m/z 97, the contribution of the cycloalkanes to the mass spectra of calibration gas 5 cannot be determined due to mass overlap with the alkenes and other linear alkanes present. Due to their lower protonation efficiencies, we concluded that the cycloalkanes made at most a minor contribution to the observed ion signals at m/z 43, 57 and 85, and the majority of the observed ion signals at these m/z in the mass spectra of calibration gas 5, were a result of the alkenes.

Table 3.12: The outcome of the mass spectral interpretation procedure (Figure 3.1) for the alkanes present in the H_3O^+ Spectra of Calibration Gas 5. The numbered references are listed in Table 3.1.

Compound	PA kJ mol ⁻¹	MW	m/z	Product ion	Decision	Ref
Ethane	596.3	30	No reaction			[8]
Propane	625.7	44	No reaction			[8]
Sum C ₄ alkanes	677.8	58	57	(M-H) ⁺	Possibly detected with significant interference, and poor sensitivity	[8]
			75	MH ⁺ (H ₂ O)	Not detected	
Sum C ₅ alkanes	<PA (H ₂ O)	72	No reaction			[9]
Sum C ₆ Alkanes	~PA (H ₂ O)	86	43 57 71 85 105	(M-C ₃ H ₇) ⁺ (M-C ₂ H ₅) ⁺ (M-CH ₃) ⁺ (M-H) ⁺ MH ⁺ (H ₂ O)	Possibly detected with significant interference, and poor sensitivity	[9]
Sum C ₇ Alkanes	~PA (H ₂ O)	100	43 57 71 85	(M-C ₄ H ₉) ⁺ (M-C ₃ H ₇) ⁺ (M-C ₂ H ₅) ⁺ (M-CH ₃) ⁺	Possibly detected with significant interference, and poor sensitivity	[9] [5]
			99 100 119	(M-H) ⁺ MH ⁺ MH ⁺ (H ₂ O)	Not detected	
Sum C ₈ Alkanes	~PA (H ₂ O)	114	43 57 71	M-C ₅ H ₁₁) ⁺ (M-C ₄ H ₉) ⁺ (M-C ₃ H ₇) ⁺	Possibly detected with significant interference, and poor sensitivity	[9] [5]
			41 99 113 133	(M-C ₅ H ₁₃) ⁺ (M-CH ₃) ⁺ (M-H) ⁺ MH ⁺ (H ₂ O)	Not detected	

Table 3.12 (cont)

Compound	PA kJ mol ⁻¹	MW	m/z	Product ion	Decision	Ref
nonane	>PA (H ₂ O)	128	43	(M-C ₆ H ₁₃) ⁺	Possibly detected with significant interference, and poor sensitivity	[9] [5]
			57	(M-C ₅ H ₁₁) ⁺		
			71	(M-C ₄ H ₉) ⁺		
			85	(M-C ₃ H ₇) ⁺		
			41 147	(M-C ₆ H ₁₅) ⁺ MH ⁺ (H ₂ O)	Not detected	
decane	>PA (H ₂ O)	142	57	(M-C ₆ H ₁₃) ⁺	Possibly detected with significant interference, and poor sensitivity	[7] [5]
			71	(M-C ₅ H ₁₁) ⁺		
			85	(M-C ₄ H ₉) ⁺		
			99	(M-C ₃ H ₇) ⁺	Not detected	
undecane	>PA (H ₂ O)	156	43	(M-C ₈ H ₁₇) ⁺	Possibly detected with significant interference, and poor sensitivity	[5] [10]
			57	(M-C ₇ H ₁₅) ⁺		
			71	(M-C ₆ H ₁₃) ⁺		
			41	(M-C ₈ H ₁₉) ⁺	Not detected	
dodecane	>PA (H ₂ O)	170	43	(M-C ₉ H ₁₉) ⁺	Probably detected with significant interference	[10]
			57	(M-C ₈ H ₁₇) ⁺		
			71	(M-C ₇ H ₁₅) ⁺		
			85	(M-C ₆ H ₁₃) ⁺		
			41 99	(M-C ₉ H ₂₂) ⁺ (M-C ₅ H ₁₁) ⁺	Not detected	

Calibration gas 5 also contained 17 C₆ – C₁₀ aromatic hydrocarbons all of which are known to yield product ion signals at their respective protonated molecular ion (MH⁺). Partial dissociation also occurs for the C₈ – C₁₀ aromatics generally involving loss of a substituted alkyl group (Gueneron et al. 2015).

The results of the mass spectral interpretation the aromatic compounds in Calibration gas 5 are listed in Table 3.14. On the basis of their known product ions and proton affinities, it was determined that the sum of the C₉ aromatics (m-, p-, o- ethyltoluene, 1,2,3-, 1,2,4-, and 1,3,5- trimethylbenzene) at m/z 121, and the sum of the C₁₀ aromatics (m- and p-diethylbenzene) at m/z 135 were detected without interference.

Protonated benzene (m/z 79), protonated toluene (m/z 93) and the sum of the protonated C₈ aromatics (m-, p-, o- xylene and ethylbenzene) at m/z 107, were detected in the mass

spectra of calibration gas 5 however they suffered minor interference from the known fragment ions of C₈ and C₉ aromatics.

Table 3.13: The outcome of the mass spectral interpretation procedure (Figure 3.1) for the cycloalkanes present in the H₃O⁺ Spectra of Calibration Gas 5. The numbered references are listed in Table 3.1.

Compound	PA kJ mol ⁻¹	MW	m/z	Product ion	Decision	Ref
Methyl- cyclopentane	~PA (H ₂ O)	84	85 57 43	MH ⁺ (M-C ₂ H ₃) ⁺ (M-C ₃ H ₅) ⁺	Possibly detected with significant interference, and poor sensitivity	[5]
			83 41	(M-H) ⁺ (M-C ₃ H ₇) ⁺	Not detected	[5]
Cyclohexane	686.9	84	85 57 43	MH ⁺ (M-C ₂ H ₃) ⁺ (M-C ₃ H ₅) ⁺	Possibly detected with significant interference, and poor sensitivity	[5]
			83 41	(M-H) ⁺ (M-C ₃ H ₇) ⁺	Not detected	
Methyl- cyclohexane	~PA (H ₂ O)	98	97	(M-H) ⁺	Detected without interference, but poor sensitivity	[5]
			57	(M-C ₃ H ₅) ⁺	Possibly detected with significant interference, and poor sensitivity	

Overall, of the 55 hydrocarbons present in calibration gas 5, there were 4 compounds/compound groups that were detected without interference, they were isoprene (m/z 69), methyl cyclohexane (m/z 97), the sum of the C₉ aromatics (m/z 121), and the sum of the C₁₀ aromatics (m/z 135). The sum of these ion signals contributed 40% of the TIS observed in the mass spectra of calibration gas 5.

There were 24 compounds, mostly the aliphatic and cyclic alkanes, that were possibly detected with significant interference and poor sensitivity; there were 12 compounds, including alkenes > C₂ and the C₆ – C₈ aromatics, that were probably detected but with significant interference. The ion signals that contained contributions from multiple compounds constituted 51% of the TIS observed in the mass spectra of calibration gas 5.

An additional 5% of the TIS in the calibration gas 5 mass spectra was attributed to the ^{13}C isotopic product ions, leaving 4% of the TIS unidentified. There were 5 compounds that were not detected (acetylene, ethane, propane, and pentane isomers).

Table 3.14: The outcome of the mass spectral interpretation procedure (Figure 3.1) for the aromatics present in the H_3O^+ Spectra of Calibration Gas 5. The numbered references are listed in Table 3.1.

Compound	PA kJ mol ⁻¹	MW	m/z	Product ion	Decision	Ref
Benzene	750.4	78	79	MH ⁺	Probably detected with significant interference	[5]
Toluene	784.0	92	93	MH ⁺	Probably detected with significant interference	[5]
Styrene	839.5	104	105	MH ⁺	Probably detected with minor interference	[7]
Sum C ₈ aromatics	>788	106	107	MH ⁺	Probably detected with minor interference	[5]
			79	(M-C ₂ H ₃) ⁺	Probably detected with significant interference	
Sum C ₉ aromatics	836.2	120	121	MH ⁺	Detected without interference	[5]
			107 93 79 43	(M-CH ₃) ⁺ (M-C ₂ H ₃) ⁺ (M-C ₃ H ₅) ⁺ (M-C ₆ H ₅) ⁺	Probably detected with significant interference	
			41	(M-C ₇ H ₉) ⁺		
Sum C ₁₀ aromatics	>691	134	135	MH ⁺	Detected without interference	[7]

In summary, The five calibration gases employed in this study contained, 73 VOCs from a range of compound classes including aliphatic and cyclic alkanes, alkenes, aromatic hydrocarbons, aldehydes, ketones, chloro-benzenes and terpenoids, as well as acetylene, methanol, acetonitrile, ethyl acetate, and dimethyl sulphide.

The observed response of the H_3O^+ SRI-MS to a series of VOCs employed in this study fulfilled several theoretical expectations. Firstly, H_3O^+ underwent efficient proton transfer reactions with all VOCs that had an PA > PA(H_2O) which equated to 44 out of the 73 compounds studied. Acetylene, ethene the alkanes and cycloalkanes were poorly detected or not detected at all by the H_3O^+ SRI-MS due to their low proton affinities (Table 3.15).

Theory predicts the excess energy deposited in the product ions upon proton transfer from H_3O^+ is not sufficient to result in extensive product ion dissociation. Consequently, the H_3O^+ SRI-MS spectra of the VOCs studied was expected to be simple and predominantly comprised of protonated parent ions detected at m/z equivalent to their molecular weight (MW) plus one. The optimum situation would be where none or one product ion contributed to each mass scanned. Twenty out of the 60 compounds/ compound groups studied were reported to undergo dissociative proton transfer yielding product ions often with overlapping m/z .

Even in the absence of fragmentation, the low resolution of the H_3O^+ SRI-MS quadrupole mass spectrometer, in combination with the relative simplicity of the H_3O^+ spectra did not permit the discrimination of isomers in the mass spectra. As a result, several m/z were attributed to isomeric compound groups based on their carbon number, and not individual compounds including the C_8 -, C_9 - and C_{10} - aromatics.

The mass spectra of the calibration gases that contained fewer compounds and /or compounds that did not undergo extensive fragmentation were more highly resolved. For example, calibration gas 5 was a complex mixture containing 55 compounds, many of which were aliphatic hydrocarbons that are reported to undergo extensive fragmentation upon protonation. Only 41% of the total ion signal of calibration gas 5 was detected without interference. In comparison, calibration gases 1-3, contained fewer compounds most of which did not undergo fragmentation. Consequently, ~80 – 90% of the total ion signal of these gas mixtures was detected without interference.

Table 3.13 summarizes the compounds that could be identified without interference or with minor interference if one were to combine the H_3O^+ SRI-MS spectra of all five calibration gases and apply the mass spectral interpretation analysis described above. If the C_8 -, C_9 - and C_{10} - aromatics are considered as compound groups, there were 13 compounds/ compound groups detectable without interference and 3 compounds/ compound groups that were probably detected with minor interference out of the 60 compound/ compound groups studied.

Table 3.15: Summary of the interpretation for the combined H_3O^+ spectra of the 71 compounds present in the certified gas standards employed in this study.

COMPOUND	m/z	COMPOUND	m/z
Detected without interference			
Methanol	33	Methyl ethyl ketone	73
Acetonitrile	42	C ₉ Aromatics	121
Acetaldehyde	45	C ₁₀ Aromatics	135
Acetone	59	Chlorobenzene	113, 115
Dimethyl Sulphide	63	Dichlorobenzene	147, 149
Ethyl acetate	89, 61	Trichlorobenzene	181, 183
Isoprene	69		
Detected without interference but with poor sensitivity			
Formaldehyde	31		
Ethene	29		
Methylcyclohexane	97		
Probably detected with minor interference			
Toluene	93		
Styrene	105		
C ₈ Aromatics	107		
Probably detected with significant interference			
C ₃ – C ₆ Alkenes	41, 43, 57, 71, 85	Alpha pinene	137, 81
Dodecane	43, 57, 71, 85	1,8-cineole	137, 81
Benzene	79	Acrolein	57
		Methacrolein	71
Possibly detected with interference and poor sensitivity			
C ₄ – C ₁₁ alkanes	41, 43, 57, 71, 85		
C ₆ cycloalkanes	43, 75, 85		
Not detected			
Acetylene		Propane	
Ethane		C ₅ alkanes	

3.5 SRI-MS measurements of certified gas standards with O_2^+

The rules for mass spectral interpretation described in section 3.2, were applied to the O_2^+ SRI-MS spectra of the five calibration gases to determine the compounds that can be detected using O_2^+ , and of these, which compounds could be unambiguously identified without significant mass overlap in the mass spectra of gas mixtures of known composition.

Rule 1 (Figure 3.1) stated, “Chemical ionization reactions between M and R^+ is thermochemically favourable”. In the case of O_2^+ SRI-MS, oxygen cations undergo efficient charge transfer reactions with all species that have a lower first ionization energy (IE) than O_2 (12.07eV) (NIST). The IE of O_2 is higher than nearly all organic compounds (Figure 3.8) including the small hydrocarbons that do not react with H_3O^+ .

Thus, Rule 1 is restated as:

Rule 1: The $IE(M) < IE(O_2)$

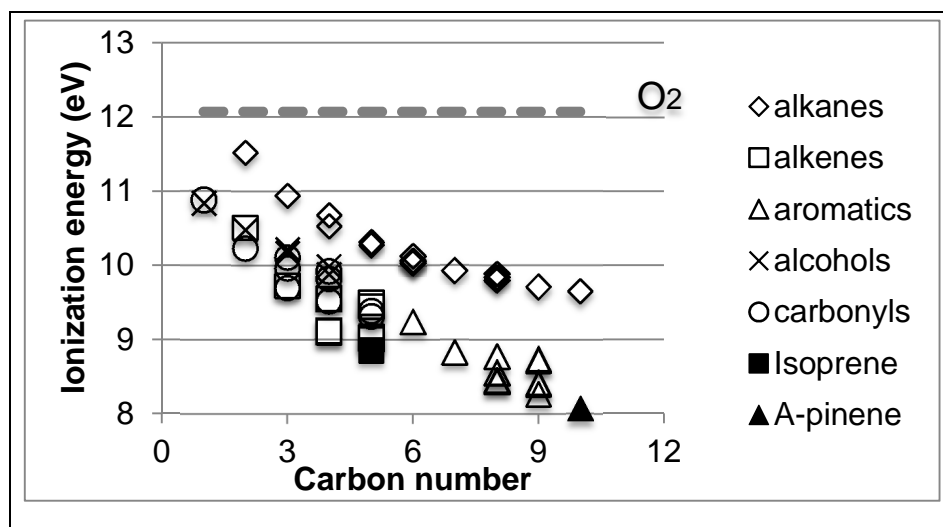


Figure 3.8: The ionization energy (IE) of a range of VOCs in relation to the IE of O_2 . If $IE(VOC) < IE(O_2)$ charge transfer reactions will occur.

The IE of each compound in the gas standards employed in this study are included in Tables 3.14 – 3.19. The IE of most VOCs is in the range of 8 – 11 eV (Figure 3.8), and there is a significant amount of excess energy deposited in the product ion upon charge transfer from O_2^+ , which may result in dissociation of the excited nascent molecular ion. The strongest single bonds in organic molecules have strengths of about 4 eV (1 eV \approx 23 kcal

mol⁻¹ \approx 96 kJ mol⁻¹) (McMurry 1992), and charge transfer from O₂⁺ to VOCs frequently results in more extensive product ion fragmentation than that observed in proton transfer from H₃O⁺. The number of compounds present in each gas standard analyzed and the number of compounds that were detected in the O₂⁺ SRI-MS mass spectra are shown in Table 3.16. Based on their known or estimated ionization energy O₂⁺ can undergo exothermic charge transfer reactions with all but one (acetonitrile) of the 73 compounds studied.

Table 3.16: The number and types of reaction products identified in the O₂⁺ SRI-MS spectra of calibration gases 1-5.

	Calibration Gas				
	1	2	3	4	5
Components	OVOcs Aromatics α -pinene acetonitrile	HCHO Acetone	Isoprene DMS E. acetate 1,8-cineole	Isoprene C ₂ – C ₅ alkanes & alkenes	Isoprene C ₂ -C ₁₂ alkanes C ₂ -C ₆ alkenes C ₆ -C ₁₀ aromatics
VOCs measured	15	2	5	12	55
VOCs detected	14	2 (1)	5	12	55
<i>Product ion types</i>					
M ⁺	10(9)		3	5	30
(M-H) ⁺	3	1 (0)	1	6	2
(M-H ₂) ⁺				2	2
(M-CH) ⁺				1	2
(M-CH ₂) ⁺				2	
(M-CH ₃) ⁺	5	1	4	5	24
(M-CH ₄) ⁺				3	2
(M-C _n H _{2n-1}) ⁺	3		1		2
(M-C _n H _{2n}) ⁺	1		1	2	7
(M-C _n H _{2n+1}) ⁺	1		1	2	33
(M-C _n H _{2n+2}) ⁺	1		1	3	26
(M-C _n H _{2n+3}) ⁺			1		24
(M-CHO) ⁺	2				
(M-CH ₅ O) ⁺			1		
(M-C _n H _{2n-1} O) ⁺			2		
(M-C _n H _{3n} O) ⁺			1		
(M+O-H _n) ⁺				1	1
(M-H ₂ O) ⁺			1		

Note: The number in brackets represents the number of compounds detected with good sensitivity.

In order to identify the major reaction processes occurring in O_2^+ SRI-MS, the number of compounds that yielded each type of reaction product ion was determined and these are also listed in Table 3.16.

Non-dissociative charge transfer yielding a molecular product ion (M^+) was a significant reaction pathway reported for many of the VOCs studied. However, the excess energy deposited in the product ions upon charge transfer from O_2^+ was sufficient in many cases to result in product ion dissociation, and a larger number and variety of fragmentation products ions were observed in the O_2^+ SRI-MS spectra in comparison to the H_3O^+ SRI-MS spectra. The products of elimination of a hydrogen atom or C_xH_y neutral fragments were the dominant fragmentation products for the compounds analysed in this study.

The O_2^+ SRI-MS mass spectra of calibration gases 1- 5 are shown in Figures 3.2 – 3.6. The reaction products of each compound studied and the results of the mass spectral interpretation for each calibration gas are summarized in Tables 3.17 – 3.22 and are discussed in turn below.

Calibration Gas 1: The O_2^+ SRI-MS spectra of calibration gas 1 is presented in Figure 3.2 and the results of the mass interpretation are listed in Table 3.17. With the exception of acetonitrile, all components in Calibration gas 1 had an $IE < IE(O_2)$ and it was assumed efficient charge transfer occurred for these compounds.

Based on their known product ions and branching ratios it was determined that there were eight compounds present in calibration gas 1 that were detected without interference at their charged parent ion m/z . They were methacrolein (m/z 70), methyl ethyl ketone (m/z 72), benzene (m/z 78), m-xylene (m/z 106), trimethylbenzene (m/z 121), chlorobenzene (m/z 112), dichlorobenzene (m/z 146), and trichlorobenzene (m/z 180). Acrolein was detected without interference at m/z 55 which corresponded to the $(M-H)^+$ fragment ion. Combined, the product ion signals detected without interference or minor interference contributed 63% of the total ion signal in the O_2^+ SRI-MS mass spectra of calibration gas 1.

The signal at m/z 93 which contributed an additional 8% to the TIS, was attributed to toluene with interference from alpha-pinene fragment ions. Acetone and acetaldehyde are known to entirely fragment to m/z 43 which constituted 18% of the TIS. 6% of the TIS was attributable to the presence of isotopes or products of reactions with H_3O^+ present as an impurity in the reagent ion matrix and the remaining 5% of the TIS was unidentified.

Acetonitrile, which was present in calibration gas 1 has an ionization energy of 12.20eV, which is marginally higher than the IE (O_2), and charge transfer from O_2^+ to acetonitrile occurs very slowly. It is likely acetonitrile made at most, a very minor contribution to the peak at m/z 41 observed in the mass spectra of calibration gas 1 (Figure 3.2) and the bulk of the ion signal can be attributed to other compounds.

Table 3.17: The results of the mass spectral interpretation procedure for the O_2^+ SRI-MS spectra of Calibration Gases 1 and 2. The numbered references are listed in Table 3.2.

Compound	IE (eV)	MW	m/z	Product ion	Decision	Ref
Formaldehyde CH ₂ O	10.88	30	29	(M-H) ⁺	Detected without interference, but with poor sensitivity	[1]
			30	M ⁺	Not detected	
Methanol CH ₄ O	10.84	32	32	M ⁺	Not detected	[2]
			31	(M-H) ⁺		
Acetaldehyde C ₂ H ₄ O	10.23	44	43	(M-H) ⁺	Probably detected with significant interference	[3]
Acrolein C ₃ H ₄ O	10.11	56	55	(M-H) ⁺	Detected without interference	[1]
			28	(M-CHO) ⁺		
			56	M ⁺	Not detected	
Acetone C ₃ H ₆ O	9.70	58	43	(M-CH ₃) ⁺	Probably detected with significant interference	[3]
Methacrolein C ₄ H ₆ O	9.92	70	70	M ⁺	Detected without interference	[3]
			69	(M-H) ⁺		
			41	(M-CHO) ⁺	Probably detected with minor interference	
			43	(M-C ₂ H ₃) ⁺	Probably detected with significant interference	
Methyl ethyl ketone C ₄ H ₈ O	9.52	72	72	M ⁺	Detected without interference	[1]
			57	(M-CH ₃) ⁺		
			43	(M-C ₂ H ₅) ⁺	Probably detected with significant interference	
Acetonitrile CH ₃ CN	12.20	41	41	M ⁺	Possibly detected with significant interference & poor sensitivity	[3]

Table 3.17 (cont)

Compound	IE (eV)	MW	m/z	Product ion	Decision	Ref
Alpha-pinene C ₁₀ H ₁₆	8.07	136	121	(M-CH ₃) ⁺	Detected without interference	[4]
			107	(M-C ₂ H ₅) ⁺		
			94	(M-C ₃ H ₆) ⁺		
			93	(M-C ₃ H ₇) ⁺		
			92	(M-C ₃ H ₈) ⁺	Probably detected with significant interference	
			136	M ⁺	Not detected	
			108	(M-C ₂ H ₄) ⁺		
			80	(M-C ₄ H ₈) ⁺		
Benzene C ₆ H ₆	9.24	78	78	M ⁺	Detected without interference	[3]
Toluene C ₇ H ₈	8.83	92	92	M ⁺	Probably detected with significant interference	[3]
m-xylene C ₈ H ₁₀	8.55	106	106	M ⁺	Detected without interference	[5]
			91	(M-CH ₃) ⁺		
Trimethylbenzene C ₉ H ₁₂	8.40	120	120	M ⁺	Detected without interference	[5]
			105	(M-CH ₃) ⁺		
Chlorobenzene C ₆ H ₅ Cl	9.07	112	112	M ⁺	Detected without interference	[6]
			114	³⁷ Cl M ⁺		
Dichlorobenzene C ₆ H ₄ Cl ₂	9.06	146	146	M ⁺	Detected without interference	[6]
			148	³⁷ Cl M ⁺		
Trichlorobenzene C ₆ H ₃ Cl ₃	9.04	180	180	M ⁺	Detected without interference	[6]
			182	³⁷ Cl M ⁺		

Studies of charge transfer from O₂⁺ to methanol observed product ion signals at m/z 32 and 31 (Spanel & Smith 1997). The ion signal at m/z 32 was not directly measured in this study as it coincides with the O₂⁺ reagent ion signal. Consequently the charged methanol ion at m/z 32 was not measured in the tests on calibration gas 1. No significant ion signal at m/z 31 was observed in the mass spectra of calibration gas 1 and it was concluded that methanol was not detected by O₂⁺ SRI-MS in this study.

Calibration Gas 2: The O₂⁺ SRI-MS spectra of calibration gas 2 is presented in Figure 3.3 and the results of the interpretation are listed in Table 3.16. Calibration gas 2 contained only acetone and formaldehyde both of which have IE < IE(O₂) and it was assumed efficient charge transfer occurred for these compounds.

Previous mass spectral studies in both SIFT-MS (Spanel et al. 1997) and EI-MS (Stein 2005) of formaldehyde have reported ion signals at m/z 29 and 30. In this study, the ion signal at m/z 30 was not measured as it coincides with the NO^+ reagent ion (Table 3.4). A trace ion signal (0.7% TIS) was observed at m/z 29 and it was concluded that formaldehyde was detected at m/z 29 without interference but with poor sensitivity.

Acetone was detected at m/z 43 without interference. Combined the acetone signal at m/z 43 and the formaldehyde signal at 29 constituted 86% of the TIS.

Ion signals at m/z 31 and 59 composed 22% of the TIS and were attributed to the presence of products of reactions with H_3O^+ present as an impurity in the reagent ion matrix. The remaining 2% of the TIS was unidentified.

Calibration Gas 3: The O_2^+ SRI-MS spectra of calibration gas 3 is presented in Figure 3.4 and the results of the O_2^+ SRI-MS mass spectral interpretation are listed in Table 3.18. All of the compounds in calibration gas 3 had $\text{IE} < \text{IE}(\text{O}_2)$ and efficient charge transfer occurred in each case.

Based on their known product ions and proton affinities, dimethyl sulphide (m/z 62, 47), isoprene (m/z 68, 67, 53), ethyl acetate (m/z 61, 55, 45), and 1,8-cineole (154, 139, 136, 108, 81 & others) were detected without interference. Combined, these ion signals constituted 59% of the total ion signal (TIS) observed in the O_2^+ SRI-MS spectra of calibration gas 3.

In the O_2^+ SRI-MS spectra of calibration gas 3, the peak at m/z 43, which comprised 30% TIS, contained contributions from acetone and ethyl acetate fragment ions. Of the TIS, 6% was attributable to the presence of isotopes or products of reactions with H_3O^+ present as an impurity in the reagent ion matrix. The remaining 6% of the TIS was unidentified.

Table 3.18: The results of the mass spectral interpretation procedure for the O₂⁺ SRI-MS spectra of Calibration Gas 3. The numbered references are listed in Table 3.2.

Compound	IE (ev)	MW	m/z	Product ion	Decision	Ref
Acetone C ₃ H ₆ O	9.70	58	43	(M-CH ₃) ⁺	Probably detected with significant interference	[3]
Dimethyl sulphide C ₂ H ₆ S	8.69	62	62 47	M ⁺ (M-CH ₃) ⁺	Detected without interference	[7]
Isoprene C ₅ H ₈	8.86	68	68 67 53	M ⁺ (M-H) ⁺ (M-CH ₃) ⁺	Detected without interference	[5]
Ethyl Acetate C ₄ H ₈ O ₂	10.31	88	61 55 45 43	(M-C ₂ H ₃) ⁺ (M-CH ₅ O) ⁺ (M-C ₂ H ₃ O) ⁺ (M-C ₂ H ₅ O) ⁺	Detected without interference Probably detected with significant interference	[3]
1,8-cineole C ₁₀ H ₁₈ O	>IE(O ₂)	154	154 139 136 126 111 108 96 84 81 71	M ⁺ (M-CH ₃) ⁺ (M-H ₂ O) ⁺ (M-C ₂ H ₄) ⁺ (M-C ₃ H ₇) ⁺ (M-C ₂ H ₆ O) ⁺ (M-C ₄ H ₁₀) ⁺ (M-C ₅ H ₁₀) ⁺ (M-C ₅ H ₁₃) ⁺ (M-C ₄ H ₇ O) ⁺	Detected without interference	[8]

Calibration Gas 4: The O₂⁺ SRI-MS spectra of calibration gas 4 is presented in Figure 3.5 and the results of the interpretation are listed in Table 3.19. Calibration gas 4 contained 12 C₂ – C₅ alkenes, alkanes and isoprene all of which have IE < IE (O₂).

Based on their known product ions and branching ratios it was determined that ethene (m/z 26, 15), the sum of the 2-butene isomers (m/z 55), the sum of the 2-pentene isomers (m/z 70) and the sum of the C₅ alkanes (m/z 57), and isoprene (m/z 68, 67, 53) were detected without interference. Combined, these ion signals comprised 30% of the TIS observed in the O₂⁺ SRI-MS spectra of calibration gas 4.

The ions detected at m/z 56, 43, 42, 41, 29 and 28 which comprised 66% of the TIS in the O₂⁺ SRI-MS spectra of calibration gas 4 contained contributions from multiple compounds.

Only 0.5% of the TIS could be uniquely attributed to the presence of isotopes or H_3O^+ reaction products, and the remaining 3.5% of the TIS was unidentified.

Table 3.19: The results of the mass spectral interpretation procedure for the O_2^+ SRI-MS spectra of Calibration Gas 4. The numbered references are listed in Table 3.2.

Compound	IE (eV)	MW	m/z	Product ion	Decision	Ref
Ethene	10.51	28	26 15	$(\text{M}-\text{H}_2)^+$ $(\text{M}-\text{CH})^+$	Detected without interference	[9]
			43 42 28	$(\text{M}+\text{O}-\text{H})^+$ $(\text{M}+\text{O}-\text{H}_2)^+$ M^+	Possibly detected with significant interference	
Ethane	11.52	30	29 28 30	$(\text{M}-\text{H})^+$ $(\text{M}-\text{H}_2)^+$ M^+	Detected with minor interference Possibly detected with significant interference Not detected	[10]
Propene	9.73	42	42 41	M^+ $(\text{M}-\text{H})^+$	Probably detected with significant interference	[10]
Propane	10.94	44	43 29	$(\text{M}-\text{H})^+$ $(\text{M}-\text{CH}_3)^+$	Probably detected with significant interference	[10]
Σ cis- & trans-2-butene isomers	<IE(O_2)	56	55 41	$(\text{M}-\text{H})^+$ $(\text{M}-\text{CH}_3)^+$	Detected without interference Probably detected with significant interference	[5]
n-butane	10.53	58	43 42 28 58	$(\text{M}-\text{CH}_3)^+$ $(\text{M}-\text{CH}_4)^+$ $(\text{M}-\text{C}_2\text{H}_6)^+$ M^+	Probably detected with significant interference Not detected	[5]

Table 3.19 (cont.)

Compound	IE (eV)	MW	m/z	Product ion	Decision	Ref
Isoprene	8.86	68	68 67	M ⁺ (M-H) ⁺	Detected without interference	[5]
			53	(M-CH ₃) ⁺	Not detected	
Σ cis- & trans- 2-pentene isomers	<9.05	70	70	M ⁺	Detected without interference	[5]
			56 42	(M-CH ₂) ⁺ (M-C ₂ H ₄) ⁺	Probably detected with significant interference	
C ₅ alkanes	<10.32	72	57	(M-CH ₃) ⁺	Detected without interference	[5]
			56 43 42	(M-CH ₄) ⁺ (M-C ₂ H ₅) ⁺ (M-C ₂ H ₆) ⁺	Probably detected with significant interference	
			72	M ⁺	Not detected	

Calibration Gas 5, contained 55 hydrocarbons including acetylene, C₂ – C₆ alkenes, C₂–C₁₂ alkanes, C₆ and C₇ cycloalkanes and C₆ – C₁₀ aromatics, all of which have IE < IE(O₂). The O₂⁺ SRI-MS spectra of calibration gas 5 is presented in Figure 3.6 and the results of the interpretation are listed in Tables 3.20 – 3.23.

Based on their known product ions and branching ratios it was determined that ethene (m/z 15), propane (m/z 44), the sum of the C₄ alkanes (m/z 58), isoprene (m/z 67, 68), methylcyclohexane (m/z 83), styrene (m/z 104), the sum of the C₈ aromatics (m/z 106), the sum of the C₉ aromatics (m/z 120), and the sum of the C₁₀ aromatics (m/z 134) were detected without interference in the O₂⁺ SRI-MS spectra of calibration gas 5. Acetylene was detected at m/z 26 with minor interference from ethane fragment ions. Combined, these product ions contributed 35% of the total ion signal.

Table 3.20: The results of the mass spectral interpretation procedure for the O_2^+ SRI-MS spectra of the unsaturated hydrocarbons in Calibration Gas 5. The numbered references are listed in Table 3.2.

Compound	IE (eV)	MW	m/z	Product ion	Decision	Ref				
Acetylene C ₂ H ₂	11.4	26	26	M ⁺	Probably detected with minor interference	[10]				
Ethene C ₂ H ₄	10.51	28	15	(M-CH) ⁺	Detected without interference	[9]				
			43	(M+O-H) ⁺	Probably detected with significant interference					
			42	(M+O-H ₂) ⁺						
			28	M ⁺						
			26	(M-H ₂) ⁺						
Propene C ₃ H ₆	9.73	42	42 41	M ⁺ (M-H) ⁺	Probably detected with significant interference	[10]				
Sum butenes C ₄ H ₈	<9.55	56	56 43 41	M ⁺ (M-CH) ⁺ (M-CH ₃) ⁺	Probably detected with significant interference	[5]				
			Isoprene C ₅ H ₈	8.86	68		68 67	M ⁺ (M-H) ⁺	Detected without interference	[5]
							53	(M-CH ₃) ⁺	Not detected	
Sum pentenes C ₅ H ₁₀	<9.49	70	70 55 42	M ⁺ (M-CH ₃) ⁺ (M-C ₂ H ₄) ⁺	Probably detected with significant interference	[5]				
			1-hexene C ₆ H ₁₂	9.44	84		84 69 56 55 43 42	M ⁺ (M-CH ₃) ⁺ (M-C ₂ H ₆) ⁺ (M-C ₂ H ₅) ⁺ (M-C ₃ H ₅) ⁺ (M-C ₃ H ₆) ⁺	Probably detected with significant interference	[11]
							29	(M-C ₄ H ₇) ⁺	Not detected	

Table 3.21: The results of the mass spectral interpretation procedure for the O_2^+ SRI-MS spectra of the aliphatic alkanes in Calibration Gas 5. The numbered references are listed in Table 3.2.

Compound	IE (eV)	MW	m/z	Product ion	Decision	Ref
Ethane C_2H_6	11.52	30	28	$(M-H_2)^+$	Probably detected with significant interference	[10]
			30	M^+	Not detected	
			29	$(M-H)^+$		
Propane C_3H_8	10.94	44	44	M^+	Detected without interference	[10]
			43	$(M-H)^+$	Probably detected with significant interference	
			29	$(M-CH_3)^+$	Not sensitively detected	
C_4 alkanes C_4H_{10}	<10.32	58	58	M^+	Detected without interference	[5]
			43	$(M-CH_3)^+$	Probably detected with significant interference	[10]
			42	$(M-CH_4)^+$		
			28	$(M-C_2H_6)^+$		
$C_5 - C_{12}$ alkanes C_nH_{2n+2} $n = >4 <11$	<10.69	72 to 170	85	$(M-C_nH_{2n+1})^+$	Probably detected with significant interference	[5] [12] [13]
			71			
			57			
			43			
			84	$(M-C_nH_{2n+2})^+$		
			70			
			56			
			42			
			55	$(M-C_nH_{2n+3})^+$		
			41			
			27			
			170	M^+	Not detected	
			156			
			142			
			128			
			114			
			100			
			86			
			72			
			58			
			155	$(M-H)^+$		
			113	$(M-H)^+$		
			112	$(M-H_2)^+$		
			99	$(M-C_nH_{2n+1})^+$		
			98	$(M-C_nH_{2n+2})^+$		
			39	?		
			29	$(M-C_nH_{2n+1})^+$		
			27	$(M-C_nH_{2n+3})^+$		

Table 3.22: The results of the mass spectral interpretation procedure for the O_2^+ SRI-MS spectra of the cycloalkanes in Calibration Gas 5. The numbered references are listed in Table 3.2.

Compound	IE (eV)	MW	m/z	Product ion	Decision	Ref
Methyl-cyclopentane C ₆ H ₁₂	9.70	84	84	M ⁺	Probably detected with significant interference	[13]
			69	(M-CH ₃) ⁺		
			56	(M-C ₂ H ₄) ⁺		
			55	(M-C ₂ H ₅) ⁺		
			43	(M-C ₃ H ₅) ⁺		
			42	(M-C ₃ H ₆) ⁺		
			41	(M-C ₃ H ₇) ⁺		
			39	(M-C ₃ H ₉) ⁺	Not detected	
Cyclohexane C ₆ H ₁₂	9.88	84	84	M ⁺	Probably detected with significant interference	[13]
			69	(M-CH ₃) ⁺		
			56	(M-C ₂ H ₄) ⁺		
			55	(M-C ₂ H ₅) ⁺		
			42	(M-C ₃ H ₆) ⁺		
			41	(M-C ₃ H ₇) ⁺		
				39	(M-C ₃ H ₉) ⁺	Not detected
Methyl-cyclohexane C ₇ H ₁₄	9.64	98	83	(M-CH ₃) ⁺	Detected without interference	[13]
			70	(M-C ₂ H ₄) ⁺	Probably detected with significant interference	
			69	(M-C ₂ H ₅) ⁺		
			56	(M-C ₃ H ₆) ⁺		
			55	(M-C ₃ H ₇) ⁺		
			42	(M-C ₄ H ₈) ⁺		
			41	(M-C ₄ H ₉) ⁺		
			98	M ⁺	Not detected	
			82	(M-CH ₃) ⁺		

Table 3.23: The results of the mass spectral interpretation procedure for the O_2^+ SRI-MS spectra of the aromatic compounds in Calibration Gas 5. The numbered references are listed in Table 3.2.

Compound	IE (eV)	MW	m/z	Product ion	Decision	Ref
Benzene C ₆ H ₆	9.24	78	78	M ⁺	Probably detected with significant interference	[3]
Toluene C ₇ H ₈	8.83	92	92	M ⁺	Probably detected with significant interference	[3]
Styrene C ₈ H ₈	8.46	104	104	M ⁺	Detected without interference	[13]
			78	(M-C ₂ H ₂) ⁺	Probably detected with significant interference	
Sum C ₈ aromatics C ₈ H ₁₀	<8.77	106	106	M ⁺	Detected without interference	[5]
			91	(M-CH ₃) ⁺	Probably detected with minor interference	
Sum C ₉ aromatics C ₉ H ₁₂	≤8.73	120	120	M ⁺	Detected without interference	[5]
			105 91	(M-CH ₃) ⁺ (M-C ₂ H ₅) ⁺	Probably detected with significant interference	
			79	(M-C ₃ H ₅) ⁺	Not detected	
Sum C ₁₀ aromatics C ₁₀ H ₁₄	<8.49	134	134 119	M ⁺ (M-CH ₃) ⁺	Detected without interference	[13]
			105		Probably detected with significant interference	

In measurements of the atmosphere, acetylene is considered useful as an inert tracer for combustion and its concentration ratio with other VOCs and with CO can be used to estimate the photochemical age of an air parcel (McKeen & Liu 1993, de Gouw et al. 2005). Given its importance to understanding the atmospheric chemistry of an air sample, the ability to measure acetylene in the atmosphere would be considered a significant advantage of O_2^+ SRI-MS.

In the O_2^+ SRI-MS spectra of calibration gas 5, multiple alkenes, alkanes and cycloalkanes contributed to the peaks at m/z 85, 84, 71, 70, 69, 57, 56, 55, 43, 42, 41, 29 and 28. The peaks at m/z 105, 92, 91, and 78 contained contributions from multiple aromatic compounds present in calibration gas 5. Combined, these ion signals comprised 64% of the TIS in the O_2^+ SRI-MS spectra of calibration gas 5. Only 2% of the TIS could be uniquely

attributed to the presence of isotopes or H_3O^+ reaction products and <1% of the TIS was unidentified.

In summary, the observed response of the O_2^+ SRI-MS to a series VOC mixtures employed in this study fulfilled several theoretical expectations. Firstly, O_2^+ underwent efficient charge transfer with all VOCS that had an IE < IE (O_2) which equated to 72 out of the 73 compounds studied. This is significantly more than the 44 out of 73 compounds detected by the SRI-MS when operating with H_3O^+ as the primary reagent ion (Section 3.4). Thus, O_2^+ SRI-MS can be considered an almost universal VOC detector as it responded to almost all of the VOCs including the small hydrocarbons, present in the certified gas standards employed in this study.

The molecular product ion (M^+) of many of the compounds tested were identified in the mass spectra. However, due to more energetic nature of O_2^+ ionization fragmentation products were also frequently observed. The products of H-elimination and loss of C_xH_y neutral fragments were the most commonly identified fragment ions in the mass spectra of the compounds studied here.

Due to the large number of compounds detectable by O_2^+ SRI-MS, and the high degree of fragmentation associated with charge transfer reactions of O_2^+ , the mass spectra of the complex gas mixtures employed here were often poorly resolved. In the O_2^+ SRI-MS spectra of calibration gases 1, 3, 4, & 5, between 30 and 63% of the total ion signal was attributed to a single compound without interference. The remaining peaks in each of the mass spectra contained contributions from more than one compound.

Table 3.24 summarizes the compounds that could be identified without interference or with minor interference if one were to combine the O_2^+ SRI-MS spectra of all five calibration gases and apply the mass spectral interpretation analysis described above.

Three important VOCs were not detected or detected with very low sensitivity by O_2^+ SRI-MS in this study. They were formaldehyde, methanol and acetonitrile. As a result, product ion signals were observed for 68 out of the 71 VOCs present in the certified gas standards employed in this study.

Table 3.24: Summary of the interpretation for the combined O₂⁺ spectra of the 71 compounds present in the certified gas standards employed in this study.

Detected without interference	
Ethene	15
Dimethyl sulphide	62, 47
Isoprene	68, 67
Ethyl acetate	61, 45
Methyl cyclohexane	83
Styrene	104
C ₈ aromatics	106
C ₉ aromatics	120
C ₁₀ aromatics	134, 119
α-pinene	121, 107, 93
1,8-cineole	154, 139, 136, 126, 111, 108, 96, 81
Chlorobenzene	112, 114
Dichlorobenzene	146, 148
Trichlorobenzene	180, 182
Detected with minor interference	
Acetylene	26
Probably detected with significant interference	
Acetaldehyde	43
Acrolein	55, 28
Acetone	43
MACR	70, 69
MEK	72, 57
C ₂ – C ₆ alkenes	26, 28, 29, 41, 42, 43, 55, 56, 57, 69, 70, 84
C ₂ – C ₁₂ alkanes	28, 29, 41, 42, 43, 55, 56, 57, 70, 71, 84, 85
Methycyclopentane & cyclohexane	41, 42, 55, 56, 69, 70, 84
Benzene	78
Toluene	92
Not detected or detected with poor sensitivity	
Formaldehyde	
Methanol	
Acetonitrile	

The C₈-, C₉- and C₁₀- aromatics were considered as compound groups, and it was determined that there were 12 compounds / compound groups detected without significant interference or with minor interference. These were: ethene (m/z 15), acetylene (m/z 26), DMS (m/z 62), isoprene (m/z 68, 67), ethyl acetate (m/z 61, 45), styrene (m/z 104), the sum of the C₈ aromatics (m/z 106) the sum of the C₉ aromatics (m/z 120), the sum of the C₁₀

aromatics (m/z 134, 119), chlorobenzene (m/z 112, 114), dichlorobenzene (m/z 146, 148), and trichlorobenzene (m/z 180, 182), α -pinene (m/z 121, 107, 93), 1,8-cineole (m/z 154, 139, 136 and others).

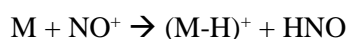
In addition while some compounds could not be individually identified the presence of a series of characteristic peaks may be useful to infer the presence of a broad class of compounds. For example, peaks at m/z that coincide with the C_nH_{2n+1} may be useful to infer the presence of alkanes (e.g. m/z 43, 57, 71, 85), and presence of peaks at m/z that coincide with C_nH_{2n-1} may be used to infer the presence of alkenes and cycloalkanes (e.g. m/z 41, 55, 69).

The ability to measure acetylene, an important atmospheric tracer, and the sum of the non-aromatic hydrocarbons, alongside compounds routinely measured by PTR-MS such as isoprene and aromatic compounds, represents a significant advantage of O_2^+ SRI-MS

3.6 SRI-MS measurements of certified gas standards with NO^+

NO^+ can undergo charge transfer reactions with compounds with an $IE < IE(NO)$, (9.26 eV). The IE of a range of VOCs is plotted in relation to the IE of NO in Figure 4.3.7. This plot shows that, unlike O_2^+ , NO^+ undergoes charge transfer with a limited number of VOCs, specifically the aromatics, alkenes $> C_4$, isoprene and monoterpenes. NO^+ will not undergo charge transfer reactions with most alkanes, ethene, propene, and oxygenated VOCs $< C_6$.

The reaction chemistry of NO^+ and VOCs is not limited to charge transfer processes. If the heat of formation of the products is lower than the heat of formation of the reactants, NO^+ may undergo hydride ion (H^-) transfer reactions. The molecular product ion is detected as the molecular mass minus one.



Reaction 3.1

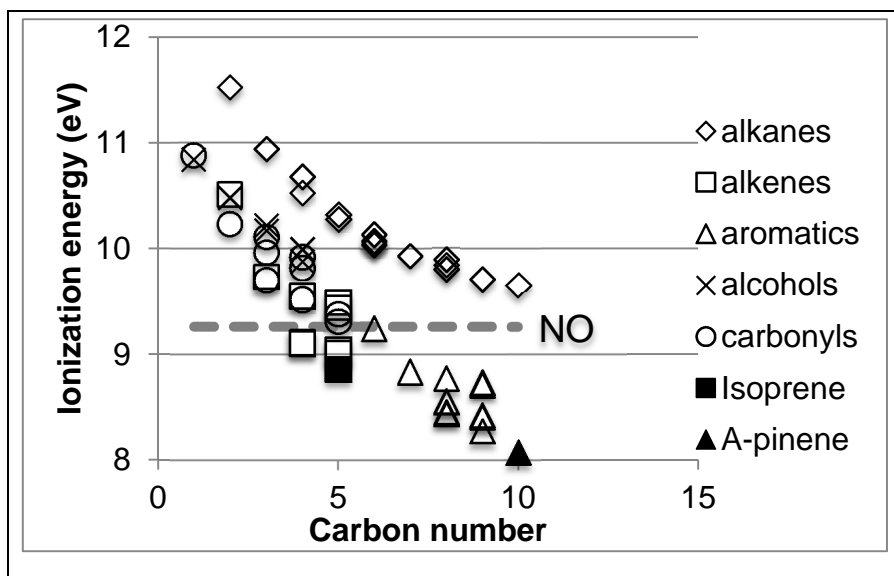
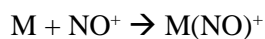


Figure 3.9: The ionization energy (IE) of a range of VOCs in relation to the IE of NO. If $IE(\text{VOC}) < IE(\text{NO})$ charge transfer reactions will occur.

NO^+ can also undergo hydroxide ion ($-\text{OH}$) transfer reactions yielding $(\text{M}-\text{OH})^+$ product ions, and alkoxide ion ($-\text{OR}$) transfer yielding $(\text{M}-\text{OR})^+$ ions.

NO^+ can also undergo association reactions with some compounds. The molecular product ion is detected as the molecular mass plus 30 due to NO^+ addition.



Reaction 3.2

This process is similar to the hydration reactions observed in the H_3O^+ reagent ion regime. That being the case, it was expected that association reactions with NO^+ would be suppressed by the high collision energies resulting from the applied voltage of 448V in the SRI-MS drift tube employed in this study.

The reactions of NO^+ with VOCs usually proceeds via only one of these reaction processes resulting in only one or two product ions, but for some compounds two reaction processes can occur simultaneously.

The procedure for interpreting SRI-MS mass spectra described in section 3.2 was applied to the NO^+ SRI-MS spectra of four calibration gases employed in this study. Rule 1 (Figure 3.1) states, “Chemical ionization reactions between M and R^+ is thermochemically favourable”. Given that the IE of a compound was not the only predictor of whether efficient ionization reactions with NO^+ occurred, Rule 1 of the mass spectral interpretation procedure was modified. Specifically, Rule 1 was restated in two parts as

Rule 1a: $\text{IE}(\text{M}) < \text{IE}(\text{NO})$

Rule 1b: $k_{\text{obs}} / k_{\text{coll}} > 0.8$

In the case where Rule 1a was determined to be false, the ratio of the observed reaction rate (k_{obs}) versus the calculated collision rate (k_{coll}) was used to determine if efficient ionization reactions, other than charge transfer, could occur.

The calculated and observed reaction rates of some components present in the certified gas standards employed in this study were unknown, in which case the ratio $k_{\text{obs}} / k_{\text{coll}}$ was estimated to be simply $<$ or > 0.8 based on the calculated and observed reaction rates of closely related compounds.

The difference between the IE of the VOCs and NO is smaller than in O_2^+ reaction regime. Consequently, less excess energy is deposited in the product ions upon charge transfer from NO^+ , which would be expected to result in less dissociation of the molecular ion.

Table 3.23 summarises the number and types of reaction products identified in the NO^+ mass spectra of the four calibration gases studied. The reaction products of charge transfer and hydride ion transfer were the dominant product ions identified in the NO^+ mass spectra in this study. As predicted the excess energy deposited in the product ions in the ionization reactions with NO^+ was not sufficient to result in extensive product ion dissociation, and a smaller number and variety of fragment ions were identified in the NO^+ SRI-MS spectra in comparison to the O_2^+ SRI-MS spectra.

Products of association reactions were not frequently observed as the formation of association complexes was suppressed by the presence of the applied electric field in the SRI-MS drift tube.

Table 3.23: The number and types of reaction products identified in the NO^+ SRI-MS spectra of calibration gases 1-4.

	Calibration Gas			
	1	2	3	4
Components	OVOCs Aromatics α -pinene acetonitrile	HCHO Acetone	Isoprene DMS Ethyl acetate 1,8-cineole	Isoprene $\text{C}_2 - \text{C}_5$ alkanes & alkenes
VOCs measured	15	2	5	12
VOCs detected	14	1	5	9
<i>Product ion types</i>				
M^+	8		3	5
$(\text{M}-\text{H})^+$	3 (2)		1	6 (4)
$(\text{M}-\text{CH}_2)^+$				2
$(\text{M}-\text{CH}_3)^+$	1(0)	1(0)	4 (3)	2
$(\text{M}-\text{C}_n\text{H}_{2n-1})^+$	1		1	
$(\text{M}-\text{C}_n\text{H}_{2n})^+$				2
$(\text{M}-\text{C}_n\text{H}_{2n+1})^+$	1			
$(\text{M}-\text{C}_n\text{H}_{2n+2})^+$	1			
$(\text{M}-\text{C}_n\text{H}_{2n+3})^+$			1	
$(\text{M}-\text{CHO})^+$	1			
$(\text{M}-\text{CHO}-\text{H}_2-\text{H})^+$	1			
$(\text{M}-\text{CH}_5\text{O})^+$			1	
$(\text{M}-\text{C}_2\text{H}_3\text{O})^+$			1	
$(\text{M}-\text{C}_2\text{H}_5\text{O})^+$			1	
$(\text{M}-\text{H}_2\text{O})^+$			1	
$\text{M}(\text{NO})^+$	2 (0)	1(0)	2	
$(\text{M} + \text{NO}-\text{C}_3\text{H}_6)^+$				1

Note: The number in brackets represents the number of compounds detected with good sensitivity.

The rules for mass spectral interpretation described in section 3.2, were applied to the NO^+ SRI-MS spectra of the four calibration gases, containing 29 VOCs, and the outcome of this process is described for each calibration gas in turn below.

Calibration Gas 1: The NO^+ SRI-MS spectra of calibration gas 1 are presented in Figure 3.1 and the results of the mass spectral interpretation are listed in Table 3.24.

Charge transfer product ions (M^+) were observed for compounds whose $\text{IE} < \text{IE}(\text{NO})$, namely the aromatic compounds and alpha-pinene. Peaks in the mass spectra were observed that corresponded to the hydride ion transfer products ($(\text{M}-\text{H})^+$) of acetaldehyde, acrolein, methacrolein and the methyl anion transfer product ($(\text{M}-\text{CH}_3)^+$) of acetone. A trace peak at m/z 102, was observed that corresponded with the association reaction product ion $(\text{M}(\text{NO})^+)$ of methyl ethyl ketone. No known reaction products were detected for methanol in the mass spectra of calibration gas 1 and it was concluded that methanol was not detected by NO^+ in this study.

Based on their known product ions and branching ratios it was determined that methacrolein (m/z 69), alpha-pinene (m/z 136, 93), benzene (m/z 78), m-xylene, (m/z 106), trimethylbenzene (m/z 120), chlorobenzene (m/z 112, 114), trichlorobenzene (m/z 146, 148) and trichlorobenzene (m/z 180, 182) were detected without interference. Combined, these ion signals comprised 66 % of the TIS observed in the NO^+ SRI-MS spectra of calibration gas 1. Known product ions of acrolein (m/z 55) and methyl ethyl ketone (m/z 102) were detected but with poor sensitivity. Combined, these ion signals comprised <2% of the TIS.

In the NO^+ SRI-MS spectra of calibration gas 1, multiple compounds contributed to the peaks at m/z 92, 43, 41, and 39, which comprised 24% of the TIS in the NO^+ SRI-MS spectra of calibration gas 1. Five percent of the TIS could be uniquely attributed to the presence of isotopes or H_3O^+ reaction products, and the remaining 3 % of the TIS was unidentified.

Table 3.24: The results of the mass spectral interpretation procedure for the NO⁺ SRI-MS spectra of Calibration Gas 1.

Compound	IE (eV)	k _{obs} /k _c	MW	m/z	Product ion	Decision	Ref
Formaldehyde	10.88	0.0	30	No reaction		Not detected	[1] [3]
Methanol	10.84	0.0	32	62	M(NO) ⁺	Not detected	[2] [3]
Acetaldehyde	10.23	≥0.8	44	43 41 39	(M-H) ⁺ ? ?	Probably detected with significant interference and poor sensitivity	[1] [4]
Acrolein	10.11	≥0.8	56	55	(M-H) ⁺	Detected without interference	[1] [3]
Acetone	9.70	0.4	58	43	(M-CH ₃) ⁺	Probably detected with significant interference and poor sensitivity	[1] [4]
				88	M(NO) ⁺	Not detected (Cal. Gas 1) Detected without interference but poor sensitivity (Cal. Gas 2)	
Methacrolein	9.92	0.8	70	69	(M-H) ⁺	Detected without interference	[4] [5]
				43 41 39	(M-C ₂ H ₃) ⁺ (M-CHO) ⁺ (M-CHO-H ₂ -H) ⁺	Probably detected with significant interference	
Methyl ethyl ketone	9.52	0.9	72	102	M(NO) ⁺	Detected without interference but poor sensitivity	[1] [3]
				72	M ⁺	Not detected	
Acetonitrile	12.20	0.0	41	41	M ⁺	Possibly detected with significant interference & poor sensitivity	[4] [6]
				71	M(NO) ⁺	Not detected	

Table 3.24 (cont.)

Compound	IE (eV)	$k_{\text{obs}}/k_{\text{c}}$	MW	m/z	Product ion	Decision	Ref
α -pinene	8.07	0.8	136	136	M^+	Detected without interference	[7]
				93	$(\text{M}-\text{C}_3\text{H}_7)^+$		
				92	$(\text{M}-\text{C}_3\text{H}_8)^+$	Probably detected with significant interference	
				166	$\text{M}(\text{NO})^+$	Not detected	
Benzene	9.24	0.9	78	78	M^+	Detected without interference	[4]
Toluene	8.83	0.9	92	92	M^+	Probably detected with minor interference	[4]
m-xylene	8.55	1	106	106	M^+	Detected without interference	[8] [9]
Trimethylbenzene	8.40	1	120	120	M^+	Detected without interference	[8] [9]
Chlorobenzene	9.07	≥ 0.8	112	112 114	M^+ $^{37}\text{Cl } \text{M}^+$	Detected without interference	[9]
Dichlorobenzene	9.06	≥ 0.8	146	146 148	M^+ $^{37}\text{Cl } \text{M}^+$	Detected without interference	[9]
Trichlorobenzene	9.04	≥ 0.8	180	180 182	M^+ $^{37}\text{Cl } \text{M}^+$	Detected without interference	[9]

Calibration Gas 2: The NO^+ SRI-MS spectra of calibration gas 2 are presented in Figure 3.2 and the results of the mass interpretation are listed in Table 3.24. Overall, the peaks observed in the mass spectra are two orders of magnitude lower than those observed in the O_2^+ and H_3O^+ SRI-MS spectra of calibration gas 2 illustrating the poor sensitivity of the NO^+ SRI-MS to these compounds.

Previous mass spectral studies of the reactions of NO^+ with formaldehyde with SIFT-MS (Spanel et al. 1997) reported that no reaction occurred. No peaks corresponding to formaldehyde were observed in this study and it was concluded that formaldehyde was not detected.

Acetone was detected at m/z 43 without interference. A trace peak at m/z 88 was also observed that corresponded with the NO^+ association reaction product ($\text{M}(\text{NO})^+$) of acetone. Combined, these signals contributed 27% to the TIS in the NO^+ SRI-MS spectra of calibration

gas 2. A second trace peak observed at m/z 59 (3% TIS) was presumably due to reactions of acetone with H_3O^+ present as an impurity in the reagent ion matrix. The remaining 70% of the TIS is unidentified, but consists mainly of instrument noise in the order of < 1 ncps on multiple m/z .

Calibration Gas 3: The NO^+ SRI-MS spectra of calibration gas 3 is presented in Figure 3.3 and the results of the NO^+ SRI-MS mass spectral interpretation are listed in Table 3.25. Product ion signals from multiple NO^+ ionization reaction processes were identified in the mass spectra of calibration gas 3 including: charge transfer in the case of dimethyl sulphide, isoprene and 1,8-cineole; association reactions in the case of ethyl acetate and 1,8-cineole. Multiple fragment ion signals were observed for many compounds in calibration gas 3. These may have been products of dissociative charge transfer or hydride/ alkyl ion transfer

Based on their known product ions and proton affinities, dimethyl sulphide (m/z 62), isoprene (m/z 68), ethyl acetate (m/z 118, 61, 55, 45) and 1,8-cineole (184, 154, 139, 136, 95) were detected without interference. Combined, these ion signals comprised 53% of the total ion signal (TIS) observed in the NO^+ SRI-MS spectra of calibration gas 3

Significant peaks were observed at m/z 67 and 53 in the NO^+ mass spectra of calibration gas 3, which were also observed in the O_2^+ SRI-MS mass spectra of calibration gas 3, and attributed to isoprene. Product ions at m/z 67 and 53 have not been previously reported for reactions of NO^+ with isoprene. However, the intensity of the peaks observed here indicated they were previously unreported products of charge transfer from NO^+ to isoprene, rather than products of reactions with impurity O_2^+ reagent ions present in trace amounts in the reagent ion matrix.

Likewise, a peak at m/z 47 was also observed in both the NO^+ and O_2^+ mass spectra of calibration gas 3 that was attributed to dimethyl sulphide and the intensity of this peak indicated this was a previously unreported product ion from charge transfer of NO^+ with DMS. Combined, the fragment ion signals at m/z 47, 53, and 67 contributed an additional 21% of the TIS that was identified without interference.

In the NO^+ SRI-MS spectra of calibration gas 3, the peak at m/z 43, which comprised 5% TIS, contained a minor contribution from acetone and a significant contribution from ethyl acetate fragment ions. 2% of the TIS was uniquely attributable to the presence of isotopes or

products of reactions with H_3O^+ present as an impurity in the reagent ion matrix. The remaining 19% of the TIS was unidentified.

Table 3.25: The results of the mass spectral interpretation procedure for the NO^+ SRI-MS spectra of Calibration Gas 3.

Compound	IE (ev)		MW	m/z	Product ion	Decision	Ref
Acetone	9.70	0.4	58	43	$(\text{M}-\text{CH}_3)^+$	Probably detected with significant interference and poor sensitivity	[4]
Dimethyl sulphide	8.69	1.0	62	62 47 ^a	M^+ $(\text{M}-\text{CH}_3)^+$	Detected without interference	[10]
Isoprene	8.86	1.0	68	68 67 ^a 53 ^a	M^+ $(\text{M}-\text{H})^+$ $(\text{M}-\text{CH}_3)^+$	Detected without interference	[8] [11]
Ethyl Acetate	10.31	0.9	88	118 61 55 45	$\text{M}(\text{NO})^+$ $(\text{M}-\text{C}_2\text{H}_3)^+$ $(\text{M}-\text{CH}_5\text{O})^+$ $(\text{M}-\text{C}_2\text{H}_3\text{O})^+$	Detected without interference	[4]
				43	$(\text{M}-\text{C}_2\text{H}_5\text{O})^+$	Probably detected with minor interference	
1,8-cineole	>9.26	1	154	184	$\text{M}(\text{NO})^+$	Detected without interference	[12]
				154	M^+		
				139	$(\text{M}-\text{CH}_3)^+$		
				136	$(\text{M}-\text{H}_2\text{O})^+$		
				95	$(\text{M}-\text{C}_4\text{H}_{11})^+$		

^a Previously unreported product ions, that were positively identified in this study.

Calibration Gas 4: The NO^+ SRI-MS spectra of calibration gas 4 are presented in Figure 3.4 and the results of the interpretation are listed in Table 3.26.

No known product ions of ethene, ethane, and propene were identified in the mass spectra and it was determined that these compounds were not detected. The $\text{C}_4 - \text{C}_5$ alkenes and isoprene have $\text{IE} < \text{IE}(\text{NO})$ and charge transfer products (M^+) for each were identified in the mass spectra. The alkanes, with the exception of isopentane, do not undergo efficient ionization reactions with NO^+ and their contribution to the mass spectra of calibration gas 3 was determined to be minor. Isopentane has been reported to undergo efficient hydride ion transfer reactions with NO^+ and a peak at m/z 71 was identified in the mass spectra of calibration gas 3 that was largely attributed to the $\text{M}-\text{H}^+$ product ion of isopentane, with a minor contribution from n-pentane.

Based on their known product ions and branching ratios it was determined that the sum of the 2-butene isomers (m/z 56, 55, 42, 29 & others), the sum of the 2-pentene isomers (m/z 70) and the sum of the C_5 alkanes (m/z 71), and isoprene (m/z 68, 67, 53) were detected without interference. Combined, these ion signals comprised 88% of the TIS observed in the NO^+ SRI-MS spectra of calibration gas 4. The remaining 12% of the TIS was unidentified.

Table 3.26: The results of the mass spectral interpretation procedure for the NO^+ SRI-MS spectra of Calibration Gas 4.

Compound	IE (eV)	k_{obs}/k_c	MW	m/z	Product ion	Decision	Ref
Ethene	10.51	0.0	28	58	$M(NO)^+$	Not detected	[13]
Ethane	11.52	0.0	30	No reaction			[13]
Propene	9.73	0.0	42	72	$M(NO)^+$	Not detected	[13]
Propane	10.94	0.0	44	43	$(M-H)^+$	Detected without interference but poor sensitivity	[13] [13]
Σ cis- & trans- 2-butenes	<9.12	>0.8	56	56 55 44 42 41 28	M^+ $(M-H)^+$ $(M+NO-C_3H_6)^+$ $(M-CH_2)^+$ $(M-CH_3)^+$ $(M-C_2H_4)^+$	Detected without interference	[4] [13]
n-butane	10.53	0.0	58	57	M^+	Not detected ^a	[13] [14]
Isoprene	8.86	1.0	68	68 67 ^a 53 ^a	M^+ $(M-H)^+$ $(M-CH_3)^+$	Detected without interference	[8] [11]
Σ cis- & trans- 2-pentenenes	<9.05	1.0	70	70	M^+	Detected without interference	[8]
n-pentane	10.28	0.0	72	71	$(M-H)^+$	Possibly detected with significant interference and poor sensitivity	[8]
isopentane	10.32	0.9	72	71	$(M-H)^+$	Probably detected with minor interference	[8]

^a Previously unreported product ions, that were positively identified in this study.

^bThe peak at m/z 57 visible in the mass spectra of calibration gas 4 can be wholly attributed to the ^{13}C isotologue signal of m/z 56.

In summary, The NO^+ SRI-MS was exposed to 4 certified gas mixtures containing 32 VOCs including oxygenated VOCs, alkenes, alkanes, isoprene, terpenoids, aromatics and chlorobenzenes. The observed response of the NO^+ SRI-MS to the VOCs studied fulfilled several theoretical expectations. Firstly, NO^+ underwent efficient charge transfer reactions with all VOCs that had an $\text{IE} < \text{IE}(\text{NO})$. These included, isoprene, alpha-pinene, 1,8-cineole, $\text{C}_4 - \text{C}_5$ alkenes, the $\text{C}_6 - \text{C}_9$ aromatic compounds, the mono-, di- and tri- substituted chlorobenzenes and dimethyl sulphide.

The reaction products of charge transfer, M^+ , and hydride ion transfer, $(\text{M-H})^+$, were the dominant product ions identified in the NO^+ mass spectra in this study. As predicted charge transfer from NO^+ was not sufficiently energetic to result in extensive product ion dissociation, and a smaller number and variety of fragment ions were identified in the NO^+ SRI-MS spectra in comparison to the analogous O_2^+ SRI-MS spectra.

The formation of association complexes was largely suppressed by the presence of the applied electric field in the SRI-MS drift tube. Minor product ion signals from association reactions were identified for methyl ethyl ketone, ethyl acetate, and 1,8-cineole.

Previous NO^+ SRI-MS studies have exploited the formation of these NO^+ association products for the differentiation of isomeric species including aldehydes and ketones (Wyche et al. 2005, Jordan et al. 2009). In order to exploit association processes when operating the SRI-MS with NO^+ as the reagent ion a lower drift tube voltage, than was used in this study, should be employed. Further work is required to optimize SRI-MS operation to maximize the formation of NO^+ association complexes, and consequently maximize the information content of the NO^+ mass spectra.

In the NO^+ SRI-MS spectra of the four calibration gases studied, between 27 and 88% of the total ion signal was composed of product ions detected without interference. Table 3.27 summarizes the compounds that could be identified without interference or with minor interference if one were to combine the NO^+ SRI-MS spectra of all four calibration gases and apply the mass spectral interpretation analysis described above.

Table 3.27: Summary of the interpretation for the combined NO⁺ spectra of the 29 compounds present in the certified gas standards employed in this study.

Detected without interference	
Methacrolein	69
Ethyl acetate	118, 61, 45 & others
Dimethyl sulphide	62, 47
Isoprene	68, 67
α-pinene	136, 93
1,8-cineole	154, 139, 136, 95
Benzene	78
2-butene	56
2-pentene	70
C ₅ alkanes	71
m-xylene	106
1,3,5-trimethylbenzene	120
Chlorobenzene	112, 114
Dichlorobenzene	146, 148
Trichlorobenzene	180, 182
Detected without interference but poor sensitivity	
MEK	102
Probably detected with significant interference	
Acetaldehyde	43
Acrolein	55
Toluene	92
Detected with significant interference and poor sensitivity	
Acetone	43, 88
Acetonitrile	41
Not detected	
Formaldehyde	
Methanol	
Ethene	
Ethane	
n-butane	

There were 15 compounds / compound groups detected without significant interference. These were: methacrolein, ethyl acetate, dimethyl sulphide, isoprene, 2-butenes, 2-pentenenes, C₅ alkanes, benzene, m-xylene, trimethyl benzene, chlorobenzene, dichlorobenzene, trichlorobenzene, α -pinene, 1,8,-cineole. A number of compounds were determined as “not detected” by NO⁺ SRI-MS, including formaldehyde, methanol, ethene, ethane, propene, and butane. Several other compounds were designated as “possibly” or “probably detected but with poor sensitivity”. These included acetaldehyde, acetone, acetonitrile, propane, and pentane.

3.7 SRI-MS Sensitivity

The sensitivity, *S*, of the SRI-MS to compounds that underwent non-dissociative ionization reactions and whose product ion signals could be qualitatively identified, was determined empirically from the calibration measurements via Equation 3.1. In the following *I*_{A+} refers to the ion signal of the analyte, *A*, normalized to a primary reagent ion signal of 10⁶ counts per second (cps). The sensitivity was expressed as normalized counts per second at a volume-mixing ratio of 1 ppbv (ncps ppbv⁻¹).

$$S_A \text{ (ncps ppbv}^{-1}\text{)} = I_{A+}(\text{ncps})/[A](\text{ppbv}) \quad \text{Equation 3.1}$$

For compounds whose ion signals could be reliably identified and underwent dissociative ionization for which the branching ratio (BR) was known, the sensitivity was determined from the fragment ion signal, *I*_{F+}, via Equation 3.2:

$$S_A \text{ (ncps ppbv}^{-1}\text{)} = I_{F+} \text{ (ncps)} / (\text{BR}_{F+} \times [A](\text{ppbv})) \quad \text{Equation 3.2}$$

The sensitivity, determined for each compound in each reagent ion mode, was plotted versus the product ion *m/z* in Figure 3.10. A line of fit based on a second order regression was applied to the sensitivity data for compounds between 45 – 200 amu that underwent chemical ionization reactions at a rate close to the collisional limit.

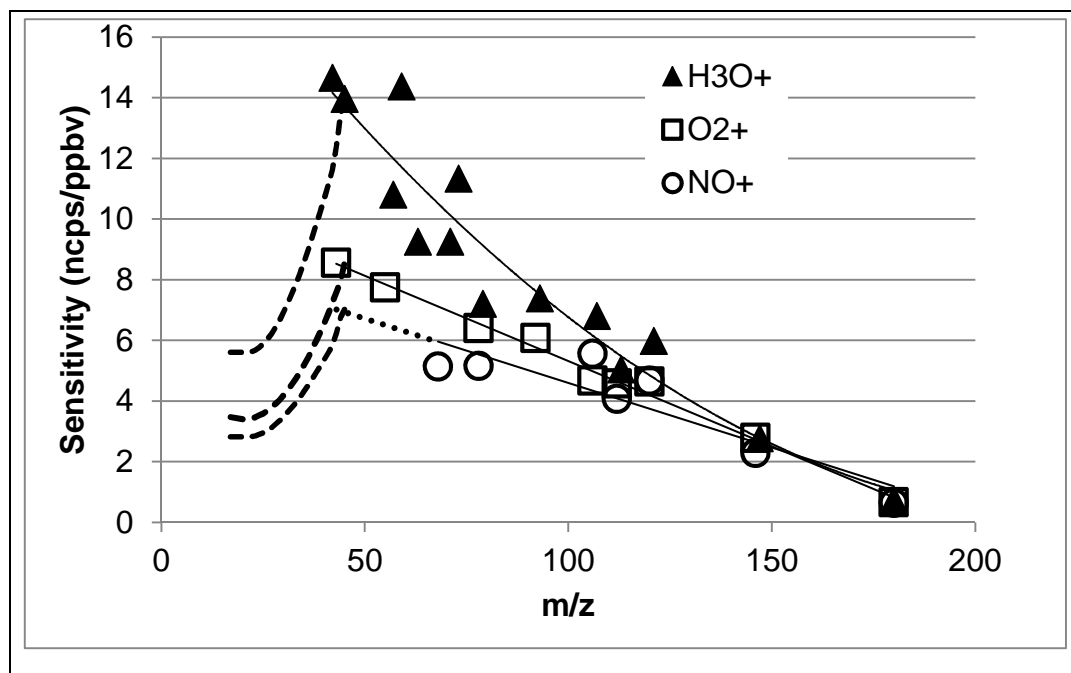


Figure 3.10: The measured sensitivity and interpolated sensitivity curves for the SRI-MS in H_3O^+ , O_2^+ and NO^+ reagent ion modes. (Dashed Lines) an interpolated sensitivity curve for $m/z < 45$ determined from the measured sensitivity at m/z 45 and the SRI-MS software output for the mass dependent transmission of ions with m/z 15 – 45 (see text below).

The sensitivity of a SRI-MS instrument to a particular compound is dependent on the chemical ionization reaction rate and the mass dependent transmission of ions through the quadrupole mass spectrometer. Tuning the mass spectrometer can alter the mass at which the mass dependent transmission is at its maxima. Heavier ions spend more time in fringing fields and are thus less efficiently transmitted through the quadrupole (Dawson 1976). The quadrupole of the PTR-MS instrument used in this study had a maximum mass dependent transmission efficiency at ~ 45 amu.

The sensitivity of the SRI-MS for lighter ions ($m/z < 45$) could not be empirically determined in this study due to a lack of measurable compounds in the calibration standards that occur in that m/z range. The SRI-MS sensitivity decreases rapidly for m/z below that of the maxima, in this case m/z 45, due to the scattering losses of lighter ions caused by collisions with buffer gas molecules at the entrance to the quadrupole.

In the absence of sufficient empirical calibration data for $m/z < 45$ from this study, we used the mass dependent transmission curve from the PTR-MS Control Software Version (Ionicon Analytik GmbH) fitted to the maximum response found at m/z 45. Thus, the sensitivity to a compound (A) whose product ion (a) occurs at $m/z < 45$ is calculated via:

$$S_{m/z\ a} = T_{m/z\ a} \times S_{\max} \quad \text{Equation 3.3}$$

where $T_{m/z\ a}$ is the transmission at $m/z = a$ determined by the transmission algorithm embedded in the PTR-MS control software, and S_{\max} is the measured sensitivity at the transmission maxima, in this case m/z 45.

Table 3.28: Equations from fits in Figure 3.10 used to interpolate the sensitivity at each m/z for each reagent ion.

Reagent ion	Observed S ($m/z > 45$)	S max ncps/ppbv	Interpolated S ($m/z < 45$)
H_3O^+	$S = 0.0004 \times m/z^2 - 0.183 \times m/z + 20.9$ $R^2 = 0.87$	14.7	$S = 0.013 \times m/z^2 - 0.524 \times m/z + 10.81$
O_2^+	$S = -0.056 \times m/z + 10.94$ $R^2 = 0.99$	8.84	$S = 0.008 \times m/z^2 - 0.321 \times m/z + 6.621$
NO^+	$S = -0.043 \times m/z + 8.87$ $R^2 = 0.82$	7.07	$S = 0.0064 \times m/z^2 - 0.256 \times m/z + 5.280$

Mass dependent sensitivity curves such as those in Figure 3.10 can be used in calculations to determine the volume-mixing ratio at m/z where no reliable empirical calibration is available. Using interpolated or measured sensitivities, the concentration of VOCs detected at $m/z = x$ can be calculated via:

$$[VOC]_A \text{ (ppbv)} = \frac{I_{A^+}(\text{ncps})}{S_{A(\text{ncps/ppbv})}} \quad \text{Equation 3.4}$$

$$[VOC]_{A=(\text{ppbv})} = \frac{I_{F^+}(\text{ncps})}{S_{A(\text{ncps/ppbv})} \cdot BR_{F^+}} \quad \text{Equation 3.5}$$

The measured sensitivities shown in Figure 3.10 were lower in NO^+ and O_2^+ reagent ion modes than in H_3O^+ mode. The mass dependent transmission efficiency of the mass spectrometer is equivalent in all reagent ion modes. The lower sensitivity in NO^+ and O_2^+ reagent ion modes is a consequence of lower reaction rates (k) for the charge transfer reactions in comparison to proton transfer from H_3O^+ . According to collision theory, the NO^+ and O_2^+ reactions occur at a slower rate due to the lower collision frequency that is a result of

the higher reduced mass of the ion-molecule colliding partners (Pilling and Seakins, 1995). In theoretical predictions of ion-molecule collisions the reduced mass, commonly represented by the symbol μ , is calculated via:

$$\mu = m_1 m_2 / (m_1 + m_2) \quad \text{Equation 3.6}$$

Where m_1 and m_2 are the masses of the ion and the neutral molecule, respectively.

There are a number of theoretical approaches for determining ion-molecule reaction rate coefficients, and a detailed discussion is beyond the scope of this chapter. However, a simple early model developed by Langevin is sufficient to demonstrate that the higher the reduced mass (μ) of the ion-neutral pair the lower the collision rate (k_L):

$$k_L = \sqrt{\frac{\pi \alpha q^2}{\mu \epsilon_0}} \quad \text{Equation 3.7}$$

Where, α is the polarizability of the neutral; q is the charge; and ϵ_0 is the permittivity of free space.

The question then arises, can the observed difference in sensitivity between H_3O^+ , O_2^+ and NO^+ be explained by the difference in their ion-molecule reaction rates in the drift tube? If the answer to this question is yes, then the following ratios should be unity:

$$(\text{S}_{\text{O}_2^+}/\text{S}_{\text{H}_3\text{O}^+})/(\text{k}_{\text{O}_2^+} / \text{k}_{\text{H}_3\text{O}^+}) = 1; \text{ and} \quad \text{Equation 3.8}$$

$$(\text{S}_{\text{NO}^+}/\text{S}_{\text{H}_3\text{O}^+})/(\text{k}_{\text{NO}^+} / \text{k}_{\text{H}_3\text{O}^+}) = 1 \quad \text{Equation 3.9}$$

where, S is the sensitivity (ncps ppbv⁻¹) of the SRI-MS to each compound in each reagent ion mode, and k refers to the respective reaction rates.

The ratios in equations 3.8 and 3.9 were determined for a series of aromatic and chlorobenzene compounds employed in this study. These compounds were selected because: their reaction rates with H_3O^+ , O_2^+ and NO^+ are known (Spanel & Smith 1998b, Spanel & Smith 1999, Francis et al. 2009); they do not undergo extensive fragmentation; and they are detected at roughly the same m/z for all reagent ion modes thus negating the effect of transmission on the comparison.

If the difference in sensitivity between O_2^+ , NO^+ and H_3O^+ reagent ion regimes is largely due to the difference in reaction rates (k), and the values of k were approximately correct, the ratios should be close to unity. The average ratio for $(S_{O_2^+}/S_{H_3O^+})/(k_{O_2^+}/k_{H_3O^+})$ was 1.00 ± 0.12 and 1.10 ± 0.25 for $(S_{NO^+}/S_{H_3O^+})/(k_{NO^+}/k_{H_3O^+})$. The ratios for each compound are listed in Table 3.29.

Table 3.29: the reaction rates (k) for reactions between each of the reagent ions and several aromatic compounds from the literature; the SRI-MS sensitivities (S) to each compound in each reagent ion mode determined in this work; and the ratios $(S_{O_2^+}/S_{H_3O^+})/(k_{O_2^+}/k_{H_3O^+})$ and $(S_{NO^+}/S_{H_3O^+})/(k_{NO^+}/k_{H_3O^+})$.

	Reaction rate ($10^{-9} \text{ cm}^3 \text{ molecule}^{-1} \text{ s}^{-1}$)			Sensitivity (ncps/ppbv)			$\frac{S_{O_2^+}/S_{H_3O^+}}{k_{O_2^+}/k_{H_3O^+}}$	$\frac{S_{NO^+}/S_{H_3O^+}}{k_{NO^+}/k_{H_3O^+}}$
	$k_{H_3O^+}$	$k_{O_2^+}$	k_{NO^+}	$S_{H_3O^+}$	$S_{O_2^+}$	S_{NO^+}		
Benzene	1.9	1.5	1.6	7.2	6.4	5.1	1.1	0.8
Toluene	2.2	1.8	1.7	7.4	6.1	8.3	1.0	1.5
m-Xylene	2.3	1.9	1.9	6.8	4.7	5.5	0.8	1.0
Trimethylbenzene	2.3	1.9	1.9	6.0	4.6	4.7	0.9	0.9
Chlorobenzene	2.9	2.4	2.4	5.0	4.6	4.0	1.1	1.0
Trichlorobenzene	2.8	2.2	2.3	0.8	0.7	0.6	1.1	0.9

We can conclude that the sensitivity curves for each reagent ion mode observed in this study fulfilled theoretical expectations based on the ion-molecule collision theory and our understanding of the mass dependent transmission of ions through a quadrupole mass spectrometer.

3.7 Conclusions

The SRI-MS mass spectra of five of certified gas standards containing 73 VOCs were determined in each reagent ion mode (H_3O^+ , O_2^+ , NO^+). A series of simple rules were developed for the interpretation of the mass spectra to determine which compounds were detected in each reagent ion mode, and of these which compounds could be identified in the mass spectra without interference. Table 3.28 summarises the compound classes detected in each reagent ion mode.

Across all reagent ion modes, the number of compounds that could be identified in the mass spectra of the VOC mixtures was dependent on the number of compounds present and their potential for fragmentation upon ionization, as both of these factors increased the total number of product ions in the mass spectra and therefore the probability that mass overlap would occur.

The H_3O^+ SRI-MS was capable of detecting almost all of the compound classes studied with the notable exceptions of the acetylene, and the short chain alkanes. Due to the “soft” ionization processes associated with H_3O^+ , the mass spectra were generally simple and well resolved. The protonated parent ion was the dominant reaction product observed across all of the H_3O^+ mass spectra, with some minor fragmentation products also observed.

Table 3.28: Comparison of compounds detected in each SRI-MS reagent ion mode in this study.

Reagent ion	H_3O^+	O_2^+	NO^+
Detectable organic compounds	Alkenes > C_3 Isoprene & terpenes Aromatics Chlorobenzenes Methanol Aldehydes Ketones Ethyl acetate Acetonitrile Dimethyl sulphide	Alkanes Alkenes Acetylene Isoprene & terpenes Aromatics Chlorobenzenes Aldehydes (excl HCHO) Ketones Ethyl acetate Dimethyl sulphide	Alkenes > C_3 Isoprene & terpenes Aromatics Chlorobenzenes Aldehydes (excl HCHO) Ethyl acetate Dimethyl sulphide

Of the 46 compounds detected by the H_3O^+ SRI-MS, there were 16 compounds / compound groups that could be identified without interference or with minor interference, including: methanol, acetaldehyde, acetone, methyl ethyl ketone, ethyl acetate, acetonitrile, dimethyl sulphide, isoprene, $\text{C}_6 - \text{C}_9$ aromatics, and the mono-, di- and tri- substituted chlorobenzenes. In addition, formaldehyde, ethene, and methylcyclohexane were detected without interference but with poor sensitivity. As has been demonstrated for formaldehyde (Hansel et al. 1997, Inomata et al. 2008), detailed calibrations may be required to quantify the concentration of ethene, and methylcyclohexane from the unique trace ion signals they produce.

The O_2^+ SRI-MS can almost be regarded as a universal VOC detector as it was capable of detecting 70 out of the 73 compounds present in the five certified gas standards, including the small alkanes not detectable with H_3O^+ .

The molecular product ion (M^+) of many of the compounds tested were identified in the mass spectra. However, due to more energetic nature of O_2^+ ionization, a large number and variety of fragmentation products were also observed and the mass spectra were less well resolved than the H_3O^+ spectra.

14 out of the 70 compounds detectable by O_2^+ SRI-MS were identified in the mass spectra without interference or with minor interference including: acetylene, ethane, isoprene, C_8 – C_{10} aromatics, mono-, di- and tri- substituted chlorobenzenes, α -pinene, 1,8 cineole, dimethyl sulphide and ethyl acetate.

Individual alkanes and alkenes were not unambiguously identified in the mass spectra, which would apparently negate a potential advantage of using O_2^+ for measurements of the atmosphere. However characteristic peaks were observed in the O_2^+ spectra that may be used to infer the presence of alkanes and alkenes in mixtures of unknown composition.

The NO^+ SRI-MS was exposed to 32 compounds, 27 of which it was capable of detecting with the notable exceptions of the ketones, and the small alkanes. Due to the “soft” ionization processes associated with NO^+ , the mass spectra were generally simple and well resolved. The reaction products of charge transfer, M^+ , and hydride ion transfer, $(\text{M}-\text{H})^+$, were the dominant product ions identified in the NO^+ mass spectra in this study. As predicted charge transfer from NO^+ was not sufficiently energetic to result in extensive product ion dissociation, and a smaller number and variety of fragment ions were identified in the NO^+ SRI-MS spectra in comparison to the O_2^+ SRI-MS spectra.

Previous studies have demonstrated the usefulness of the formation of NO^+ association complexes to distinguish between isomeric aldehydes and ketones (Wyche et al. 2005, Jordan et al. 2009) which is not possible with H_3O^+ SRI-MS. The high drift tube voltage used in this study suppressed the formation of these ions. Further work is required to optimize the SRI-MS to exploit this reaction pathway and maximize the information content of the NO^+ SRI-MS mass spectra.

Across the NO^+ SRI-MS spectra of the four certified gas standards studied, there were 15 compounds / compound groups identified without interference, including C_5 alkanes, C_4 & C_5 alkenes, isoprene, terpenes, benzene, xylenes, trimethylbenzene, mono-, di- and tri-substituted chlorobenzenes, methacrolein, ethyl acetate, and dimethyl sulphide. The results of this analysis suggest that in measurements of the atmosphere, with the operating conditions employed in this study the NO^+ SRI-MS wouldn't provide any significant additional information to H_3O^+ SRI-MS measurements alone.

The rules for mass spectral interpretation developed for this analysis provide a useful tool for determining whether or not unequivocal identification of a compound present in a mixture of known composition has been achieved.

The compounds employed here along with many others, have been previously detected in the atmosphere (Heald et al 2008). While the relative concentrations of the compounds employed here do not reflect typical atmospheric concentrations, the number and diversity of species is a reasonable simulation of atmospheric composition. This analysis therefore provides important information on which compounds the SRI-MS could detect in the atmosphere, and of these, which compounds are more likely to be identified in the mass spectra of air without significant mass overlap.

Finally, empirically derived instrument sensitivities for each reagent ion mode were determined. The observed differences between the sensitivities in each reagent ion mode fulfilled theoretical expectations based on the ion-molecule collision theory and our understanding of the mass dependent transmission of ions through a quadrupole mass spectrometer.

Part B: Measurements of VOCs in urban air with SRI-MS

Chapter 4. An exploratory study of the use of switchable reagent ion mass spectrometry (SRI-MS) for the measurement of VOCs in urban air

4.1 Introduction

Proton transfer mass spectrometry (PTR-MS) has proven to be a useful tool for the measurement of VOCs in the atmosphere. The major limitation of measurements of VOCs in complex air matrices by PTR-MS is that product ions of the same nominal molecular weight cannot be readily distinguished using quadrupole mass spectrometers.

One approach to overcome this limitation is to exploit the use of alternative reagent ions to differentiate compounds on the basis of differences in their ionization reactions or fragmentation products. Blake et al. (2006) and Jordan et al. (2009) reported the development of PTR-MS instruments with switchable reagent ion capability (SRI-MS) in which different reagent ion source gases and ion source tuning were used to selectively produce O_2^+ , NO^+ , NH_4^+ or H_3O^+ reagent ions.

The deployment of SRI-MS in measurements of the atmosphere has so far been limited to only a small number of field studies, (Norman et al 2007, Knighton et al 2009, Karl et al 2012, Karl et al 2014) with a combined total of 24 days of data reported. These field studies have focused on the measurement of a handful of individual compounds of specific interest.

Norman et al (2007) achieved highly sensitive measurements of ammonia in the atmosphere over an intensely managed grassland by employing O_2^+ as a reagent ion in their SRI-MS instrument. Measurements of ammonia are not possible using conventional H_3O^+ PTR-MS, as NH_4^+ produced from air back-streaming into the ion source generates a significant background signal at m/z 18 resulting in prohibitively high detection limits for the measurement of ambient ammonia at its protonated mass (m/z 18).

Knighton et al. (2009) employed NO^+ reagent ions to selectively measure 1,3-butadiene in an urban air sample, over 7 days. In conventional PTR-MS using H_3O^+ reagent ions, the measurement of 1,3 butadiene at m/z 55 suffers significant interference from other compounds and water clusters. In addition to 1,3-butadiene, $\text{C}_6 - \text{C}_{10}$ aromatic compounds

were also identified in the ambient mass spectra measured with NO^+ as the primary reagent ion.

In two separate field studies, Karl et al (2012, 2014) were able to selectively measure two important biogenic VOCs, isoprene and 2-methyl-3-buten-2-ol (2,3,2-MBO), by employing NO^+ as a reagent ion. In conventional PTR-MS, 2,3,2-MBO undergoes fragmentation resulting in a dominant ion peak at m/z 69 that coincides with the isoprene parent ion. However in NO^+ reagent ion mode, these 2 compounds underwent different reaction processes resulting in distinct ion signals, with isoprene detected at m/z 68 and MBO detected at m/z 69.

Overall, the application of SRI-MS to measurements of inorganic and organic compounds in the atmosphere is still in its infancy and further work is required to determine what, if any, additional information can be acquired through the use of reagent ions other than H_3O^+ .

In the study reported here a special data analysis technique was utilized to select the key m/z from the mass scans of ambient air, for each reagent ion mode, that had sufficiently high ion signals to be reliably quantified. Based on the mass spectral studies performed for this thesis (Chapter 3) and those available in the literature, probable product ion identities were assigned to the key m/z identified in each reagent ion mode.

Secondly, this chapter presents a real-world inter-comparison of the mixing ratios of selected VOCs measured by H_3O^+ SRI-MS with parallel integrated VOC adsorbent tube (AT-VOC) samples analysed by GC-MS and parallel VOC integrated samples captured on DNPH cartridges and analysed by HPLC.

Finally, the VOCs measured by the SRI-MS in O_2^+ and NO^+ reagent ion modes are compared with conventional H_3O^+ SRI-MS measurements. The agreements, disagreements, and possible reagent chemistry underlying the results of all inter-comparisons are presented.

4.2 Methodology

4.2.1 Study location

The SRI-MS sampled ambient air in an urban area of Sydney, Australia in summer from 18th February – 7th March 2011. In Sydney, VOC emissions are dominated by biogenic emissions (isoprene, monoterpenes, methanol) and emissions from motor vehicles (hydrocarbons) and the products of photochemical oxidation (aldehydes, ketones, dicarbonyls, carboxylic acids). Bushfires can be also significant intermittent sources of VOCs to the Sydney airshed (CSIRO 2008, Cope et al. 2014).

The sampling site (33.8°S, 150.9°E) was located in the suburb of Westmead, in the grounds of a hospital greater than 500m from major roads.

4.2.2 SRI-MS measurement set-up

For the study of urban air in Sydney 2011, equipment was located in a demountable building with sample inlet ~1 m above the roofline, the main sample line consisted of a ~80 mm O.D. glass inlet of ~ 2 m length connected to a ~ 4m length of ¼ inch O.D silco steel tubing. A constant flow of ambient air was drawn at a flow rate of 1.5 L/min through the PTR-MS auxiliary system and the SRI-MS sampled 300 mL/min from the auxiliary system.

The instrument employed in this work was a commercially built PTR-MS (Ionicon Analytik GmbH, Innsbruck Austria) and subsequently factory modified with the addition of a switchable reagent ion source system to enable the use of NO⁺ and O₂⁺ reagent ions in addition to H₃O⁺. Briefly, the instrument consists of an ion source where the reagent ions are generated, a drift tube where the reagent ions and the sample are mixed and chemical ionization reactions occur between the reagent and the analyte, and a quadrupole mass spectrometer (Balzers QMG422) and secondary electron multiplier (SEM) for sorting and detecting the reagent and product ions.

In the hollow cathode ion source, the relevant source gas was ionized by electron impact to produce the desired reagent ions either: H₃O⁺, O₂⁺ or NO⁺. The H₃O⁺ reagent ions were produced from water vapour introduced at a flow of ~ 6 mL min⁻¹ (STP). The source gas for the O₂⁺ reagent ions was UHP O₂ (BOC, Australia) introduced to the ion source at a flow rate of 5 mL min⁻¹ (STP). The source gas for the NO⁺ reagent ions was a combination of UHP O₂

and UHP N₂ (BOC, Australia) introduced to the ion source at flow rates of 5.0 mL min⁻¹ (STP) and 3.8 mL min⁻¹ (STP), respectively.

The hollow cathode ion source generated high intensity ion signals (10⁷ cps) in all three reagent ion modes. The mean ion signals and the relative concentration of trace impurity ions for each reagent ion system are listed in Table 4.1. The ion source was tuned to produce the primary reagent ions with a purity of >95% but there were always other ions present in trace amounts in the reagent ion matrix as a result of air back-streaming into the ion source and the humidity of the sampled air (Table 4.1). The presence of these trace impurity reagent ions complicated the SRI-MS spectra, as they also undergo chemical ionization reactions with VOCs present in the reagent–analyte matrix.

Table 4.1: Primary reagent ion signals and the relative concentration of impurity ions. Also listed are the ionization energies (IE) and proton affinities (PA) of primary and impurity reagent ions.

Primary reagent ion	Mean primary reagent ion signal (cps)	Impurity reagent ions	% primary reagent ion signal
H ₃ O ⁺	2.8 ± 0.1 × 10 ⁷	O ₂ ⁺ NO ⁺ H ₃ O ⁺ (H ₂ O)	2.9 – 3.5% 0.4 – 0.6% 1.5 – 6.0%
O ₂ ⁺	4.3 ± 0.1 × 10 ⁷	H ₃ O ⁺ NO ⁺ NO ₂ ⁺	2.2 – 7.0 % 4.6 – 5.4% 0.4 – 0.6%
NO ⁺	5.0 ± 0.2 × 10 ⁷	H ₃ O ⁺ O ₂ ⁺ NO ₂ ⁺	0.2 – 0.3% 0.6 – 1.1% 4.8 – 8.2%

The intense ion signals of the primary reagent ions H₃O⁺, O₂⁺ and NO⁺ overwhelm the ion detection system and shorten the lifetime of the SEM. In order to avoid this, the ion isotopes of the reagent ion were measured rather than the primary ion signal: H₃¹⁸O⁺ detected at m/z 21 was multiplied by 500 to approximate the H₃O⁺ signal at m/z 19; ¹⁵NO⁺ detected at m/z 31, was multiplied by 274 to approximate the NO⁺ signal at m/z 30; and, ¹⁸O ¹⁶O⁺ detected at m/z 34, was multiplied by 250 to approximate the ¹⁶O₂⁺ signal at m/z 32. Likewise, the ion isotopes of impurity reagent ions were measured rather than the primary ion signal: H₃¹⁸O⁺(H₂O) or H₃O⁺(H₂¹⁸O) detected at m/z 39 was multiplied by 250 to approximate the H₃O⁺(H₂O) signal at m/z 37; and, ¹⁴N¹⁸O¹⁶O⁺ detected at m/z 48 was multiplied by 250 to approximate the NO₂⁺ signal at m/z 46.

In the present study, the drift tube was operated at 60°C and an applied voltage of 445 V. The pressure in the reactor was 2.16 mbar when sampling in H_3O^+ mode, 2.26 mbar in NO^+ mode and 2.23 mbar in O_2^+ mode. The SRI-MS quadrupole continuously scanned 181 masses between 14 and 200 amu. The dwell time for a single mass measurement was 1 second, generating a full mass scan approximately every 3 minutes.

The PTR-MS operated with the aid of custom built auxiliary equipment that regulated the flow of air in the sample inlet and controlled whether the PTR-MS was sampling ambient or zero air or calibration gas. Zero readings were made by diverting the air through a zero furnace (350°C) with a Platinum wool catalyst that destroyed VOCs in the air before it entered the PTR-MS. Zero measurements were conducted in H_3O^+ , O_2^+ and NO^+ mode twice per day. Background corrections were performed for all measurements described in this study. All ion signals from calibration and ambient air measurements referred to in this study are background corrected. The zero corrected data can have negative values because they are calculated from the difference between the ion signals during a zero measurement and an ambient measurement. At lower concentrations, in the presence of some measurement noise, negative values can result from the difference.

The minimum detectable level (MDL) for each m/z was determined from the scatter in the zero measurements during a zero period of a half-hour or hour, using the principles of ISO6879 (1995). The MDL was set at a level where 5% of the zero measurements gave a false positive reading above the mean zero value. Because of the nature of the noise affecting the PTR-MS signal (Poisson statistics), lower MDLs can be achieved by the use of longer averaging times.

The production of a stable NO^+ plasma is more sensitive to the operating parameters of the ion source, in particular the extraction voltage and the discharge current (Knighton et al. 2009). At the time of this study, it was not possible to automatically change the discharge current on the ion source during measurement and the hollow cathode ion source was operated with a discharge current of 4.8 mA which was an optimized setting for H_3O^+ reagent ion production. For NO^+ reagent ion production a discharge current of ~ 6 mA is recommended. As a result of the sub-optimal ion source settings for NO^+ production used in this study, the instrument background was not stable during NO^+ measurement periods.

The signal at m/z 25 is commonly regarded as a measure of the background ‘noise’ in the ion signal, as there are no known compounds that contribute to the signal at m/z 25, and the

signal at m/z 25 arises from dark counts, or from light escaping the ion source and travelling into the detection system and is ideally < 5 cps.

During NO^+ measurements, the m/z 25 exhibited a steady decrease over the measurement period. Figure 4.1 shows the m/z 25 ion signal across a typical NO^+ measurement cycle in which ambient measurement occurred from 12:00 am – 1:00 am, zero measurement occurred from 1:00 am – 1:30 am, and calibration measurement occurred from 1:30 – 2:00 am. As a result of the unstable background signal, an additional noise correction, based on the difference between the m/z 25 signals during ambient and zero measurements, was applied to the hourly average NO^+ data and the NO^+ calibration data.

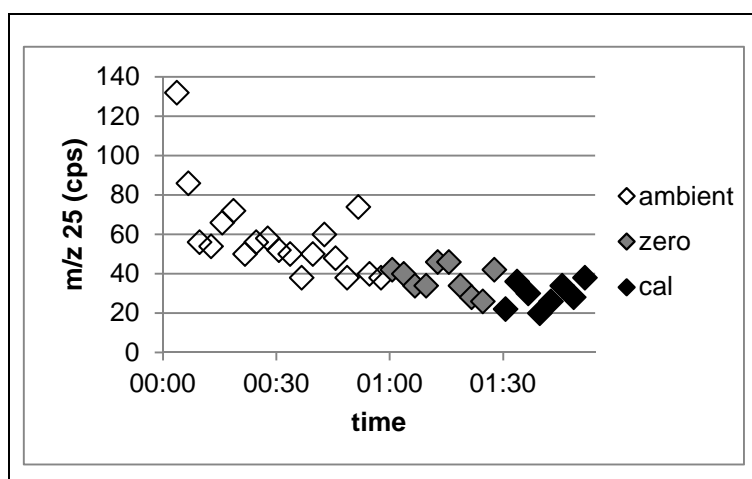


Figure 4.1: The m/z 25 ion signal for a typical ambient measurement period. The signal at m/z 25, commonly regarded as a measure of the background ‘noise’ in the ion signal.

There were also several occasions during measurement in which the NO^+ plasma became unstable and the reagent ion signal “dropped out”. These measurement periods were excluded from the following analysis. Following this study, further modification of the SRI-MS instrument has allowed the automatic switching of the source current when switching between reagent ion source gases.

4.3 SRI-MS calibrations

During the field study in Sydney 2011, the SRI-MS was calibrated with certified gas standards in H_3O^+ mode twice per day and in O_2^+ and NO^+ mode once per day for a duration of 30 minutes each.

For each calibration measurement a set flow of 10 – 20 mL min⁻¹ of the calibration standard was diluted in a flow of 1500 mL min⁻¹ of ambient air that had been passed through the zero furnace and delivered to the SRI-MS inlet. This zero air had the same mole fractions of H₂O and CO₂ as the ambient air being sampled, neglecting minor contributions from the oxidation of VOCs present.

The calibration gases used in this study, were described in chapter 3 and were referred to as calibration gases 1 – 3. These certified gas standards were supplied by AiR Environmental Inc, and Air Liquide-Scott Specialty Gases. The stated accuracy for each component in the standards was $\pm 5\%$. The SRI-MS spectra of the gas standards employed in this study were described in detail in Chapter 3 and the components of each are listed in Chapter 3, Table 3.5.

Table 4.2: The calibration factors in ncps ppbv⁻¹ for each of the VOCs used in this work in each reagent ion mode (H₃O⁺, O₂⁺, NO⁺). The error limits represent \pm the relative standard deviation of the mean. N represents the number of 30 min calibration periods used to calculate the sensitivity statistics.

	MW	H ₃ O ⁺			N	O ₂ ⁺			N	NO ⁺			N
		m/z	Calibration Factor (ncps ppbv ⁻¹)			m/z	Calibration Factor (ncps ppbv ⁻¹)			m/z	Calibration Factor (ncps ppbv ⁻¹)		
Formaldehyde	30	31	0.94 \pm 16%	19	43	8.55 \pm 4%	11						
Acetaldehyde	44	45	13.65 \pm 10%	28									
Acetone	58	59	12.43 \pm 7%	55									
MACR	70	71	8.05 \pm 12%	28									
MEK	72	73	10.61 \pm 10%	28									
Isoprene	68	69	3.37 \pm 6%	8	67	3.05 \pm 2%	3	68	5.12 \pm 2%	2			
α -pinene	136	81	3.66 \pm 10%	28	93	3.26 \pm 10%	14	93	1.65 \pm 14%	5			
Benzene	78	79	6.72 \pm 10%	28	78	5.97 \pm 8%	14	78	4.80 \pm 4%	5			
Toluene	92	93	6.81 \pm 13%	28	92	6.31 \pm 12%	14	92	9.01 \pm 8%	5			
m-xylene	106	107	6.19 \pm 13%	28	106	3.99 \pm 11%	14	106	5.06 \pm 13%	5			
1,3,5-trimethyl benzene	120	121	5.38 \pm 15%	28	120	4.17 \pm 16%	14	120	4.20 \pm 17%	5			

The response of the SRI-MS to the compounds analysed in this study were determined empirically from the calibration measurements via Equation 4.1. In the following I_{A+} refers to the ion signal of the analyte, A, normalized to a primary reagent ion signal of 10⁶ counts per second (cps). The sensitivity was expressed as normalized counts per second at a volume-mixing ratio of 1 ppbv (ncps ppbv⁻¹).

$$\text{Calibration factor (A) (ncps ppbv}^{-1}\text{)} = I_{A+}(\text{ncps})/[A](\text{ppbv}) \quad \text{Equation 4.1}$$

The empirically derived SRI-MS calibration factors used in this work are presented in Table 4.2 for each reagent ion mode. The scatter ($\pm 1 \sigma$) in the calibration measurements was ~10% for all reagent ion modes within a range of 2 – 17% (Table 4.2).

4.4 Selection and identification of key m/z

A specially developed data analysis technique was utilized to select the m/z from the mass scans of ambient air, for each reagent ion mode, that had persistently high ion signals. It was enacted as follows.

Firstly, the ion signals of the primary reagent ions, impurity reagent ions and their isotopes (Table 4.1) were excluded from further consideration. Secondly, two bulk properties of the data sets, described as measures, were examined to identify the m/z of interest in each data set (Galbally et al. 2008). The first data measure is the fraction of occasions throughout the whole dataset for a given m/z where the ion signal was above the MDL for that m/z . This measure is expressed as a dimensionless fraction represented by $T > MDL$ varying from 0 - 1. This first measure is essentially “for a particular mass, during what portion of the measurements is a signal being detected?”

The second measure is the ratio for each mass of the 95th percentile, P , to the MDL. This peak to noise ratio measure is expressed as a dimensionless fraction represented by P/MDL . The second measure is essentially “how large are the peak concentrations compared with the MDL?” This fraction will have a lower limit of 1.65 for a normally distributed random noise signal. For signals that do not arise from instrument noise there is no upper limit of P/MDL .

For each reagent ion mode, for each m/z , $T > MDL$ was plotted against P/MDL (Figure 4.2). The plot is divided into 4 regions. The data points in the bottom left region of the plots can be considered m/z where little or no VOCs are detected and the signal is dominated by ‘noise’. A line of fit was applied to the ‘noise’ data that divides the plot horizontally. The $T > MDL$ value on the x-axis, where the noise data ends, divides the plot vertically.

Data points in the bottom right are m/z with persistent low concentrations; top left, are m/z with concentrations generally below the MDL with occasional high peaks; and the top right are m/z with persistent high concentrations.

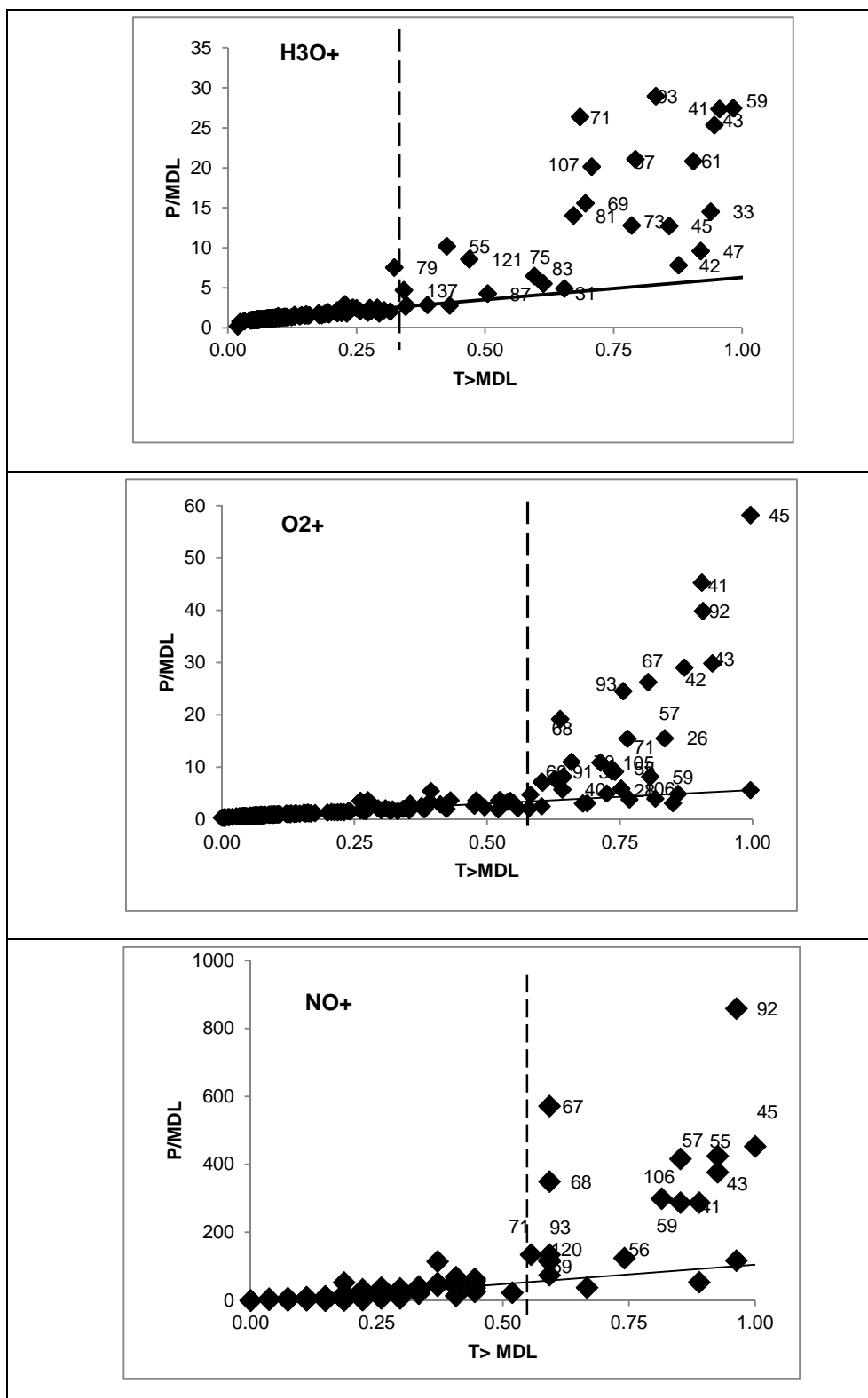


Figure 4.2: Plots of $T > \text{MDL}$ and P/MDL for each reagent ion mode. The m/z in the top right quadrant had persistent high concentrations and were identified as key m/z .

The m/z with persistently high concentrations (key m/z) were selected for further analysis. Firstly, based on the mass spectral studies performed for this thesis and those available in the literature, probable product ion identities were assigned to the key m/z identified in each reagent ion mode. The key m/z and their probable identities are listed for the H_3O^+ SRI-MS, O_2^+ SRI-MS and NO^+ SRI-MS measurements in Table 4.3.

Table 4.3: Key m/z identified in the H_3O^+ , O_2^+ and NO^+ SRI-MS mass scans of urban air and their probable compound identities.

Reagent ion	Major m/z	Formula	Probable Compound / Group
H_3O^+	33	CH_4O^+	Methanol
	47, 61	$C_nH_{2n+1}O_2^+$	Carboxylic acids / esters
	31	CH_3O^+	Formaldehyde
	45	$C_2H_5O^+$	Acetaldehyde
	59	$C_3H_7O^+$	Acetone/ Propanal
	71	$C_4H_7O^+$	MACR/ MVK
	73	$C_4H_9O^+ / C_3H_3O_2^+$	MEK / Butanal / Methyl glyoxal
	75	$C_nH_{2n+1}O_2^+$	Multifunctional compounds
	69	$C_5H_9^+$	Isoprene
	81 & 137	$C_6H_9^+ \& C_{10}H_{17}^+$	Monoterpenes
	79	$C_6H_7^+$	Benzene
	93	$C_7H_9^+$	Toluene
	107	$C_8H_{11}^+$	C_8 Aromatics
	121	$C_9H_{13}^+$	C_9 Aromatics
	42	CH_4CN^+	Acetonitrile
	41, 43, 57, 83, 85	$C_xH_y / C_xH_yO / C_xH_yO_2$	Multiple compounds

Table 4.3 (cont.)

Reagent ion	Major m/z	Formula	Probable Compound / Group
O ₂ ⁺	26, 28, 41, 42, 55, 57, 70, 71	C _x H _y ⁺	Hydrocarbons
	67, & 68	C ₅ H ₇ ⁺ & C ₅ H ₈ ⁺	Isoprene
	93	C _n H _{2n-5} ⁺	Monoterpenes
	39, 43, 45, 69, 70, 83	C _x H _y ⁺ / C _x H _y O ⁺ / C _x H _y O ₂ ⁺	Multiple compounds
	92 106, 91, 105	C ₇ H ₈ ⁺ C ₈ H ₁₀ ⁺ C ₈ H ₉ ⁺	Toluene C ₈ Aromatics C ₉ Aromatics fragment ion
NO ⁺	41, 55, 56, 57	C _x H _y ⁺	Hydrocarbons
	43, 69, 71	C _x H _y ⁺ / C _x H _y O ⁺	Multiple compounds
	45, 59	C _x H _y O ⁺ , C _x H _y O ₂ ⁺	Multiple compounds
	67 & 68	C ₅ H ₇ ⁺ & C ₅ H ₈ ⁺	Isoprene
	93	C ₇ H ₉ ⁺	Monoterpenes
	92 106 120	C ₇ H ₈ ⁺ C ₈ H ₁₀ ⁺ C ₉ H ₁₂ ⁺	Toluene C ₈ Aromatics C ₉ Aromatics

4.5 Supporting Measurements

The SRI-MS was deployed alongside a number of other instruments (Table 4.4) as a part of a more extensive study to provide a detailed characterization of the chemical and aerosol composition of the urban atmosphere in Sydney (Cope et al. 2014).

Samples were collected for VOCs on one each of the Marke's Carbograph 1TD/Carbopack X adsorbent tubes adsorbent tubes and for carbonyls on DNPH cartridges three times daily over periods that coincided with the PTR-MS measurement sequences: one 8-hour sample was collected in the morning (5 am – 10 am); one 8-hour sample was collected in the afternoon (11am – 7pm); and, one 10-hour sample was collected overnight (7pm – 5am). See Table 4.5.

The timing and duration of SRI-MS sampling in H₃O⁺, O₂⁺ and NO⁺ reagent ion modes are listed in Table 4.5, alongside the sampling times for the AT-VOC and DNPH samples.

Table 4.4: Summary of measurement systems deployed in the field study in Sydney 2011
Source: Cope et al., (2014).

Instrument	Measurement		Frequency
Particles	HiVol PM _{2.5}	PM _{2.5} , OC/EC, sugars (incl. Levoglucosan), water soluble ions	Integrated (2 samples/day) on all days
	Aerosol Mass Spectrometer	Particle composition as function of size >500nm	Continuous during 2 select periods
Criteria gas	Ecotech, Teco analysers	CO, NO, NO ₂ , NO _y , O ₃ , SO ₂	Continuous
Acid/alkaline gas	Gas filter sampler	NH ₃ , SO ₂ , HNO ₃	Integrated (2 samples/day) on all days
VOCs	VOC adsorbent tubes	VOCs	Integrated (3 samples/ day on all days)
	DNPH cartridges	Carbonyls	
	SRI-MS	VOCs	Continuous
Meteorology	Met station	Temp, RH, wind speed/direction	Continuous

The concentration of 27 VOCs, including alkanes, aromatic and biogenic compounds (Table 4.6) were determined from the air samples collected onto Marke's Carbograph 1TD/Carbopack X adsorbent tubes (Markes International Inc, Delaware, USA) using constant-flow air sampling pumps at a set flow rate of 20 mL min⁻¹. The tubes were analysed using an Automated Thermal Desorber and gas chromatograph (GC) equipped with a Flame Ionization Detector (FID) and a Mass Selective Detector (MSD). It should be noted that the GC-FID-MSD was calibrated with several of the same certified gas standards used to calibrate the SRI-MS (Chapter 3, Calibration gases 1, 3 and 5, components are listed in Tables 3.5 – 3.6). The adsorbent tube VOC samples will be referred to as AT-VOC samples in the following discussions.

The concentrations of 15 aldehydes and ketones (Table 4.6) were determined from air samples collected onto Supelco LpDNPH S10 air monitoring cartridges (Supelco Pennsylvania, USA) using constant flow air pumps at a set flow rate of 1 L min⁻¹. A KI ozone scrubber was placed in front of the sample cartridges. Carbonyls are trapped on the cartridge

where they are converted to the hydrazine derivatives. The derivatives are eluted from the cartridge in acetonitrile and analysed by HPLC.

Table 4.5: A summary of the sampling times for each measurement system.

	<u>Sampling times</u>		
	<i>Morning</i>	<i>Afternoon</i>	<i>Night</i>
H ₃ O ⁺ SRI-MS	5:00 – 10:00	11:00 – 15:00 <i>plus</i> 18:00 – 19:00	19:00 – 23:00 <i>plus</i> 4:00 – 5:00
O ₂ ⁺ SRI-MS		17:00 – 18:00	3:00 – 4:00
NO ⁺ SRI-MS		15:00 – 16:00	0:00 – 1:00
AT-VOC & DNPH	5:00 – 10:00	11:00 – 19:00	19:00 – 5:00

Table 4.6: Compounds measured in the AT-VOC samples and analysed by GC-FID-MS and in the DNPH samples analysed by HPLC.

AT-VOC			DNPH	
n-Butane	Isoprene	Benzene	Formaldehyde	Acetone
2-Methyl butane	α-Pinene	Toluene	Acetaldehyde	Acrolein
n-Pentane	β-Pinene	m-Xylene	Propanal	Methacrolein
2-Methyl pentane	p-Cymene	p-Xylene	Butenal	Benzaldehyde
3-Methyl pentane	D-Limonene	o-Xylene	Butanal	Tolualdehyde
n-Hexane	Eucalyptol	Ethylbenzene	Pentanal	Glyoxal
3- Methyl hexane	Camphor	o-Ethyltoluene	Hexanal	
n-Heptane		m-Ethyltoluene	Methyl ethyl ketone	
Methyl-cyclopentane		1,2,4-Trimethylbenzene	Methylglyoxal	
Cyclohexane		1,3,5-Trimethylbenzene		

4.6 Considerations for quantitative inter-comparisons

In this study, we will present inter-comparisons of the mixing ratios of several compounds that were measured by both the SRI-MS and in the parallel integrated AT-VOC and DNPH samples. In order to maximize the quality of an inter-comparison there several important factors that must be considered:

- Differences in the timing and duration of sampling between the two techniques being compared
- The signal/noise ratio of the data being analysed

- Appropriate regression analysis techniques for comparing observational data.

Firstly, in a comparison between two collocated measurement systems with equal sample timing and duration, any differences in their reported mixing ratios will largely arise from differences between the analytical techniques. As shown in Table 4.5, in the present study, the SRI-MS sampling times did not entirely overlap with the parallel, integrated AT-VOC and DNPH samples. Consequently, differences between the reported mixing ratios from the SRI-MS and AT-VOC or DNPH samples may arise, at least in part, from sampling bias. When comparing independent measurements of compounds, especially those with short atmospheric lifetimes (hours) such as isoprene, monoterpenes and higher aromatics (Atkinson & Arey 2003), the difference in timing between the measurement techniques can contribute significantly to their reported concentrations.

Table 4.7: Sample acquisition times for each reagent ion mode used in the inter-comparison of H_3O^+ , O_2^+ and NO^+ SRI-MS measurements.

O_2^+	H_3O^+
17:00 – 18:00	18:00 – 19:00
3:00 – 4:00	4:00 – 5:00
NO^+	H_3O^+
15:00 – 16:00	14:00 – 15:00
0:00 – 1:00	22:00 – 23:00 <i>plus</i> 4:00 – 5:00
NO^+	O_2^+
15:00 – 16:00	17:00 – 18:00
0:00 – 1:00	3:00 – 4:00

For each day of sampling three 5-hour averages (morning, afternoon, night) were calculated from the H_3O^+ SRI-MS data (Table 4.5) that coincided, as much as possible, with the AT-VOC and DNPH sampling times.

During the study in Sydney 2011, the SRI-MS sequentially sampled in H_3O^+ , O_2^+ and NO^+ reagent ion modes and the sampling periods could not overlap. The O_2^+ 1h average mixing ratios were compared with the consecutive 1 h average mixing ratios determined in H_3O^+ reagent ion mode (Table 4.7).

There was a 2-hour gap between H_3O^+ and NO^+ sampling times at night. In order to minimise sampling bias, the 1h average NO^+ mixing ratios were compared with the average of the combined H_3O^+ SRI-MS measurements from 22:00 – 23:00 and 4:00 – 5:00 (Table 4.7).

The second factor considered in the inter-comparison of measurement techniques was the signal to noise ratio of the m/z being analysed. The relative error of most instrument systems including SRI-MS, increases with decreasing VMR (Horwitz 1982, de Gouw & Warneke 2007). Therefore it is useful to check if the data being compared is substantially above the noise (MDL) level, otherwise the comparison will be dominated by the influence of random instrument noise.

To do this the ratio of the median of the sample set to the MDL was calculated for the SRI-MS, AT-VOC and DNPH measurements. Median/MDL values above 10 were considered suitable for a robust quantitative comparison as 50% of the data was >10 times the MDL. Measurements of some compounds with median/MDL ratios < 10 were compared; however the low VMRs precluded an accurate quantitative comparison.

As discussed in 4.2.2, the instrument background during NO^+ SRI-MS measurements was high and unstable in comparison to H_3O^+ and O_2^+ reagent ion modes. As a result, the minimum detection limits of the NO^+ SRI-MS measurements were significantly higher (Table 4.8) and the median/MDL ratios for the NO^+ SRI-MS measurements were < 10 for all m/z studied. The results for several key NO^+ SRI-MS m/z are compared with measurements in H_3O^+ reagent ion mode in 4.9, however the low median/MDL ratios observed limited the accuracy of the quantitative inter-comparison.

Table 4.8: The minimum detection limits (MDL) for several VOC compounds measured in this study.

	H_3O^+ SRI-MS		O_2^+ SRI-MS		NO^+ SRI-MS	
	m/z	MDL (ppbv)	m/z	MDL (ppbv)	m/z	MDL (ppbv)
Benzene	79	0.02	78	0.02	78	0.11
Toluene	93	0.02	92	0.02	92	0.08
C_8 aromatics	107	0.02	106	0.07	106	0.09
C_9 aromatics	121	0.02	120	0.05	120	0.08
Isoprene	69	0.04	67	0.01	68	0.08
Monoterpenes	81	0.03	93	0.01	93	0.08

Finally, reduced major axis (RMA) regression analysis was used to determine the quantitative agreement between the SRI-MS in each reagent ion mode and the independent measurement techniques for the selected compounds. When comparing two observational datasets RMA regression is preferable to simple linear regression as RMA can account for random measurement errors on both the x- and y- variables, rather than only the y-variable (Ayers 2001).

For the inter-comparisons reported in this study, acceptable quantitative agreement between two independent measurements was defined as a slope from RMA regression analysis equal to $1 \pm 20\%$.

4.7 SRI-MS measurements of selected VOCs in urban air with H_3O^+

Twenty-two key m/z were identified in the H_3O^+ SRI-MS mass scans of urban air, according to the criteria in section 4.4. Of these, there were 11 m/z attributed to compounds measured by both the H_3O^+ SRI-MS and one of the independent VOC measurement techniques (DNPH/AT-VOC).

Both the AT-VOC technique and the H_3O^+ SRI-MS measured benzene (m/z 79), toluene (m/z 93), the sum of the C_8 aromatics (m/z 107), the sum of the C_9 aromatics (m/z 121), isoprene (m/z 69) and the sum of the monoterpenes (m/z 81, 137). The common species measured by both the DNPH and H_3O^+ SRI-MS were formaldehyde (m/z 31), acetaldehyde (m/z 45), acrolein (m/z 57), acetone (m/z 59), and methacrolein (m/z 71).

The ratio of the median benzene concentration versus the MDL (ppb/ppb) for the whole data set was 1.4 which is significantly less than the value of 10, specified for a robust quantitative comparison and benzene is not considered further here.

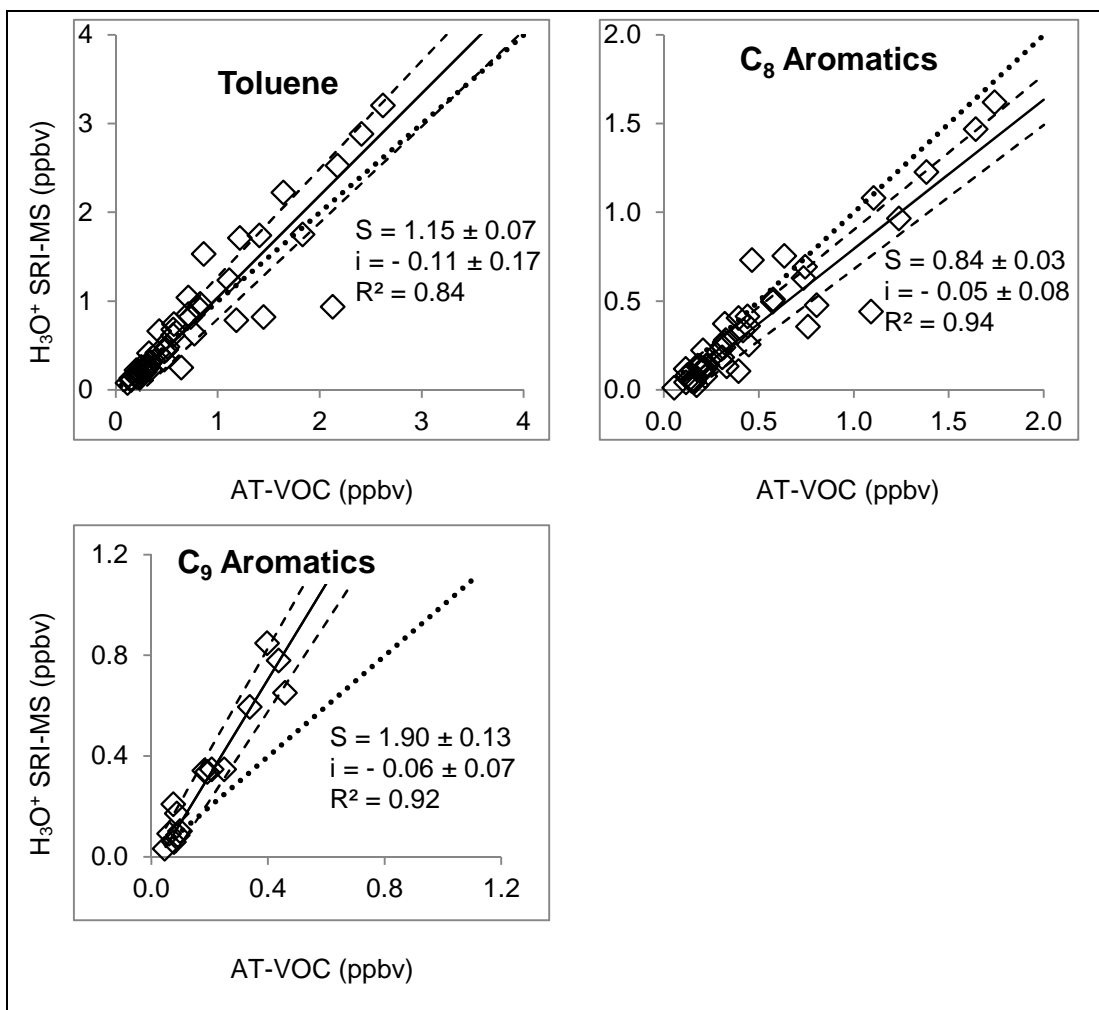


Figure 4.3: Comparisons of toluene, and the C₈- and C₉- aromatics measured by H₃O⁺ SRI-MS and in the AT-VOC samples analysed by GC-FID-MS from Sydney 2011. Dotted line is 1:1. Also included are the Slopes (S)(solid line), error limits (dashed lines), intercepts (i), and correlation coefficients (R²) from the reduced major axis regression analysis.

4.7.1 H₃O⁺ SRI-MS m/z 93: Toluene

The ratio of the median toluene concentration measured by the H₃O⁺ SRI-MS versus the MDL (ppb/ppb) for the whole data set was 18 and the mixing ratios observed in the morning afternoon and nighttime sampling periods are sufficiently high enough to perform a meaningful quantitative comparison with all AT-VOC data (N = 48).

The results of the RMA regression analysis yielded good agreement between the H₃O⁺ SRI-MS signal at m/z 93 and the AT-VOC data for toluene with, R² of 0.83, a slope of 1.21 ± 0.07 , and an intercept of -0.10 ± 0.19 ppb (Figure 4.3).

It is possible the slope > 1 is a result of contributions to the H_3O^+ SRI-MS signal at m/z 93 from compounds other than toluene. In measurements of certified gas standard mixtures, (Chapter 3, sect 3.4) when the SRI-MS was operating with H_3O^+ , protonated toluene was detected at m/z 93 with minor contributions from several C_9 aromatic compounds (m-, p-, o-ethyl toluene, 1,2,3-trimethylbenzene) that have branching ratios to m/z 93 of $\sim 3\%$.

Another minor positive contribution at m/z 93 has been reported to result from the presence of fragment ions of some monoterpenes (de Gouw & Warneke 2007, Ambrose et al. 2010). α -pinene, β -pinene and p-cymene have branching ratios to m/z 93 of 7%, 7% and 66% respectively (Warneke et al. 2003, Maleknia et al. 2007).

In this study, m- and o-ethyl toluene, α - and β -pinene and p-cymene were measured in the AT-VOC samples. The AT-VOC reported concentration of each of these compounds was multiplied by their empirically determined branching ratios (de Gouw et al. 2003, Warneke et al. 2003, Maleknia et al. 2007, Gueneron et al. 2015) to estimate their possible contribution to m/z 93. When the contributions from the C_9 aromatics, α - and β -pinene, and p-cymene were added to the toluene concentration measured in the AT-VOC samples the slope of the RMA regression was 1.15 ± 0.07 and intercept of -0.11 ± 0.17 ($R^2 = 0.84$) (Figure 4.3). We concluded that these compounds comprised only a minor fraction of the signal at m/z 93 in this study.

The quantitative agreement between H_3O^+ SRI-MS and the AT-VOC samples analysed by GC-MS in this study were consistent with many previous inter-comparison studies with GC techniques most of which have reported good quantitative agreement (slopes 0.52 – 1.18) (Warneke et al. 2001, de Gouw et al. 2003, Warneke et al. 2003, Kato et al. 2004, Kuster et al. 2004, de Gouw & Warneke 2007).

In summary, in the H_3O^+ SRI-MS measurements of urban air in this study, the signal at m/z 93 contained substantial contributions of toluene with minor contributions ($< 10\%$) from fragment ions of terpenes and C_9 aromatic compounds. Despite the presence of these additional compounds the H_3O^+ SRI-MS measurements of toluene at m/z 93 quantitatively agreed with the AT-VOC reported values within the criteria of $\pm 20\%$.

4.7.2 H_3O^+ SRI-MS m/z 107: C_8 Aromatics

In measurements of the atmosphere with H_3O^+ SRI-MS the signal at m/z 107 is commonly regarded as a measure of the sum of the C_8 aromatic isomers: m-, p-, o- xylenes plus ethylbenzene. The ratio of the median concentration measured at m/z 107 by the H_3O^+ SRI-MS versus the MDL for the whole data set was 13 and the mixing ratios observed are sufficiently high enough to perform a meaningful quantitative comparison with the sum of the C_8 aromatics measured in the AT-VOC samples for all data ($N = 48$).

The results of the reduced major axis regression analysis for the H_3O^+ SRI-MS measurements at m/z 107 versus the C_8 aromatics measured in the AT-VOC samples from Sydney yielded a slope of 0.84 ± 0.03 , intercept of -0.05 ± 0.08 , $R^2 = 0.94$ (Figure 4.3).

In measurements of the atmosphere, the H_3O^+ SRI-MS signal at m/z 107 may also contain contributions from benzaldehyde (de Gouw et al. 2003, Warneke et al. 2003). A ~5% contribution of $\text{C}_7\text{H}_7\text{O}^+$ product ions was observed in the H_3O^+ SRI-MS signal at m/z 107 in PTR-TOF measurements of ambient air in a region of oil and gas extraction (Warneke et al. 2015).

In this study, benzaldehyde, measured in the DNPH samples, was on average 5% (range: 0-19%) of the C_8 aromatic concentrations measured in the AT-VOC samples. The sum of the C_8 aromatics plus benzaldehyde was calculated from the AT-VOC and DNPH data sets. The results of the reduced major axis regression analysis for the H_3O^+ SRI-MS measurements at m/z 107 versus the [C_8 aromatics + benzaldehyde] measured in the AT-VOC and DNPH samples from Sydney indicate benzaldehyde was a very minor fraction of the signal at m/z 107 (slope = 0.83 ± 0.03 , intercept of -0.06 ± 0.08 , $R^2 = 0.94$).

During the field study, in Sydney the H_3O^+ SRI-MS was calibrated with a certified standard containing m-xylene but not p-, o- xylene or ethylbenzene. In a separate laboratory study, when the H_3O^+ SRI-MS was exposed to a certified gas standard containing m-, p- and o-xylene plus ethylbenzene, among other components, the sensitivity at m/z 107 was 10% lower than in measurements of the standard containing only m-xylene. Applying an adjusted calibration factor to the data from Sydney improved the slope of the relationship between the H_3O^+ SRI-MS and AT-VOC data for the C_8 aromatics to 0.91.

The quantitative agreement between H_3O^+ SRI-MS and the AT-VOC samples analysed by GC-MS in this study was consistent with many previous inter-comparison studies with GC techniques most of which have reported good quantitative agreement (slopes 0.78 – 1.02) (de Gouw et al. 2003, Warneke et al. 2003, Kato et al. 2004, Kuster et al. 2004, Steinbacher et al. 2004, de Gouw & Warneke 2007).

In conclusion, the C_8 aromatic compounds dominated the H_3O^+ SRI-MS signal at m/z 107. The sum of the C_8 aromatic compounds measured at m/z 107 by H_3O^+ SRI-MS and the sum of the C_8 aromatic compounds measured in the AT-VOC samples quantitatively agreed within the criteria of $\pm 20\%$.

4.7.3 H_3O^+ SRI-MS m/z 121: C_9 aromatics

In measurements of the atmosphere, the signal at m/z 121 is attributed to the sum of the C_9 aromatics (1,2,3-, 1,2,4- and 1,3,5-trimethylbenzene, m-, p-, o-ethyl toluene, propyl benzene and, isopropyl benzene).

The ratio of the median of the m/z 121 signal versus the MDL for the whole dataset was 4.1, which is significantly less than the value of 10, specified for a robust quantitative comparison. However, the median/MDL ratio for the morning sampling periods was 14.6 and only the data from the morning sampling period were analysed further.

Only four of the possible eight C_9 aromatic isomers were measured in the AT-VOC samples (1,2,4- and 1,3,5-, trimethylbenzene, and m-, o-ethyl toluene). These other compounds (1,2,3-trimethyl benzene, p-ethyl toluene, and propyl- and isopropyl- benzene) while detected, failed to meet the criteria for quantitative measurement with regard to field blanks and breakthrough.

The H_3O^+ SRI-MS reported values for the C_9 aromatics were highly correlated with the sum of C_9 aromatics measured in the AT-VOC integrated samples ($R^2 = 0.92$), however the quantitative agreement significantly differed from unity with a slope of 1.90 ± 0.13 and intercept of -0.06 ± 0.07 ($N = 15$) (Figure 4.3).

In measurements of the atmosphere the H_3O^+ SRI-MS signal at m/z 121 may also contain contributions from tolualdehyde (de Gouw et al. 2003, Warneke et al. 2003). $\text{C}_8\text{H}_9\text{O}^+$ product

ions contributed 10% to the observed signal at m/z 121 in PTR-TOF measurements of ambient air in a region of oil and gas extraction (Warneke et al. 2015).

In this study, tolualdehyde, measured in the DNPH samples, was on average 5% (range: 0-7%) of the C_9 aromatic concentrations measured in the AT-VOC samples. Adding the tolualdehyde in the DNPH samples to the sum of the $\Sigma[C_9 \text{ Aromatics}]$ in the AT-VOC samples had a negligible effect on the results of the RMA regression indicating that tolualdehyde made at most a very minor contribution to the signal at m/z 121 in this study.

Previous inter-comparison studies between PTR-MS and GC techniques have observed slopes of 0.98 – 2.0 (Kato et al 2004, Kuster et al 2004, de Gouw et al 2003a) with the agreement dependent upon whether all eight C_9 -aromatic isomers were determined accurately for the inter-comparison.

In the present study, an insufficient number of the C_9 aromatics were measured in the AT-VOC samples to make a quantitative comparison with the H_3O^+ SRI-MS signal at m/z 121. However, we concluded that the H_3O^+ SRI-MS signal at m/z 121 contained substantial contributions from C_9 aromatic compounds.

4.7.4 H_3O^+ SRI-MS m/z 69: Isoprene

In measurements of the atmosphere, the signal at m/z 69 is commonly regarded as a measure of isoprene. The ratio of the median m/z 69 signal measured by the H_3O^+ SRI-MS versus the MDL (ppb/ppb) for the whole dataset was 11.4 the mixing ratios observed in the sufficient to perform a meaningful quantitative comparison with all of the AT-VOC data ($N=48$).

The H_3O^+ SRI-MS measurements of isoprene at m/z 69 and AT-VOC data for isoprene differed significantly from unity with a slope of 2.13 ± 0.11 and intercept of 0.13 ± 0.25 (R^2 of 0.76). As can be seen in the scatterplot in Figure 4.4, there were two outliers in the data. These occurred consecutively on the night of the 19/2 followed by the morning sample on the 20/2. When these outliers are removed, the slope of the RMA regression becomes 1.84 ± 0.06 and intercept of 0.11 ± 0.16 , $R^2 = 0.90$).

The slope > 1 may be a result of contributions to m/z 69 from compounds other than isoprene. Park et al (2013) observed three peaks at m/z 69 in the PTR- Time of Flight (PTR-

ToF) spectra of ambient air in an orange orchard: $\text{C}_3\text{H}_2\text{O}_2\text{H}^+$ (m/z 68.997), $\text{C}_4\text{H}_4\text{OH}^+$ (m/z 69.034) and $\text{C}_5\text{H}_8\text{H}^+$ (m/z 69.071) with mean 24h mixing ratios of 0.037, 0.052 and 0.28 ppb respectively.

GC-PTR-MS analysis has also shown that multiple other species can contribute to the ion signal at m/z 69. Specifically, 2-/3- methyl-butanal and 1-penten-3-ol in urban air (de Gouw et al. 2003), and furan in air masses impacted by biomass burning (Christian et al. 2004). In air impacted by emissions from pine trees, 2-methyl-3-buten-2-ol, was reported to contribute ~20 – 50 % of the m/z 69 ion signal (Karl et al. 2012).

Protonated 2-methyl-3-buten-2-ol, 1-penten-3-ol, and 2-/3-methyl-butanal are detected at m/z 87, with a fragment ion signal at m/z 69 (Amelnyck et al. 2005, Michel et al. 2005). In this study, the correlation of m/z 87 with m/z 69 was $R^2 = 0.66$ indicating a contribution at m/z 69 from C_5 aldehydes and unsaturated alcohols did occur.

For the m/z 69 data in the present study, the contribution of hydrocarbon (C_xH_y) versus oxygenated ($\text{C}_x\text{H}_y\text{O}_z$) product ions was investigated by analysing the ^{13}C isotopologue of the ion signal at m/z 69. The natural ^{13}C isotopic abundance is 1.11%; thus if the signal at m/z 69 was dominated by C_5 compounds, 5.5% of the signal at m/z 69 would have been detected at m/z 70. The observed ratio of m/z 70: m/z 69 was 0.059 ($R^2 = 0.85$), indicating the signal at m/z 69 was dominated by C_5 product ions.

Previous inter-comparison studies between PTR-MS and GC techniques have observed slopes of 0.96 – 2.15 often with significant (14 – 120 pptv) offsets (Kato et al 2004, Kuster et al 2004, de Gouw et al 2003a). In general, isoprene measurements at m/z 69 in air that is not dominated by biogenic emissions are considered to be affected by interference (de Gouw & Warneke 2007).

In conclusion, C_5 compounds dominated the H_3O^+ SRI-MS ion signal at m/z 69. The H_3O^+ SRI-MS signal at m/z 69 was significantly higher than the AT-VOC reported values for isoprene. The presence of compounds other than isoprene that produce ion signals at m/z 69 probably contributed to the positive interference.

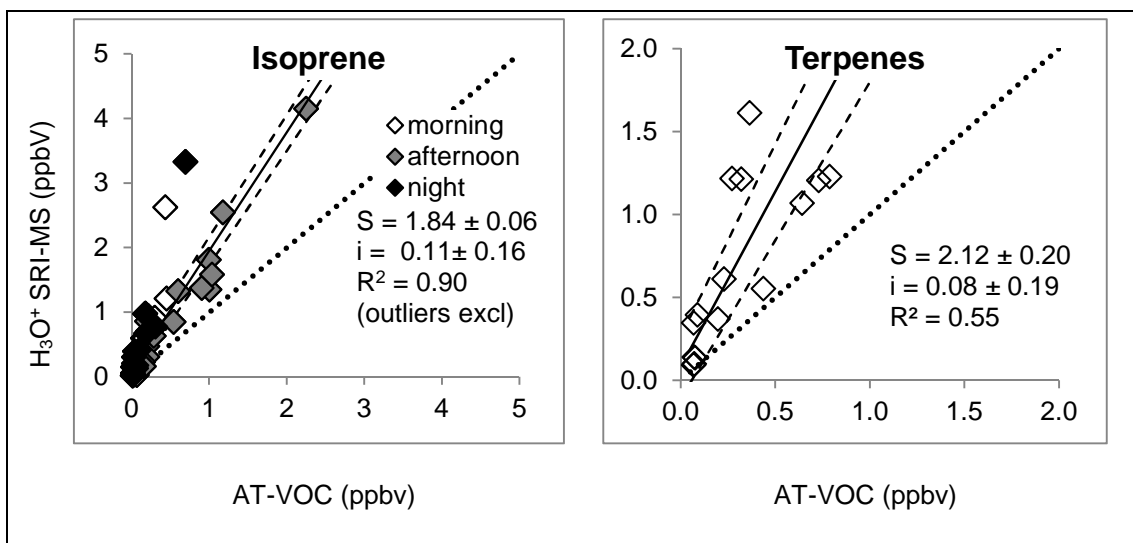


Figure 4.4: Scatterplots of isoprene and terpene measurements by H_3O^+ SRI-MS and the AT-VOC samples analysed by GC-FID-MS from Sydney 2011. Dotted line is 1:1. Also included are the Slopes (S)(solid line), error limits (dashed lines), intercepts (i), and correlation coefficients (R^2) from the reduced major axis regression analysis.

4.7.5 H_3O^+ SRI-MS m/z 81 & 137: Monoterpenes

In H_3O^+ SRI-MS, the protonated molecular ion (m/z 137) and a $\text{C}_6\text{H}_8\text{H}^+$ (m/z 81) fragment ion are the dominant product ions from most monoterpenes (Tani et al. 2003). However these ion signals may also contain contributions from sesquiterpenes and oxygenated terpenoids (Lee et al. 2005). In this study the signals at m/z 81 and 137 were highly correlated (Slope = 1.17 ± 0.02 , intercept = 0.03 ± 0.02 , $R^2 = 0.99$). Given the higher ion signals, m/z 81, was used to measure monoterpenes in this study.

In the study in Sydney, the ratio of the median concentration measured at m/z 81 by the H_3O^+ SRI-MS versus the MDL for the whole dataset was 10.7 and the mixing ratios observed are sufficiently high enough to perform a meaningful quantitative comparison with the AT-VOC data ($N = 48$). However, when comparing independent measurements of compounds with short atmospheric lifetimes such as monoterpenes (atmospheric lifetimes $\sim 1\text{h}$) (Atkinson & Arey 2003), the difference in timing between the measurement techniques is important. In the present study, the timing and duration of the H_3O^+ SRI-MS and AT-VOC sampling were roughly equivalent only in the morning sampling period (5:00 – 10:00) and only the mixing ratios for this period were analysed further.

α -pinene β - pinene, D-limonene, p-cymene, 1,8-cineole and camphor were measured in the AT-VOC samples in this study. Camphor and p-cymene are not known to produce ion

signals at m/z 81 or 137 and are not considered further. For this analysis, the H_3O^+ SRI-MS signal at m/z 81 was compared with the sum of terpenoids measured in the AT-VOC samples, here referred to as $\Sigma[\text{terpenx}]$, where:

$$\Sigma[\text{terpenx}] = [\alpha\text{-pinene}] + [\beta\text{-pinene}] + [\text{D-limonene}] + [1,8\text{ cineole}]$$

Figure 4.4 contains a scatterplot of the m/z 81 versus $\Sigma[\text{terpenx}]$. The qualitative agreement between the H_3O^+ SRI-MS measurements at m/z 81 and the AT-VOC reported values $\Sigma[\text{terpenx}]$ was poor ($R^2 = 0.55$) and the slope of the RMA regression differed from unity (Slope = 2.12 ± 0.20 , intercept = 0.08 ± 0.19 , $N = 15$).

The H_3O^+ SRI-MS was calibrated with a certified gas standard containing α -pinene. Individual monoterpenes and oxygenated monoterpenes have different reaction rates and branching ratios in reactions with H_3O^+ (Schoon et al. 2003, Tani et al. 2003, Amelnyck et al. 2005). 57% of the α -pinene signal has been observed to occur at m/z 81 in comparison to 70% for β -pinene, 72% for D-limonene, and 56% for 1,8-cineole (Maleknia et al. 2007).

Also the relative concentrations of each of the terpenoids in the AT-VOC samples differed: α -pinene (17%), β -pinene (48%), D-limonene (10%), and 1,8-cineole (25%). Therefore, the accuracy of the calibration factor based on α -pinene would have been dependent on the relative concentration of all terpeneoid compounds present that yielded signals at m/z 81.

Furthermore, over 5000 isomers of monoterpenes, sesquiterpenes, diterpenes and other terpenoids have been identified in the atmosphere, with a subset of 14 monoterpenes commonly emitted from a variety of tree species (Geron et al. 2000). Thus, $\Sigma[\text{terpenx}]$ identified in the AT-VOC samples in this study are likely to be a considerable but not complete fraction of the terpenes actually present.

Previous inter-comparisons of PTR-MS with GC techniques have reported slopes from 0.80 – 1.93, R^2 0.94 – 0.66 (de Gouw et al. 2003, Lee et al. 2005, de Gouw & Warneke 2007). The slope of 1.93 ($R^2 = 0.66$) was reported by de Gouw and Warneke (2007) and was attributed to two factors: only α - and β -pinene were measured in the air samples analysed by the GC; and, there was a minor difference in sampling times (20 secs) between the two methods, which contributed to the scatter observed.

Analysis of ambient air by a high resolution PTR-ToF located in an orange orchard observed two peaks at m/z 81 identified as $C_6H_8H^+$ (terpenx fragment ion) and a smaller peak at $C_5H_4OH^+$ with 24 h mean mixing ratios of 0.5 and 0.05 ppb respectively. It is therefore possible oxygenated product ions also made a minor contribution to the ion signal at m/z 81 in this study.

For the m/z 81 data in the present study, the contribution of hydrocarbon (C_xH_y) versus oxygenated ($C_xH_yO_z$) product ions was investigated by analysing the ^{13}C isotopologue of the ion signal at m/z 81. The natural ^{13}C isotopic abundance is 1.109%; thus if the signal at m/z 81 was dominated by C_6 compounds, ~ 6.7% of the signal at m/z 81 would have been detected at m/z 82. The observed ratio of m/z 82: m/z 81 was 0.074 ($R^2 = 0.71$) in this study, indicating the signal at m/z 81 was dominated by C_6 product ions.

We concluded that the H_3O^+ SRI-MS signal at m/z 81 contained substantial contributions from monoterpene fragment ions but an insufficient number of the terpenes were measured in the AT-VOC samples to make a quantitative comparison. Furthermore, non-equivalent sampling times may have contributed to the scatter observed.

4.7.6 H_3O^+ SRI-MS m/z 31: Formaldehyde

The ratio of the median H_3O^+ SRI-MS signal measured at m/z 31 versus the MDL for the whole dataset was 6.7. However, the mean/MDL ratio for the afternoon sampling periods (11:00 – 19:00) was 11.7, and only the data from the afternoon sampling period were analysed further here ($N= 12$).

The accurate quantitative measurement of formaldehyde with H_3O^+ SRI-MS is complex as its proton affinity is only slightly greater than the proton affinity of water and loss via back reaction in humid air is non-negligible (Inomata et al., 2008). As a result, significant scatter was observed in the calibration measurements of formaldehyde in this study ($\pm 16\%$). To account for this variability, a moving calibration factor was applied to the data.

Formaldehyde was also measured in the DNPH samples from Sydney 2011. There was a significant discrepancy between the DNPH reported values and the H_3O^+ SRI-MS measurements for multiple carbonyl compounds for the period 18 / 2/2011 – 21/2/2011. The cause of this discrepancy was unclear however as shown in Figure 4.5, the effect appeared larger for ketones (acetone) than for the aldehydes (formaldehyde). Ketones are less reactive

than aldehydes in the derivatization with DNPH, resulting in poorer collection efficiencies (Ho et al. 2014).

This period coincided with high ambient temperatures, in excess of 30 °C which may have impacted the collection efficiency and/or sample stability of the DNPH cartridges. The data from this period was excluded from the comparison of the H_3O^+ SRI-MS and DNPH data.

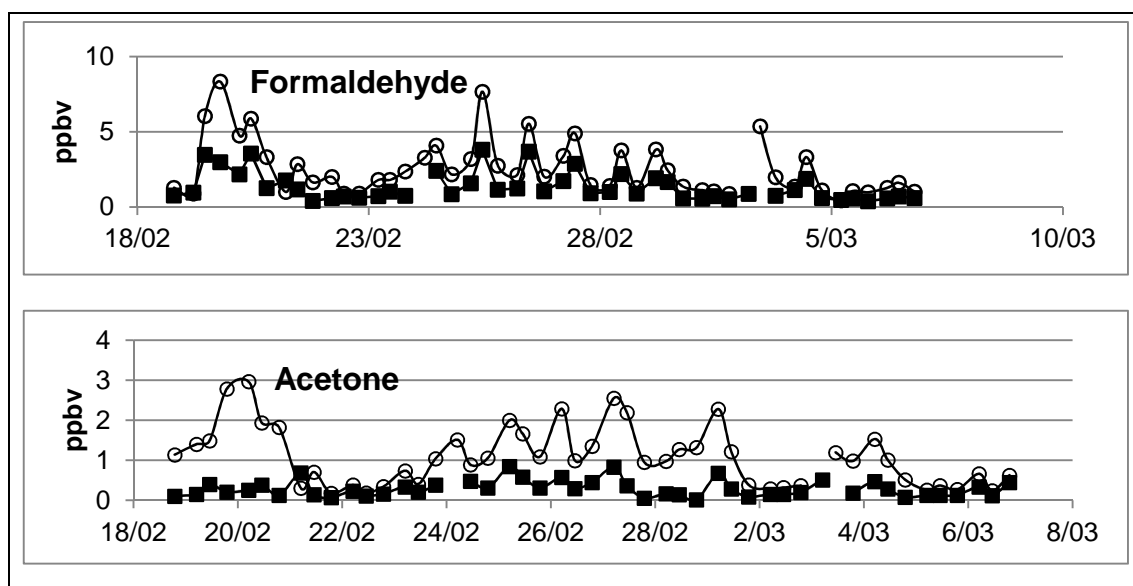


Figure 4.5: Time series of formaldehyde and acetone measured by both the H_3O^+ SRI-MS (open circles) and in the DNPH samples (black squares) from Sydney 2011. Note the large discrepancy in the two datasets for the period 18/2/11 – 21/02/11.

The results of the reduced major axis regression analysis between the H_3O^+ SRI-MS measurements at m/z 31 and formaldehyde in the DNPH samples from Sydney 2011 are shown in Figure 4.6. The concentration of formaldehyde in the DNPH samples was well correlated with the VMRs reported for m/z 31 with R^2 of 0.95. The quantitative agreement between the H_3O^+ SRI-MS and DNPH data for formaldehyde differed from unity with a slope of 1.81 ± 0.13 and intercept of -0.01 ± 0.26 ($N = 12$).

Several authors have reported DNPH values for formaldehyde that were systematically lower by 15 – 35% than those reported by other analytical methods (DOAS, FTIR, Hantzsch, TDLAS) (Kleindienst et al. 1988, Lawson et al. 1990, Gilpin et al. 1997, Hak et al. 2005).

Variable results were reported for DNPH and PTR-MS measurements of formaldehyde undertaken across a range conditions (humidity, ozone) as part of an inter-comparison study in an atmosphere simulation chamber (Apel et al. 2008, Wisthaler et al. 2008). The

formaldehyde measured in the DNPH samples was on average 38% lower than the known concentration of formaldehyde in the chamber (range -89% to +15%). A PTR-MS specially optimized for formaldehyde measurements, reported values on average 5% higher than the known concentration of formaldehyde in the chamber (range -26% to +70%).

Overall, formaldehyde made a considerable contribution to the H_3O^+ SRI-MS signal at m/z 31. The H_3O^+ SRI-MS observed substantially more formaldehyde than the DNPH technique however the comparison presented here alongside other published studies, casts doubt on both methods.

4.7.7 H_3O^+ SRI-MS m/z 45: Acetaldehyde

The ratio of the median acetaldehyde concentration measured at m/z 45 by the H_3O^+ SRI-MS versus the MDL (ppb/ppb) for the whole dataset was 17, and the mixing ratios observed are sufficiently high enough to perform a meaningful quantitative comparison with all DNPH data ($N = 37$).

The results of the reduced major axis regression analysis between the H_3O^+ SRI-MS measurements at m/z 45 and acetaldehyde in the DNPH samples from Sydney 2011 are shown in Figure 4.6. The concentration of acetaldehyde in the DNPH samples correlated well with the VMRs reported for m/z 45 with R^2 of 0.82. The quantitative agreement between the H_3O^+ SRI-MS and DNPH data for acetaldehyde significantly differed from unity with a slope of 1.75 ± 0.12 and intercept of 0.00 ± 0.07 ($N = 37$).

The inter-comparison study of oxygenated VOC measurements in an atmosphere simulation chamber (Apel et al., 2008) reported measurements by DNPH method significantly underestimated the concentration of acetaldehyde (slope ~ 0.6 , intercept ~ 0.5 ppb, $R^2 \sim 0.65$). The reasons for the discrepancy were related to the calibration standards employed, the collection efficiency and variability of the DNPH sample cartridges. In the same study, three PTR-MS instruments measured acetaldehyde at m/z 45 with good agreement (Slopes $\sim 0.7 - 1.0$, intercept ~ 0 , $R^2 > 0.98$).

It is also possible compounds other than acetaldehyde contributed to the signal at m/z 45. Due to structural constraints the signal at m/z 45 can be either $\text{C}_2\text{H}_5\text{O}^+$, protonated carbon dioxide (HCO_2^+) or CH_3NO^+ . The contribution of carbon dioxide should be removed during zero correction and the signal at m/z 45 is expected to be solely $\text{C}_2\text{H}_5\text{O}^+$. Studies of ambient

air by high resolution PTR-TOF confirm a single peak at m/z 45 consisting of $C_2H_5O^+$ (Park et al. 2013, Warneke et al. 2015).

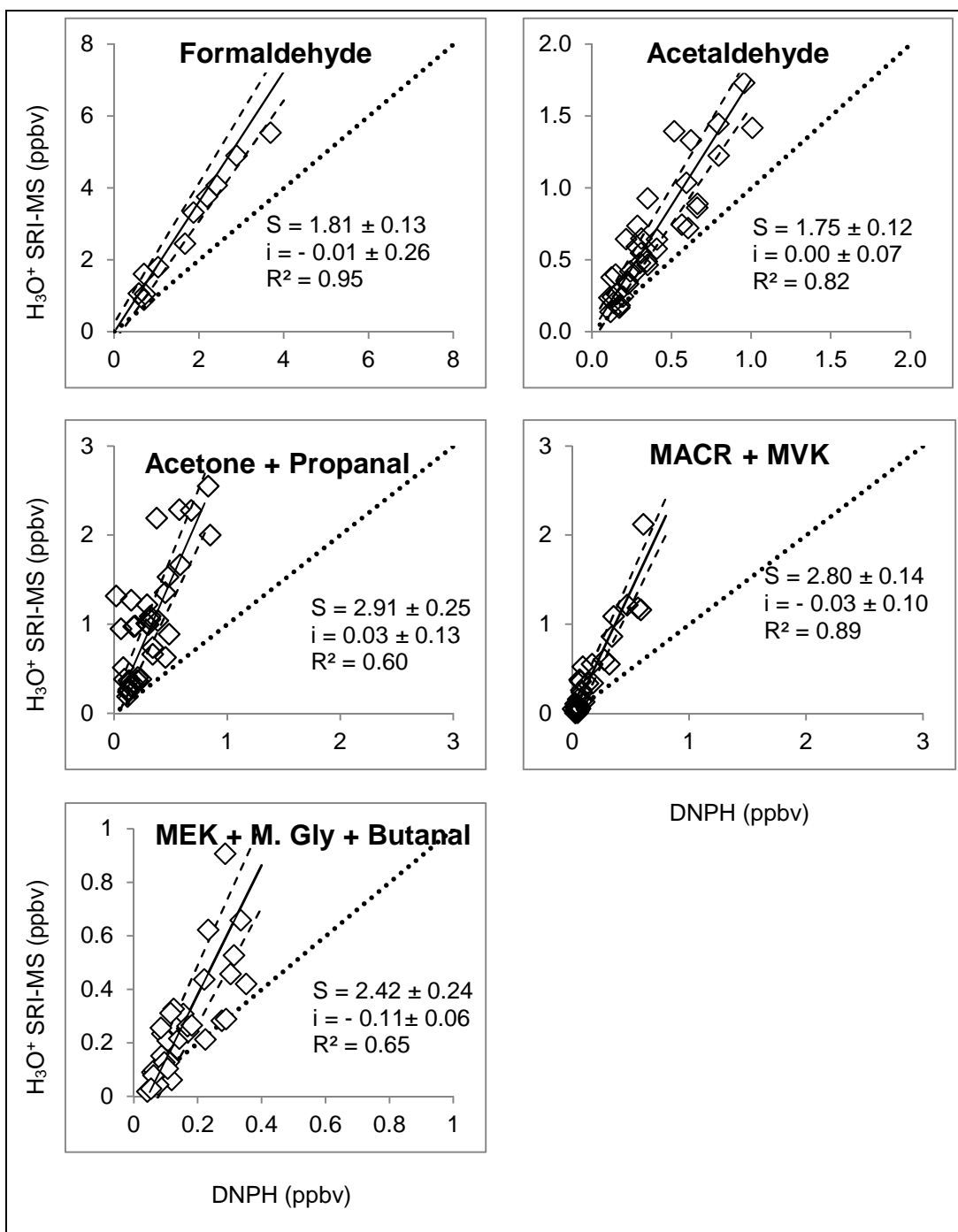


Figure 4.6: Comparisons for the aldehydes and ketones measured by the H_3O^+ SRI-MS and the DNPH samples analysed by HPLC for Sydney 2011. Dotted line is 1:1. Also included are the Slopes (S)(solid line), error limits (dashed lines), intercepts (i), and correlation coefficients (R^2) from the reduced major axis regression analysis.

In addition to protonated acetaldehyde, $C_2H_5O^+$ may also be protonated vinyl alcohol and/or protonated ethylene oxide but the occurrence of these compounds in the atmosphere is

unknown. Ethylene glycol, ($\text{C}_2\text{H}_6\text{O}_2$) emitted from vehicles, (Wood et al. 2015), produces a significant fragment ion signal at m/z 45 but it was unlikely to be consistently present in concentrations sufficient to account for the large slope observed in this study.

A fragment ion signal at m/z 45 was observed in the mass spectra of ethanol and 2-propanol, methyl ethyl ketone, methyl glyoxal, and methyl isobutyl ketone (Chapter 2) but this is a minor fragmentation pathway for these compounds ($< 10\%$) under the SRI-MS conditions employed in this study, and it is reasonable to assume they had a minor influence on the m/z 45 ion signal measured in Sydney 2011.

Interestingly, m/z 45 was also identified as a key m/z in the O_2^+ and NO^+ measurements in this study (Figure 4.2) and the ion signals at m/z 45 in all three reagent ion modes correlate with one another ($R^2 > 0.73$). Acetaldehyde is not detected at m/z 45 in O_2^+ and NO^+ reagent ion modes. This suggests the presence of a compound/s that undergoes dissociative chemical ionization reactions with H_3O^+ , O_2^+ and NO^+ yielding a significant product ion signal at m/z 45 with a similar temporal behavior to acetaldehyde.

A previous study comparing H_3O^+ SRI-MS measurements of acetaldehyde with GC-MS reported a slope of 1.56 ($R^2 > 0.86$). The discrepancy between the two methods was attributed a decline in the acetaldehyde mixing ratio in the calibration standard over time resulting in a calibration factor for acetaldehyde that was 1.6 times lower than in earlier calibrations (de Gouw et al. 2003).

The stability of acetaldehyde in the calibration standard used in the study in Sydney 2011 could not be determined due to changes in the tuning of the mass spectrometer following this study that varied the instrument response at m/z 45 for a fixed input of acetaldehyde.

Overall, the H_3O^+ SRI-MS signal at m/z 45 contained substantial contributions from acetaldehyde with some contributions from other unknown compounds. The H_3O^+ SRI-MS reported values were significantly higher than the acetaldehyde measured in the DNPH samples, however the comparison presented here alongside other published studies, casts doubt on both methods.

4.7.8 H_3O^+ SRI-MS m/z 59: Acetone & Propanal

The ratio of the median concentration measured at m/z 59 by the H_3O^+ SRI-MS versus the MDL (ppb/ppb) for the whole dataset was 44, and the mixing ratios observed are sufficiently high enough to perform a meaningful quantitative comparison with all DNPH data ($N = 37$).

In measurements of the atmosphere with H_3O^+ SRI-MS, the ion signal at m/z 59 is commonly regarded as a measure of acetone, but may also contain contributions from propanal (de Gouw & Warneke 2007). Protonated glyoxal ($\text{C}_2\text{H}_3\text{O}_2^+$) would also occur at m/z 59, however, tests of a prepared gaseous standard of glyoxal described in chapter 2, and recent published studies (Thalman et al. 2015) suggest there is no detectable response to glyoxal at m/z 59. Furthermore, PTR-ToF measurements of the atmosphere observe a single peak attributed to $\text{C}_3\text{H}_7\text{O}^+$ (Park et al. 2013, Warneke et al. 2015). Glyoxal was not considered to have contributed to m/z 59 in this study.

Acetone, and propanal were also measured in the DNPH samples in this study. The agreement between the sum of acetone and propanal in the DNPH samples with the VMRs reported for m/z 59 was poor with R^2 of 0.60, and a slope of 2.91 ± 0.25 , intercept = 0.03 ± 0.13 (Figure 4.6).

The poor agreement for acetone observed between the between the H_3O^+ SRI-MS and the DNPH may be due to contributions to the signal at m/z 59 from compounds other than acetone and propanal. No other possible candidates with product ion signals at m/z 59 that are known to be present in the atmosphere in sufficient concentrations to generate significant ion signals could be found.

Interestingly, m/z 59 was also identified as a key m/z in the O_2^+ and NO^+ measurements in this study (Figure 4.2). The correlation of the H_3O^+ SRI-MS ion signal at m/z 59 with the O_2^+ and NO^+ SRI-MS ion signals at m/z 59 were R^2 of 0.84 and 0.51 respectively. Acetone is not detected at m/z 59 in O_2^+ and NO^+ reagent ion modes. This suggests the presence of a compound/s that undergo dissociative chemical ionization reactions with H_3O^+ , O_2^+ and NO^+ yielding a product ion signal at m/z 59.

On average propanal was 16 ± 22 % of the acetone concentration measured in the DNPH samples. However, the H_3O^+ SRI-MS m/z 59 signal was more highly correlated with the concentration of propanal in the DNPH samples ($R^2 = 0.59$) than the concentration of acetone.

Of these two compounds, acetone is known to be the dominant species in the atmosphere (Singh et al. 1994) and the low correlation of m/z 59 with DNPH acetone is possibly a result of an analytical bias.

Ho et al. (2014) identified significant negative biases in the collection efficiency of acetone on DNPH cartridges that were related to relative humidity (RH), sample flow rates, and sampling time. While a different DNPH cartridge type was employed in the study by Ho et al. (2014), these authors reported collection efficiencies of $< 20\%$ under similar conditions as those experienced in this study (RH~ 50%, sampling times $> 8\text{h}$, sampling rates of 1 L min^{-1}).

In an inter-comparison of oxygenated VOC measurements in an atmosphere simulation chamber (Apel et al., 2008), measurements by DNPH method underestimated the concentration of acetone (slope ~ 0.7 , intercept $\sim 0.5\text{ ppb}$, $R^2 \sim 0.90$). In the same study, three PTR-MS instruments measured acetone at m/z 59 showing good agreement (Slopes $\sim 0.8 - 1.0$, intercept ~ 0 , $R^2 > 0.98$).

Conversely, comparisons of H_3O^+ SRI-MS measurements of acetone with GC techniques observe good agreement with slopes ~ 1 and intercepts of $-0.5 - 0.0\text{ ppb}$, $R^2 > 0.85$ (de Gouw et al. 2003, Kuster et al. 2004).

It was concluded that in this study the H_3O^+ SRI-MS signal at m/z 59 contained substantial contributions from acetone and propanal with possible minor contributions from other unknown compounds. The signal at m/z 59 was considerably higher than the sum of acetone and propanal in the DNPH samples. Again, the comparison presented here alongside other published studies, casts doubt on both methods.

4.7.9 H_3O^+ SRI-MS m/z 71: Methacrolein & Methyl Vinyl Ketone

The ratio of the mean concentration measured at m/z 71 by the H_3O^+ SRI-MS versus the MDL (ppb/ppb) for the whole dataset was 15, and the mixing ratios observed are sufficiently high enough to perform a meaningful quantitative comparison with all DNPH data ($N = 37$).

In measurements of the atmosphere, the H_3O^+ SRI-MS signal at m/z 71 is attributed to the sum of the isoprene oxidation products methacrolein (MACR) and methyl vinyl ketone (MVK) (de Gouw et al. 2003).

Methacrolein was measured in the DNPH samples in Sydney 2011 but MVK was not. Protonated (E)-2-butenal (crotonaldehyde) also measured in the DNPH samples produces an ion signal at m/z 71 in H_3O^+ SRI-MS measurements of ambient air. The VMR of (E)-2-butenal was on average 10% ($\pm 15\%$) of the MACR values.

The concentration of [MACR + (E)-2-butenal] in the DNPH samples was well correlated with the VMRs reported for m/z 71 with R^2 of 0.89. The slope differed significantly from unity (Slope = 2.80 ± 0.14 and intercept of -0.03 ± 0.10 , $N=37$) (Figure 4.6) which was expected given methyl vinyl ketone was not measured in the DNPH samples.

In this study, the calibration factor applied to the m/z 71 ion signal was determined empirically from a certified standard containing MACR but not MVK. The H_3O^+ SRI-MS sensitivity (S) to MACR and MVK differs such that the ratio $S(MVK)/S(MACR) \sim 0.74$ (Warneke et al. 2003). In the measurements of ambient air in Sydney, the accuracy of this calibration factor was dependent on the relative abundance of MVK to MACR which was unknown. Stroud et al (2001) reported the ratio of $[MVK]/[MACR]$ in the atmosphere can vary from 1 at night, to 2 during the day.

The presence of compounds other than MACR, MVK and 2-butenal that also yield product ion signals at m/z 71 may also have contributed to the large slope observed. Measurements of certified gas standards presented in Chapter 3 demonstrated that product ions from several alkenes, alkanes and cycloalkanes $> C_5$ can yield $C_5H_{11}^+$ product ions that contribute to the signal at m/z 71.

Contributions from hydrocarbons at m/z 71 were also observed in a recent study located within a region of high density oil and gas extraction industry with a higher mass resolution PTR-ToF, Warneke et al (2015) that observed two separate peaks at m/z 71 identified as $C_5H_{11}^+$ (80%) and $C_4H_7O^+$ (20%).

Conversely, measurements with a PTR-ToF located in an orange orchard also reported a peak corresponding to $C_3H_3O_2^+$, in addition to $C_4H_7O^+$, $C_5H_{11}^+$ with 24 h mean mixing ratios of 0.04, 0.30 and 0.05 ppbv respectively (Park et al. 2013). In measurements using PTR-ToF at a pine forest site determined $\sim 15\%$ of the signal at m/z 71 was due to a $C_4H_7O^+$ fragment ion from 2-hydroxy, 2-methyl propanal ($C_4H_8O_2$) (Kaser et al. 2013).

If the signal at m/z 71 in ambient air in this study was dominated by $C_4H_7O^+$ ions, 4.4% of the signal at m/z 71 should have been detected at m/z 72 due to the presence of ^{13}C isotopologues. The observed ratio of m/z 72 : m/z 71 was 0.047 in this study, indicating the signal at m/z 71 was dominated by $C_4H_7O^+$.

It is also possible that analytical differences contributed to the observed relationship between the H_3O^+ SRI-MS and the DNPH reported values. In the previously mentioned inter-comparison study of OVOC measurements in a simulated atmosphere, Apel et al. (2008) reported a significant underestimation of the measurements of MACR by DNPH method (slope ~ 0.3). The reasons for the discrepancy were related to the calibration standards, collection efficiency and variability of the DNPH sample cartridges. Underestimation of unsaturated carbonyls such as MACR in DNPH measurements may also be the result of loss due to dimerization of the carbonyl-DNP-hydrazone prior to analysis (Ho et al. 2011). In the atmospheric chamber study by Apel et al., four PTR- MS/-ToF instruments measured MACR+ MVK at m/z 71 with good agreement (Slopes ~ 1.0 , $R^2 > 0.99$).

Published inter-comparisons between H_3O^+ SRI-MS and GC techniques that measured both MACR and MVK show good agreement with slopes ~ 1 and $R^2 > 0.96$ (de Gouw et al. 2003, de Gouw & Warneke 2007).

One plausible explanation for the slope of 2.8 between the H_3O^+ SRI-MS measurement at m/z 71 and the DNPH measurements of [MACR + butenal] is that an equivalent concentration of MVK was also present in the atmosphere during sampling and was detected at m/z 71 but was not measured in the DNPH samples; and, the DNPH samples significantly underestimated the concentration of MACR.

In summary, the signal at m/z 71 contained substantial contributions from MACR and minor contributions from butenal. It is probable MVK made equivalent or larger contributions as MACR to the signal at 71, however only MACR and butenal were measured in the DNPH samples and the contribution of MVK to the signal at m/z 71 could not be quantified in this study. Consistent with the previous DNPH and H_3O^+ SRI-MS comparisons, the results presented here, alongside other published studies, casts doubt on both methods.

4.7.10 H_3O^+ SRI-MS m/z 73: Methyl Ethyl Ketone, Methyl Glyoxal & Butanal

The ratio of the median H_3O^+ SRI-MS signal measured at m/z 73 versus the MDL (ppb/ppb) for the whole dataset was 17 and the mixing ratios observed are sufficiently high enough to perform a meaningful quantitative comparison with the selected DNPH data ($N = 37$).

In measurements of the atmosphere, the H_3O^+ SRI-MS signal at m/z 73 can be attributed to methyl ethyl ketone (MEK), methyl glyoxal and butanal (de Gouw et al. 2003, Thalman et al. 2015). The concentration of MEK, methyl glyoxal and butanal were measured in the DNPH samples in Sydney 2011 with mean (\pm stdev) VMRs (ppbv) of 0.06 ± 0.06 , 0.54 ± 0.54 , and 0.46 ± 0.21 respectively.

RMA regression analysis was performed for the signal at m/z 73 versus the sum of MEK, methyl glyoxal and butanal in the DNPH samples yielding a slope of 0.32 ± 0.04 and R^2 value of 0.29 ($N = 48$).

In tests of prepared gas standards described in Chapter 2, proton transfer from H_3O^+ to methyl glyoxal and MEK had branching ratios to m/z 73 of ~15% and 96% respectively under the SRI-MS operating conditions used in this study. Proton transfer to butanal also results in a minor (7%) product ion signal at m/z 73 (Buhr et al 2002).

In this study, when the concentration of MEK, methyl glyoxal and butanal measured in the DNPH samples were multiplied by their respective branching ratios and their sum was compared with the VMR measured at m/z 73 by H_3O^+ SRI-MS, the results of the RMA regression changed significantly with a slope of 2.42 ± 0.24 , an intercept of -0.11 ± 0.09 ppb and an R^2 value of 0.65 (Figure 4.6).

In this study, the calibration factor applied to the m/z 73 ion signal was determined empirically from a certified standard containing MEK but not butanal or methyl glyoxal. The accuracy of a calibration factor based solely on MEK would have been sensitive to the relative abundance of MEK, butanal and methyl glyoxal present, as the instrument response to each compound is expected to differ due to differences in their branching ratios, as described above, and their reaction rates with H_3O^+ .

The H_3O^+ SRI-MS sensitivity (S) to MEK and butanal differs such that the ratio $S(\text{MEK})/S(\text{Butanal}) \sim 1.2$ (Warneke et al. 2003). No published reaction rates or explicit descriptions of instrument sensitivity to methyl glyoxal have been published, however some authors have observed potential memory effects due to the ‘sticky’ nature of this compound (de Gouw et al. 2003, Thalman et al. 2015).

Interference may occur in the calibration and measurement of compounds at m/z 73 from $\text{H}_3\text{O}^+(\text{H}_2\text{O})_3$ cluster ions (de Gouw et al. 2003, Thalman et al. 2015). In the study in Sydney 2011, the background signal at m/z 73, was relatively small and quite stable across the study period (mean = 2.19 ± 0.35 ncps) and did not significantly affect the measurement and calibration of m/z 73 compounds.

Again it is important to highlight the work by Ho et al. (2014) that identified significant negative biases in the collection efficiency of methyl ethyl ketone on DNPH cartridges that were related to relative humidity (RH), sample flow rates, and sampling time. While a different DNPH cartridge type was employed in the study by Ho and co-workers, reported collection efficiencies of MEK were as low as 50% under similar conditions as those experienced in this study (RH~ 50%, sampling times 8 - 10h, sampling rates of 1 L min^{-1}).

In summary, the concentrations of MEK, methyl glyoxal and butanal measured in the DNPH samples explained a significant fraction of the variability in the H_3O^+ SRI-MS ion signal at m/z 73. However, the quantitative agreement between the two methods was poor due to uncertainty in the applied branching ratios and calibration factors of the of the H_3O^+ SRI-MS and a possible negative bias to ketones in the DNPH samples.

4.7.11 Summary of the comparison of measurements of VOCs in urban air with H_3O^+ SRI-MS, AT-VOC and DNPH techniques

A comparison was performed for 10 compounds/ compound groups measured by both the H_3O^+ SRI-MS and one of the independent methods (AT-VOC and DNPH). The number of compounds compared was limited by the availability of quality observations in the atmosphere that were well above the analytical detection limit.

For toluene and the C_8 aromatics, the H_3O^+ SRI-MS and AT-VOC values were highly correlated ($R^2 > 0.8$) and in absolute agreement within $\pm 20\%$. We can conclude that the H_3O^+ SRI-MS provided reliable measurements of toluene and C_8 aromatics in this study.

For the remaining comparisons differences between the H_3O^+ SRI-MS and the independent VOC measurement methods (AT-VOC and DNPH) were observed. The observed differences were due to one or more of the following factors:

- Contributions of non-target compounds in the H_3O^+ SRI-MS measurements of the m/z of interest;
- Where multiple target compounds were detected at a single m/z, (e.g. C_9 aromatics, monoterpenes, MACR + MVK) in some cases not all target compounds were measured in the AT-VOC or DNPH samples;
- Where multiple target compounds were detected at a single m/z, (e.g. C_9 aromatics, monoterpenes, MACR + MVK) the use of a calibration factor determined for a single compound in H_3O^+ SRI-MS may result in measurement uncertainty;
- Significant negative bias, perhaps as large as 50%, in the DNPH measurements, due to issues with the calibration, and collection efficiency of the DNPH sample cartridges (Gilpin et al. 1997, Ho et al. 2014). The effect of this negative bias could not be accurately quantified for the individual compounds in this study.

The factors that contributed to the specific results of the inter-comparison for each compound are summarized in Table 4.9. These are discussed as follows:

The H_3O^+ SRI-MS measurements of C_9 aromatic compounds at m/z 121 were systematically higher (Slope = 1.9) than the AT-VOC measurements as not all of the C_9 aromatic compounds detected by the H_3O^+ SRI-MS were also measured in the AT-VOC samples. This was also the case for the H_3O^+ SRI-MS measurements of the sum of MACR+ MVK+ Butenal at m/z 71, which were systematically higher than the DNPH measurements (Slope ~ 2.8) as MVK was not measured in the DNPH samples.

The H_3O^+ SRI-MS measurements of isoprene at m/z 69 were also systematically higher (slope ~ 1.8) than the AT-VOC measurements due to contributions of non-target compounds to the ion signal at m/z 69.

Poor agreement (Slope ~ 2) and a high degree of scatter was observed in the comparison between the H_3O^+ SRI-MS measurements of the sum of monoterpenes measured at m/z 81, and the sum of four monoterpenes measured in the AT-VOC samples. This difference was

attributed to two factors: 1) not all of the monoterpenes detected by the H_3O^+ SRI-MS were also measured in the AT-VOC samples; and, 2) uncertainty due to the use of a calibration factor determined for a single compound.

The H_3O^+ SRI-MS measurements of formaldehyde (m/z 31), acetaldehyde (m/z 45) and the sum of acetone and propanal (m/z 59) were systematically higher than the DNPH measurements of these species (slopes ~ 1.8 to 2.9). The differences was attributed to two factors: 1) Contributions of non-target compounds in the H_3O^+ SRI-MS measurements of the m/z of interest; and, 2) Significant negative analytical bias in the DNPH measurements, due to issues with the calibration, and collection efficiency.

Poor agreement (Slope ~ 2.4) and a high degree of scatter was observed in the comparison between the H_3O^+ SRI-MS measurements at m/z 73 and the sum of MEK, methyl glyoxal and butanal measured in the DNPH samples. This difference was attributed to two factors: 1) Significant negative analytical bias in the DNPH measurements, due to issues with the calibration, and collection efficiency; and, 2) uncertainty due to the use of a calibration factor determined for a single compound.

Table 4.9: Correlation coefficients (R^2), and the slopes and intercepts from the RMA regression analysis between the H_3O^+ SRI-MS and the AT-VOC and DNPH measurements of selected VOCs.

m/z	Compound	Slope	Intercept (ppbv)	R^2	N	Comment
<i>H_3O^+ SRI-MS v AT-VOC</i>						
93	Toluene	1.21 ± 0.07	-0.10 ± 0.19	0.83	8	Agreement within $\pm 20\%$
107	C ₈ Aromatics	0.84 ± 0.03	-0.05 ± 0.08	0.94	8	Agreement within $\pm 20\%$
121	C ₉ Aromatics	1.90 ± 0.13	-0.06 ± 0.07	0.92	5	-ve bias in AT-VOC: not all C ₉ aromatics measured
69	Isoprene	1.82 ± 0.06	0.11 ± 0.16	0.90	8	+ve bias in H_3O^+ SRI-MS: contributions of non-target compounds
81	Terpenes	2.06 ± 0.20	0.08 ± 0.19	0.55	5	Low R^2 due to calibration uncertainty -ve bias in AT-VOC: not all terpenes measured

Table 4.9 (cont.)

m/z	Compound	Slope	Intercept (ppbv)	R ²	N	Comment
<i>H₃O⁺ SRI-MS v DNPH</i>						
31	Formaldehyde	1.81 ± 0.13	-0.01 ± 0.26	0.95	12	+ve bias in H ₃ O ⁺ SRI-MS: unexplained -ve bias in DNPH: low collection efficiencies
45	Acetaldehyde	1.75 ± 0.12	0.00 ± 0.07	0.82	37	+ve bias in H ₃ O ⁺ SRI-MS: contributions of non-target compounds -ve bias in DNPH: low collection efficiencies
59	Acetone & Propanal	2.91 ± 0.03	0.03 ± 0.13	0.60	37	+ve bias in H ₃ O ⁺ SRI-MS: of non-target compounds at m/z 59 -ve bias in DNPH due to low collection efficiencies
71	MACR, Butenal MVK	2.80 ± 0.14	-0.03 ± 0.10	0.89	37	-ve bias in DNPH: MVK not measured
73	MEK, Methyl Glyoxal & Butanal	2.42 ± 0.24	-0.11 ± 0.09	0.65	37	Low R ² and +ve bias in H ₃ O ⁺ SRI-MS: due to calibration uncertainty -ve bias in DNPH due to low collection efficiencies

4.8 SRI-MS measurements of VOCs in urban air with O₂⁺

Of the 21 key m/z identified according to the criteria in section 4.4 in the O₂⁺SRI-MS measurements of urban air in this study, there were 6 compounds measured by the both the O₂⁺SRI-MS and H₃O⁺ SRI-MS techniques.

Measurements of certified gas standards in section 3.5, demonstrated that O₂⁺SRI-MS could detect benzene (m/z 78), toluene (m/z 92), the sum of the C₈ aromatics (m/z 106), the sum of the C₉ aromatics (m/z 120), isoprene (m/z 67) and the sum of the monoterpenes (m/z 93) with only minor, if any interference. In this study, an inter-comparison between the O₂⁺ and H₃O⁺ reported values was undertaken for these compounds, with the exception of benzene, from the measurements in urban air in Sydney 2011. As discussed the VMRs of benzene observed in this study were frequently close to the MDL. The ratio of the median O₂⁺ SRI-MS benzene signal at m/z 78 versus the MDL was 1.2. This is significantly less than the

value of 10, specified for a robust quantitative comparison, and benzene will not be discussed further here.

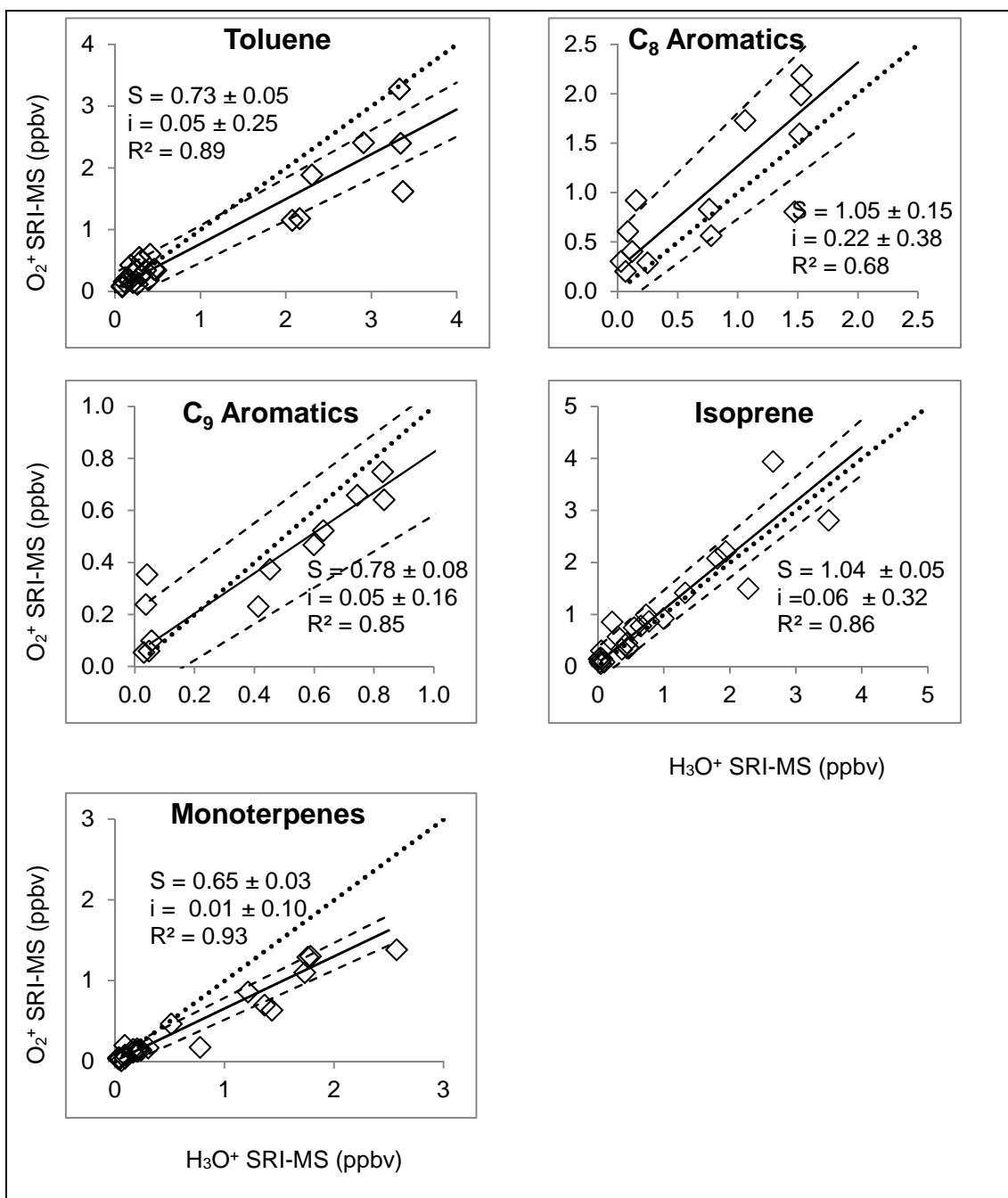


Figure 4.7: Scatterplots of the O_2^+ SRI-MS versus the H_3O^+ SRI-MS measurements of toluene, C_8 aromatics, C_9 aromatics, isoprene and monoterpenes in urban air in Sydney 2011. Dotted line is 1:1. Also included are the Slopes (S)(solid line), error limits (dashed lines), intercepts (i), and correlation coefficients (R^2) from the reduced major axis regression analysis.

As discussed in section 4.3, empirically derived sensitivities were determined from daily calibration measurements for each of these compounds in both H_3O^+ and O_2^+ reagent ion

modes over the sampling period. For each day of sampling two 1-hour averages (afternoon, night) were calculated from the ambient O_2^+ SRI-MS data (Table 4.6). In total there were twenty-seven 1 h averages acquired in O_2^+ SRI-MS over the 16 days of sampling. The 1 h O_2^+ SRI-MS averages were compared with the H_3O^+ SRI-MS 1 h averages obtained in the hour of ambient sampling directly following O_2^+ measurements (Table 4.6).

The difference in sampling times between the 1h average O_2^+ SRI-MS ambient measurements versus the AT-VOC integrated ambient samples periods were too large to perform a quantitative comparison and only the correlation coefficients with the AT-VOC data will be reported here.

4.8.1 O_2^+ SRI-MS m/z 92: Toluene

The ratio of the median m/z 92 concentrations versus the MDL for the whole data set was 22 and the mixing ratios observed were sufficiently high to perform a meaningful quantitative comparison with the H_3O^+ SRI-MS 1 h average data ($N = 37$).

The 1 h average O_2^+ SRI-MS m/z 92 data were well correlated with the consecutive 1h average H_3O^+ SRI-MS data for m/z 93 ($R^2 = 0.89$) and the AT-VOC reported toluene mixing ratios ($R^2 = 0.92$). This confirms that toluene made substantial contributions to the O_2^+ SRI-MS signal at m/z 92.

In the comparison of H_3O^+ SRI-MS measurements at m/z 93 and the AT-VOC measurements of toluene in section 4.7.1, the slope of 1.2 was at least partly attributed to the presence of fragment ions of C_9 aromatics at m/z 93. Unlike H_3O^+ reagent ion mode, when the SRI-MS is operating with O_2^+ reagent ions, fragment ions of C_9 aromatics do not overlap with the toluene product ion signal at m/z 92. This may partly explain the slope of ~ 0.7 observed in the comparison of the O_2^+ SRI-MS m/z 92 signal versus H_3O^+ SRI-MS m/z 93 signal in this study (slope = 0.73 ± 0.05 , intercept = 0.22 ± 0.38 ($N=15$)) (Figure 4.7).

In conclusion, in this study the O_2^+ SRI-MS ion signal at m/z 92, was dominated by toluene. The O_2^+ SRI-MS measurements at m/z 92 were $\sim 30\%$ lower than the consecutive H_3O^+ SRI-MS measurements at m/z 93. There were fewer compounds identified that could contribute to the O_2^+ SRI-MS signal at m/z 92 than the H_3O^+ SRI-MS signal at m/z 93 and it is possible the O_2^+ SRI-MS could provide a more selective measurement of toluene, in comparison to the standard H_3O^+ SRI-MS technique.

4.8.2 O₂⁺ SRI-MS m/z 106: C₈ Aromatic compounds

In measurements of certified gas standards with O₂⁺ SRI-MS the signal at m/z 106 was attributed to the sum of the C₈ aromatic isomers: m-, p-, o- xylenes and ethylbenzene (Section 3.5).

For the study in Sydney 2011, the ratio of the median m/z 106 concentration versus the MDL was highest for 3:00 AM – 4:00 AM data (median/MDL = 9.4) which was only slightly less than the value of 10, specified for a robust quantitative comparison. Only the m/z 106 data from the 3:00 AM – 4:00 AM sampling period were analysed further here.

The O₂⁺ SRI-MS data for m/z 106 were correlated with the values for m/z 107 reported by the H₃O⁺ SRI-MS ($R^2 = 0.68$) as well as the AT-VOC reported mixing ratios for the sum of the C₈ aromatics ($R^2 = 0.73$). This indicates the C₈ aromatics made significant contributions to the O₂⁺ SRI-MS signal at m/z 106.

The low volume mixing ratios of C₈ aromatics encountered in this study (O₂⁺ SRI-MS median/MDL = 9.4) contributed to the high degree of scatter in the inter-comparison with H₃O⁺ SRI-MS ($R^2 = 0.68$) due to the increased influence of random instrument noise in both reagent ion modes.

In section 4.7.2 we demonstrated that the H₃O⁺ SRI-MS provided a reliable measurement of Σ [C₈ Aromatics] in comparison with the AT-VOC reported values over equivalent sampling times. Therefore, in this case the H₃O⁺ SRI-MS can be considered a reference method for comparison with O₂⁺ SRI-MS. The RMA regression analysis for the O₂⁺ SRI-MS m/z 106 values versus the H₃O⁺ SRI-MS m/z 107 values, yielded a slope of 1.05 ± 0.11 , intercept = 0.22 ± 0.38 (N=15) (Figure 4.7).

There was a significant zero-offset (0.22 ppb) in the O₂⁺ SRI-MS data for C₈ aromatics. It is likely another species was detected at m/z 106. In the measurement of C₈ aromatics at m/z 107 by H₃O⁺ SRI-MS contributions of benzaldehyde were determined to be at most minor and we can assume this was also the case for the signal at m/z 106 in O₂⁺ SRI-MS. Despite investigation, no other possible candidates with product ion signals at m/z 106, that are known to be present in the atmosphere in sufficient concentrations to explain the offset observed were found.

We concluded that, in this study the O_2^+ SRI-MS signal at m/z 106 was dominated by C_8 aromatic compounds. The 1 h average O_2^+ SRI-MS measurements of C_8 aromatics at m/z 106 were systematically higher than the consecutive 1 h average H_3O^+ SRI-MS measurements of C_8 aromatics at m/z 107. This was likely due to the presence of other compounds at m/z 106 that could not be identified in this study.

4.8.3 O_2^+ SRI-MS m/z 120: C_9 Aromatic compounds

In measurements of certified gas standards with O_2^+ SRI-MS the signal at m/z 120 was attributed to the sum of the C_9 aromatic isomers: 1,2,4- and 1,3,5-, trimethylbenzene, m-, p- and o-ethyl toluene, and propyl- and isopropyl- benzene (Section 3.5).

In the present study, the ratio of the median m/z 120 concentrations versus the MDL was highest for the 3:00 AM – 4:00 AM data (median/MDL = 4.4), which is significantly less than the value of 10, specified for a robust quantitative comparison. As this is one of the first field deployments of O_2^+ SRI-MS, the results of the analysis of the 3:00 AM – 4:00 AM data for m/z 120 were included here to demonstrate whether the O_2^+ SRI-MS can qualitatively identify C_9 aromatics at m/z 120 in urban air.

The 1h average O_2^+ SRI-MS m/z 120 data were well correlated with the H_3O^+ SRI-MS data for m/z 121 ($R^2 = 0.85$) and the AT-VOC values for the sum of the C_9 aromatics ($R^2 = 0.82$) confirming the C_9 aromatics made a substantial contribution to the O_2^+ SRI-MS signal at m/z 120.

The 1h average O_2^+ SRI-MS data for m/z 120 was slightly lower than the H_3O^+ SRI-MS data for m/z 120 with a slope of 0.78 ± 0.08 , intercept = 0.05 ± 0.16 (Figure 4.7). The reasons for the negative bias are unclear as there were no species identified that would contribute substantially to the H_3O^+ SRI-MS signal at m/z 121, but not the O_2^+ SRI-MS signal at m/z 120.

In summary, the O_2^+ SRI-MS signal at m/z 120 contained substantial contributions from the C_9 aromatic isomers. The O_2^+ SRI-MS reported slightly lower concentrations than the H_3O^+ SRI-MS and the reasons for this negative bias remain unclear. However the low VMRs observed in this study precluded an accurate quantitative comparison.

4.8.4 O_2^+ SRI-MS m/z 67: Isoprene

The O_2^+ SRI-MS ion signals at m/z 67 and 68 were attributed to isoprene in measurements of certified gas standards described in Section 3.5. The higher ion signals at m/z 67 were used for the following analysis.

The ratio of the median m/z 67 concentration versus the MDL for the whole data set was 35 and the mixing ratios observed were sufficient to perform a meaningful quantitative comparison with the H_3O^+ SRI-MS data from the afternoon and night-time sampling periods ($N = 27$).

The 1h average O_2^+ SRI-MS m/z 67 data showed good agreement with the consecutive 1h average H_3O^+ SRI-MS data at m/z 69. The RMA regression analysis yielded a slope of 1.04 ± 0.05 , intercept = 0.06 ± 0.32 and an R^2 value of 0.86 (Figure 4.7).

Given the contributions from compounds other than isoprene observed in the H_3O^+ SRI-MS m/z 69 signal reported in section 4.7.4, the slope of ~ 1 suggests equivalent contributions from compounds other than isoprene in the O_2^+ SRI-MS signal at m/z 67 observed here.

In measurements of certified gas standard mixtures containing over 70 VOC species (Chapter 3, sect 3.5) when the SRI-MS was operating with O_2^+ , only isoprene was detected at m/z 67.

Unlike H_3O^+ reagent ion mode, reactions of O_2^+ with C_5 unsaturated alcohols, C_5 aldehydes, and furan do not yield fragment ions that overlap with the isoprene product ion signal at m/z 67 (Wang et al. 2004, Michel et al. 2005).

In measurements of air impacted by biomass burning with O_2^+ SRI-MS, charged pyrrole ($\text{C}_4\text{H}_5\text{N}^+$) may make a contribution to the signal at m/z 67 (Spaniel & Smith 1998c, Wang et al. 2004). For the present study, removing days impacted by biomass burning emissions did

not affect the agreement between the O_2^+ SRI-MS signal at m/z 67 and H_3O^+ SRI-MS signal at m/z 69 (Slope = 1.03, $R^2 = 0.85$).

No other possible candidates with product ion signals at both m/z 67 in O_2^+ SRI-MS, and m/z 69 in H_3O^+ SRI-MS, that are known to be present in the atmosphere in sufficient concentrations could be found.

Overall, we concluded that in O_2^+ SRI-MS measurements of urban air in this study, the ion signal at m/z 67 was dominated by isoprene. The O_2^+ SRI-MS and H_3O^+ SRI-MS were in close agreement. Given the contributions from compounds other than isoprene observed in the H_3O^+ SRI-MS m/z 69 signal the slope of ~ 1 observed here suggests equivalent contributions from compounds other than isoprene in the O_2^+ SRI-MS signal at m/z 67. The identity of these compounds could not be determined.

4.8.5 O_2^+ SRI-MS m/z 93: Monoterpenes

The signal at m/z 93 was attributed to α -pinene in measurements of a certified gas standards mixture when the SRI-MS was operating with O_2^+ (Chapter 3, sect 3.5). In the same tests, 1,8-cineole did not yield a product ion signal at m/z 93 and the O_2^+ SRI-MS response to other monoterpenes was not determined.

In measurements of a series of six monoterpenes by O_2^+ SIFT-MS α -pinene, β -pinene, D-Limonene, carene, and myrcene were observed to yield product ion signals at m/z 93 and for the purposes of this study the O_2^+ SRI-MS signal at m/z 93 will be compared with H_3O^+ SRI-MS signal at m/z 81 as a measurement of the sum of the monoterpenes.

The ratio of the median m/z 93 concentration versus the MDL for the whole data set was 12 and the mixing ratios observed were sufficient to perform a meaningful quantitative comparison with the H_3O^+ SRI-MS data from the afternoon and night-time sampling periods ($N = 27$).

The 1h average O_2^+ SRI-MS m/z 93 data were well correlated with the H_3O^+ SRI-MS data for m/z 81 ($R^2 = 0.93$) and moderately correlated with the AT-VOC data for the sum of α -pinene, β -pinene, and D-Limonene ($R^2 = 0.67$). Notably, this R^2 value is higher than that observed for the inter-comparison of the H_3O^+ SRI-MS signal at m/z 81 and the sum of the monoterpenes in the AT-VOC samples ($R^2 = 0.55$) (4.7.5). The quantitative agreement

between the O_2^+ SRI-MS m/z 93 data and the H_3O^+ SRI-MS data for m/z 81 was poor with a slope of 0.64 ± 0.03 , intercept = 0.01 ± 0.10 (Figure 4.7).

In this study, the calibration factor applied to the O_2^+ SRI-MS m/z 93 ion signal was determined empirically from a certified standard containing α -pinene but no other monoterpenes. In the measurements of ambient air in Sydney, the accuracy of this calibration factor was dependent on the relative abundance of all of the monoterpenes and their individual instrument responses.

In measurements of a series of six monoterpenes by O_2^+ SIFT-MS the reaction rates of monoterpenes with O_2^+ did not significantly differ ($\pm 10\%$) but their branching ratios to m/z 93 did: α -pinene, β -pinene, D-Limonene, carene, myrcene and camphene had branching ratios to m/z 93 between 13 and 61% (Schoon et al. 2003). Consequently, the slope of 0.64 observed may be a result of error in the application of a calibration factor based on one monoterpene compound when the instrument response among the multiple monoterpene isomers present at m/z 93 differs significantly.

More work is required to determine which species are detected at m/z 93 in O_2^+ SRI-MS measurements of the atmosphere, and to characterise their individual instrument responses. In lieu of quantitative measurements, the signal at m/z 93 may be useful to infer the presence of monoterpenes in O_2^+ SRI-MS measurements of the atmosphere.

4.8.6 Summary of the comparison of measurements of VOCs in urban air with O_2^+ and H_3O^+ SRI-MS

A comparison was performed for five compounds/ compound groups measured by both the O_2^+ SRI-MS and H_3O^+ SRI-MS. The number of compounds compared was limited by the availability of quality observations well above the analytical detection limit in the atmosphere.

The O_2^+ SRI-MS reported values for all compounds were generally well correlated with the H_3O^+ SRI-MS measurements (R^2 0.68 - 0.93) however the O_2^+ SRI-MS reported values tended to be lower than H_3O^+ SRI-MS values (mean slope = 0.8). The observed differences were due to one or more of the following factors:

- Contributions of non-target compounds in the H_3O^+ SRI-MS measurements at the m/z of interest;
- Contributions of non-target compounds in the O_2^+ SRI-MS measurements at the m/z of interest;
- Where multiple target compounds were detected at a single m/z, (e.g. monoterpenes) in some cases the compounds detected by the O_2^+ SRI-MS differed to those measured in the AT-VOC or DNPH samples;
- Where multiple target compounds were detected at a single m/z, (e.g. C_9 aromatics, monoterpenes,) the use of a calibration factor determined for a single compound may result in uncertainty in both O_2^+ and H_3O^+ SRI-MS measurements;

The factors that contributed to the specific results of the inter-comparison for each compound are summarized in Table 4.10. These are discussed as follows:

In the case of toluene O_2^+ SRI-MS measurements do not show the positive bias of ~20 - 30% identified in the H_3O^+ SRI-MS measurements due to contributions compounds other than toluene. Thus it appears O_2^+ SRI-MS may provide more selective measurements of toluene than conventional H_3O^+ SRI-MS.

The O_2^+ SRI-MS measurements of C_8 aromatics were systematically higher than the consecutive H_3O^+ SRI-MS measurements (intercept = 0.22 ppbv). Given the good agreement of H_3O^+ SRI-MS with the independent measurements of C_8 aromatics in the AT-VOC samples, O_2^+ SRI-MS measurements of C_8 aromatics are probably positively biased due to contributions of non-target compounds, which could not be identified in this study.

The O_2^+ SRI-MS measurement of isoprene at m/z 67 was in close agreement H_3O^+ SRI-MS measurement of isoprene at m/z 69 (slope = 1.05, $R^2 = 0.86$). Given the contributions from compounds other than isoprene observed in the H_3O^+ SRI-MS m/z 69 signal in this study, the slope of ~1 observed here suggests equivalent contributions from compounds other than isoprene in the O_2^+ SRI-MS signal at m/z 67.

Table 4.10: Correlation coefficients (R^2), and the slopes and intercepts from the RMA regression analysis between the O_2^+ SRI-MS and H_3O^+ SRI-MS measurements of selected VOCs from Sydney 2011.

	SRI-MS		Slope	Intercept (ppbv)	R^2	N	Comment
	O_2^+ m/z	H_3O^+ m/z					
Toluene	92	93	0.73 ± 0.05	0.05 ± 0.25	0.89	27	+ve bias in H_3O^+ SRI-MS: contributions from non-target compounds
C ₈ Aromatics	106	107	1.05 ± 0.11	0.22 ± 0.38	0.68	15	+ve offset in O_2^+ SRI-MS: contributions from non-target compounds
C ₉ Aromatics	120	121	0.78 ± 0.08	0.05 ± 0.16	0.85	15	Slope >1, $R^2 < 0.7$ due to calibration uncertainty in H_3O^+ and O_2^+ SRI-MS
Isoprene	67	69	1.04 ± 0.05	0.06 ± 0.32	0.86	27	Agreement within $\pm 10\%$
Monoterpenes	93	81	0.64 ± 0.03	0.01 ± 0.10	0.93	27	-ve bias due to calibration uncertainty and differences in compounds detected by O_2^+ & H_3O^+

It is highly likely that the O_2^+ SRI-MS signal at m/z 93 contains substantial contributions from monoterpenes given its high correlation ($R^2 = 0.93$) with the H_3O^+ SRI-MS measurement of monoterpenes at m/z 81. However, the O_2^+ SRI-MS values were ~35% lower than the H_3O^+ SRI-MS values. The reasons for the discrepancy remain unclear and may result from both the sensitivity of the calibrations in both reagent ion modes, and the differences in the monoterpenes detected by each of the two methods. At this stage it is not possible to identify whether the H_3O^+ or O_2^+ SRI-MS measurements are more reliable.

Overall, few compounds were selectively measured by O_2^+ SRI-MS in comparison to conventional H_3O^+ SRI-MS. In particular, the O_2^+ SRI-MS was not able to selectively measure the oxygenated VOCs, which are measured by the H_3O^+ SRI-MS. These results suggest the use of O_2^+ SRI-MS for speciated VOC measurements of the atmosphere, did not provide any additional information in comparison to conventional H_3O^+ SRI-MS.

O_2^+ SRI-MS is capable of detecting acetylene and small alkanes not measureable with conventional H_3O^+ SRI-MS. The measurement of these compounds represents a significant potential advantage of O_2^+ SRI-MS not explored here and further inter-comparisons are required to demonstrate this application of O_2^+ SRI-MS.

4.9 SRI-MS measurements of VOCs in urban air with NO^+

Of the 15 key m/z identified according to the criteria in section 4.4 in the NO^+ SRI-MS mass scans of urban air, there were 6 compounds that were also measured by the H_3O^+ SRI-MS and O_2^+ SRI-MS techniques.

Measurements of certified gas standards in section 3.6, demonstrated that the NO^+ SRI-MS could detect benzene (m/z 78), toluene (m/z 92), the sum of the C_8 aromatics (m/z 106), the sum of the C_9 aromatics (m/z 120), isoprene (m/z 68) and the sum of the monoterpenes (m/z 93) with only minor, if any interference. In this study, an inter-comparison between the NO^+ and H_3O^+ SRI-MS measurements of these compounds in urban air in Sydney 2011 was undertaken.

As discussed in section 4.3, empirically derived sensitivities were determined from daily calibration measurements for each of these compounds in both NO^+ and H_3O^+ reagent ion modes over the sampling period.

For each day of sampling two 1-hour averages (afternoon, night) were calculated from the NO^+ SRI-MS data (Table 4.6). In total there were twenty-seven 1 h averages acquired in NO^+ SRI-MS over the 16 days of sampling. The 1h average NO^+ SRI-MS mixing ratios were compared with the average of the combined H_3O^+ SRI-MS measurements from 22:00 – 23:00 and 4:00 – 5:00 (Table 4.6).

The difference in sampling times between the 1h average NO^+ SRI-MS ambient measurements versus the AT-VOC integrated ambient samples periods were too large to perform a quantitative comparison and only the correlation coefficients with the AT-VOC data will be reported here.

The median/MDL ratio for the NO^+ SRI-MS measurement of benzene (m/z 78), the sum of the C_9 aromatics (m/z 120) and the sum of the monoterpenes (m/z 93) were < 1.5 and these compounds were not analysed further here.

As discussed in section 4.6, the signals at m/z 92 (toluene), m/z 120 (C_8 aromatics), and m/z 68 (isoprene) had median/MDL ratios of 4 – 7.2 which is significantly less than the value of 10, specified for a robust quantitative comparison. However, in lieu of better data and as this was one of the first field deployments of NO^+ SRI-MS, the results for these m/z were

included to assess the potential for these compounds to be qualitatively identified, in a series of measurements of urban air, at their respective m/z .

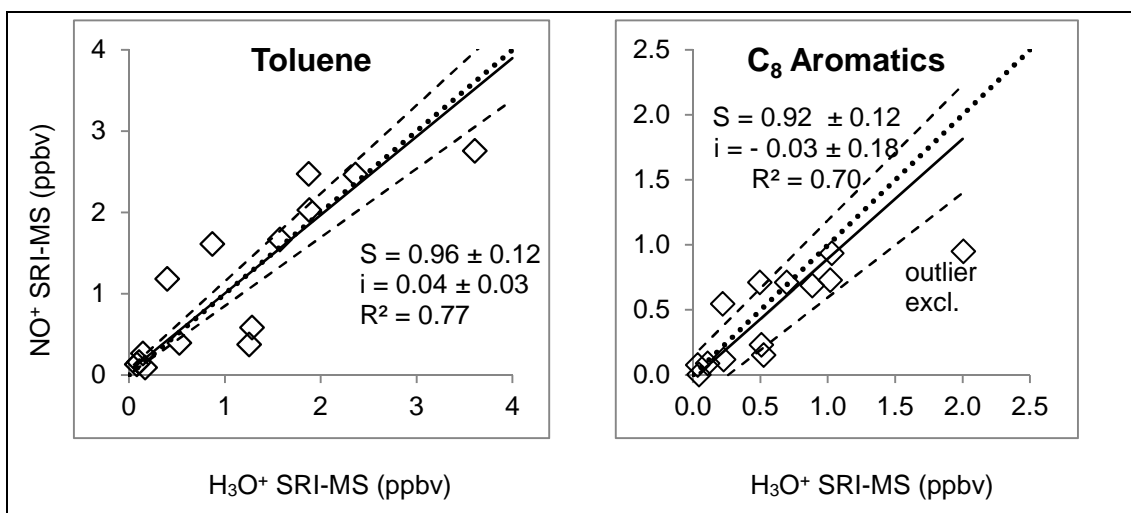


Figure 4.8: Scatterplots of the NO^+ SRI-MS versus the H_3O^+ SRI-MS measurements of toluene, and the C_8 aromatics in urban air in Sydney 2011. Dotted line is 1:1. Also included are the Slopes (S)(solid line), error limits (dashed lines), intercepts (i), and correlation coefficients (R^2) from the reduced major axis regression analysis.

4.9.1 NO^+ SRI-MS m/z 92: Toluene

The NO^+ SRI-MS signal at m/z 92 was attributed to toluene (Section 3.6). The highest median/MDL ratio of 7.2 was observed for data from the sampling period 0:00 – 1:00 and only the data from these sampling periods were analysed further.

The NO^+ SRI-MS signal at m/z 92 was well correlated with the H_3O^+ SRI-MS data for m/z 93 with $R^2 = 0.77$. The correlation of the NO^+ SRI-MS m/z 92 data with the AT-VOC reported toluene mixing ratios was lower with $R^2 = 0.68$.

In section 4.7.1, we demonstrated that the H_3O^+ SRI-MS provided a reliable measurement of toluene with minor contributions from some other compounds when compared with the AT-VOC samples over equivalent sampling times. The results of the RMA regression for the NO^+ SRI-MS ion signal at m/z 92 and the H_3O^+ SRI-MS signal at m/z 93 yielded a slope of 0.96 ± 0.12 and intercept of 0.04 ± 0.03 ($N = 15$) (Figure 4.8).

As was the case for the H_3O^+ SRI-MS signal at m/z 93, it is likely monoterpene fragment ions also comprised a minor fraction of the NO^+ SRI-MS signal at m/z 92 in this study. In measurements of certified gas standards mixtures (Chapter 3, sect 3.5) when the SRI-MS was

operating with NO^+ , protonated toluene was detected at m/z 92 with minor contributions from α - pinene fragment ions.

α - pinene, β - pinene and D-Limonene have branching ratios to m/z 92 of 8%, 1% and 1% respectively (Schoon et al. 2003). These branching ratios were expected to be greater in this study due to the higher collision energy in the SRI-MS drift tube.

However, the correlation (R^2) of the NO^+ SRI-MS m/z 92 signal with α - pinene, β - pinene and D-Limonene measured in the AT-VOC samples in this study were all < 0.2 indicating monoterpenes, did not substantially contribute to the NO^+ SRI-MS m/z 92 ion signal in this study.

The positive bias of $\sim 20\%$ in the H_3O^+ SRI-MS measurements of toluene at m/z 93 versus the AT-VOC measurements reported in section 4.7.1, was at least partly attributed to the presence of fragment ions of C_9 and higher aromatics at m/z 93. Unlike H_3O^+ reagent ion mode, when the SRI-MS is operating with NO^+ , fragment ions of C_9 aromatics do not overlap with the toluene product ion signal at m/z 92.

In conclusion, in this study the NO^+ SRI-MS ion signal at m/z 92, was dominated by toluene. The NO^+ SRI-MS measurements at m/z 92 agreed with the H_3O^+ SRI-MS measurements at m/z 93 within the criteria of $\pm 20\%$. There were fewer compounds identified that could contribute to the NO^+ SRI-MS signal at m/z 92 than the H_3O^+ SRI-MS signal at m/z 93 and it is possible NO^+ SRI-MS may provide a more selective measurement of toluene, in comparison to the standard H_3O^+ SRI-MS technique.

4.9.2 NO^+ SRI-MS m/z 106: C_8 Aromatics

In NO^+ SRI-MS the signal at m/z 106 can be attributed to C_8 aromatics (m-, p- and o-xylene plus ethylbenzene) (Section 3.6). A median/MDL ratio of 2.5 was observed for the data from the 0:00 – 1:00 NO^+ SRI-MS sampling period. This was higher than the median/MDL ratio for the afternoon NO^+ SRI-MS sampling period and only data from the period 0:00 – 1:00 were analysed further here.

The NO^+ SRI-MS signal at m/z 106 correlated well with the H_3O^+ SRI-MS data for m/z 107 with $R^2 = 0.70$. The correlation of the NO^+ SRI-MS m/z 106 data with the sum of the C_8 aromatics in the AT-VOC samples was $R^2 = 0.65$.

In section 4.7.2 we demonstrated that the H_3O^+ SRI-MS provided a reliable measurement of $\Sigma [\text{C}_8 \text{ Aromatics}]$ in comparison with the AT-VOC reported values over equivalent sampling times. The RMA regression analysis between the NO^+ SRI-MS ion signal at m/z 106 and the H_3O^+ SRI-MS signal at m/z 107 yielded a slope of 0.67 ± 0.10 and intercept of 0.04 ± 0.22 ($N = 15$) (Figure 4.8). The presence of a single high value that occurred on the night of the 23rd of February, had a strong influence on the slope of the fitted line. When this value was excluded, the NO^+ SRI-MS ion signal at m/z 106 and the H_3O^+ SRI-MS values signal at m/z 107 were in agreement with a slope of 0.92 ± 0.12 , intercept = -0.03 ± 0.18 , and $R^2 = 0.75$.

In summary, C_8 aromatic compounds dominated the NO^+ SRI-MS signal at m/z 106. The NO^+ SRI-MS signal at m/z 106 and the H_3O^+ SRI-MS signal at m/z 107 agreed within the criteria of $\pm 20\%$.

4.9.3 NO^+ SRI-MS m/z 68: Isoprene

In the measurements of certified gas standards described in Section 3.6, the NO^+ SRI-MS ion signals at m/z 67 & 68 were unique to isoprene. The stronger ion signals at m/z 68 were used for the purposes of this inter-comparison.

The ratio of the median m/z 68 signal versus the MDL was highest (median/MDL = 4.0) in the afternoon sampling period from 15:00 – 16:00 and only the data from the afternoon sampling periods were analysed further.

The NO^+ SRI-MS signal at m/z 68 was highly correlated with the H_3O^+ SRI-MS data for m/z 69 with $R^2 = 0.83$. The correlation between the NO^+ SRI-MS m/z 68 data and the isoprene in the AT-VOC samples was $R^2 = 0.77$ confirming isoprene made a significant contribution to the O_2^+ SRI-MS signal at m/z 68.

The RMA regression analysis of the NO^+ SRI-MS m/z 68 and the H_3O^+ SRI-MS m/z 69 data yielded a slope of 0.65 ± 0.06 , intercept = 0.06 ± 0.68 . The presence of a single high value that occurred on the afternoon of the 19th of February, had a strong influence on the slope of the fitted line. When this value was excluded, the NO^+ SRI- the slope became 1.25 ± 0.10 , intercept = -0.41 ± 0.37 , and $R^2 = 0.85$.

In the present study, at low VMRs (< 0.8 ppbv) the NO^+ SRI-MS signal at m/z 68 was $> 20\%$ lower than the H_3O^+ SRI-MS signal at m/z 69. Previous studies have reported that in air masses with low isoprene VMRs, contributions from compounds other than isoprene can be a significant fraction of the H_3O^+ SRI-MS signal at m/z 69 (Warneke et al. 2003). For instance, reactions of H_3O^+ , with C_5 aldehydes, and 2-methyl-3-buten-2-ol can yield product ions that overlap with the isoprene product ion signal at m/z 69 (Michel et al. 2005, Karl et al. 2012). Unlike H_3O^+ , the reactions of NO^+ with these compounds do not yield product ions that coincide with the isoprene signal at m/z 68 (Amelnyck et al. 2005, Michel et al. 2005) and NO^+ has been shown to provide a more selective measurement of isoprene in some cases (Karl et al. 2012).

At higher mixing ratios of isoprene the H_3O^+ SRI-MS has been demonstrated to perform well against GC techniques (slopes $0.9 - 1.2$) (de Gouw et al. 2003, Kuster et al. 2004, de Gouw & Warneke 2007). In the present study, at volume mixing ratios between 0.8 ppbv - 2.6 ppbv the NO^+ SRI-MS measurements of isoprene at m/z 68 and the H_3O^+ SRI-MS measurements at m/z 69 agreed within the criteria of $\pm 20\%$. There was only one isoprene value > 2.6 ppbv in this study and the performance of the NO^+ SRI-MS at higher isoprene VMRS could not be determined.

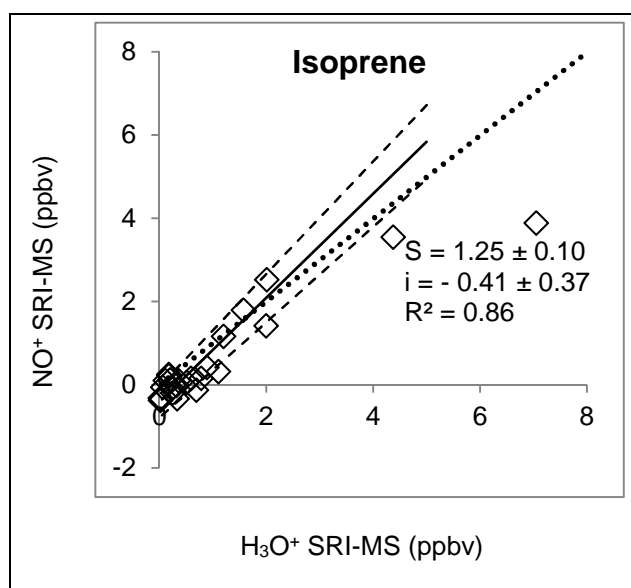


Figure 4.9: Scatterplot of the NO^+ SRI-MS versus the H_3O^+ SRI-MS measurements of isoprene in urban air in Sydney 2011. Dotted line is 1:1. Also included are the Slopes (S)(solid line), error limits (dashed lines), intercepts (i), and correlation coefficients (R^2) from the reduced major axis regression analysis.

Overall, the NO^+ SRI-MS ion signal at m/z 68 contained significant contributions from isoprene. The H_3O^+ SRI-MS and NO^+ SRI-MS measurements agreed within the criteria of \pm

20%. Fewer compounds were identified that could contribute to the NO^+ SRI-MS signal at m/z 68, and in air masses with low isoprene VMRs. The quantitative comparison presented here suggests the NO^+ SRI-MS could provide more selective measurements of isoprene in comparison to conventional H_3O^+ SRI-MS.

4.9.4 Summary of the comparison of measurements of VOCs in urban air with NO^+ and H_3O^+ SRI-MS

A comparison was performed for toluene, the C_8 aromatics and isoprene measured by both the NO^+ SRI-MS and H_3O^+ SRI-MS. The number of compounds compared was limited by the lack of availability of quality observations well above the detection limit in the atmosphere. The factors that contributed to the specific results of the inter-comparison for each compound are summarized in Table 4.11.

The NO^+ SRI-MS observations for toluene and the C_8 aromatics were in agreement with the H_3O^+ SRI-MS within the criteria of $\pm 20\%$.

Table 4.11: Correlation coefficients (R^2), and the slopes and intercepts from the RMA regression analysis between the O_2^+ SRI-MS and H_3O^+ SRI-MS measurements of selected VOCs from Sydney 2011.

	SRI-MS		Slope	Intercept (ppbv)	R^2	N	Comment
	NO^+ m/z	H_3O^+ m/z					
Toluene	92	93	0.96 ± 0.12	0.04 ± 0.03	0.77	15	Agreement within $\pm 20\%$
C_8 Aromatics	106	107	0.92 ± 0.12	-0.03 ± 0.18	0.75	14	Agreement within $\pm 20\%$
Isoprene	68	69	1.25 ± 0.06	-0.41 ± 0.37	0.85	14	+ve offset in H_3O^+ SRI-MS due to contributions from non-target compounds Agreement within $\pm 20\%$ at VMRS 0.8 – 2.6 ppb

At VMRS of isoprene (< 2.6 ppbv) the NO^+ SRI-MS observations were less than or equal to the H_3O^+ SRI-MS reported values. This was attributed to a positive bias in the H_3O^+ SRI-MS isoprene measurements due to contributions from non-isoprene compounds at the target m/z that was more apparent at low VMRS (< 0.8 ppbv). Unlike H_3O^+ , the reactions of NO^+

with these non-target compounds do not yield product ions that coincided with the NO^+ SRI-MS isoprene signal and NO^+ provided a more selective measurement of isoprene.

Given that isoprene is the most abundantly emitted VOC globally, and plays an important role in photochemistry and climate (Seinfeld & Pandis 2006), the higher selectivity of NO^+ SRI-MS measurements of isoprene represents a significant potential advantage of NO^+ SRI-MS over conventional H_3O^+ SRI-MS. In previous studies, Karl and co-workers (2012, 2014) have demonstrated the use of NO^+ for selective SRI-MS measurements of isoprene in a forest ecosystem.

With the exception of higher selectivity measurements of isoprene and perhaps toluene, the results of this analysis suggest that in measurements of the atmosphere, with the operating conditions employed in this study, the NO^+ SRI-MS wouldn't provide any significant additional information to H_3O^+ SRI-MS measurements alone.

Previous laboratory studies have demonstrated the usefulness of the formation of NO^+ association complexes to distinguish between isomeric aldehydes and ketones that are not possible with H_3O^+ SRI-MS (Wyche et al. 2005, Jordan et al. 2009). The high drift tube voltage used in this study suppressed the formation of these ions. Further work is required to optimize the SRI-MS to exploit this reaction pathway and maximize the information content of the NO^+ SRI-MS mass spectra.

4.10 Conclusions

This chapter presented a real-world inter-comparison of the mixing ratios of selected VOCs measured by H_3O^+ SRI-MS with two independent measurement techniques (AT-VOC and DNPH). The H_3O^+ SRI-MS measurements were also compared with the measurements obtained when the SRI-MS was operating in O_2^+ and NO^+ reagent ion modes.

The H_3O^+ SRI-MS and AT-VOC for toluene and the C_8 aromatics were within the $\pm 20\%$ specified for quantitative agreement.

The H_3O^+ SRI-MS signal at m/z 69 correlated well with the isoprene in the AT-VOC samples but the quantitative agreement (slope ~ 1.8) suggests interference from non-isoprene compounds occurred.

Where multiple compounds were detected at a single m/z , the agreement between the H_3O^+ SRI-MS and the independent VOC measurements was often poor and this was in part due to uncertainty in the calibration factor applied to the ion signal which was determined from only one of the multiple species detected at a given m/z .

The comparisons of the H_3O^+ SRI-MS and AT-VOC measurements of the C_9 aromatics, and monoterpenes were less quantitative because not all of the C_9 aromatics and monoterpenes detected by the SRI-MS were also measured in the AT-VOC samples. Furthermore, where multiple target compounds were detected at a single m/z , (e.g. C_9 aromatics, monoterpenes) the use of a calibration factor determined for a single compound may have contributed to some scatter and bias in the measurements.

This was also the case for the H_3O^+ SRI-MS measurements of the sum of MACR+ MVK+ Butenal at m/z 71, which were systematically higher than the DNPH measurements (Slope ~ 2.8) as MVK was not measured in the DNPH samples. In addition, the sensitivity at m/z 71 was determined from calibration with MACR only.

The comparison of H_3O^+ SRI-MS measurements of carbonyl compounds with the DNPH samples were less quantitative (slopes of 1.8 – 2.8) than those reported in the H_3O^+ SRI-MS comparison with AT-VOC. These comparisons were potentially affected by a significant negative bias, in the DNPH measurements, that has been identified in previous studies, and attributed to issues with the calibration and collection efficiency of the DNPH sample cartridges (2014). The results presented here, alongside other published studies (Apel et al. 2008, Wisthaler et al. 2008), casts doubt on both (DNPH and H_3O^+ SRI-MS) methods.

Overall, the H_3O^+ SRI-MS measurements of C_9 aromatics, monoterpenes and the carbonyl compounds correlated well with those reported in the AT-VOC and DNPH samples however, the measurements by the independent VOC techniques (AT-VOC and DNPH) employed in this study, suffered from their own inherent analytical biases and could not be considered as a reference method against which the quantitative accuracy of the H_3O^+ SRI-MS measurements of these compounds could be assessed.

In the present study, O_2^+ SRI-MS performed similarly to H_3O^+ SRI-MS for measurements of toluene and isoprene. The O_2^+ SRI-MS detected the sum of the C_8 aromatics, C_9 aromatics and the sum of the terpenes. However, more work is required to characterize their instrument response in order to achieve accurate measurements.

For the measurements of toluene, C₈ aromatics and isoprene the NO⁺ SRI-MS and H₃O⁺ SRI-MS were in close agreement. The measurement of benzene, C₉ aromatics and monoterpenes by NO⁺ SRI-MS could not be assessed in this study as their respective ion signals were not sufficient for a quantitative comparison with H₃O⁺ SRI-MS.

The results of this study suggest that the O₂⁺ and NO⁺ SRI-MS could provide equivalent or more selective measurements of isoprene and toluene, in comparison to conventional H₃O⁺ SRI-MS. With the exception of higher selectivity measurements of these species, the NO⁺ and O₂⁺ SRI-MS did not provide any significant additional information in comparison to the H₃O⁺ SRI-MS measurements alone. The measurement of small hydrocarbons including acetylene with O₂⁺ SRI-MS, and the discrimination between isomeric aldehydes and ketones with NO⁺ represents a significant potential advantage of SRI-MS not explored here and further inter-comparisons are required to demonstrate this application of SRI-MS.

Chapter 5. Interference in the PTR-MS measurement of acetonitrile at m/z 42 in polluted urban air – A study using switchable reagent ion PTR-MS

This thesis chapter is in the same form as the final manuscript published in the peer reviewed *International Journal of Mass Spectrometry*. The full reference for the published paper is:

Dunne, E., Galbally, I.E., Lawson, S., Patti, A., (2012) “Interference in the PTR-MS measurement of acetonitrile at m/z 42 in polluted urban air – A study using switchable reagent ion PTR-MS”, *Int. J. Mass Spectrom.*, 319-320, 40 – 47.



Interference in the PTR-MS measurement of acetonitrile at m/z 42 in polluted urban air—A study using switchable reagent ion PTR-MS

Erin Dunne^{a,b,*}, Ian E. Galbally^a, Sarah Lawson^a, Antonio Patti^c

^a Centre for Australian Weather and Climate Research, CSIRO Marine and Atmospheric Research, PMB 1, Aspendale, Vic. 3195, Australia

^b School of Applied Science, Monash University, Gippsland, Vic., Australia

^c Centre for Green Chemistry, Monash University, Clayton, Vic., Australia

ARTICLE INFO

Article history:

Received 30 January 2012

Received in revised form 4 May 2012

Accepted 7 May 2012

Available online 20 May 2012

Keywords:

Acetonitrile

Switchable reagent ion

PTR-MS

Mass interference

Urban air

ABSTRACT

In Proton Transfer Reaction Mass Spectrometer (PTR-MS) measurements of the atmosphere, the signal at m/z 42 is commonly regarded as a unique measure of acetonitrile. However, two other ions potentially contribute to the signal at m/z 42. These are ^{13}C isotopologues of C_3H_5^+ and the product ion C_3H_6^+ produced by reaction of NO^+ and O_2^+ (present in trace amounts in the H_3O^+ reagent gas), with a number of volatile organic compounds. Thus, there is the possibility of interference in the measurement of acetonitrile at m/z 42 by PTR-MS.

Interference in the measurement of acetonitrile at m/z 42 was quantified in urban air over 17 days in Sydney, Australia, in summer. A PTR-MS with Switchable Reagent Ion capability was used for measurements at m/z 41 and 42 in three different primary reagent ion modes, O_2^+ , NO^+ and H_3O^+ , to quantify the contribution of non-acetonitrile compounds to the signal at m/z 42 when the PTR-MS was operating in H_3O^+ reagent ion mode. Acetonitrile dominated the ion signal at m/z 42; however non-acetonitrile ions contributed 5–41% of the total ion signal at m/z 42. The average corrected and uncorrected acetonitrile concentrations were 120 pptv and 148 pptv respectively.

The interference in the m/z 42 signal was calculated from known or interpolated concentrations of compounds identified as potential interferences. Overall the isotopologue correction is due to alkenes including isoprene with probable contributions from other compounds not measured in this study. The other component of the interference, produced by reactions of O_2^+ , is due to alkanes and alkenes.

Levogluconan, a biomass burning tracer in atmospheric particulate matter was more highly correlated with the corrected acetonitrile signal than the uncorrected acetonitrile signal.

Measurements of acetonitrile by PTR-MS at m/z 42 in urban air will frequently require correction because of the non-trivial concentrations of alkanes and alkenes commonly observed in urban air.

© 2012 Published by Elsevier B.V. All rights reserved.

1. Introduction

Biomass burning is a major source of gases and particles to the atmosphere at concentrations that have a significant influence on atmospheric chemistry at local, regional and global scales [1]. Acetonitrile is almost exclusively emitted from biomass burning and has an atmospheric lifetime of many months [2]. Consequently, it is commonly used as a tracer for biomass burning. In the urban atmosphere measurements of acetonitrile are a useful indicator of the contribution to air quality of controlled and uncontrolled biomass burning, wood fuelled heating, and any other biomass combustion.

Proton transfer mass spectrometry (PTR-MS) observations have been useful in identifying biomass burning plumes and observing their transport and chemical processing [e.g., 3,4]. PTR-MS instruments are capable of detecting numerous VOCs including acetonitrile and other nitrogen-containing VOCs as well as oxygenated VOCs, aromatics and some alkenes [5,6] online with fast response and high sensitivity (sub-ppb). The principal of the PTR-MS is the utilization of proton transfer reactions from H_3O^+ compounds with a proton affinity (PA) > H_2O (166.5 kcal mol⁻¹) to produce charged products.

The ion detection system in a standard PTR-MS consists of a quadrupole mass spectrometer that separates the ions according to their mass/charge ratio (m/z) and a secondary electron multiplier (SEM) operated in count mode that detects the number of impinging ions at each m/z channel with a mass resolution of 1 amu. The major practical limitation of PTR-MS is its inability to distinguish between ions with the same mass to charge ratio (m/z) [7]. The low

* Corresponding author at: Private Bag 1, Aspendale, Vic. 3195, Australia.

Tel.: +61 3 9239 4428; fax: +61 3 9239 4444.

E-mail address: Erin.Dunne@csiro.au (E. Dunne).

selectivity of PTR-MS needs to be considered when measuring air with complex VOC mixtures, such as urban air and smoke plumes, which contain many different VOCs with the same molecular or fragment ion mass.

In the identification of a signal from PTR-MS, one must consider the contributions to a particular m/z ratio from a number of reaction pathways involving constituents of the sample being analysed and the multiple components of the reagent ion matrix. These contributions include:

- Product ions with molecular mass plus one due to proton addition.
- Product ions from fragmentation of molecular ions following proton transfer.
- Product ions that are isotopologues including those containing ^{13}C , ^{18}O , ^{35}S , etc.
- Product ions from reactions with the impurity reagent ions O_2^+ , NO^+ and $\text{H}_3\text{O}^+\cdot\text{H}_2\text{O}$.

The ion source of the PTR-MS instrument is a hollow cathode that produces H_3O^+ ions via electron impact ionization of water vapour. The ion source is tuned to produce reagent H_3O^+ ions with a purity of >95% but there are always some O_2^+ , NO^+ , $\text{H}_3\text{O}^+\cdot(\text{H}_2\text{O})_n$ and other ions present in the reagent ion matrix as a result of air back-streaming into the ion source. The instrument manufacturer (Ionicon Analytik GmbH) suggests that <2% of O_2^+ and NO^+ impurities is optimal.

PTR-MS mass spectra can be further complicated by the presence of these trace reagent ions including O_2^+ , NO^+ , $\text{H}_3\text{O}^+\cdot(\text{H}_2\text{O})_n$ in the reagent ion matrix. As well as proton transfer from the H_3O^+ primary reagent ion, the other trace constituents in the reagent ion matrix (O_2^+ , NO^+ , and $\text{H}_3\text{O}^+\cdot(\text{H}_2\text{O})_n$) also undergo chemical ionization reactions involving proton transfer, charge transfer, association reactions and hydride ion transfer, depending on the VOCs and other constituents within the sample.

The majority of PTR-MS instruments are operated with H_3O^+ as the only primary chemical ionization reagent ion. Recently, Jordan et al. [8] described a modified PTR-MS system with a switchable reagent ion capability (SRI+PTR-MS) which allows switching between 3 primary reagent ions: H_3O^+ , O_2^+ and NO^+ . In each mode there was always 3 or 4 reagent ions present in the reagent ion matrix: a primary reagent ion present at a purity of ~95% and 2 or 3 trace reagent ion species.

The use of other primary reagent ions O_2^+ and NO^+ in PTR-MS with switchable reagent ion capability was designed by Jordan et al. [8] for the separation of isomers and identification of VOCs previously indistinguishable with ionization via H_3O^+ alone. Measurements using the 3 different reagent ions can also be used to determine interference from O_2^+ and NO^+ reaction products when the PTR-MS is operating with H_3O^+ as the primary reagent ion and O_2^+ and NO^+ are trace constituents in the reagent ion matrix.

In atmospheric measurements the PTR-MS signal at m/z 42 is commonly regarded as a unique measure of acetonitrile [7]. However, two other ions potentially contribute to the signal at m/z 42. These are ^{13}C isotopologues of C_3H_5^+ and the product ion C_3H_6^+ .

In this paper we examine the interferences in the measurement of acetonitrile in the urban atmosphere, and quantify the interference.

2. PTR-MS selectivity at m/z 42

When the PTR-MS is operating with H_3O^+ as the primary reagent ion, there are 12 possible reaction pathways that yield four different product ions with m/z 42: CH_3CNH^+ , C_3H_6^+ , and the ^{13}C isotopologues of CH_3CN^+ and C_3H_5^+ . The reaction pathways and product

ions that may contribute to the signal at m/z 42, and to the either the measurement of acetonitrile or interference with acetonitrile measurement, are listed in Table 1. Each reaction pathway is discussed in turn.

When the PTR-MS used in this study was exposed to a prepared pure gaseous standard of acetonitrile, a single product ion was observed at m/z 42, most likely CH_3CNH^+ . The PA of acetonitrile ($186.2\text{ kcal mol}^{-1}$) is not sufficient for exothermic proton transfer with $\text{H}_3\text{O}^+\cdot(\text{H}_2\text{O})$ reagent ions ($\text{PA}(\text{H}_3\text{O}^+\cdot(\text{H}_2\text{O})) = 195.7\text{ kcal mol}^{-1}$) [9], so this reaction pathway does not influence the signal at m/z 42. The contributions to the ion signal at m/z 42 may result from dissociative ligand switching reactions with $\text{H}_3\text{O}^+\cdot(\text{H}_2\text{O})$ (reaction 2, Table 1), however the protonated product usually co-occurs with the non-dissociative ligand switching product $\text{CH}_3\text{CNH}^+\cdot\text{H}_2\text{O}$ (m/z 60) which is not observed in the mass spectra. Thus, reaction pathway 2 is unlikely to be significant.

O_2^+ ions undergo charge transfer reactions with compounds whose ionization energies are >12.06 eV, including some that yield product ions of C_3H_6^+ at m/z 42 (reactions 3 and 4, Table 1). Laboratory studies using O_2^+ chemical ionization have observed molecular and fragment ions at m/z 42 amu as a result of reactions with C_3 – C_5 alkanes and alkenes [10–12].

Measurements using PTR-MS with gas chromatographic pre-separation of urban air samples observed peaks in the chromatogram at mass 42 attributed to reactions of O_2^+ impurity ions with C_3 – C_4 alkanes [7]. When the PTR-MS used in this study, operating with O_2^+ as the primary reagent ion, was exposed to a pure gaseous standard mixture of 12 C_2 – C_5 hydrocarbons (ethane, ethene, propane, propene, *n*-butane, *cis*-2- and *trans*-2-butene, *n*-pentane, isopentane, *cis*-2- and *trans*-2-pentene, isoprene), the m/z 42 signal was 11% of the total ion signal (the sum of the ion signals for all m/z in the range 14–200 amu excluding reagent ion signals). Thus, contributions to the signal at m/z 42 due to reactions 3 and 4 are possible.

Laboratory studies using NO^+ as the primary reagent ion have observed a product ion at m/z 42 from charge transfer reactions of NO^+ with cyclopropane and 1-butene [12,13]. When the PTR-MS used in this study, operating with NO^+ as the primary reagent ion, was exposed to a pure gaseous standard mixture of 12 C_2 – C_5 hydrocarbons, the m/z 42 signal was 3% of the total ion signal. Contributions to the signal at m/z 42, due to reactions 5 and 6, are therefore possible.

The m/z 41 ion signal is often significantly larger than the m/z 42 signal when sampling urban air as there are many reaction pathways involving H_3O^+ , O_2^+ and NO^+ and common atmospheric VOCs that will yield a product ion at m/z 41 (reactions 7–10). The most likely product ion at m/z 41 is C_3H_5^+ . As a result of the natural ^{13}C isotopic abundance, a component of the signal at m/z 41 will be detected at m/z 42 as the ^{13}C isotopologues of the ^{12}C compound C_3H_5^+ . The natural ^{13}C isotopic abundance is 1.109%; thus, for a given C_3 compound, 3.3% of the signal at m/z 41 will appear at m/z 42 due to the isotopologues. Therefore, contributions to the signal at m/z 42 from reactions 7–10 are possible.

When the PTR-MS used in this study, operating with H_3O^+ as the primary reagent ion, was exposed to a pure gaseous standard of C_2 – C_5 hydrocarbons mentioned previously, a dominant peak at m/z 41 was observed that constituted 37% of the total ion signal. A fragment ion signal at m/z 41 was also observed when this PTR-MS, operating with H_3O^+ as the primary reagent ion, was exposed to individual prepared gaseous standards of pure isoprene, acetaldehyde, C_3 and C_4 alcohols, and C_4 and C_5 formate esters. Product ions at m/z 41 have been observed as a result of reactions with H_3O^+ for methacrolein and 1-butene [13], propyne [7] and C_4 – C_9 saturated and unsaturated alcohols [14,15]. Thus all of these compounds contribute through their fragmentation to m/z 41, and their single ^{13}C isotopologue to the signal at m/z 42.

Table 1

Reaction pathways and product ions that contribute to the signal at m/z 42 when the PTR-MS is operating with H_3O^+ as the primary reagent ion.

Product ion	Analytes	Reaction	Reaction pathway
CH_3CNH^+	Acetonitrile	1	$H_3O^+ + CH_3CN \rightarrow CH_3CNH^+ + H_2O$
		2	$H_3O^+ \cdot H_2O + CH_3CN \rightarrow CH_3CNH^+ + 2H_2O$
$C_3H_6^+$	Propene, cyclopropane	3	$O_2^+ + C_3H_6 \rightarrow C_3H_6^+ + O_2$
	C_4 – C_5 hydrocarbons (A)	4	$O_2^+ + A \rightarrow C_3H_6^+ + N + O_2$
	Cyclopropane, propene	5	$NO^+ + C_3H_6 \rightarrow C_3H_6^+ + NO$
	C_4 – C_5 hydrocarbons	6	$NO^+ + A \rightarrow C_3H_6^+ + N + NO$
$^{13}C^{12}C_2H_5^+$	Propyne	7	$H_3O^+ + (C_3H_4) \rightarrow ^{13}C^{12}C_2H_5^+ + H_2O$
	Multiple compounds (A_i)	8	$H_3O^+ + A_i \rightarrow ^{13}C^{12}C_2H_5^+ + N + H_2O$
		9	$O_2^+ + A_i \rightarrow ^{13}C^{12}C_2H_5^+ + N + O_2$
		10	$NO^+ + A_i \rightarrow ^{13}C^{12}C_2H_5^+ + N + NO$
$^{13}C^{12}CH_3N^+$	Acetonitrile	11	$O_2^+ + ^{13}C^{12}CH_3N \rightarrow ^{13}C^{12}CH_3N^+ + O_2$
		12	$NO^+ + ^{13}C^{12}CH_3N \rightarrow ^{13}C^{12}CH_3N^+ + NO$

The CH_3CN^+ ion does not contribute significantly to the ion signal at m/z 41 as the reaction rate coefficients for charge transfer reactions from NO^+ or O_2^+ to acetonitrile are only 0.9×10^{-9} and $0.2 \times 10^{-9} \text{ cm}^3 \text{ s}^{-1}$, respectively [16]. When the PTR-MS, operating with H_3O^+ as the primary reagent ion, with 4.2% O_2^+ impurity ions, was exposed to a pure gaseous standard of acetonitrile, the m/z 41 (CH_3CN^+) signal was 0.01% of the m/z 42 signal (CH_3CNH^+). Consequently, the ^{13}C isotopologue of CH_3CN^+ would not make a significant contribution to the ion signal at m/z 42, and reactions 11 and 12 are unlikely to be significant.

Overall, this analysis of reaction pathways that yield a product ion at m/z 42 in PTR-MS reveals that m/z 42 is not a unique measure for acetonitrile.

3. Accurate quantification of acetonitrile from the signal at m/z 42

Here a method is formulated to accurately determine the concentration of acetonitrile in urban air in PTR-MS measurements by quantifying and subtracting the interference of non-acetonitrile compounds at m/z 42. For the following analysis I_A , I_B and I_C refer to ion signals, measured in the primary reagent ion modes A (H_3O^+), B (O_2^+) and C (NO^+), (Table 2). There is an ion signal on most masses when zero (VOC-free) air is passed into the PTR-MS. This zero signal is measured (see Section 4.1) and has been subtracted from the ion signals reported here.

When the PTR-MS is operating in reagent ion mode A (H_3O^+ as the primary reagent ion), the uncorrected acetonitrile concentration is calculated from the total ion signal at m/z 42, $I_A(m/z$ 42) and a calibrated sensitivity for acetonitrile, S_{CH_3CN} , where $I_X(P^+, R^+)$ refers to the ion signal, I , in ion mode X , (where X = reagent ion mode A, B or C), of the enclosed product ion, P^+ , from reactions with reagent ion, R^+ . Ion signals are normalized to a primary reagent ion signal of 10^6 counts per second, expressed as normalized counts per second (ncps) and the sensitivity is expressed as ncps/ppbv.

$I_A(m/z$ 42) is composed of the sum of the ion signals from the 3 product ions CH_3CNH^+ , $C_3H_6^+$ and $^{13}C^{12}C_2H_5^+$ expressed using the nomenclature above:

$$[CH_3CN]_{uncorr} = \frac{I_A(m/z\ 42)}{S_{CH_3CN}} \quad (1a)$$

$$[CH_3CN]_{uncorr} = \frac{I_A(CH_3CNH^+, H_3O^+)}{S_{CH_3CN}} + \frac{I_A(^{13}C^{12}C_2H_5^+, H_3O^+)}{S_{CH_3CN}} + \frac{I_A(C_3H_6^+, O_2^+)}{S_{CH_3CN}} + \frac{I_A(C_3H_6^+, NO^+)}{S_{CH_3CN}} \quad (1b)$$

The corrected acetonitrile concentration, $[CH_3CN]_{corr}$ which is the first term on the right-hand side of Eq. (1b), can be determined

by quantifying and subtracting the interference of the other ions from the total ion signal at m/z 42 by re-arranging Eq. (1b):

$$[CH_3CN]_{corr} = \frac{I_A(CH_3CNH^+, H_3O^+)}{S_{CH_3CN}} \quad (2a)$$

$$[CH_3CN]_{corr} = \frac{I_A(m/z\ 42)}{S_{CH_3CN}} - \frac{I_A(^{13}C^{12}C_2H_5^+, H_3O^+)}{S_{CH_3CN}} - \frac{I_A(C_3H_6^+, O_2^+)}{S_{CH_3CN}} - \frac{I_A(C_3H_6^+, NO^+)}{S_{CH_3CN}} \quad (2b)$$

This equation allows the acetonitrile concentration to be calculated. The first term on the right-hand side of Eq. (2b) represents the PTR-MS observed signal. The following three terms on the right-hand side of Eq. (2b) are examined in the following three sections.

3.1. Quantifying the signal of the ^{13}C isotopologue of $C_3H_5^+$

The contribution from the ^{13}C isotopologue of $C_3H_5^+$ at m/z 42 can be quantified from the ion signal at m/z 41, $I_A(m/z$ 41), via the following equation:

$$I_A(^{13}C^{12}C_2H_5, H_3O^+) = 3 \times \frac{^{13}C}{^{12}C} \times I_A(m/z\ 41) \quad (3)$$

Note: it is standard procedure to correct for the mass dependent transmission efficiency of the PTR-MS detector when quantifying the concentration from the raw signals. The ratio of the measured transmission efficiency of m/z 42: m/z 41 was close to unity. Thus, transmission will have a minor effect on the calculation of the isotopologue interference and is not included in the analysis.

3.2. Quantifying the O_2^+ reaction product ion signal

The contribution to the m/z 42 ion signal resulting from O_2^+ reactions when the PTR-MS is operating with H_3O^+ as the primary reagent ion, and O_2^+ is present as a trace reagent ion can be determined by measurements at m/z 42 with the PTR-MS switched to O_2^+ mode, provided the results are scaled according to the respective concentrations of O_2^+ in the two different modes (it is assumed that the sample has the same composition when measured in all three modes).

$$I_A(C_3H_6^+, O_2^+) = \frac{I_A(O_2^+)}{I_B(O_2^+)} \times I_B(C_3H_6^+, O_2^+) \quad (4)$$

3.3. Quantifying the NO^+ reaction product ion signal

Similarly, the contribution of NO^+ reactions to the total ion signal at m/z 42 when the PTR-MS is operating with H_3O^+ as the primary

Table 2
Reagent ion signals and relative concentration of impurity ions in this study.

Reagent ion mode	Primary reagent ion	Mean primary reagent ion signal (cps)	Trace reagent ions (% primary reagent ion signal)	
A	H ₃ O ⁺	2.75 ± 0.11 × 10 ⁷	O ₂ ⁺	2.9–3.5%
			NO ⁺	0.4–0.6%
B	O ₂ ⁺	4.26 ± 0.14 × 10 ⁷	H ₃ O ⁺	2.2–7.0%
			NO ⁺	4.6–5.4%
			NO ₂ ⁺	0.4–0.6%
C	NO ⁺	5.01 ± 0.16 × 10 ⁷	H ₃ O ⁺	0.2–0.3%
			O ₂ ⁺	0.6–1.1%
			NO ₂ ⁺	4.8–8.2%

reagent ion can be determined by measurements at *m/z* 42 with the PTR-MS switched to NO⁺ mode via:

$$I_A(\text{C}_3\text{H}_6^+, \text{NO}) = \frac{I_A(\text{NO}^+)}{I_C(\text{NO}^+)} \times I_C(\text{C}_3\text{H}_6^+, \text{NO}) \quad (5)$$

3.4. Quantifying the acetonitrile ion signal

To determine the corrected concentration of acetonitrile $[\text{CH}_3\text{CN}]_{\text{corr}}$ from the protonated acetonitrile ion signal $I_A(\text{CH}_3\text{CNH}^+, \text{H}_3\text{O}^+)$, the measured ion signals from the isotopeologue product ions and O₂⁺ and NO⁺ reaction products are subtracted from the total ion signal at *m/z* 42:

$$[\text{CH}_3\text{CN}]_{\text{corr}} = \frac{I_A(\text{CH}_3\text{CNH}^+, \text{H}_3\text{O}^+)}{S_{\text{CH}_3\text{CN}}} \quad (6a)$$

$$[\text{CH}_3\text{CN}]_{\text{corr}} = \frac{I_A(m/z\ 42)}{S_{\text{CH}_3\text{CN}}} - \frac{[3 \times (^{13}\text{C}/^{12}\text{C}) \times I_A(m/z\ 41)]}{S_{\text{CH}_3\text{CN}}} - \frac{[(I_A(\text{O}_2^+)/I_B(\text{O}_2^+)) \times I_B(\text{C}_3\text{H}_6^+)]}{S_{\text{CH}_3\text{CN}}} - \frac{[(I_A(\text{NO}^+)/I_C(\text{NO}^+)) \times I_C(\text{C}_3\text{H}_6^+)]}{S_{\text{CH}_3\text{CN}}} \quad (6b)$$

Thus, from switchable reagent ion measurements it is possible to accurately determine the concentration of acetonitrile in urban air using a sequential pattern of measurements at *m/z* 41 and 42 with O₂⁺, NO⁺ and H₃O⁺ as the primary reagent ions.

4. Methodology

4.1. PTR-MS measurements

A PTR-MS with switchable reagent ion capability (SRI + PTR-MS) was utilized to make sequential measurements with different ion source tuning to generate primary reagent ions H₃O⁺, NO⁺ and O₂⁺ [8]. The SRI + PTR-MS sampled ambient air in an urban area of Sydney, Australia in summer from 18th February–7th March 2011. The sampling site (33.8°S, 150.9°E) was located in an open park land area greater than 30 m from other buildings and >100 m from any major roads. Air was sampled at a height of 4 m via a glass inlet of ~2 m connected to silco steel tubing at a flow rate of 1.5 L min^{−1} of which the PTR-MS sampled 300 mL min^{−1} (STP).

The PTR-MS measurements were made as a part of a more extensive study to provide a detailed characterization of the chemical and aerosol composition of the urban atmosphere in Sydney. A full description of that study is beyond the scope of this paper and will be presented elsewhere at a later date.

Daily, the PTR-MS switched sequentially through the 3 reagent ion modes: H₃O⁺, NO⁺ and O₂⁺. In the hollow cathode ion source, H₃O⁺ reagent ions were produced from water vapour introduced at a flow of ~6 mL min^{−1} (STP). The source gas for the O₂⁺ reagent ions

was UHP O₂ (BOC, Australia) introduced to the ion source at a flow rate of 5 mL min^{−1} (STP). The source gas for the NO⁺ reagent ions was a combination of UHP O₂ and N₂ (BOC, Australia) introduced to the ion source at flow rates of 5.0 mL min^{−1} (STP) and 3.8 mL min^{−1} (STP), respectively.

The drift tube reaction chamber was maintained at 60 °C and an applied voltage of 445 V. The pressure in the reactor was 2.16 mbar when sampling in H₃O⁺ mode, 2.25 mbar in NO⁺ mode, and 2.23 mbar in O₂⁺ mode.

The hollow cathode ion source with switchable reagent ion capability generates a high density plasma of either H₃O⁺, NO⁺ or O₂⁺ with high purity. However, there are always some impurity reagent ions present. Reagent ion signals from this study and the relative concentration of impurity ions are presented in Table 2. The NO⁺ plasma in the ion source was unstable at times due to the low ion source operating current used for this study.

The PTR-MS quadrupole was run in scanning mode, operating between masses 14 amu and 200 amu. The dwell time for a single mass measurement was 1 s, generating a full mass scan approximately every 3 min. To preserve the lifetime of the SEM, the signal of the reagent ion isotopes were measured rather than the primary ion signal. H₃¹⁸O⁺ detected at *m/z* 21 was multiplied by 500 to approximate the H₃O⁺ signal at *m/z* 19; ¹⁵NO⁺, detected at *m/z* 31, was multiplied by 274 to approximate the NO⁺ signal at *m/z* 30; and, ¹⁸O¹⁶O⁺, detected at *m/z* 34, was multiplied by 250 to approximate the O₂⁺ signal at *m/z* 32.

The PTR-MS operated with the aid of custom built auxiliary equipment that regulates the flow of air in the sample inlet and controls whether the PTR-MS is sampling ambient or zero air or calibration gas. Zero readings were made by diverting the air through a zero furnace (350 °C) with a platinum wool catalyst that destroyed VOCs in the air before they entered the PTR-MS. Zero measurements were made 5 times daily: for 30 min commencing at 01:00 h, 02:30 h, 10:00 h, 16:00 h and 23:00 h. Zero measurements occurred in H₃O⁺, O₂⁺ and NO⁺ mode twice per day. The minimum detection limit (MDL) at *m/z* 42 for a 1 s observation was 46 pptv.

Over the 17 days of sampling, calibrations against certified gas standards were performed on the PTR-MS four times per day. Calibrations occurred in H₃O⁺ mode twice per day and in O₂⁺ and NO⁺ mode once per day. A gas standard supplied by AiR Environmental Inc (Broomfield, Colorado), which contained 15 compounds including 980 ppb acetonitrile, determined the PTR-MS sensitivity to acetonitrile of 14.6 (±0.7) ncps ppbv^{−1} at *m/z* 42.

4.2. Supporting measurements

The concentration of levoglucosan, a biomass burning tracer in atmospheric particulate matter, was determined from 8-h filter samples taken on 16 days (11 am–7 pm), collected on quartz filters using a HiVol sampler (Ecotech Pty Ltd, Blackburn, Victoria, Australia). A 6.25 cm² portion of the filter was extracted in deionized water and analysed by high performance anion exchange

Table 3Ambient measurement parameters, m/z at which they are measured, reagent ion mode used, and the reagent ion switching times for the two sampling sequences.

Measurement parameter	m/z	Reagent ion mode	Primary reagent ion	Sequence 1 13:00–20:00	Sequence 2 21:00–5:59
$I_A(m/z\ 42)$	42				
$I_A(C_3H_5^+, H_3O^+)$	41	A	H_3O^+	13:00–14:59	21:00–22:59
$I_A(O_2^+)$	32			18:00–20:00	4:00–5:59
$I_A(NO^+)$	30				
$I_B(O_2^+)$	42	B	O_2^+	15:00–15:59	0:00–0:59
$I_B(C_3H_6^+, O_2^+)$	32				
$I_C(NO^+)$	30	C	NO^+	17:00–17:59	3:00–3:59
$I_C(C_3H_6^+, NO^+)$	42				

chromatography with pulsed amperometric detection (HPAEC-PAD) as described in Iinuma et al. [17]. An Ecotech EC 9830 CO analyser and Ecotech NO_x Chemiluminescence analyser were used to determine the concentration of carbon monoxide and nitrogen oxides (NO_x).

The concentrations of 32 VOCs, including alkanes, aromatic and biogenic compounds, were determined from air samples collected onto Markes Carbograph 1TD/Carbopack X adsorbent tubes (Markes International Inc., Rhondda Cynon Taff, United Kingdom) using constant-flow air sampling pumps. The tubes were analysed using an automated thermal desorber and gas chromatograph (GC) equipped with a flame ionization detector (FID) and a mass selective detector (MSD).

The concentrations of 15 aldehydes and ketones were determined from air samples collected onto Supelco LpDNPH H10 air monitoring cartridges (Supelco, Pennsylvania, USA) using constant flow air pumps. Carbonyls were trapped on the cartridge where they were converted to the hydrazine derivatives. The derivatives were eluted from the cartridge in acetonitrile and analysed by HPLC. Samples were collected on the Markes Carbograph 1TD/Carbopack X adsorbent tubes and DNPH cartridges twice daily over periods that coincided with the PTR-MS measurement sequences: one 8-h sample was collected in the afternoon (11 am–7 pm) and one 10-h sample was collected overnight (7 pm–5 am).

4.3. Data analysis

For this analysis, a subset of the PTR-MS data was used which were grouped into 2 distinct sampling sequences each day according to time of day (Table 3).

Sequence 1 was a period of sampling in switchable reagent ion mode from afternoon to early evening and Sequence 2 was a period of sampling in switchable reagent ion mode from late evening to early morning. Overall, 31 periods of H_3O^+ reagent ion mode data and 27 periods of NO^+ and O_2^+ reagent ion mode data were obtained over the 17 days of sampling.

Daily zero measurements in each reagent ion mode for each mass were subtracted from the raw signal. Ambient measurements corresponded to the 1-h averaged ion signals (cps) for sampling periods when the PTR-MS was operating with NO^+ and O_2^+ as the primary reagent ions. Ambient measurements with H_3O^+ as the primary reagent ion were a combined 4-h average of the data that span the 2 h prior to and the 2 h following the NO^+ and O_2^+ sampling times (Table 3). This bracketing of the NO^+ and O_2^+ measurements by 2 sets of H_3O^+ measurements is to ensure, as much as possible, that the ambient air VOC concentrations in the samples were approximately equivalent in all three reagent ion modes. The measurement parameters used for the corrected quantification of acetonitrile at $m/z\ 42$, and described in Section 2, are listed in Table 3.

There were 4 periods in which no data were collected in NO^+ and O_2^+ reagent ion modes; thus, the correction for the interference

could only be made for the isotopologue interference. The linear relationship between the O_2^+ interference (cps) and the concentration of toluene (ppbv) measured by PTR-MS ($R^2 = 0.75$) was used to interpolate the O_2^+ interference for the missing periods. The corrected acetonitrile ion signals (cps) determined using interpolated values showed very good agreement with measured values for the entire dataset (slope = 0.996, $R^2 = 0.99$); thus, the 4 interpolated data points were included for all analyses in this study.

5. Results and discussion

5.1. Contributions to the ion signal at $m/z\ 42$

The extent of interference from $C_3H_6^+$ ions and the ^{13}C isotopologues of $C_3H_5^+$ in the measurement of acetonitrile at $m/z\ 42$ were determined using Eq. (6). Interference in the signal for the measurement of acetonitrile at $m/z\ 42$ was observed for every sampling period (Fig. 1).

The contributions of the ^{13}C isotopologues of $C_3H_5^+$ to the signal at $m/z\ 42$ were quantitatively determined from the signal at $m/z\ 41$ ($C_3H_5^+$). The ion signal at $m/z\ 42$ of the ^{13}C isotopologue of $C_3H_5^+$ contributed 2.7–21.1% of the total $m/z\ 42$ signal (Fig. 1). Isotopologue ions contributed >10% to the signal at $m/z\ 42$ in 16 of the 31 measurement periods (Fig. 1).

The impurity reagent ions O_2^+ and NO^+ were present at levels of ~3% and <1% of the H_3O^+ reagent ion signal, respectively (Table 2). In this study, $C_3H_6^+$ ions resulting from reactions of VOCs with O_2^+ contributed 0.4 to 20.1% of the total $m/z\ 42$ signal and were >10% in eight out of 31 measurement periods (Fig. 1). The contribution of $C_3H_6^+$ ions to $m/z\ 42$, resulting from reactions of VOCs with NO^+ , was always negligible (<1.2% of the total $m/z\ 42$ signal).

Protonated acetonitrile ions dominated the signal at $m/z\ 42$ (Fig. 1) contributing an average of $81 \pm 9\%$ with a range of 59–95% of the total ion signal. The contribution of the protonated acetonitrile ion was >90% on 7 out of the 31 measurement periods in this study (Fig. 1).

5.2. Calculation of the acetonitrile interference from other individual compounds

In this section we provide an explanation to account for the observed interference in the signal at $m/z\ 42$ by calculating the interference from the known or interpolated concentrations of compounds identified as potential interferences. The potential interferences identified for this analysis are C_3 – C_6 alkenes (including isoprene) and alkanes, methacrolein and acetaldehyde. The concentrations of the potential interferences, with the exception of short chain alkenes, were measured in this study by PTR-MS, GC-MS and DNPH derivatization.

The concentrations of C_3 – C_5 alkenes, apart from isoprene, were not measured in this study. Small alkenes contribute to the interference in the $m/z\ 42$ signal as they produce ^{13}C isotopologues of $C_3H_5^+$

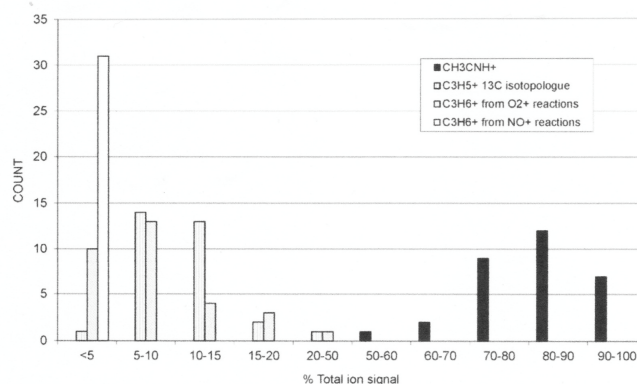


Fig. 1. Frequency distribution of the relative contributions from, protonated acetonitrile ions, ^{13}C isotopologue ions of C_3H_5^+ , and C_3H_6^+ ions from O_2^+ and NO^+ reactions for the 31 measurement periods in this study.

and O_2^+ reaction products at m/z 42. In the absence of better data, we drew upon a dataset where the concentrations of C_3 – C_6 alkenes, as well as C_3 – C_7 alkanes, and a range of aromatic compounds were measured in 82 hourly samples taken in 3 urban locations, during the day (7 am–5 pm) in summer in Sydney, 2006 [18] near the site of this study. The linear relationship (y -intercept = 0) observed between each of the alkene groups and isopentane from the 2006 study was used to interpolate C_3 – C_6 alkene concentrations from the isopentane concentrations observed in this study (Table 4). The observed isopentane and calculated C_3 – C_6 alkene concentrations in this analysis correspond with the concentrations observed in 2006.

The interference due to the ^{13}C isotopologue of C_3H_5^+ ions can be calculated by using Eq. (7):

$$\text{isotopologue interference} = [\text{A}] \times \text{BR}_{m/z\ 41} \times \left(\frac{^{13}\text{C}}{^{12}\text{C}} \text{ ratio} \times 3 \right) \quad (7)$$

where $[\text{A}]$ is the concentration of an analyte that produces a fragment at m/z 41 when the PTR-MS is operating with H_3O^+ as the primary reagent ion. In this analysis the concentrations of C_3 – C_6 alkenes, isoprene, acetaldehyde and methacrolein were considered as they are known to produce a product ion at m/z 41.

For the sum of the C_3 – C_6 alkenes, a branching ratio (BR) of 37% at m/z 41 was determined from measurements performed when the PTR-MS, operating with H_3O^+ as the primary reagent ion, was exposed to a pure gaseous standard of C_2 – C_5 hydrocarbons. Branching ratios to m/z 41 of 19% for isoprene and 2% for acetaldehyde were determined in the laboratory from measurements when the PTR-MS, operating in H_3O^+ mode, was exposed to individual prepared pure gaseous standards of these compounds. These branching ratios were determined using the same drift tube operating parameters (pressure, voltage, temperature) as used in

the urban air monitoring in this study. The branching ratio to m/z 41 for methacrolein was 4% [14].

The presence of C_3 – C_6 alkenes and isoprene, with minor contributions from acetaldehyde and methacrolein, explained the observed ^{13}C isotopologue interference (Table 5) within the overlapping uncertainty limits of the two techniques. Further contributions to the ^{13}C isotopologue interference may have resulted from compounds that produce a fragment ion at m/z 41 that were not included in this analysis. This is because their concentrations could not be quantitatively determined or estimated. These compounds include C_3 – C_9 saturated and unsaturated alcohols [14,15], C_4 – C_5 formate esters [15], cyclopropane [12] and propyne [7].

The interference due to O_2^+ reaction products can be calculated using Eq. (8):

$$\text{O}_2^+ \text{ reaction products interference} = [\text{A}] \times \text{BR}_{m/z\ 42} \times \left(\frac{[\text{O}_2^+]}{[\text{H}_3\text{O}^+]} \right) \quad (8)$$

where $[\text{A}]$ is the sum of the concentrations of propene, pentenes and C_4 – C_7 alkanes. When the PTR-MS, operating with O_2^+ as the primary reagent ion, was exposed to a pure gaseous standard of C_2 – C_5 hydrocarbons, the peak at m/z 42 constituted 11% of the total ion signal. Therefore, we assumed BR of 0.11 for the sum of propene, pentenes and C_4 – C_7 alkanes this analysis. A product ion at m/z 42 was not observed as a result of charge transfer from O_2^+ to butenes and hexenes [12,13] so they were excluded in this analysis. The reagent ion ratio $[\text{O}_2^+]/[\text{H}_3\text{O}^+]$ used in Eq. (8) was 3%. The calculated and observed O_2^+ reaction product interference showed good agreement within the uncertainties of the two methods. The presence of C_3 – C_7 alkanes, propene and the sum of the pentenes

Table 4
Linear interpolation equations derived from measurements in Sydney 2006 [20] used to estimate alkene concentrations in the present study.

Alkene	Isopentane linear interpolation (Sydney, 2006)	Interpolated conc. (Sydney, 2011) (ppb)
Propene	$[\text{Propene}] = 0.391 \times [\text{Isopentane}]$ $R^2 = 0.64$	0.88 ± 0.75
Sum of butenes	$[\text{Butenes}] = 0.362 \times [\text{Isopentane}]$ $R^2 = 0.73$	0.82 ± 0.69
Sum of pentenes	$[\text{Pentenes}] = 0.336 \times [\text{Isopentane}]$ $R^2 = 0.81$	0.76 ± 0.64
Sum of hexenes	$[\text{Hexenes}] = 0.088 \times [\text{Isopentane}]$ $R^2 = 0.64$	0.20 ± 0.17

Table 5

Quantification of the contribution of individual compounds or compound groups to the interference at m/z 42.

Compounds	Concentration (ppb) (mean \pm stdev)	Branching ratio	Calculated ^{13}C Isotopologue Interference (ppt)	Calculated O_2^+ reaction product interference (ppt)
^{13}C isotopologue interference				
C_3 – C_6 alkenes ^a	2.66 \pm 2.25	0.37	32.5 (5–60)	–
Isoprene	1.02 \pm 1.37	0.19	6.4 (0–15)	–
Acetaldehyde MACR	0.40 \pm 0.27	0.02	0.3 (0.1–0.4)	–
	0.17 \pm 0.20	0.04	0.2 (0–0.5)	–
O_2^+ reaction products interference				
C_4 – C_7 alkanes, propene, pentene	12.16 \pm 9.79	0.11	–	40.1 (7.8–72.4)
Total calculated interference			39 (5–76)	40 (8–72)
Total observed interference			15 \pm 10	12 \pm 12

^a C_3 – C_6 alkenes did not include isoprene.

explained the interference due to O_2^+ reaction products within the overlapping uncertainty limits of the two techniques (Table 5).

5.3. Characteristics of the corrected acetonitrile data

The 4-hourly average corrected and uncorrected concentrations of acetonitrile are shown in Fig. 2. The 4-hourly mean corrected acetonitrile concentration was 120 pptv (± 54) and ranged from 47 to 251 pptv. The 4-hourly mean, uncorrected acetonitrile concentration was 148 pptv (± 65) and ranged from 53–311 pptv. The mean difference between corrected and uncorrected acetonitrile concentrations was 28 pptv (± 20). The greatest difference of 87 pptv occurred during the evening sampling period on 23rd February identified as a high pollution day in Fig. 2 when enhanced concentrations of VOCs, CO and NO_x were observed with only average concentrations of acetonitrile.

A clear diurnal cycle of acetonitrile was observed (Fig. 2) with a daytime minima of 99 pptv (± 65) and nighttime maxima of 189 pptv (± 60) predominantly driven by atmospheric stability at night that prevented dispersion of acetonitrile.

The corrected acetonitrile concentrations, uncorrected acetonitrile concentrations and acetonitrile interference were each correlated with the concentrations of a number of other atmospheric constituents. An examination was undertaken to identify the compounds that are likely to be related to the real acetonitrile signal and those that contribute to the interference in the m/z 42 signal (Table 6).

Levogluconan is a major component of smoke particles from biomass burning and, like acetonitrile, it is used as a tracer of emissions from biomass burning [19]. During a biomass burning event on the 25th and 26th of February, a maximum corrected

acetonitrile concentration of 251 pptv (uncorrected 311 pptv) and a maximum levoglucosan concentration of 268 ng m^{-3} was observed (Fig. 2). For this limited dataset ($N=15$), the corrected acetonitrile concentrations were more strongly correlated with levoglucosan ($R^2=0.66$) than the uncorrected acetonitrile concentrations ($R^2=0.54$). The acetonitrile interference (the uncorrected acetonitrile concentration minus the corrected acetonitrile concentration), was uncorrelated with levoglucosan ($R^2=0.00$) indicating the interference in the acetonitrile signal does not have a biomass burning origin. Therefore, the urban interference causes an apparent acetonitrile contribution.

5.4. Interference from urban pollutants

The following is an analysis of the interference in the measurement of background acetonitrile in urban air, with no direct biomass burning influence. When a subset of the data was taken that excluded the period of biomass burning on the 25th and 26th of February, it was possible to analyse more sensitively the correlations of the interference in the measurement of the acetonitrile concentration with urban pollutants.

The corrected acetonitrile concentration in this subset of data was less well correlated with 6 measures of urban pollutant sources (CO, NO_x , C_4 – C_7 alkanes, aromatic VOCs, biogenic VOCs and secondary VOC oxidation products) than the uncorrected acetonitrile concentration (Table 6). Alkanes and aromatic VOCs in the Sydney urban atmosphere are primarily emitted by vehicles [20]. The C_4 – C_7 alkanes measured by GC–MS in this analyses included isobutane, *n*-butane, 2-methyl butane, *n*-pentane, 2- and 3-methyl pentane, *n*-hexane, methyl cyclopentane, cyclohexane, 3-methyl hexane and *n*-heptane. Aromatics measured by GC–MS in this analyses included benzene, toluene, ethylbenzene, *p*-, *m*- and *o*-xylenes, *m*- and *o*-ethyltoluene, 1,3,5- and 1,2,4-trimethylbenzenes. Biogenic VOCs measured by GC–MS in this analyses included isoprene, α - and β -pinene, *o*-cymene, *D*-limonene, eucalyptol and camphor measured by GC–MS. VOC oxidation products is the sum of formaldehyde, acetaldehyde, acetone, propanal, methacrolein, methyl ethyl ketone, butanal, benzaldehyde, glyoxal, pentanal, methyl glyoxal and hexanal measured by DNPH derivatization.

The interference in the acetonitrile signal caused by the ^{13}C isotopologue of C_3H_5^+ was significantly correlated with CO, C_4 – C_7 alkanes, aromatics, biogenic emissions and VOC oxidation products. The interference is a result of dissociative proton transfer reactions of H_3O^+ with small alkenes, isoprene, and methacrolein resulting in a product ion at m/z 41 with an associated ^{13}C isotopologue ion at m/z 42. The PTR–MS does not detect CO, and aromatics and alkanes are not observed to fragment to m/z 41; therefore, the observed correlation with the ^{13}C isotopologue is a proxy for other processes in the urban atmosphere, coincidental source regions, or meteorology that leads to a correlation between various atmospheric pollutants.

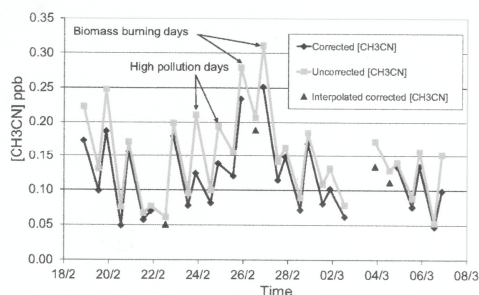


Fig. 2. Corrected (diamonds) and uncorrected (squares) acetonitrile concentrations from 17 days of ambient sampling in urban air in summer in Sydney 2011. Interpolated corrected acetonitrile concentrations (triangles) (see Section 4.3).

Table 6

Correlation coefficients (R^2) for the linear regression of the corrected and uncorrected acetonitrile concentration, the ^{13}C isotopologue correction and the O_2^+ reaction products correction versus 6 measures of urban pollutant sources. Bold text indicates $R^2 > 0.51$.

	Corrected CH_3CN	Uncorrected CH_3CN	^{13}C Isotopologue correction			O_2^+ reaction products correction		
	All	All	All	Day	Night	All	Day	Night
CO	0.40	0.58	0.58	0.64	0.49	0.46	0.41	0.44
NO_x	0.09	0.31	0.48	0.04	0.50	0.79	0.31	0.81
$\text{C}_4\text{--C}_7$ alkanes	0.12	0.37	0.72	0.20	0.79	0.79	0.31	0.76
Aromatic VOCs	0.08	0.24	0.53	0.18	0.81	0.44	0.06	0.71
Biogenic VOCs	< 0.01	< 0.01	0.12	0.79	0.12	< 0.01	0.22	0.10
VOC oxidation products	< 0.01	0.01	0.14	0.67	0.41	0.02	0.53	0.11

Measurement of short chain alkenes ($\text{C}_2\text{--C}_6$) not undertaken here, is obviously central to describing the interference.

The O_2^+ reaction product ions were strongly correlated with the concentrations NO_x , $\text{C}_4\text{--C}_7$ alkanes and aromatics. The interference in the acetonitrile signal caused by O_2^+ reaction products was a result of dissociative and non-dissociative charge transfer reactions of O_2^+ with alkanes and alkenes resulting in a product ion at m/z 42. The PTR-MS does not detect NO_x and aromatics do not fragment to m/z 42, therefore the observed correlation with the O_2^+ reaction product ions are due to other processes that lead to a correlation between the concentrations of various atmospheric pollutants.

6. Conclusions

A systematic study was conducted into the interference in the PTR-MS measurement of acetonitrile at m/z 42 in Sydney, Australia. Two other ions contributed to the signal at m/z 42. These are ^{13}C isotopologues of C_3H_5^+ and the product ion C_3H_6^+ . The signal from the ^{13}C isotopologue of C_3H_5^+ at m/z 42, is due to alkenes including isoprene with probable contributions from other compounds not measured in this study. The signal from C_3H_6^+ is produced by reactions of O_2^+ with alkanes and alkenes.

A correction was applied to the m/z 42 signal to accurately quantify the acetonitrile concentration. The correction for the ^{13}C isotopologue of C_3H_5^+ can be made utilizing the signal at m/z 41. The correction for the C_3H_6^+ product ion signal from O_2^+ reactions can be corrected for by utilizing switchable reagent ion PTR-MS in O_2^+ mode or reduced by minimizing the O_2^+ component in the H_3O^+ primary reagent ion matrix. The correction to the apparent acetonitrile concentrations from 17 days of observations in Sydney, Australia ranged from 5 to 41%.

The corrected acetonitrile concentration is more highly correlated with levoglucosan, a marker of biomass burning, and less highly correlated with benzene and toluene, compounds from motor vehicles, than the uncorrected concentrations. The corrected acetonitrile concentrations show no significant influence from motor vehicles. The method formulated in this study to quantify and subtract the interference of non-acetonitrile compounds in PTR-MS measurements at m/z 42 resulted in a more accurate quantification of the concentration of acetonitrile and consequently, a more sensitive tracer for biomass burning in polluted urban air.

Acknowledgements

This work was carried out as part of the Sydney Particle Study 2011 Summer Observation Program for the NSW Dept. of

Environment and Climate Change. This work was supported by The Centre for Australian Weather and Climate Research and a Monash University Faculty of Science Postgraduate Scholarship. The authors gratefully acknowledge P. Selleck and M. Cheng from CAWCR for their supporting measurements.

References

- [1] J.M. Lobert, D.H. Scharff, W.M. Hao, P.J. Crutzen, *Nature* 346 (1990) 552.
- [2] J.A. de Gouw, C. Warneke, D.D. Parrish, J.S. Holloway, M. Trainer, F.C. Fehsenfeld, *Journal of Geophysical Research* 108 (D11) (2003) 4329.
- [3] M.O. Andreae, P. Artaxo, H. Fisher, S.R. Freitas, J.-M. Gregoire, A. Hansel, P. Hoor, R. Kormann, R. Krejci, L. Lange, J. Lelieveld, W. Lindinger, K. Longo, W. Peters, M. de Reus, B. Scheeren, M.A.F. Silva Dias, J. Strom, P.F.J. van Velthoven, *Geophysics Research Letters* 28 (2001) 951–954.
- [4] J. Lelieveld, P.J. Crutzen, V. Ramanathan, M.O. Andreae, C.A.M. Brenninkmeijer, T. Campos, G.R. Cass, R.R. Dickerson, H. Fisher, J.A. de Gouw, A. Hansel, A. Jefferson, D. Kley, A.T.J. de Laat, S. Lal, M.G. Lawrence, J.M. Lobert, O.L. Mayol-Bracero, A.P. Mitra, T. Novakov, S.J. Oltmans, K.A. Prather, T. Reiner, H. Rodhe, H.A. Scheeren, D. Sikka, J. Williams, *Science* 291 (2001) 1031–1036.
- [5] W. Lindinger, A. Hansel, A. Jordan, *International Journal of Mass Spectrometry and Ion Processes* 173 (1998) 191–241.
- [6] J. de Gouw, C. Warneke, *Mass Spectrometry Reviews* 26 (2007) 223–257.
- [7] C. Warneke, J.A. de Gouw, W.C. Kuster, P.D. Goldan, R. Fall, *Environmental Science and Technology* 37 (2003) 2494–2501.
- [8] A. Jordan, S. Haidacher, G. Hanel, E. Hartungen, J. Herbig, L. Mark, R. Schotkowsky, H. Seehauser, P. Sulzer, T.D. Mark, *International Journal of Mass Spectrometry* 286 (2009) 32–38.
- [9] NIST Chemistry Web Book, in: P.J. Lindstrom, W.G. Mallard (Eds.), EBNIST Standard Reference Database Number 69, National Institute of Standards and Technology, Gaithersburg, MD, 2005, <http://webbook.nist.gov>.
- [10] P. Spänel, D. Smith, *International Journal of Mass Spectrometry* 181 (1998) 1–10.
- [11] A.M. Diskin, T. Wang, D. Smith, P. Spänel, *International Journal of Mass Spectrometry* 218 (2002) 87–101.
- [12] P.F. Wilson, C.G. Freeman, M.J. McEwan, *International Journal of Mass Spectrometry* 229 (2003) 143–149.
- [13] R.S. Blake, K.P. Wyche, A.M. Ellis, P.S. Monks, *International Journal of Mass Spectrometry* 254 (2006) 85–93.
- [14] M. Demarcke, C. Amelynck, N. Schoon, F. Dhooque, J. Rimetz-Planchon, H. Van Langenhove, J. Dewulf, *International Journal of Mass Spectrometry* 290 (2010) 14–21.
- [15] K. Buhr, S. van Ruth, C. Delahunty, *International Journal of Mass Spectrometry* 221 (2002) 1–7.
- [16] P. Spänel, D. Smith, *International Journal of Mass Spectrometry* 176 (1998) 203–211.
- [17] Y. Iinuma, G. Engling, H. Puxbaum, H. Herrmann, *Atmospheric Environment* 43 (2009) 1367–1371.
- [18] M. Azzi, A.R. Tibbet, R.J. Heywood, D.E. Angove, J.N. Carras, ET/IR 880R (2007), Department of Environment and Climate Change NSW, Sydney, NSW, Australia (not published).
- [19] H. Puxbaum, A. Caseiro, A. Sanchez-Ochoa, A. Kasper-Giebl, M. Claeys, A. Gelencser, M. Legrand, S. Preunkert, C. Pio, *Journal of Geophysical Research* 112 (2007) D23S05.
- [20] DECC, Department of Environment and Climate Change NSW, Sydney, NSW, Australia, 2007, Available: <http://www.environment.nsw.gov.au/air/inventory.htm>.

Chapter 6. Measurement of total non-methane organic carbon (TNMOC) in urban air using O₂⁺ SRI-MS

6.1 Introduction

Typical field studies of the atmosphere observe 30 -100 organic compounds (Heald et al. 2008), and field studies with comprehensive separation have observed > 500 organic compounds in the atmosphere (Lewis et al. 2000). It has been estimated that in excess of 10⁴ organic compounds have been observed and the number of compounds actually present in the atmosphere far exceeds the number of measured species (Goldstein & Galbally 2007). Developing technologies to deal with this range of organic compounds is a key challenge in atmospheric chemistry.

While a multitude of speciated VOC measurement systems exist, far fewer techniques to measure total VOCs have been developed. A number of techniques were developed to measure total non-methane organic carbon (TNMOC) in source streams and highly polluted environments (e.g. Howe et al. (1983), Zielinska et al (1996). However, few techniques exist to measure bulk total volatile organic compounds or TNMOC at concentrations typical in ambient air with high time resolutions.

Roberts et al. (1998) developed a technique to measure gas-phase TNMOC via cryogenic collection, pre-separation of CO₂, CO and CH₄, back flushing the NMOC off the GC column, conversion of the NMOC to CH₄, and measurement by flame ionization detector (Roberts et al 1998). In measurements at Chebogue Point Nova Scotia, Roberts et al (1998) observed TNMOC concentrations greater than or equal to the sum of the speciated VOCs on all but a few occasions.

Maris et al (2003) developed a 2-channel instrument capable of simultaneously analyzing TNMOC using a modified version of the technique described above, and speciated VOCs via standard GC-FID. In measurements of primary pollution sources (diesel exhaust and petrol vapor), air masses close to primary sources (roads, light industry) and air masses where there was minimal photochemistry Maris et al (2003) reported the speciated measurements gave 85-95% of the TNMOC concentrations observed. However, in photochemically aged air masses the speciated measurements reported 55 – 80% of the unspciated TNMOC observed.

Overall, these measurements of total organic carbon and speciated VOCs confirm that a significant fraction of organic carbon in the atmosphere remains unidentified with conventional VOC measurement techniques. Consequently the organic carbon budget remains poorly constrained (Heald et al. 2008) and the role of this unidentified organic carbon in the formation of ozone and secondary organic aerosol is uncertain.

Proton transfer mass spectrometry (PTR-MS) has proven to be a useful tool for the measurement of VOCs in the atmosphere. The tests against gas standards described in Chapters 2 and 3, demonstrated that standard PTR-MS employing H_3O^+ reagent ions is capable of detecting almost all compound classes including oxygenated VOCs, aromatics, alkenes including isoprene, and terpenes, with the notable exceptions of the small alkanes which make up a considerable fraction of total VOCs in urban air.

Oxygen cations (O_2^+) will undergo efficient charge transfer reactions with all species that have a lower first ionization energy (IE) than O_2 (12.07eV) (Lias 2015). The IE of O_2 is higher than nearly all organic compounds including the small hydrocarbons that do not react with H_3O^+ .

The use of O_2^+ as a reagent ion in PTR-MS has been explored in previous chapters of this thesis (Chapters 3 and 5). The laboratory studies described in Chapter 3 demonstrated that an SRI-MS operating with O_2^+ as the primary reagent ion can almost be regarded as a universal VOC detector as it was capable of detecting 70 out of 73 compounds present in five certified gas standards, including the small alkanes not detectable with H_3O^+ . However, due to the large number of compounds that undergo reactions with O_2^+ and the more energetic nature of O_2^+ ionization which results in more extensive product ion fragmentation, the mass spectra from O_2^+ SRI-MS were less well resolved than the H_3O^+ SRI-MS spectra, and O_2^+ SRI-MS is not suitable for speciated VOC measurements.

The approach explored here is to evaluate the use of O_2^+ reagent ions in SRI-MS to measure the concentration of “total” volatile organic compounds in an urban atmosphere. If one assumes O_2^+ SRI-MS is responding to almost all VOCs present in a given sample, the sum of the ion signals in the m/z range should be proportional to the total volatile organic carbon concentration in the sample. The following discussion outlines the development of a methodology for quantifying total non-methane organic carbon (TNMOC) from the O_2^+ SRI-MS signal. This technique was applied to the measurements of urban air undertaken in

Sydney, Australia in summer 2011 and the results are compared with the sum of the speciated VOCs measured using standard measurement techniques.

Definitions of total non-methane organic carbon

VOCs are organic compounds and are generally defined by a boiling point or volatility range and ability to participate in photochemical reactions. In general VOCs have boiling points which allow them to exist in the gas phase at ambient temperatures (50 – 250 °C). However there are a number of definitions of VOCs in use. Methane is generally not included in VOCs, as it does not significantly contribute to photochemistry due to its low reactivity (Seinfeld & Pandis 2006). A simple definition of “total” VOCs is the sum of the concentration of these individual compounds in the sample mixture. In studies of ambient air, there is no consistent term used to describe “total” VOCs. In practice, the sampling and analysis techniques employed to measure the sum of the VOCs operationally defines “total” VOC.

Heald et al (2008) in a synthesis of measurements of VOCs in the atmosphere measured individually across a large number of measurement platforms referred to total observed organic carbon (TOOC) ($\mu\text{gC m}^{-3}$).

In the companion papers by Maris and Chung et al (Chung et al. 2003, Maris et al. 2003) GC measurements of total VOCs without compound identification were referred to as the “sum of speciated VOCs” and direct measurements via FID were referred to as total non-methane organic carbon TNMOC, expressed in units of ppbC. This definition was also used for FID measurements by Roberts et al (1998).

The VOCs (excluding methane) that currently make the dominant contribution on a mass or mole fraction basis to the total measured in air include:

1. C₂ – C₁₂ alkanes and cycloalkanes
2. C₂ – C₇ alkenes
3. C₄ – C₆ dienes including isoprene
4. C₂ – C₃ alkynes
5. C₆ – C₁₀ aromatics
6. C₁₀ monoterpenes
7. C₁ – C₇ carbonyls
8. C₁ – C₆ alcohols
9. Other oxygenates (ethers, carboxylic acids, esters, multifunctionals)
10. Halogenated derivatives of 1 – 10

Thus, while the terms and definitions used to describe “total” VOCs are not consistent, they generally refer to the sum of 1 to 10 above. The “total” VOCs measured by each method employed in this study can be defined as:

O₂⁺ SRI-MS - the sum of VOCs that have ionization energies greater than the ionization energy of O₂. Generally, this will include the sum of the compounds in 1 – 10 above.

H₃O⁺ SRI-MS - the sum of VOCs that have proton affinities greater than the proton affinity of water. Generally, this will include the sum of the compounds in 2 – 10 above (excluding ethene).

Sum of the Speciated VOCs - the sum of compounds that can be efficiently captured in VOC adsorbent tubes (AT-VOC) and quantified by GC-FID-MS plus the sum of carbonyl VOCs that can be efficiently captured on DNPH cartridges and quantified by HPLC. Thus [Sum Sp. VOCs] will include selected compounds from 1, 3, and 5 - 7 above.

In this study we will use the term total non-methane organic carbon [TNMOC] expressed in units of parts per billion of carbon (ppbC). ppbC is equivalent to the summation, for all speciated compounds present, of the product of the volume mixing ratio (ppbv) and the number of carbon atoms of each compound.

Three methods for measurement of TNMOC will be discussed: O_2^+ SRI-MS, H_3O^+ SRI-MS and the sum of the speciated VOCs measured by the combination of two independent VOC measurement techniques.

For the sum of the VOCs measured by the independent methods (AT- VOC and DNPH), we will use the same term, “Sum of the speciated VOCs”, or (Sum Sp. VOC) also expressed both in units of ppbC.

6.2 Methodology

The sampling site, SRI-MS set-up and supplementary measurements were described in detail in Chapter 5. Briefly, The SRI-MS sampled ambient air in an urban area of Sydney, Australia in summer from 18th February – 7th March 2011. The sampling site was located in an urban area, in the grounds of a hospital greater than 500m from major roads. The SRI-MS was deployed alongside a number of other instruments (Table 6.1) as a part of a more extensive study to provide a detailed characterization of the chemical and aerosol composition of the urban atmosphere in Sydney (Cope et al. 2014).

6.2.1 Speciated VOC measurements

Two independent VOC measurement techniques were deployed alongside the SRI-MS in the field study in Sydney 2011. These were described in detail in the previous chapters and in Cope et al. (2014). Briefly, the concentration of 27 VOCs, (Table 6.1) were determined from the air samples collected onto Marke’s Carbograph 1TD/Carbopack X adsorbent tubes (Markes International Inc, Delaware, USA) using constant-flow air sampling pumps. The tubes were analysed using an Automated Thermal Desorber and gas chromatograph (GC) equipped with a Flame Ionization Detector (FID) and a Mass Selective Detector (MSD). The adsorbent tube VOC samples will be referred to as AT-VOC samples in the following discussions.

The concentrations of 15 aldehydes and ketones (Table 6.1) were determined from air samples collected onto Supelco LpDNPH S10 air monitoring cartridges (Supelco Pennsylvania, USA) using constant flow air pumps. Carbonyls are trapped on the cartridge where they are converted to the hydrazine derivatives. The derivatives are eluted from the cartridge in acetonitrile and analysed by HPLC.

Table 6.1: Compounds measured in the AT-VOC samples and analysed by GC-FID-MS and in the DNPH samples analysed by HPLC the sum of which is referred to as [Sum Sp. VOC] in this study.

AT-VOC		
n-butane	isoprene	Benzene
2-methyl butane	α -pinene	Toluene
n-pentane	β -pinene	m-xylene
2-methyl pentane	p-cymene	p-xylene
3-methyl pentane	D-limonene	o-xylene
n-hexane	Eucalyptol	ethylbenzene
3- methyl hexane	Camphor	o-ethyltoluene
n-heptane		m-ethyltoluene
methyl cyclopentane		1,2,4-trimethylbenzene
cyclohexane		1,3,5-trimethylbenzene
DNPH		
Formaldehyde	Acrolein	
Acetaldehyde	Methacrolein	
Propanal	Benzaldehyde	
Butenal	m-Tolualdehyde	
Butanal	Glyoxal	
Pentanal	Methyl glyoxal	
Hexanal	Acetone	
	Methyl ethyl ketone	

6.2.2 SRI-MS set-up

The instrument employed in this work was a commercially built PTR-MS (Ionicon Analytik GmbH, Innsbruck Austria) and subsequently factory modified with the addition of a switchable reagent ion source system to enable the use of NO^+ and O_2^+ reagent ions in addition to H_3O^+ . The SRI-MS instrument employed in this study is described in detail in Chapters 3 and 5.

Briefly, in the hollow cathode ion source, UHP O_2 (BOC, Australia) was ionized by electron impact to produce the desired O_2^+ reagent ions with high intensity (10^7 cps) and high purity ($\sim 95\%$).

The SRI-MS drift tube was operated at 60°C and an applied voltage of 445 V and drift tube pressure of 2.23 mbar which equates to E/N of ~ 100 Td. The SRI-MS quadrupole

continuously scanned 181 masses between 14 and 200 amu. The dwell time for a single mass measurement was 1 second, generating a full mass scan approximately every 3 minutes.

The SRI-MS operated with the aid of custom built auxiliary equipment that regulated the flow of air in the sample inlet and controlled whether the PTR-MS was sampling ambient or zero air or calibration gas. Zero readings were made by diverting the air through a zero furnace (350°C) with a Platinum wool catalyst that destroyed VOCs in the air before it entered the PTR-MS. Zero measurements were conducted in, O_2^+ mode twice per day. Background corrections were performed for all measurements described in this study. All ion signals from calibration and ambient air measurements referred to in this paper are background corrected. Note, the zero corrected data can have small negative values because they are calculated from the difference between the ion signals during a zero measurement and an ambient measurement and at lower concentrations, with some measurement noise, negative values result from the difference.

During the field study in Sydney 2011, the SRI-MS was calibrated with certified gas standards in O_2^+ mode once per day for a duration of 30 minutes. The SRI-MS response, to the VOCs contained in each of the gas standards employed in this work were discussed in detail in Chapter 3. The components, of each gas standard are listed in Chapter 3, Tables 3.5 – 3.6.

6.3 O_2^+ SRI-MS Sensitivity

The sensitivity, S , of the SRI-MS to compounds that underwent non-dissociative ionization reactions and whose product ion signals could be qualitatively identified, was determined empirically from the calibration measurements via:

$$S_A \text{ (ncps ppbv}^{-1}\text{)} = I_{A^+}(\text{ncps})/[A](\text{ppbv}) \quad \text{Equation 6.1}$$

Equation 6.1. In the following I_{A+} refers to the background corrected ion signal of the analyte, A, normalized to a primary reagent ion signal of 10^6 counts per second (cps). The sensitivity was expressed as normalized counts per second at a volume-mixing ratio of 1 ppbv (ncps ppbv⁻¹). For compounds whose ion signals could be reliably identified and underwent dissociative ionization for which the branching ratio (BR) was known, the sensitivity was determined from the fragment ion signal, I_{F+} , via Equation 6.2:

$$S_A \text{ (ncps ppbv}^{-1}\text{)} = I_{F+} \text{ (ncps)} / (\text{BR}_{F+} \times [A] \text{ (ppbv)}) \quad \text{Equation 6.2}$$

The sensitivity, determined for each compound in each reagent ion mode, was plotted versus the product ion m/z in Figure 6.1. A line of fit based on a linear regression was applied to the sensitivity data for compounds between 43 – 200 amu that underwent chemical ionization reactions at a rate close to the collisional limit.

The sensitivity of a SRI-MS instrument to a particular compound is dependent on the chemical ionization reaction rate and the mass dependent transmission of ions through the quadrupole mass spectrometer (Chapter 3). Heavier ions spend more time in fringing fields and are thus less efficiently transmitted through the quadrupole (Dawson 1976). Tuning the mass spectrometer can alter the mass at which the mass dependent transmission is at its maxima. The quadrupole of the PTR-MS instrument used in this study had a maximum mass dependent transmission efficiency at ~ 45 amu.

The sensitivity of the SRI-MS for lighter ions ($m/z < 43$) could not be empirically determined in this study due to a lack of measurable compounds in the calibration standards that occur in that m/z range. The SRI-MS sensitivity decreases rapidly for m/z below that of the maxima, in this case m/z 43, due to the scattering losses of lighter ions caused by collisions with buffer gas molecules at the entrance to the quadrupole.

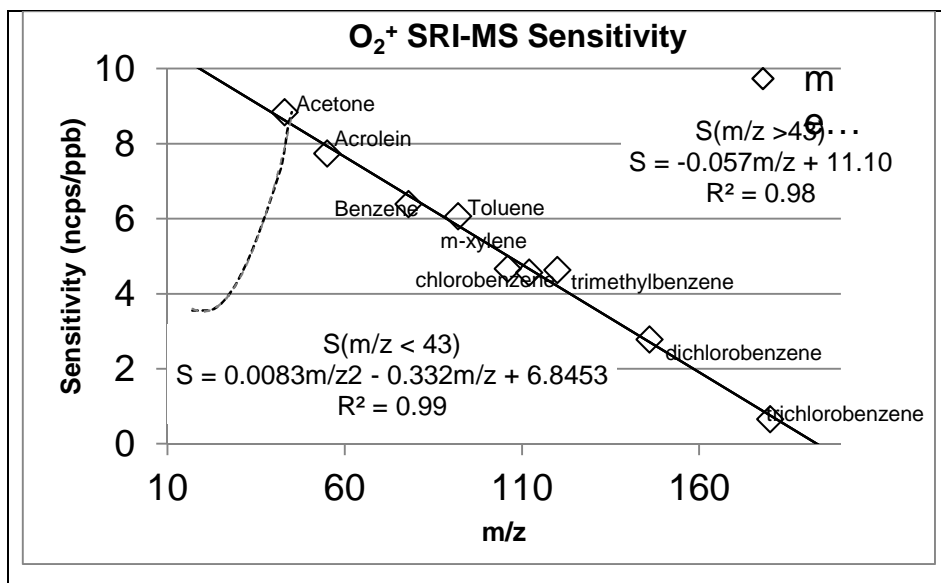


Figure 6.1: The measured sensitivity of the O_2^+ SRI-MS to 9 compounds with product ions that are detected across the m/z range scanned. (Solid Line) An interpolated sensitivity curve determined from the measured sensitivity factors for $m/z > 43$. (Dashed line) An interpolated sensitivity curve for $m/z < 43$ determined from the measured sensitivity at m/z 43 and the SRI-MS software output for the mass dependent transmission of ions with m/z 15 - 43.

In the absence of sufficient empirical calibration data for $m/z < 45$ from this study, we used the mass dependent transmission curve from the PTR-MS Control Software (Ionicon Analytik GmbH) fitted to the maximum response found. Thus, the sensitivity to a compound (X) whose product ion (X^+) occurs at $m/z = x$ where x is < 45 is calculated via:

$$S_{m/z \ x} = T_{m/z \ x} \times S_{\max} \quad \text{Equation 6.3}$$

where $T_{m/z \ x}$ is the mass dependent transmission at $m/z = x$ determined by the transmission algorithm embedded in the PTR-MS control software, and S_{\max} is the measured sensitivity at the transmission maxima, in this case m/z 45.

The fits in Figure 6.1 were used in subsequent calculations to determine to the volume-mixing ratio at m/z where no reliable calibration was available. Using the interpolated or measured sensitivities, the concentration of VOCs detected at $m/z = x$ can be calculated via:

$$[\text{VOC}]_{m/z \ x} (\text{ppbv}) = \frac{I_{m/z \ x} (\text{ncps})}{S_{m/z \ x} (\text{ncps ppbv}^{-1})} \quad \text{Equation 6.4}$$

where, $[VOC]_{m/z\ x}$ is the volume mixing ratio of the VOC product at $m/z = x$; $I_{m/z\ x}$ is the ion signal at $m/z = x$ in ncps and $S_{m/z\ x}$ is the sensitivity of the SRI-MS to VOCs at $m/z = x$ in units of ncps ppbv⁻¹ determined from the sensitivity curves in Figure 6.1.

6.4 Quantification of total non-methane organic carbon [TNMOC] from the O_2^+ SRI-MS signal

The concentration of TVOC in units of ppbv can be determined from the sum of the [VOC] concentrations measured at each of the m/z in the mass range scanned (e.g. $m/z\ a$ to x)

$$[TVOC](ppbv) = \Sigma \{ [VOC]_{m/z\ a} + [VOC]_{m/z\ b} + \dots [VOC]_{m/z\ x} \}$$

$$[TVOC](ppbv) = \Sigma \left\{ \left(\frac{I_{m/z\ a}}{S_{m/z\ a}} \right) + \left(\frac{I_{m/z\ b}}{S_{m/z\ b}} \right) + \dots \left(\frac{I_{m/z\ x}}{S_{m/z\ x}} \right) \right\} \quad \text{Equation 6.5}$$

If the number of carbon atoms in the product ion/s detected at each m/z are known, the concentration of organic carbon [OC], in parts per billion of carbon (ppbC), at each m/z can be calculated:

$$[OC]_{m/z\ x}(ppbC) = [VOC]_{m/z\ x} \times CN_x$$

$$[OC]_{m/z\ x}(ppbC) = \left(\frac{I_{m/z\ x}}{S_{m/z\ x}} \right) \times CN_x \quad \text{Equation 6.6}$$

where, $[OC]_{m/z\ x}$, is the VMR of organic carbon at $m/z = x$, CN_x is the carbon number of the organic carbon product ion/s at $m/z = x$.

The total non-methane organic carbon (TNMOC) present in the sample can be determined from the sum of the organic carbon measured at each m/z (e.g. $m/z\ a - x$).

$$[TNMOC](ppbC) = \Sigma\{[OC]_{m/z\ a} + [OC]_{m/z\ b} + \dots [OC]_{m/z\ x}\}$$

$$[TNMOC](ppbC)$$

$$= \Sigma\{([VOC]_{m/z\ a} \times CN_a) + ([VOC]_{m/z\ b} \times CN_b) + \dots ([VOC]_{m/z\ x} \times CN_x)\}$$

$$[TNMOC](ppbC) = \Sigma\left\{\left(\frac{I_{m/z\ a}}{S_{m/z\ a}} \times CN_a\right) + \left(\frac{I_{m/z\ b}}{S_{m/z\ b}} \times CN_b\right) + \dots \left(\frac{I_{m/z\ x}}{S_{m/z\ x}} \times CN_x\right)\right\}$$

Equation 6.7

In an air sample the carbon number of product ions occurring at each m/z would be unknown. Carbon number is constrained by m/z such that the integer of $(m/z)/12$, 12 being the molecular weight of carbon, is the upper limit of carbon number for a given m/z , but allowance must be made for organic molecules that also contain oxygen and nitrogen etc.

In order to determine likely carbon numbers for each m/z in the mass spectra of a sample containing a range of atmospherically relevant VOCs, the mass spectra of 73 atmospherically important VOCs contained in 4 certified gas standard mixtures were measured. Probable product ion identities were assigned to each of the m/z , and the carbon number of the product ions was derived for each m/z . For m/z where more than one product ion could be assigned, an average carbon number was determined.

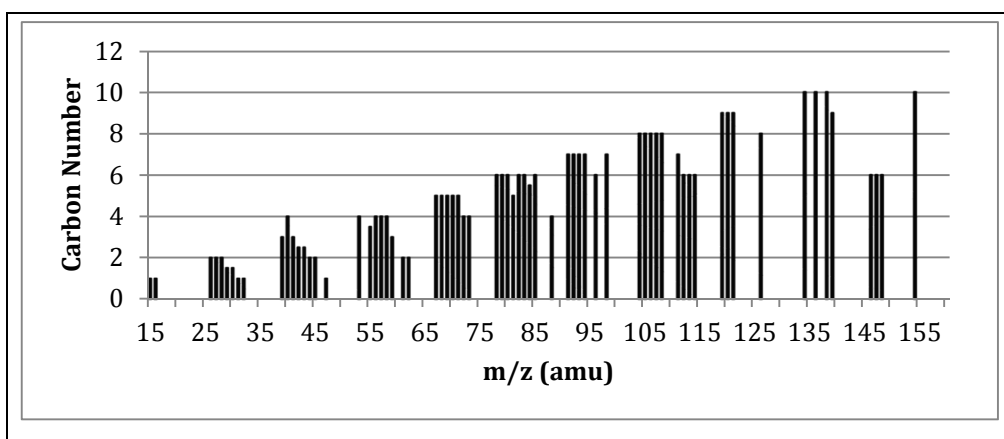


Figure 6.2: Carbon numbers assigned to each m/z in the O_2^+ mass spectra ($m/z\ 15 - 160\ amu$) for the calculation of $[TNMOC]$ (ppbC) in this study.

6.6 Tests against certified gas standards

In order to evaluate the performance of O_2^+ SRI-MS for quantifying TNMOC, four certified gas standards containing 73 different VOCs were measured when the SRI-MS was operating with O_2^+ as the primary reagent ion. The four certified gas standards, numbered 1-3, and 5 coincide with those employed in the studies described in Chapters 3 and 5. The concentration of TNMOC in each standard was determined from the O_2^+ SRI-MS measurements using Equation 6.6. For this analysis, only the sensitivity factors interpolated from the fits in Figure 6.1 were used to calculate the VMR of VOCs detected at each m/z by the O_2^+ SRI-MS.

The TNMOC measured by the O_2^+ SRI-MS was compared with the calculated concentration of TNMOC. The ratio of the measured versus calculated TNMOC values are presented in Table 6.2 as % TNMOC recovery. For the purposes of comparison the TNMOC concentrations were also quantified from the H_3O^+ SRI-MS measurements of the same certified gas standards using an analogous methodology to that outlined above.

Calibration gas 1 contained 15 VOCs including oxygenated VOCs, acetonitrile, aromatics, chlorobenzenes and a monoterpene. The O_2^+ SRI-MS and H_3O^+ SRI-MS measurements of TVOC in calibration gas 1 was $\sim 100\%$ of the known TNMOC concentration in the standards. This was unsurprising given almost all components in calibration gas 1 had $PAs > PA(H_2O)$ and $IEs < IE(O_2)$ and therefore underwent fast exothermic chemical ionization reactions with both O_2^+ and H_3O^+ reagent ions and were detected by both techniques. The exception was acetonitrile which has an $IE \sim IE(O_2)$ and was not detected by O_2^+ SRI-MS.

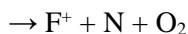
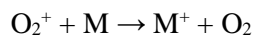
Table 6.2: % Recovery of TNMOC from four certified gas standards containing 73 different VOC compounds by H_3O^+ and O_2^+ SRI-MS

Cal. Gas	Contents	SRI-MS	
		H_3O^+ % Recovery	O_2^+ % Recovery
1	OVOCs (6) C ₆ – C ₉ Aromatics (7) α -Pinene Acetonitrile	100%	98%
2	HCHO Acetone	99%	88%
3	Isoprene DMS Ethyl acetate 1,8-cineole	61%	61%
5	Acetylene Isoprene C ₂ - C ₁₂ Alkanes (27) C ₂ - C ₆ Alkenes (8) C ₆ - C ₁₀ Aromatics (18)	45%	83%

Calibration gas 2 contained acetone and formaldehyde. The H_3O^+ SRI-MS reported recovery for [TNMOC] in calibration gas 2 was 99%. Previous studies have reported charge transfer from O_2^+ to formaldehyde results in the product ions HCHO^+ (m/z 30) and CHO^+ (m/z 29) (Spanel et al. 1997). As discussed, m/z 30 was not measured in this study to preserve the lifetime of the SEM. Consequently the formaldehyde product ion at m/z 30 was not measured. No significant ion signal was observed at m/z 29 in the measurements of calibration gas 2 in this study and it was concluded that formaldehyde was not detected by O_2^+ SRI-MS. Due to the non-detection of formaldehyde, the O_2^+ SRI-MS recovery of [TNMOC] in calibration gas 2 was 88%.

Calibration gas 5 was a certified PAMS standard containing 55 C₂ – C₁₂ hydrocarbons including alkanes, alkenes, alkynes, cyclic- and aromatic VOCs. The O_2^+ chemical ionization technique measured 83% of the TNMOC in calibration gas 5 as all components undergo fast exothermic charge transfer reactions with O_2^+ . In contrast, proton transfer from H_3O^+ to alkanes, which composed 53% of the TNMOC in the standard, is endothermic. Consequently these alkanes were not detected resulting in the poor recoveries of 45% of TNMOC observed. The ability to detect alkanes is the major advantage of employing O_2^+ chemical ionization when using SRI-MS as a total carbon analyzer as alkanes are a significant component of TVOC in the atmosphere (Heald et al 2008).

For both O_2^+ and H_3O^+ SRI-MS measurements of [TNMOC] the % recovery of TNMOC can be < 100% due to fragmentation processes. For instance, charge transfer from O_2^+ to VOCs can be dissociative (Reaction 6.1b) yielding a charged fragment ion (F^+) and a neutral fragment (N) or non-dissociative (Reaction 6.1a) yielding the charged parent ion (M^+):



Reaction 6.1

The TNMOC concentration determined from Equation 6.7 may underestimate the actual TNMOC concentration present as only the organic carbon present in the charged product ions is detected. Carbon present in the neutral fragments is not detected by the mass spectrometer and as such is not quantified via equation 6.7. The compounds in calibration gas 3, are known to undergo extensive fragmentation in SRI-MS (Chapter 3. Sections 3.4 and 3.5) and the TNMOC recovery in both O_2^+ and H_3O^+ reagent ion modes was 61%. Likewise the aliphatic hydrocarbons in calibration gas 5, also undergo extensive fragmentation in reactions with O_2^+ and as a result the TNMOC recovery for this standard was 83%.

The recoveries < 100% observed for both H_3O^+ SRI-MS and O_2^+ SRI-MS for calibration gas 2, 3, and 5 was in some part a result of the non-detection of neutral carbon reaction products. As observed in Chapter 3 extensive fragmentation frequently occurs in ionization reactions between O_2^+ (and H_3O^+) with VOCs, and the neutral fragments of the reactions frequently contain carbon atoms. Consequently, in measurements of TNMOC using equation 6.7, the quantity of neutral carbon not quantified is likely to be non-negligible.

In addition, there are also a number of compounds not detected by O_2^+ and H_3O^+ SRI-MS due to poor instrument response or due to mass interference from reagent ions. Consequently the carbon in these compounds, referred to here as $[\text{OC}]_{\text{nd}}$, is not quantified in the calculation of TNMOC via equation 6.7.

Thus, the TNMOC present in a sample is a product of the ionic and neutral organic carbon products of the charge transfer reactions and the carbon present in non detectable species:

$$[\text{TNMOC}] = [\text{OC}]_{\text{ion}} + [\text{OC}]_{\text{neut}} + [\text{OC}]_{\text{nd}} \quad \text{Equation 6.8}$$

Therefore, as the SRI-MS only detects the ionic component the concentration of organic carbon measured by the SRI-MS, $[\text{OC}]_{\text{meas}}$ will be equivalent to:

$$[\text{OC}]_{\text{meas}} = [\text{OC}]_{\text{ion}} = [\text{TNMOC}] - ([\text{OC}]_{\text{neut}} + [\text{OC}]_{\text{nd}}) \quad \text{Equation 6.9}$$

The amount of organic carbon not detected, $[\text{OC}]_{\text{nd}}$, due to these factors was determined from the ionization energy of each component in the calibration standards and the reaction pathways and branching ratios from published mass spectral data. The fraction of total organic carbon not detectable in each standard is also presented in Table 6.3 as $\Sigma[\text{OC}]_{\text{nd}}$.

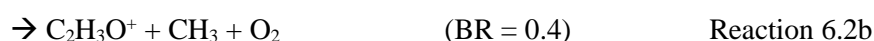
In order to correctly quantify TNMOC measured by O_2^+ SRI-MS, the carbon in both the ionic and neutral reaction products must be quantified. If the composition, reaction pathways and branching ratios (BR) for each component present in the sample are known, the ratio of total carbon to the carbon in the ion and neutral products can be calculated for each component via:

$$[\text{I}_{\text{a}+}]/[\text{A}] = \text{BR}(\text{I}_{\text{a}+}) * \text{CN}(\text{I}_{\text{a}+}) / \text{CN}(\text{A}) \quad \text{Equation 6.10}$$

$$[\text{N}_{\text{a}}] / [\text{A}] = \text{BR}(\text{I}_{\text{a}+}) * \text{CN}(\text{N}_{\text{a}}) / \text{CN}(\text{A}) \quad \text{Equation 6.11}$$

where , $[\text{I}_{\text{a}+}]/[\text{A}]$ is the ratio of ionic carbon to the total carbon of the analyte, A, in ppbC/ppbC; $\text{BR}(\text{I}_{\text{a}+})$ is the branching ratio for the reaction pathway producing an ion at $m/z = a$, $\text{I}_{\text{a}+}$, and a neutral N_{a} ; $\text{CN}(\text{I}_{\text{a}+})$, $\text{CN}(\text{A})$ and $\text{CN}(\text{N}_{\text{a}})$ are the carbon numbers of the product ion, the analyte and the neutral respectively.

For example, charge transfer from O_2^+ to acetone can proceed as follows:



Thus, the branching ratios for the charged products is calculated via:

$$\begin{aligned}
 [\text{C}_3\text{H}_6\text{O}^+] / [\text{C}_3\text{H}_6\text{O}] \text{ (ppbC)/(ppbC)} &= \text{BR}(\text{C}_3\text{H}_6\text{O}^+) * \text{CN}(\text{C}_3\text{H}_6\text{O}^+) / \text{CN}(\text{C}_3\text{H}_6\text{O}) \\
 &= 0.6 * 3/3 \\
 &= 0.6
 \end{aligned}
 \tag{Equation 6.12}$$

$$\begin{aligned}
 [\text{C}_2\text{H}_3\text{O}^+] / [\text{C}_3\text{H}_6\text{O}] \text{ (ppbC)/(ppbC)} &= \text{BR}(\text{C}_2\text{H}_3\text{O}^+) * \text{CN}(\text{C}_2\text{H}_3\text{O}^+) / \text{CN}(\text{C}_3\text{H}_6\text{O}) \\
 &= 0.4 * 2/3 \\
 &= 0.27
 \end{aligned}
 \tag{Equation 6.13}$$

And the branching ration for the neutral products is calculated via:

$$\begin{aligned}
 [\text{CH}_3] / [\text{C}_3\text{H}_6\text{O}] \text{ (ppbC)/(ppbC)} &= \text{BR}(\text{C}_2\text{H}_3\text{O}^+) * \text{CN}(\text{CH}_3) / \text{CN}(\text{C}_3\text{H}_6\text{O}) \\
 &= 0.4 * 1/3 \\
 &= 0.13
 \end{aligned}
 \tag{Equation 6.14}$$

If the composition of the sample is known, and the reaction rates and branching ratios of each components can be determined experimentally or from the literature, one can estimate the fraction of total organic carbon in the sample that will occur in the ionic and neutral reaction products. This methodology was applied to the measurements of the 4 certified gas standards analysed in this study.

For each compound in the gas standard the fraction of organic carbon that would occur as ionic products ($[\text{OC}]_{\text{ion}}$) was calculated from the sum of the products of Equations 6.12 and 6.13. The sum of the $[\text{OC}]_{\text{ion}}$ values for all compounds in the gas standard was determined ($\Sigma[\text{OC}]_{\text{ion}}$). The ratios of $\Sigma[\text{OC}]_{\text{ion}}/[\text{TNMOC}]_{\text{total}}$, were calculated for each gas standard, and are presented in Table 6.3 as a percentage.

Likewise, for each compound in the gas standard the fraction of organic carbon that would occur as neutral products ($[\text{OC}]_{\text{neutral}}$) was calculated from Equation 6.14. The sum of the $[\text{OC}]_{\text{neutral}}$ values for all compounds in the gas standard was determined ($\Sigma[\text{OC}]_{\text{neutral}}$). The ratios of $\Sigma[\text{OC}]_{\text{neutral}}/[\text{TNMOC}]$, were also calculated for each gas standard, and are presented in Table 6.3 as a percentage.

The fraction of organic carbon detected as product ions $[OC]_{meas}$ by the SRI-MS are shown in Table 6.3. As described by Equation 6.9, the SRI-MS only measures the ionic component in the gas standard, and if the branching ratios and SRI-MS response is properly characterized the ratio of $[OC]_{meas} / \Sigma[OC]_{ion}$ should be ~ 1 .

Given the uncertainty associated with using branching ratios determined in different instruments, and operating conditions, the ratio between the measured $[OC]_{ion}$ and the calculated values of $[OC]_{ion}$ were close to unity, with 0.75 – 1.44 for the O_2^+ SRI-MS and 0.76 – 1.03 for the H_3O^+ SRI-MS.

Table 6.3: The fraction of organic carbon detected as product ions $[OC]_{meas}$ by the SRI-MS. The fraction of TNMOC predicted to occur as ionic ($[OC]_{ion}$), neutral ($[OC]_{neutral}$) and non-detected $[OC]_{nd}$ organic carbon for each gas standard based on known branching ratios of each component. If the branching ratios and SRI-MS response is properly characterized the ratio $[OC]_{meas} / [OC]_{ion}$ should be ~ 1 .

Cal. Gas	H_3O^+ SRI-MS				O_2^+ SRI-MS			
	Measured	Calculated			Measured	Calculated		
	$[OC]_{meas}$	$\Sigma[OC]_{ion}$	$\Sigma[OC]_{neutral}$	$\Sigma[OC]_{nd}$	$[OC]_{meas}$	$\Sigma[OC]_{ion}$	$\Sigma[OC]_{neutral}$	$\Sigma[OC]_{nd}$
	% of $[OC]_{total}$				% of $[OC]_{total}$			
1	100%	97%	3%		98%	92%	8%	
2	99%	100%			88%	61%	27%	12%
3	61%	88%	12%		61%	81%	19%	
5	45%	59%	1%	40%	83%	73%	27%	

In practice, the composition of the air is usually unknown and the reaction pathways that yield the ionic and neutral carbon cannot be derived from the mass spectra. Empirically, the tests on gas standards reported here indicate the O_2^+ SRI-MS reported values of [TNMOC] may be an underestimate due to $\sim 20\%$ of the organic carbon present occurring as neutral and/or undetected products of the ionization process.

Overall, the tests on gas standards described here suggest that in measurements of the atmosphere O_2^+ SRI-MS will frequently detect a larger fraction of TNMOC present than H_3O^+ SRI-MS due to the added ability of O_2^+ SRI-MS to detect short chain alkanes.

6.7 TNMOC measurements in urban air

In measurements in an urban area of Sydney in 2011, the SRI-MS was operated with O_2^+ as the primary reagent ion for two hours per day. The O_2^+ SRI-MS [TNMOC] data presented here are 1 hour averages measured at 3:00 – 4:00 and 17:00 – 18:00 daily. Overall, 27 one-hour averages were determined from the O_2^+ data. For comparison, [TNMOC] was also calculated from the H_3O^+ SRI-MS data for the one hour periods directly proceeding the O_2^+ SRI-MS measurements (4:00 – 5:00, and 18:00 – 19:00).

The performance of the O_2^+ SRI-MS as a total VOC analyzer was also evaluated with reference to the sum of the speciated VOCs, [Sum Sp. VOC] which was the sum of the VMRs of VOCs (ppbC) measured on the adsorbent tubes analysed with GC-FID-MS plus the carbonyl VOCs measured on the DNPH cartridges analysed by HPLC.

Laboratory studies of the O_2^+ SRI-MS response to 73 compounds contained in 5 certified gas standards (Chapter 3) demonstrated SRI-MS cannot detect formaldehyde and methanol when operating with O_2^+ as the primary reagent ion. For the following analysis we have excluded formaldehyde and methanol from the H_3O^+ SRI-MS measurements of TNMOC by subtracting the signal at m/z 31 and m/z 33 which correspond to protonated formaldehyde and methanol. Formaldehyde detected by the DNPH technique was not included in the calculation of the [Sum Sp. VOC] and methanol was not measured by either the AT-VOC or DNPH techniques so is not also included in [Sum Sp. VOC].

The RMA regression between the O_2^+ and H_3O^+ SRI-MS data for [TNMOC] (ppbC) yielded a slope of 1.45 ± 0.10 , and a significant and highly variable offset of 17.91 ± 23.05 , $R^2 = 0.86$ (Figure 6.3a). A substantial fraction of the additional VOC observed by the O_2^+ SRI-MS is likely to be a result of the presence of alkanes $< \text{C}_8$ which are detected with good sensitivity by the O_2^+ SRI-MS but not by the H_3O^+ SRI-MS (Chapter 3).

When the organic carbon (ppbC) in sum of the alkanes measured in the AT-VOC samples was added to the H_3O^+ SRI-MS [TNMOC] values, the agreement with the O_2^+ SRI-MS [TNMOC] values was improved with the RMA regression yielding a slope of 1.13 ± 0.07 , intercept = 11.24 ± 12.87 , $R^2 = 0.91$ (Figure 6.3b).

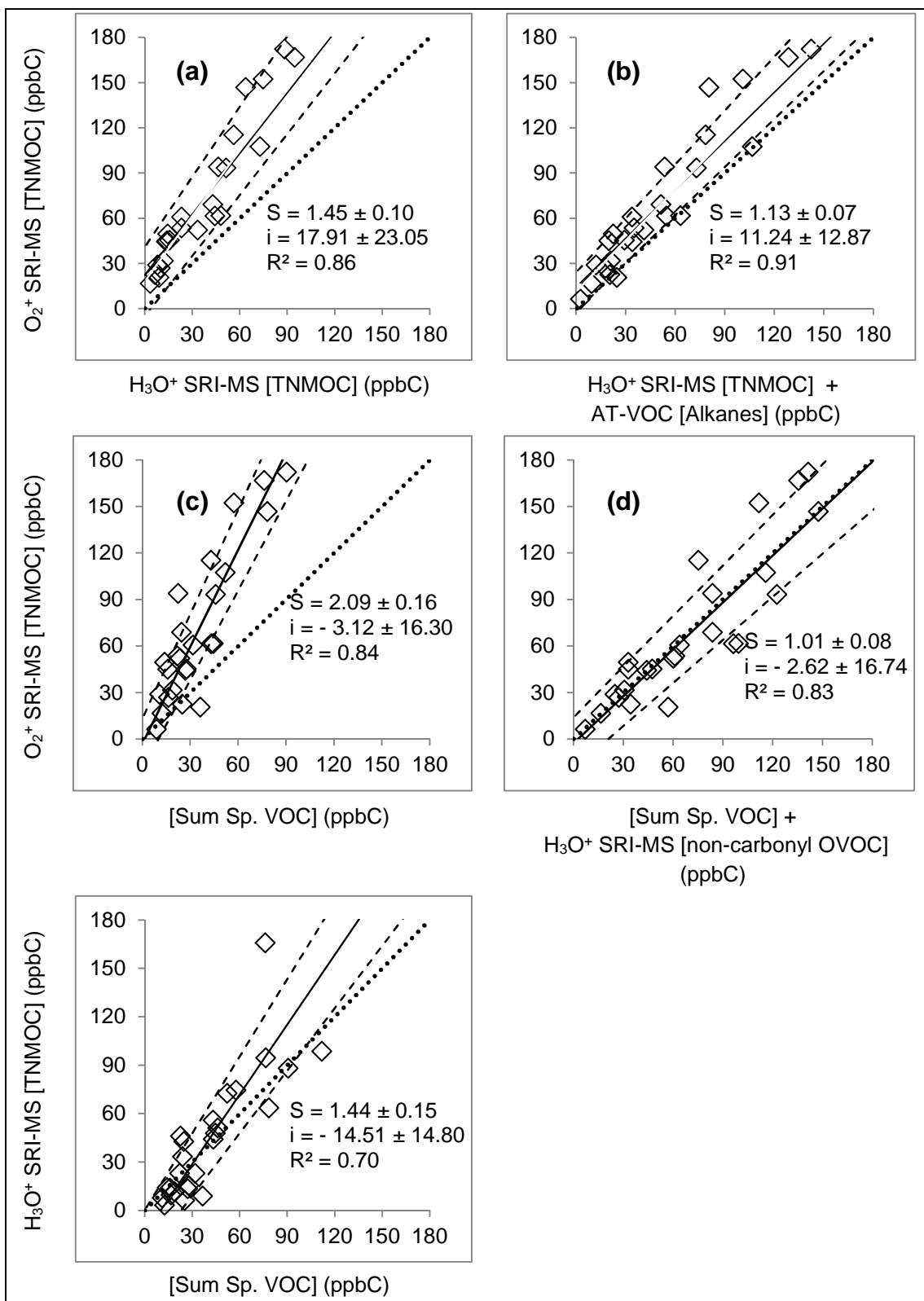


Figure 6.2: Scatterplots with the Slope (S) and intercept (i) form the reduced major axis regression analysis between: (a) O_2^+ SRI-MS and H_3O^+ SRI-MS [TNMOC], (b) O_2^+ SRI-MS [TNMOC] and the sum of H_3O^+ SRI-MS [TNMOC] plus [alkanes] measured in the AT-VOC samples, (c) O_2^+ SRI-MS [TNMOC] and [Sum Sp. VOC], and (d) O_2^+ SRI-MS [TNMOC] and [Sum Sp. VOC] plus the [non-carbonyl OVOCs] measured by the H_3O^+ SRI-MS. Dotted line is 1:1.

It was concluded that, in measurements of the atmosphere with SRI-MS in this study, the difference between the O_2^+ and H_3O^+ SRI-MS measurements of [TNMOC] was largely due to the presence of short chain alkanes, which are only detected when the SRI-MS is operating with O_2^+ as the primary reagent ion. This fulfills theoretical expectations based on the ionization energies and proton affinities of short chain alkanes, and confirms our conclusions based on the laboratory tests of [TNMOC] recovery from a certified gas standard containing a range of short chain alkanes (Calibration gas 5, Section 6.6).

The O_2^+ SRI-MS [TNMOC] values were well correlated with the [Sum Sp. VOC] values ($R^2 = 0.84$) however the quantitative agreement was poor with a slope of 2.09 ± 0.16 , intercept = -3.12 ± 16.30 ppbC (Figure 6.3c).

The [Sum Sp. VOC] included the concentration of 14 aldehydes, ketones and dicarbonyls determined from the DNPH samples, and 1,8 cineole measured in the AT-VOC samples. The O_2^+ SRI-MS is capable of detecting all of these compounds along with a large number of other oxygenated VOCs (OVOCs) not detected by the DNPH technique including alcohols ($> \text{C}_2$), carboxylic acids, esters, oxygenated terpenoids, oxygenated aromatics, and other multifunctional compounds, as almost all of these compounds have ionization energies less than IE (O_2) (Lias 2015). Therefore, it is possible the additional organic carbon measured by the O_2^+ SRI-MS [TNMOC] was due to the presence of these non-carbonyl VOCs not measured by the AT-VOC or DNPH techniques.

H_3O^+ SRI-MS can detect carbonyls and non-carbonyl OVOCs as well as aromatics, isoprene, and monoterpenes. Concentrations of [non-carbonyl OVOC] were determined by subtracting from the H_3O^+ SRI-MS [TNMOC] the concentrations, of the known aromatic ion signals (benzene m/z 79, toluene m/z 93, C_8 aromatics m/z 107, C_9 aromatics m/z 121), the known isoprene (m/z 69) and monoterpene ion signals (m/z 81, 137) and the known carbonyl ion signals (acetaldehyde m/z 45, acetone m/z 59, MACR+ MVK m/z 71, MEK + Methyl glyoxal (m/z 73)

When the [non-carbonyl OVOC] measured by the H_3O^+ SRI-MS was added to the [Sum Sp. VOC] close agreement with O_2^+ SRI-MS [TNMOC] was observed with slope of 1.01 ± 0.08 , an intercept of -2.62 ± 16.74 and $R^2 = 0.83$ (Figure 6.3d). It was concluded that the presence of non-carbonyl OVOCs largely explains difference between the O_2^+ SRI-MS [TNMOC] and the [Sum Sp. VOC] as non-carbonyl OVOCs were not measured by the AT-VOC and DNPH techniques.

The H_3O^+ SRI-MS [TNMOC] values were less well correlated with the [Sum Sp. VOC] values ($R^2 = 0.70$) with a slope of 1.44 ± 0.15 , and a significant negative intercept of -14.51 ± 14.80 ppbC (Figure 6.3e). The large negative intercept is probably a product of the presence of short chain alkanes measured in the AT-VOC samples and quantified in [Sum Sp. VOC] but not measured by the H_3O^+ SRI-MS.

In conclusion, consistent with theoretical expectations and tests on certified gas standards, O_2^+ SRI-MS was capable of measuring a larger fraction of total VOCs present in an urban atmosphere, including short chain alkanes not detected with H_3O^+ SRI-MS and non-carbonyl OVOCs not detected by the AT-VOC and DNPH techniques employed in this study

6.8 Correlations of TNMOC with other atmospheric constituents

The formation of secondary organic aerosol in the troposphere results from the reactive chemistry of volatile organic compounds. As VOCs in the atmosphere become more oxidized, the compounds become less volatile and either nucleate to form new particles or condense out upon existing particles (Seinfeld & Pandis 2006).

This study has demonstrated that measurements of [TNMOC] with O_2^+ SRI-MS report significantly higher concentrations than conventional H_3O^+ SRI-MS and the sum of VOCs measured by AT-VOC and DNPH (Sum Sp. VOC).

Table 6.4 presents the correlations of the relationships between [TNMOC] determined by the three methods with NO_x , ($N = 27$). In addition the correlation between [TNMOC] determined by the three methods was correlated with the mass of particulate matter with diameter $\leq 2.5 \mu\text{m}$ (PM 2.5) ($N = 27$). The PM 2.5 sampling and analysis is described in detail in Cope et al. (2014).

The PM 2.5 samples were analysed to determine the fraction of total carbon present as elemental versus organic carbon. Elemental carbon (black carbon) is non-reactive and is directly emitted from fossil fuel combustion and biomass burning.

The organic carbon mass in PM 2.5 is a combination of primary organics (20 – 26%) emitted directly into the atmosphere in the solid phase primarily from combustion processes; and secondary organic aerosol (74 – 80%) formed from gas phase oxidation of VOCs to lower

vapour pressure organic species (Cope et al. 2014) which either form new particles or condense out upon existing particles.

An aerosol mass spectrometer, AMS, was employed during the field study in Sydney to determine the real-time (10 s – 10 min) size-resolved chemical composition and mass concentration of submicron aerosol particles between 60 and 600 nm (approximately PM₁). The AMS measurements are described in detail in Cope et al. (2014). The SRI-MS and AMS made simultaneous measurements with the O₂⁺ SRI-MS from 19th Feb – 24th Feb 2011, and 11 paired one-hour averages were obtained from the two datasets. The organic aerosol measured by the AMS (AMS-OA) was compared with the VMRs of [TNMOC] determined by the three VOC measurement techniques (O₂⁺ and H₃O⁺ SRI-MS and the Sum of the speciated VOCs).

Primary hydrocarbons such as alkanes and aromatics are directly emitted into the atmosphere from fossil fuel combustion alongside NO_x and elemental carbon in PM 2.5. These compounds act as precursors (or as a tracer of precursors in the case of elemental carbon) for atmospheric oxidation processes.

O₂⁺ SRI-MS is capable of measuring the primary hydrocarbons (alkanes, aromatics) that are emitted alongside NO_x, and elemental carbon. As a result of their common sources, the O₂⁺ SRI-MS [TNMOC] was significantly correlated ($p \leq 0.05$) with the precursor species NO_x ($R^2 = 0.58$), and elemental carbon measured in PM 2.5 ($R^2 = 0.22$) (Table 6.4).

Table 6.4: The correlations (R^2) between [TNMOC] measured by O_2^+ and H_3O^+ SRI-MS and the sum of the speciated VOCs from the independent VOC measurement techniques (AT-VOC and DNPH) with NO_x , the carbon mass in PM 2.5 ($\mu g C m^{-3}$) ($R^2 > 0.11$, $p \leq 0.05$) and organic aerosol ($\mu g m^{-3}$) measured by the AMS (AMS-OA) ($R^2 > 0.30$, $p \leq 0.05$).

	NO _x (ppbv) N = 27	PM 2.5 ($\mu g C m^{-3}$) N = 27			AMS-OA ($\mu g m^{-3}$) N = 11
		Total Carbon	Element. Carbon	Org. Carbon	
		Correlation coefficients (R^2)			
NO _x		0.26	0.10	0.41	0.05
O ₂ ⁺ SRI-MS [TNMOC] (ppbC)	0.58	0.37	0.22	0.27	0.43
H ₃ O ⁺ SRI-MS [TNMOC] (ppbC)	0.33	0.32	0.08	0.31	0.55
AT-VOC & DNPH [Sum Sp. VOC] (ppbC)	0.59	0.13	0.12	0.07	0.26
H ₃ O ⁺ SRI-MS & AT-VOC [TNMOC] + [alkanes] (ppbC)	0.51	0.31	0.16	0.24	0.49
H ₃ O ⁺ SRI-MS, AT-VOC & DNPH [Sum Sp. VOC] + [non-carbonyl OVOC] (ppbC)	0.47	0.32	0.06	0.26	0.53

As previously discussed, H_3O^+ SRI-MS is not capable of measuring short chain alkanes which are a significant fraction of primary VOC emissions. Consequently, the correlations of [TNMOC] measured by the H_3O^+ SRI-MS with the other primary emission species, NO_x ($R^2 = 0.33$) and elemental carbon ($R^2 = 0.08$), were considerably lower than the correlations observed for O_2^+ SRI-MS [TNMOC] (Table 6.4).

We saw in section 6.7 that when the concentration of alkanes measured by the AT-VOC is added to the [TNMOC] measured by the H_3O^+ SRI-MS the values agree well with the [TNMOC] measured by the O_2^+ SRI-MS (slope ~ 1). The correlations of the sum of (H_3O^+ SRI-MS [TNMOC] + AT-VOC [Alkanes]) with NO_x ($R^2 = 0.51$) and elemental carbon ($R^2 = 0.16$) were closer to those observed for the O_2^+ SRI-MS data (Table 6.4). Thus, the non-detection of alkanes by in H_3O^+ SRI-MS partly explains the poorer correlations between the H_3O^+ SRI-MS [TNMOC] with NO_x and elemental carbon.

The AT-VOC measurement technique used to determine [Sum Sp. VOCs] is capable of measuring the primary hydrocarbons (alkanes, aromatics) that are emitted alongside NO_x , and elemental carbon. The [Sum Sp. VOC] was significantly correlated with NO_x ($R^2 = 0.59$) but not with elemental carbon measured in PM 2.5 ($R^2 = 0.12$) (Table 6.4).

We can conclude that, based on their relationship with other precursor species, the O_2^+ SRI-MS measurements of [TNMOC] appear to capture pre-cursor VOCs better than the H_3O^+ SRI-MS and the [Sum Sp. VOC] measured by the independent measurement techniques.

Oxygenated VOC as well as a large fraction of the organic carbon in PM 2.5, and the organic aerosol measured by the AMS are products of atmospheric oxidation processes. O_2^+ SRI-MS is capable of measuring oxygenated VOCs and the O_2^+ SRI-MS measurements of [TNMOC] were significantly ($p \leq 0.05$) correlated with the organic carbon in PM 2.5 ($R^2 = 0.27$) and organic aerosol measured by the AMS ($R^2 = 0.43$) (Table 6.4).

The H_3O^+ SRI-MS is also capable of measuring oxygenated VOCs. H_3O^+ SRI-MS does not detect the short chain alkanes, and the OVOCs will constitute a larger fraction of [TNMOC] measured by H_3O^+ SRI-MS than measured by the other techniques (O_2^+ SRI-MS, speciated VOC measurement techniques). Consequently, [TNMOC] measured by the H_3O^+ SRI-MS was significantly correlated with the other oxidation products: organic carbon in PM 2.5 ($R^2 = 0.31$) and organic aerosol measured by the AMS ($R^2 = 0.55$).

The DNPH technique used to calculate the [Sum Sp. VOCs] measured the carbonyls and the AT-VOC technique measured 1,8 cineole. These compounds probably represent only a subset of the OVOC compounds actually present. Consequently, the correlations between the [Sum Sp. VOC] and the organic carbon in PM 2.5 ($R^2 = 0.07$) and organic aerosol measured by the AMS ($R^2 = 0.26$), were considerably lower than the correlations observed for O_2^+ and H_3O^+ SRI-MS [TNMOC] (Table 6.4).

We saw in section 6.7 that when the concentration of non-carbonyl OVOCs measured by the H_3O^+ SRI-MS is added to [Sum Sp. VOC] the values agree well with [TNMOC] measured by the O_2^+ SRI-MS (Slope ~ 1). The correlations of the sum of ([Sum Sp. VOC] + [non-carbonyl OVOC]) with organic carbon in PM 2.5 ($R^2 = 0.26$) and organic aerosol measured by the AMS ($R^2 = 0.53$) were closer to those observed for the O_2^+ SRI-MS [TNMOC] data. Thus, the non-detection of a non-carbonyl OVOC by the AT-VOC and DNPH techniques

largely explains the poorer correlations between the [Sum Sp. VOC] and organic PM 2.5 and organic aerosol.

We conclude that, based on their relationship with other products of atmospheric oxidation, the O_2^+ and H_3O^+ SRI-MS measurements of [TNMOC] are more closely related to the presence of organic aerosol than the [Sum Sp. VOC] measured by the AT-VOC and DNPH techniques.

As a total VOC analyzer, the O_2^+ SRI-MS performed better than the H_3O^+ SRI-MS, as well as the AT-VOC and DNPH techniques as O_2^+ SRI-MS was able to capture both the primary VOCs, which act as pre-cursors for atmospheric oxidation processes, as well as the oxygenated products of these processes.

6.9 Conclusions

A significant fraction of organic carbon in the atmosphere remains unidentified with conventional VOC measurement techniques, the organic carbon budget remains poorly constrained (Heald et al. 2008) and the role of this unidentified organic carbon in the formation of ozone and secondary organic aerosol is uncertain.

Tests on gas standards containing 73 VOCs from a range of functional groups demonstrated that O_2^+ SRI-MS is potentially an ideal total carbon analyzer as it was capable of recovering a larger percentage of TNMOC than H_3O^+ SRI-MS, including many small hydrocarbons not measurable with H_3O^+ SRI-MS.

In measurements of an urban atmosphere O_2^+ SRI-MS reported concentrations of [TNMOC] that were significantly higher than the H_3O^+ SRI-MS. When the concentration of alkanes from independent measurements by AT-VOC were added to the H_3O^+ SRI-MS [TNMOC], to account for the insensitivity of H_3O^+ SRI-MS to alkanes, the O_2^+ SRI-MS [TNMOC] values were in agreement with the H_3O^+ SRI-MS [TNMOC] *plus* AT-VOC [alkanes] (slope ~ 1).

The O_2^+ SRI-MS reported concentrations of [TNMOC] were ~ 2 times higher than the sum of the VOCs measured using a combination of AT-VOC and DNPH techniques. When the concentration of non-carbonyl OVOCs from independent measurements by H_3O^+ SRI-MS were added to the [Sum Sp. VOC], to account for the non-detection of these species by AT-

VOC and DNPH, the O_2^+ SRI-MS [TNMOC] values were in agreement with the [Sum Sp. VOC] *plus* H_3O^+ SRI-MS [non-carbonyl OVOC] (slope ~ 1).

O_2^+ SRI-MS [TNMOC] was more highly correlated with both atmospheric oxidation precursors (NO_x , elemental carbon) as well as oxidation products (organic aerosol and particles). Conversely, the [Sum Sp. VOC] correlated well with only the precursor species (NO_x); and the H_3O^+ SRI-MS [TNMOC] correlated well with only the product species (organic aerosol and particles).

Its ability to capture both the VOC pre-cursors of atmospheric oxidation processes and the oxygenated VOC products, as well as having a good correlation with organic aerosol makes O_2^+ SRI-MS a promising new tool for the measurement of TNMOC in the atmosphere.

Chapter 7. Thesis Conclusions

Two key questions regarding the use of SRI-MS to accurately identify and quantify VOCs in the atmosphere have been explored in this thesis:

- What information can be reliably determined about VOC identification from SRI-MS?
- What compounds can the SRI-MS unequivocally quantify in measurements of the atmosphere?

The key to identifying and quantifying VOCs in SRI-MS spectra is understanding the chemistry and fragmentation in the drift tube. This has been done by:

- studies of VOCs standards
- manipulation of drift tube conditions
- use of different reagent ions
- comparison of atmospheric measurements by PTR-MS with other measurement techniques.

The instrument employed in this study was a PTR-MS with switchable reagent ion capability (SRI-MS), which enables the use of O_2^+ and NO^+ as reagent ions in addition to H_3O^+ . These multiple reagent ion systems were designed to detect compounds not detectable with H_3O^+ alone, and to differentiate isobaric compounds on the basis of differences in their ionization reactions or fragmentation products. The application of SRI-MS to measurements of inorganic and organic compounds in the atmosphere is still in its infancy and studies such as those described in this thesis are critical to determine what, if any, additional information can be acquired through the use of reagent ions other than H_3O^+ .

A systematic study of the PTR-MS mass spectra of the reactions of H_3O^+ with > 90 VOCs including aromatic and aliphatic hydrocarbons, aldehydes, ketones, alcohols, carboxylic acids, esters and multifunctional compounds, contained in a series of gaseous standards is presented in Chapters 2 and 3. The mass spectra of most VOCs contained multiple product ion signals, the number and distribution of which was dependent on the drift tube operating conditions (E/N) (Chapter 2).

A series of simple rules were developed for the interpretation of the mass spectra to determine which compounds were detected in each reagent ion mode, and of these which compounds could be identified in the mass spectra without interference (Chapter 3).

When operating with H_3O^+ as the primary reagent ion the PTR-MS was capable of detecting almost all of the compound classes studied with the notable exceptions of the acetylene, the short chain alkanes and glyoxal. Of the 60 compounds detected by the H_3O^+ SRI-MS, there were 16 compounds / compound groups that could be identified without significant interference from the 60 compounds detected including: formaldehyde, methanol, acetaldehyde, acetone, methyl ethyl ketone, acetonitrile, dimethyl sulphide, isoprene, monoterpenes, and the $\text{C}_6 - \text{C}_9$ aromatics.

A systematic study of the SRI-MS spectra of five of certified gas standards containing > 70 VOCs including aromatic and aliphatic hydrocarbons, oxygenated VOCs, acetonitrile, and dimethyl sulphide were determined in each reagent ion mode (H_3O^+ , O_2^+ , NO^+) (Chapter 3). This study represents the most extensive instrument characterization of SRI-MS to date.

The O_2^+ SRI-MS can almost be regarded as a universal VOC detector as it was capable of detecting 70 out of the 73 compounds present in the five certified gas standards, including the small alkanes not detectable with H_3O^+ . Due to the more energetic nature of O_2^+ ionization, the mass spectra were less well resolved than the H_3O^+ spectra and only 14 out of the 70 compounds detected with O_2^+ SRI-MS were identified in the mass spectra without significant interference. These 14 compounds included important atmospheric species such as acetylene, ethane, isoprene, $\text{C}_8 - \text{C}_{10}$ aromatics, α -pinene, 1,8 cineole, and dimethyl sulphide.

The NO^+ SRI-MS was exposed to 32 compounds, 27 of which it was capable of detecting with the notable exception of the ketones, and the small alkanes. Due to the “soft” ionization processes associated with NO^+ , the mass spectra were generally simple and well resolved. There were 15 compounds / compound groups detected without significant interference from the 27 compounds detected including important atmospheric species such as methacrolein, dimethyl sulphide, isoprene, $\text{C}_8 - \text{C}_{10}$ aromatics, α -pinene, 1,8,-cineole.

Chapter 4, presented a real-world inter-comparison of the mixing ratios of selected VOCs measured by H_3O^+ SRI-MS with two independent measurement techniques (AT-VOC and DNPH). The H_3O^+ SRI-MS closely agreed with the AT-VOC measurements for toluene and the C_8 aromatics.

The H_3O^+ SRI-MS measurements of C_9 aromatics, monoterpenes and the carbonyl compounds correlated well with those reported in the AT-VOC and DNPH samples but the measurements by these independent VOC measurement techniques employed in this study,

suffered from their own inherent analytical biases and could not be considered as a reference method against which the quantitative accuracy of the H_3O^+ SRI-MS measurements of these compounds could be assessed.

The H_3O^+ SRI-MS measurements were also compared with the measurements obtained when the SRI-MS was operating in O_2^+ and NO^+ reagent ion modes. This study represents one of the first real-world inter-comparisons of SRI-MS to date.

The results of this study suggest that the O_2^+ and NO^+ SRI-MS could provide equivalent or more selective measurements of isoprene and toluene, in comparison to conventional H_3O^+ SRI-MS. With the exception of higher selectivity measurements of these species, the NO^+ and O_2^+ SRI-MS did not provide any significant additional information in comparison to the H_3O^+ SRI-MS measurements alone. The measurement of small hydrocarbons including acetylene with O_2^+ SRI-MS, and the discrimination between isomeric aldehydes and ketones with NO^+ represents a significant potential advantage of SRI-MS not explored here and further inter-comparisons are required to demonstrate these applications of SRI-MS.

Overall, the results of the present study demonstrate that while switching reagent ions to exploit the potential unique detection capabilities of each, continuity in measurements of two important VOCs, isoprene and toluene, is possible in all three reagent ion modes.

In Chapter 5 of this thesis, a systematic study was conducted into the interference in the PTR-MS measurement of acetonitrile at m/z 42 in Sydney, Australia. Two other ions contributed to the signal at m/z 42. These are ^{13}C isotopologues of C_3H_5^+ and C_3H_6^+ . The signal from the ^{13}C isotopologue of C_3H_5^+ at m/z 42, was due to the presence of alkenes including isoprene with probable contributions from other compounds not measured in this study. The signal from C_3H_6^+ was produced by reactions of O_2^+ , present as an impurity in the H_3O^+ reagent ion matrix, with alkanes and alkenes. The method formulated in this study to quantify and subtract the interference of non-acetonitrile compounds in PTR-MS measurements at m/z 42 resulted in a more accurate quantification of the concentration of acetonitrile and consequently, a more sensitive tracer for biomass burning in polluted urban air.

A significant fraction of organic carbon in the atmosphere remains unidentified with conventional VOC measurement techniques and the role of this unidentified organic carbon in the formation of ozone and secondary organic aerosol is uncertain. Chapter 6, of this thesis

described a novel application of O_2^+ SRI-MS for the measurement of total non-methane organic carbon (TNMOC) in an urban atmosphere.

Test on the previously described gas standards containing 73 VOCs demonstrated that the potential of application of O_2^+ SRI-MS as a total carbon analyzer as it was capable of recovering a larger percentage of TNMOC than H_3O^+ SRI-MS, including many small hydrocarbons not measurable with H_3O^+ SRI-MS.

In measurements of an urban atmosphere O_2^+ SRI-MS reported concentrations of [TNMOC] that were significantly higher than the H_3O^+ SRI-MS. Its ability to capture both the VOC pre-cursors of atmospheric oxidation processes and the oxygenated VOC products, as well as having a good correlation with organic aerosol makes O_2^+ SRI-MS a promising new tool for the measurement of TNMOC in the atmosphere.

In conclusion, the laboratory studies described in this thesis represent one of the most extensive characterizations of the performance of SRI-MS instruments for the identification and quantification of VOCs to date. This was followed by one of the first real-world comparisons of the measurement of VOCs using O_2^+ , NO^+ and H_3O^+ reagent ions in SRI-MS and this work represents a significant contribution to the available information on the application of SRI-MS to atmospheric observations of VOCs. In addition, two novel applications of SRI-MS were developed: A study of acetonitrile showed that in some cases corrections may be made for the coincidence of several VOC signals at the same mass/charge ratio, and an improved analyte signal obtained. Finally some promising results concerning the measurement of total non-methane organic carbon with SRI-MS were presented.

8. Bibliography

- Adams NG, Smith D. 1976. The Selected Ion Flow Tube (SIFT); A technique for studying ion-neutral reactions. *International Journal of Mass Spectrometry and Ion Physics* 21:349 - 359.
- Ambrose JL, Haase K, Russo RS, Zhou Y, White ML, Frinak EK, Jordan C, Mayne HR, Talbot R, Sive BC. 2010. A comparison of GC-FID and PTR-MS toluene measurements in ambient air under conditions of enhanced monoterpene loading. *Atmos. Meas. Tech.* 3:959-980.
- Amelnyck C, Schoon N, Kuppens T, Bultinck P, Arijis E. 2005. A selected ion flow tube study of the reactions of H_3O^+ , NO^+ and O_2^{*+} with some oxygenated biogenic volatile organic compounds. *International Journal of Mass Spectrometry* 247:1 - 9.
- Ammann C, Spirig C, Neftel A, Steinbacher M, Komenda M, Schaub A. 2004. Application of PTR-MS for measurements of biogenic VOC in a deciduous forest. *International Journal of Mass Spectrometry* 239:87 - 101.
- Andreae MO, Artaxo P, Fischer H., Freitas SR, Gregoire JM, Hansel A, Hoor P, Kormann R, Krejci R, Lange L, Lelieveld J, Lindinger W, Longo K, Peters W, de Reus M, Scheeren B, Silva-Dias MAF, Strom J, P.F.J. vV, Williams J. 2001. Transport of biomass burning smoke to the upper troposphere by deep convection in the equatorial region. *Geophysical Research Letters* 28.
- Apel E, Brauers T, Koppmann R, Bandowe B, Boßmeyer J, Holzke C, Tillmann R, Wahner R, Wegener R, Brunner A, Jocher M, Ruuskanen T, Spirig C, Steigner D, Steinbrecher R, Gomez Alvarez E, Müller K, Burrows JP, Schade GW, Solomon J, Ladstätter-Weissenmayer A, Simmonds P, Young D, Hopkins JR, Lewis AC, Legreid G, Reimann S, Hansel A, Wisthaler A, Blake RS, Ellis AM, Monks PS, Wyche KP. 2008. Intercomparison of oxygenated volatile organic compound measurements at the SAPHIR atmosphere simulation chamber. *J. Geophys. Res.* 113.
- Aprea E, Biasioli F, Mark TD, Gasperi F. 2007. PTR-MS study of esters in water and water/ethanol solutions: Fragmentation patterns and partition coefficients. *International Journal of Mass Spectrometry* 262:114 - 121.

- Atkinson R, Arey J. 2003. Atmospheric Degradation of Volatile Organic Compounds. *Chemical Reviews* 103:4605-4638.
- Axson JL, Takahashi K, de Haan DO, Vaida V. 2009. Gas-phase water mediated equilibrium between methylglyoxal and its geminal diol. *Proceedings of the National Academy of Science* 107:6687 - 6692.
- Ayers GP. 2001. Comment on regressin analysis of air quality data. *Atmos. Env.* 35:2423 - 2425.
- Baasandorj M, Millet DB, Hu L, Mitroo D, Williams BJ. 2015. Measuring acetic and formic acid by proton-transfer-reaction mass spectrometry: sensitivity, humidity dependence, and quantifying interferences. *Atmos. Meas. Tech.* 8:1303 - 1321.
- Baker M, Gabryelski W. 2007. Collision induced dissociation of deprotonated glycolic acid. *International Journal of Mass Spectrometry* 262:128 - 135.
- Blake RS, Monks PS, Ellis AM. 2009. Proton-Transfer Reaction Mass Spectrometry. *Chemical Reviews* 109:861 - 896.
- Blake RS, Patel M, Monks PS, Ellis AM, Inomata S, Tanimoto H. 2008. Aldehyde and ketone discrimination and quantification using two-stage proton transfer reaction mass spectrometry. *International Journal of Mass Spectrometry* 278:15-19.
- Blake RS, Wyche KP, Ellis AM, Monks PS. 2006. Chemical ionization reaction time-of-flight mass spectrometry: Multi-reagent analysis for determination of trace gas composition. *International Journal of Mass Spectrometry* 254:85-93.
- Bleaney BI, Bleaney B. 1965. *Electricity and Magnetism*. London: Oxford University Press.
- Bouchoux G, Salpin JY, Leblanc D. 1996. A relationship between the kinetics and thermochemistry of proton transfer in the gas phase. *International Journal of Mass Spectrometry and Ion Processes* 153:37 - 48.
- Brown P, Watts P, Mark TD, Mayhew CA. 2010. Proton transfer reaction mass spectrometry investigations on the effects of reduced electric field and reagent ion internal energy

- on product ion branching ratios for a series of saturated alcohols. *International Journal of Mass Spectrometry* 294:103-111.
- Buhr K, van Ruth S, Delahunty C. 2002. Analysis of volatile flavour compounds by Proton Transfer Reaction-Mass Spectrometry: fragmentation patterns and discrimination between isobaric and isomeric compounds. *International Journal of Mass Spectrometry* 221.
- Cappellin L, Karl T, Probst M, Ismailova O, Winkler PM, Soukoulis C, Aprea E, Mark TD, Gasperi F, Biasioli F. 2012. On quantitative determination of volatile organic compound concentrations using proton transfer reaction time-of-flight mass spectrometry. *Environmental Science & Technology* 46.
- Cappellin L, Makhoul S, Schuhfried E, Romano A, Sanchez del Pulgar J, Aprea E, Farneti B, Costa F, Gasperi F, Biasioli F. 2014. Ethylene: Absolute real-time high-sensitivity detection with PTR/SRI-MS. The example of fruits, leaves and bacteria. *International Journal of Mass Spectrometry* 365–366:33-41.
- Christian TJ, Kleiss B, Yokelson RJ, Holzinger R, Crutzen PJ, Hao WM, Shirai T, Blake DR. 2004. Comprehensive laboratory measurements of biomass burning emissions: 2. First intercomparison of open-path FTIR, PTR-MS, and GC-MS/FID/ECD. *Journal of Geophysical Research- Atmospheres* 109.
- Chung MY, Maris C, Krischke U, Meller R, Paulson S. 2003. An investigation of the relationship between total non-methane organic carbon and the sum of the speciated hydrocarbons and carbonyls measured by standard GC/FID: measurements in the Los Angeles air basin. *Atmospheric Environment* 37:S159-S170.
- Cope M, Keywood M, Emmerson K, Galbally IE, Boast K, Chambers S, Cheng M, Crumeyrolle S, Dunne E, Fedele R, Gillett R, Griffiths A, Harnwell J, Katzfey J, Hess D, Lawson SL, Miljevic B, Molloy S, Powell J, Reisen F, Ristovski Z, Ward J, Zhang C, Zeng J. 2014. Sydney Particle Study - Stage II. Australia: CSIRO and Office of Environment and Heritage.

- CSIRO. 2008. Sources of ozone pre-cursors and atmospheric chemistry in a typical Australian city, A report to the Air Quality section, Environment Standards Branch, Dept. Environment, Water, Heritage and the Arts. Canberra.
- Dass C. 2006. Fundamentals of Contemporary Mass Spectrometry. Hoboken NJ, USA: John Wiley and Sons.
- Dawson PH. 1975. Accetance of the quadrupole mass filter. *International Journal of Mass Spectrometry and Ion Physics* 17:423-445.
- Dawson PH. 1976. Experimental measurements of quadrupole mass analysis performance and comparison with theoretical predictions. *International Journal of Mass Spectrometry and Ion Physics* 21:317 - 332.
- Dawson PH. 1986. Quadrupole mass analyzers: Performance, design and some recent applications. *Mass Spectrometry Reviews* 5:1-37.
- de Gouw J, Goldan PD, Warneke C, Kuster WC, Roberts JM, Marchewka M, Bertman SB, Pszenny AAP, Keene WC. 2003. Validation of proton transfer reaction-mass spectrometry (PTR-MS) measurements of gas-phase organic compounds in the atmosphere during the New England Air Quality Study (NEAQS) in 2002. *Journal of Geophysical Research* 108:4682
- de Gouw J, Middlebrooke AM, Warneke C, Goldan PD, Kuster WC, Roberts JM, Fehsenfeld FC, Worsnop DR, Canagaratna MR, Pszenny AAP, Keene WC, Marchewka M, Bertman SB, Bates TS. 2005. Budget of organic carbon in a polluted atmosphere: Results from the New England Air Quality Study in 2002. *Journal of Geophysical Research* 110.
- de Gouw J, Warneke C. 2007. Measurements of volatile organic compounds in the Earth's atmosphere using proton-transfer-reaction mass spectrometry. *Mass Spectrometry Reviews* 26:223- 257.
- de Gouw J, Warneke C, Karl T, Eerdekens G, van der Veen C, Fall R. 2003. Sensitivity and Specificity of atmospheric trace gas detection by proton-transfer-reaction mass spectrometry. *International Journal of Mass Spectrometry* 223-224:365-382.

- Demarcke M, Amelnyck C, Schoon N, Dhooge F, Rimetz-Planchon J, Van Langenhove H, Dewulf J. 2010. Laboratory studies in support of the detection of biogenic unsaturated alcohols by proton transfer reaction - mass spectrometry. *International Journal of Mass Spectrometry* 290:14 - 21.
- Diskin AM, Wang T, Smith D, Spanel P. 2002. A selected ion flow tube (SIFT), study of the reactions of H_3O^+ , NO^+ and O_2^+ ions with a series of alkenes; in support of SIFT-MS. *International Journal of Mass Spectrometry* 218:87 - 101.
- Dunne E, Galbally IE, Lawson SL, Patti A. 2012. Interference in the PTR-MS measurement of acetonitrile at m/z 42 in polluted urban air - A study using switchable reagent ion PTR-MS. *International Journal of Mass Spectrometry* 319-320:40-47.
- Dupeyrat G, Rowe BR, Fahey DW, Albritton DL. 1982. Diagnostic studies of venturi inlets for flow reactors. *International Journal of Mass Spectrometry and Ion Physics* 44:1 - 18.
- Ellis AM, Mayhew CA. 2014. Proton transfer reaction mass spectrometry: principles and applications. Chichester U.K.: John Wiley & Sons Ltd.
- Erickson MH, Gueneron M, Jobson BT. 2014. Measuring long chain alkanes in diesel engine exhaust by thermal desorption PTR-MS. *Atmospheric Measurement Techniques* 7:225-239.
- Fehensfeld FC, Schmeltekopf AL, Goldan PD. 1966. Thermal energy ion-neutral reaction rates. I. Some reactions of helium ions. *J. Phys. Chem.* 44:4087 - 4094.
- Francis GJ, Langford VS, Milligan DB, McEwan MJ. 2009. Real-time monitoring of hazardous air pollutants. *Anal. Chem.* 81.
- Galbally IE, Lawson SJ, Hibberd MF, Bentley ST, Cheng M, Weeks IA, Gillett RW, Selleck PW, Dunne E. 2008. A study of VOCs during Winter 2006 at Wagerup, Western Australia. A Report to Alcoa World Alumina. Aspendale, Australia: CSIRO Marine and Atmospheric Research.

- Geron C, Rasmussen R, Arnts RR, Guenther A. 2000. A review and synthesis of monoterpene speciation from forests in the United States. *Atmos. Env.* 34:1761 - 1781.
- Gilpin T, Apel E, A. F, Wert B, Calvert J, Genfa Z, Dasgupta PK, Harder P, Heikes PW, Hopkins B, Westberg H, Kleindienst TE, Lee YN, Zhou X, Lonneman W, Sewell S. 1997. Intercomparision of six ambient [CH₂O] measurement techniques. *J. Geophys. Res.* 102:21161 - 21188.
- Gioumousis G, Stevenson DP. 1958. Reactions of gaseous molecule ions with gaseous molecules. *V> Theory. J. Chem. Phys.* 29:294.
- Glosik J, Jordan A, Skalsky V, Lindinger W. 1993. Collision induced dissociation of the isomeric ions H₂COOH⁺ and HC(OH)₂₊₁. *International Journal of Mass Spectrometry and Ion Processes* 129.
- Goldan PD, Schmeltekopf AL, Fehensfeld FC, Schiff HI, Ferguson E. 1966. Thermal energy ion-neutral reaction rates. II. Some reactions of ionospheric interest. *J. Chem. Phys.* 44:4095 - 4103.
- Goldstein AH, Galbally IE. 2007. Known and unexplored constituents in the Earth's atmosphere. *Environmental Science and Technology* 41:1514-1521.
- Graus M, Müller M, Hansel A. 2010. High Resolution PTR-TOF: Quantification and formula confirmation of VOC in real time. *J. American Soc. for Mass Spectrom.* 21:1037 - 1044.
- Gueneron M, Erickson MH, VanderSchelden GS, Jobson BT. 2015. PTR-MS fragmentation patterns of gasoline hydrocarbons. *International Journal of Mass Spectrometry* 379:97-109.
- Haase KB, Keene WC, Pszenny AAP, Mayne HR, Talbot R, Sive BC. 2012. Calibration and intercomparison of acetic acid measurements using proton-transfer-reaction mass spectrometry (PTR-MS). *Atmos. Meas. Tech.* 5:2793-2750.
- Hak C, Pundt I, Trick S, Platt U, Dommen J, Ordonez C, Prevot ASH, Junkermann W, Astorga-Llorens C, Larsen BR, Mellqvist J, Strandberg A, Yu Y, Galle B, Kleffmann

- J, Lorzer JC, Braathen GO, Volkamer R. 2005. Intercomparison of four different in-situ techniques for ambient formaldehyde measurements in urban air. *Atmos. Chem. Phys.* 5:2881 -2900.
- Hansel A, Jordan A, Holzinger R, Prazeller P, Vogel W, Lindinger W. 1995. Proton transfer reaction mass spectrometry: on-line trace gas analysis at the ppb level. *International Journal of Mass Spectrometry and Ion Processes* 149 - 150:609 - 619.
- Hansel A, Wisthaler A, Schwarzman M, Lindinger W. 1997. Energy dependencies of the proton transfer reactions $\text{H}_3\text{O}^+ + \text{CH}_2\text{O} \rightleftharpoons \text{CH}_2\text{OH}^+ + \text{H}_2\text{O}$. *International Journal of Mass Spectrometry and Ion Processes* 167-268:697 - 703.
- Harrison AG. 1992. *Chemical Ionization Mass Spectrometry*. United States of America: CRC Press
- Heald CL, Goldstein AH, Allan JD, Aiken AC, Apel E, Atlas EL, Baker AK, Bates TS, A.J. B, Blake DR, Campos T, Coe H, Crounse JD, DeCarlo PF, de Gouw JA, Dunlea EJ, Flocke FM, Fried A., Goldan PD, Griffin RJ, Herndon SC, Holloway JS, Holzinger R, Jimenez JL, Junkermann W, Kuster WC, Lewis AC, Meinardi S, Millet DB, Onasch T, Polidori A, Quinn PK, Riemer DD, Roberts JM, Salcedo D, Sive B, Swanson AL, Talbot R, Warneke C, Weber RJ, Weibring P, Wennberg PO, Worsnop DR, Wittig AE, Zhang R, Zheng J, Zheng W. 2008. Total observed organic carbon (TOOC) in the atmosphere: a synthesis of North American observations. *Atmospheric Chemistry and Physics* 8:2007-2025.
- Ho SSH, Chow JC, Watson JG, Ip HSS, Ho KF, Dai WT, Cao JJ. 2014. Biases in ketone measurements using DNPH-coated solid sorbent cartridges. *Analytical Chemistry* 6:967 - 974.
- Ho SSH, Ho KF, Liu WD, Lee SC, Dai WT, Cao JJ, Ip HSS. 2011. Unsuitability of using the DNPH-coated solid sorbent cartridge for determination of airborne unsaturated carbonyls. *Atmos. Env.* 45:261 - 265.
- Horwitz W. 1982. Evaluation of Analytical Methods Used for Regulation of Foods and Drugs. *Analytical Chemistry* 54:67 -76.

- Howe GB, Gangwal SK, Jaynaty RKM. 1983. Validation and improvement of EPA reference method 25- determination of gaseous non-methane organic emissions as carbon. . US EPA.
- Howorka F, Lindinger W, Pahl M. 1973. Ion sampling from the negative glow plasma in a cylindrical hollow cathode. *International Journal of Mass Spectrometry and Ion Physics* 12.
- Howorka F, Lindinger W, R.N. V. 1974. Reaction rate constants in steady-state hollow cathode discharges: $\text{N}_2 + \text{H}_2\text{O}$ reactions. *J. Chem. Phys.* 61:1180 - 1188.
- Hunter KC, East ALL. 2002. Properties of C-C bonds in n-alkanes: relevance to cracking mechanisms. *J. Phys. Chem. A.* 106:1346 - 1356.
- Iinuma Y, Engling G, Puxbaum H, Hermann H. 2009. A highly resolved anion-exchange chromatographic method for determination of saccharidic tracers biomass combustion and primary bio-particles in atmospheric aerosol. *Atmospheric Environment* 43:1367 - 1371.
- Inomata S, Tanimoto H. 2009. A deuterium-labeling study on the reproduction of hydronium ions in the PTR-MS detection of ethanol. *International Journal of Mass Spectrometry* 285:95-99.
- Inomata S, Tanimoto H. 2008. Differentiation of isomeric compounds by two-stage proton transfer reaction time-of-flight mass spectrometry. *Journal of the American Society for Mass Spectrometry* 19:325-331.
- Inomata S, Tanimoto H. 2010. A quantitative examination of the detection sensitivities of proton-transfer reaction mass spectrometry for gaseous 2-propanol and acetic acid. *Bulletin of the Chemical Society of Japan* 83:900 -904.
- Inomata S, Tanimoto H, Kameyama S, Tsunogai U, Irie H, Kanaya Y, Wang Z. 2008. Technical Note: Determination of formaldehyde mixing ratios in polluted air with PTR-MS: laboratory experiments and field measurements. *Atmos. Chem. Phys.* 8:273 - 284.

- Inomata S, Tanimoto H, Yamada H. 2013. Mass spectrometric detection of alkanes using NO^+ chemical ionization in proton-transfer-reaction plus switchable reagent ion mass spectrometry. *Chemistry Letters* 43:538-540.
- ISO. 1995. ISO 6879: 1995 Air Quality- Performance Characteristics and related concepts for air quality measuring methods. Geneva, Switzerland: International Organization for Standardization.
- Jordan A, Haidacher S, Hanel G, Hartungen E, Mark L, Seehauser H, Schotchkowsky R, Sulzer P, Mark TD. 2009. A high resolution and high sensitivity proton-transfer-reaction time-of-flight mass spectrometer (PTR-TOF-MS). *International Journal of Mass Spectrometry* 286:122 -128.
- Jordan A, Haidacher S, Hartungen E, Herbig J, Mark L, Schotchkowsky R, Seehauser H, Sulzer P, Mark TD. 2009. An online ultra-high sensitivity Proton-transfer-reaction-mass-spectrometer combined with switchable reagent ion capability (SRI+PTR-MS). *International Journal of Mass Spectrometry* 286:32 - 38.
- Karl T, Christian TJ, Yokelson RJ, Artaxo P, Hao WM, Guenther A. 2007. The Tropical Forest and Fire Emissions Experiment: method evaluation of volatile organic compound emissions measured by PTR-MS, FTIR, and GC from tropical biomass burning. *Atmos. Chem. Phys.* 7:5883 - 5897.
- Karl T, Hansel A, Cappellin L, Kaser L, Herdlinger-Blatt I, Jud W. 2012. Selective measurements of isoprene and 2-methyl-3-buten-2-ol based on NO^+ ionization mass spectrometry. *Atmos. Chem. Phys.* 12:11877-11884.
- Karl T, Jobson BT, Kuster WC, Williams EJ, Stutz J, Shetter R, Hall SR, Goldan PD, Fehsenfeld FC, Lindinger W. 2003. Use of proton-transfer-reaction mass spectrometry to characterize volatile organic compound sources at the La Porte super site during the Texas Air Quality Study 2000. *J. Geophys. Res.* 108:4508.
- Karl T, Kaser L, Turnipseed A. 2014. Eddy covariance measurements of isoprene and 232-MBO based on NO^+ time-of-flight mass spectrometry. *International Journal of Mass Spectrometry* 365–366:15-19.

- Kaser L, Karl T, Schnitzhofer R, Graus M, Herdinger-Blatt I, J. D, Sive B, Turnipseed A, Hornbrook R, Zheng W, Flocke F, Guenther A, Keutsch F, Apel E, Hansel A. 2013. Comparison of different real time VOC measurement techniques in a ponderosa pine forest. *Atmos. Chem. Phys.* 13:2893 - 2906.
- Kato S, Miyakawa Y, Kaneko T, Kajii Y. 2004. Urban air measurements using PTR-MS in Tokyo area and comparison with GC-FID measurements. *International Journal of Mass Spectrometry* 235:103-110.
- Kleindienst TE, Shepson PB, Nero CM, Arnts RR, Tejada SB, Mackay GI, Mayne LK, Schiff HI, Lind JA, Kok A, Lazrus AL, Dasgupta PK, Dong S. 1988. An intercomparison of formaldehyde measurement techniques at ambient concentration *Atmos. Env.* 22:1931 - 1939.
- Knighton WB, Fortner EC, Herndon SC, Wood EC, Miake-Lye RC. 2009. Adaptation of a proton transfer reaction mass spectrometer instrument to employ NO^+ as reagent ion for the detection of 1,3-butadiene in the ambient atmosphere. *Rapid Communications in Mass Spectrometry* 23:3301-3308.
- Kok A, Zeijlmans van Emmichoven PA, Niehaus A. 2003. Reactions between CH_4^+ and $\text{C}_2\text{H}_5\text{OH}$. *International Journal of Mass Spectrometry* 223 - 224:81 - 89.
- Kuster WC, Jobson BT, Karl T, Riemer D, Apel E, Goldan PD, Fehsenfeld FC. 2004. Intercomparison of Volatile Organic Carbon Measurement Techniques and Data at La Porte during the TexAQS2000 Air Quality Study. *Environmental Science & Technology* 38:221-228.
- Lagg A, Taucher J, Hansel A, Lindinger W. 1994. Applications of proton transfer reactions to gas analysis. *International Journal of Mass Spectrometry and Ion Processes* 134:55 - 66.
- Langevin M. 1905. Une formule fondamentale de th'eorie cin'etique [A fundamental formula of kinetic theory]. *Ann. Chim. Phys.* 5:245.
- Lanza M, Acton WJ, Jürschik S, Sulzer P, Breiev K, Jordan A, Hartungen E, Hanel G, Märk L, Mayhew CA, Märk TD. 2013. Distinguishing two isomeric mephedrone

- substitutes with selective reagent ionisation mass spectrometry (SRI-MS). *Journal of Mass Spectrometry* 48:1015-1018.
- Lawson DR, Biermann HW, Tuazon EC, Winer AM, Mackay GI, Schiff HI, Kok A, Dasgupta PK, Fung K. 1990. Formaldehyde measurement methods evaluation and ambient concentrations during the Carbonaceous Species Methods Comparison Study. *Aerosol Sci. Technol.* 12:64 - 76.
- Lee A, Schade GW, Holzinger R, Goldstein AH. 2005. A comparison of new measurements of total monoterpene flux with improved measurements of speciated monoterpene flux. *Atmos. Chem. Phys.* 5:505-513.
- Lelieveld J, Crutzen PJ, Ramanathan V, Andreae MO, Brenninkmeijer CAM, Campos T, Cass GR, Dickerson RR, Fischer H., de Gouw J, Hansel A, Jefferson A, Kley D, de Laat ATJ, Lal S, Lawrence MG, Lobert JM, Mayol-Bracero OL, Mitra AP, Novakov T, Oltmans SJ, Prather KA, Reiner T, Rodhe H, Scheeren HA, Sikka D, Williams J. 2001. The Indian Ocean Experiment: Widespread Air Pollution from South and Southeast Asia. *Science* 291:1031 - 1036.
- Lewis AC, Carslaw N, Marriott PJ, Kingorn RM, Morrison P, Lee AL, Bartle KD, Pilling MJ. 2000. A larger pool of ozone-forming carbon compounds in urban atmospheres. *Nature* 405:778-781.
- Lias SG. 2015. Ionization Energy Evaluation. In: Lindstrom PJ, Mallard WG, Editors. NIST Chemistry WebBook, NIST Standard Reference Database Number 69. Gaithersburg MD 20899: National Institute of Standards and Technology.
- Liggio J, Li S-M, McLaren R. 2005. Heterogenous reactions of glyoxal on particulate matter: identification of acetals and sulfate esters. *Environmental Science & Technology* 39:1532 - 1541.
- Lindinger W. 1973. Reaction-rate constants in steady-state hollow cathode discharges: Ar + H₂O reactions. *Phys. Rev. A* 7:328 - 333.

- Lindinger W, Alge E, Stori H, Varney RN, Helm H, Holzmann P, Pahl M. 1979. Investigation of ion-molecule reactions using a drift tube with separated ion source. *International Journal of Mass Spectrometry and Ion Physics* 30:251 - 261.
- Lindinger W, Hansel A, Jordan A. 1998. On-line monitoring of volatile organic compounds at pptv levels by means of proton-transfer-reaction mass spectrometry (PTR-MS) medical applications, food control and environmental research. *International Journal of Mass Spectrometry and Ion Processes* 173:191-241.
- Lindinger W, Hirber J, Paretzke H. 1993. An ion/molecule-reaction mass spectrometer used for on-line trace gas analysis. *International Journal of Mass Spectrometry and Ion Processes* 129:79 - 88.
- Lobert JM, Scharffe DH, Hao WM, Crutzen PJ. 1990. Importance of biomass burning in the atmospheric budgets of nitrogen-containing gases. *Nature* 346:552 - 554.
- Loeffler KW, Koehler CA, Paul NM, de Haan DO. 2006. Oligomer formation in evaporating aqueous glyoxal and methyl glyoxal solutions. *Env. Sci. Technol.* 40:6318 - 6323.
- Lucke RL. 1976. Counting statistics for non-negligible dead time corrections. *Rev. Scientific Instruments* 47:766 - 767.
- Maleknia S, Bell T, Adams M. 2007. PTR-MS analysis of reference and plant-emitted volatile organic compounds. *International Journal of Mass Spectrometry* 262:203 - 210.
- Maris C, Chung MY, Lueb R, Krischke U, Meller R, Fox MJ, Paulson S. 2003. Development of instrumentation for simultaneous analysis of total-non-methane organic carbon and volatile organic compounds in ambient air. *Atmospheric Environment* 37:S149-S158.
- Märk TD, Lindinger W, Howorka F, Egger F, Varney RN, Pahl M. 1972. A simple bakeable hollow cathode device for the direct study of plasma constituents. *Review of Scientific Instruments* 43:1852 - 1853.
- Mavrodineanu R. 1984. Hollow Cathode Discharges- Analytical applications. *Journal of Research of the National Bureau of Standards* 89:143 - 185.

- McFarland M, Albritton DL, Fehensfeld FC, Ferguson E, Schmeltekopf AL. 1973. Flow-drift technique for ion mobility and ion-molecule reaction rate constant measurements. I. Apparatus and mobility measurements. *J. Chem. Phys.* 59:6610 - 6619.
- McFarland M, Albritton DL, Fehensfeld FC, Ferguson EE, Schmeltekopf AL. 1973. Flow-drift technique for ion mobility and ion molecule reaction rate constant measurements. *J. Chem. Phys.* 59:6610.
- McKeen SA, Liu SC. 1993. Hydrocarbon ratios and photochemical history of air masses. *Geophys. Res. Letters* 20:2363 - 2366.
- McMurry J. 1992. *Organic Chemistry*. Belmont, California: Wadsworth Inc.
- Michel E, Schoon N, Amelnyck C, Guimbaud C, Catoire V, Arijs E. 2005. A selected ion flow tube study of the reactions of H_3O^+ , NO^+ and O_2^{*+} with methyl vinyl ketone and some atmospherically important aldehydes. *International Journal of Mass Spectrometry* 244:50 - 59.
- Munson MSB, Field FH. 1966. Chemical Ionization Mass Spectrometry. *J. American Soc. for Mass Spectrom.* 88:2621 - 2630.
- Munson MSB, Field FH. 1966. Chemical Ionization Mass Spectrometry. *J. Am. Chem. Soc.* 88:2621.
- Norman M, Hansel A, Wisthaler A. 2007. O_2^+ as reagent ion in the PTR-MS instrument: Detection of gas-phase ammonia. *International Journal of Mass Spectrometry* 265:382-387.
- Park JH, Goldstein AH, Timkovsky J, Fares S, Weber RJ, Karlik J, Holzinger R. 2013. Active Atmosphere-Ecosystem Exchange of the Vast Majority of Detected Volatile Organic Compounds. *Science* 341:643 - 647.
- Puxbaum H, Caseiro A, Sanchez-Ochoa A, Kasper-Giebl A, Claeys M, Gelencser M. 2007. Levoglucosan levels at background sites in Europe for assessing the impacts of biomass combustion on the European aerosol background. *J. Geophys. Res.* 112:D23S05.

- Richter S, Goldberg SA, Mason PB, Traina AJ, Schwieters JB. 2001. Linearity test for secondary electron multipliers used in isotope ratio mass spectrometry. *International Journal of Mass Spectrometry* 206:105 - 127.
- Roberts JM, Bertman SB, Jobson BT, Niki H, Tanner R. 1998. Measurement of total nonmethane organic carbon (C_y): Development and application at Chebogue Point, Nova Scotia, during the 1993 North Atlantic Regional Experiment campaign. *Journal of Geophysical Research* 103:13581-13592.
- Schoon N, Amelnyck C, Vereecken L, Arijs E. 2003. A selected ion flow tube study of the reactions of H_3O^+ , NO^+ and O_2^+ with a series of monoterpenes. *International Journal of Mass Spectrometry* 229:231 - 240.
- Seinfeld JH, Pandis SN. 2006. *Atmospheric Chemistry and Physics: From Air Pollution to Climate Change*. New York: J Wiley.
- Shamlouei HR, Tabrizchi M. 2008. Transmission of different ions through a drift tube. *International Journal of Mass Spectrometry* 273:78 - 83.
- Silverstein RM, Webster KX, Kiemle D. 2005. *Spectrometric identification of organic compounds*. New York, USA: John Wiley and Sons.
- Singh HB, O'Hara D, Herlth D, Sachse W, Blake DR, Bradshaw JD, Kanakidou M, Crutzen PJ. 1994. Acetone in the atmosphere: Distribution, sources and sinks. *J. Geophys. Res.* 99:1805 - 1819.
- Smith D, Španěl P. 2011. Ambient analysis of trace compounds in gaseous media by SIFT-MS. *Analyst* 136:2009-2032.
- Smith D, Španěl P. 1996. The novel Selected-ion Flow Tube approach to trace gas analysis of air and breath. *Rapid Communications in Mass Spectrometry* 10:1183 - 1198.
- Smith D, Španěl P. 2005. Selected ion flow tube mass spectrometry (SIFT-MS) for on-line trace gas analysis. *Mass Spectrometry Reviews* 24:661-700.

- Spanel P, Ji Y, Smith D. 1997. SIFT studies of the reactions of H_3O^+ , NO^+ and O_2^+ with a series of aldehydes. *International Journal of Mass Spectrometry and Ion Processes* 165 - 166:25 - 37.
- Spanel P, Ji Y, Smith D. 1997. SIFT studies of the reactions of H_3O^+ , NO^+ and O_2^+ with a series of aldehydes and ketones. *International Journal of Mass Spectrometry and Ion Processes* 165 - 166:25 - 37.
- Spanel P, Smith D. 1999. Selected ion flow tube studies of the reactions of H_3O^+ , NO^+ and O_2^+ with several aromatic and aliphatic monosubstituted halocarbons. *International Journal of Mass Spectrometry* 189:213 - 223.
- Spanel P, Smith D. 1998b. Selected ion flow tube studies of the reactions of H_3O^+ , NO^+ , and O_2^+ with several aromatic and aliphatic hydrocarbons. *International Journal of Mass Spectrometry* 181:1-10.
- Spanel P, Smith D. 1998a. Selected ion flow tube studies of the reactions of H_3O^+ , NO^+ , and O_2^+ with some organosulphur molecules. *International Journal of Mass Spectrometry* 176.
- Spanel P, Smith D. 1998c. Selected ion flow tube studies of the reactions of H_3O^+ , NO^+ and O_2^+ with several amines and some other nitrogen containing molecules. *International Journal of Mass Spectrometry* 176:203 - 211.
- Spanel P, Smith D. 1997. SIFT studies of the reactions of H_3O^+ , NO^+ and O_2^+ with a series of alcohols. *International Journal of Mass Spectrometry and Ion Processes* 167/168:375 - 388.
- Spanel P, Smith D. 1998. SIFT studies of the reactions of H_3O^+ , NO^+ and O_2^+ with a series of volatile carboxylic acids and esters. *International Journal of Mass Spectrometry and Ion Processes* 172:137 - 147.
- Stein SE. 2005. Mass Spectra. In: Linstrom PJ, W.G. M, Editors. NIST Chemistry WebBook, NIST Standard Reference Database Number 69. Gaithersburg MD, 20899: National Institute of Standards and Technology.

- Steinbacher M, Dommen J, Ammann C, Spirig C, Neftel A, Prevot ASH. 2004. Performance characteristics of a proton-transfer-reaction mass spectrometer (PTR-MS) derived from laboratory and field measurements. *International Journal of Mass Spectrometry* 239:117 - 128.
- Stroud CA, Roberts JM, Goldan PD, Kuster WC, Murphy PC, Williams EJ, Hereid D, Parrish DD, Sueper D, Trainer M, Fehsenfeld FC, Apel E, Riemer D, Wert B, Henry B, A. F, Martinez-Harder M, Harder H, Brune WH, Li G, Xie H, Young VL. 2001. Isoprene and its oxidation products, methacrolein and methylvinyl ketone, at an urban forested site during the 1999 Southern Oxidants Study. *J. Geophys. Res.* 106:8035 - 8046.
- Su T, Bowers MT. 1973c. Ion-polar molecule collisions: the effect of ion size on ion-polar rate constants; the parameterization of the average-dipole-orientation theory. *International Journal of Mass Spectrometry and Ion Physics* 12:347.
- Su T, Bowers MT. 1973b. Ion-polar molecule collisions. Proton transfer reactions of H_3^+ and CH_5^+ to the geometric isomers of difluoroethylene, dichloroethylene, and difluorobenzene. *J. American Chem. Soc.* 95:1370.
- Su T, Bowers MT. 1973a. Theory of ion-polar molecule collisions. Comparison with experimental charge transfer reactions of rare gas ions to geometric isomers of difluorobenzene and dichloroethylene. *J. Chem. Phys.* 58:3027.
- Su T, Chesnavich WJ. 1982. Parameterization of the ion-polar molecule collision rate constant by trajectory calculations. *J. Chem. Phys.* 76:5183.
- Sulzer P, Edtbauer A, Hartungen E, Jürschik S, Jordan A, Hanel G, Feil S, Jaksch S, Märk L, Märk TD. 2012. From conventional proton-transfer-reaction mass spectrometry (PTR-MS) to universal trace gas analysis. *International Journal of Mass Spectrometry* 321–322:66-70.
- Tani A, Hayward S, Hansel A, Hewitt CN. 2004. Effect of water vapour pressure on monoterpene measurements using proton transfer reaction-mass spectrometry (PTR-MS). *International Journal of Mass Spectrometry* 239:161 - 169.

- Tani A, Hayward S, Hewitt CN. 2003. Measurement of monoterpenes and related compounds by proton transfer reaction-mass spectrometry (PTR-MS). *International Journal of Mass Spectrometry* 223-224:561 - 578.
- Thalman R, Baeza-Romero MT, Ball SM, Borrás E, Daniels MJS, Goodall ICA, Henry SB, Karl T, Keutsch FN, Kim S, Mak J, Monks PS, Muñoz A, Orlando J, Peppe S, Rickard AR, Ródenas M, Sánchez P, Seco R, Su L, Tyndall G, Vázquez M, Vera T, Waxman E, Volkamer R. 2015. Instrument intercomparison of glyoxal, methyl glyoxal and NO₂ under simulated atmospheric conditions. *Atmos. Meas. Tech.* 8:1835-1862.
- Utterback DF, Millington DS, Gold A. 1984. Characterization and determination of Formaldehyde Oligomers by Capillary Column Gas Chromatography. *Anal. Chem.* 56:470 - 473.
- von Hartungen E, Wisthaler A, Mikovny T, Jaksch D, Boscaini E, Dunphy PJ, Mark TD. 2004. Proton-transfer-reaction mass spectrometry (PTR-MS) of carboxylic acids: Determination of Henry's law constants and axillary odour investigations. *International Journal of Mass Spectrometry* 239:243 - 248.
- Wang T, Španěl P, Smith D. 2004. A selected ion flow tube, SIFT, study of the reactions of H₃O⁺, NO⁺ and O₂⁺ ions with several N- and O-containing heterocyclic compounds in support of SIFT-MS. *International Journal of Mass Spectrometry* 237:167-174.
- Warneke C, de Gouw J, Kuster WC, Goldan PD, Fall R. 2003. Validation of atmospheric VOC measurements by proton-transfer-reaction mass spectrometry using a gas-chromatographic preseparation method. *Environmental Science and Technology* 37:2494-2501.
- Warneke C, van der Veen C, Luxembourg S, de Gouw J, Kok A. 2001. Measurements of benzene and toluene in ambient air using proton-transfer-reaction mass spectrometry: calibration, humidity dependence, and field intercomparison. *International Journal of Mass Spectrometry* 207:167 - 182.
- Warneke C, Veres P, Murphy SM, Soltis J, Field R, Koss A, Li R, Yuan B, Roberts JM, de Gouw J. 2015. PTR-QMS versus PTR-TOF comparison in a region with oil and

- natural gas extraction industry in the Uintah Basin 2013. *Atmos. Meas. Tech.* 8:411 - 420.
- Wilson PF, Freeman CG, McEwan MJ. 2003. Reactions of small hydrocarbons with H_3O^+ , O_2^+ and NO^+ ions. *International Journal of Mass Spectrometry* 229:143 - 149.
- Wisthaler A, Apel E, Bossmeyer J, Hansel A, Junkermann W, Koppmann R, Meier R, Muller K, Solomon S, Steinbrecher R, Tillman M, Brauers T. 2008. Technical Note: Intercomparison of formaldehyde measurements at the atmosphere simulation chamber SAPHIR. *Atmos. Chem. Phys.* 8.
- Wisthaler A, Hansel A, Koppmann R, Brauers T, Bossmeyer J, Steinbrecher R, Junkermann W, Müller K, Solomon SJ, Apel E. 2006. PTR-MS measurements of HCHO and results from HCHO intercomparison measurements in the atmosphere simulation chamber SAPHIR. *Geophys. Res. Abstr.* 8:04776.
- Wood EC, Knighton WB, Fortner EC, Herndon SC, Onasch TB, Franklin JP, Worsnop DR, Dallmann TR, Gentner DR, Goldstein AH, Harley RA. 2015. Ethylene Glycol Emissions from On-road Vehicles. *Environmental Science & Technology* 49:3322-3329.
- Wyche KP, Blake RS, Willis KA, Monks PS, Ellis AM. 2005. Differentiation of isobaric compounds using chemical ionization reaction mass spectrometry. *Rapid Communications in Mass Spectrometry* 19:3356-3362.
- Zhao J, Zhang R. 2004. Proton transfer reaction rate constants between hydronium ion (H_3O^+) and volatile organic compounds. *Atmospheric Environment* 38:2177 - 2185.
- Zielinska B, Sagebiel JC, Harshfield G, Gertler AW, Pierson WR. 1996. Volatile organic compounds up to C_{20} emitted from motor vehicles; measurement methods. *Atmospheric Environment* 30:2269 - 2286.